The Novel Interacting Partners of Viperin and Their Role in Establishing a Host Antiviral State

Onruedee Khantisitthiporn, M.Sc.

Discipline of Molecular and Cellular Biology

School of Biological Sciences

The University of Adelaide

THE UNIVERSITY of ADELAIDE

A dissertation submitted to The University of Adelaide

in candidature for the degree of

Doctor of Philosophy in the Faculty of Sciences

October 2017

Table of content

List of Figures

List of Tables

Abstract

Viral infection results in activation of the innate immune response that culminates in the production of the interferons and the establishment of an antiviral state through the expression of hundreds of interferon stimulated genes (ISGs). One such ISG is Viperin (*RSAD2*) that has broad antiviral activity against a range of RNA and DNA viruses. Previous work has established that viperin is antiviral against the hepatitis C virus, however the molecular mechanism(s) that underpin this antiviral activity are not well understood. It is thought that viperin interacts with the HCV NS5A protein and the host pro-viral host factor VAP-A within the HCV replication complex, although this has not formally been proven. Thus the main objective of this thesis was to investigate the localisation of viperin to the HCV replication complex at the cellular level and to identify additional viperin cellular interacting partners in the hope that we can further understand the biology of this enigmatic protein.

We therefore used a cell biology approach to visualise viperin at or within the HCV replication complex. Expression of viperin tagged to the electron microscopy (EM) tag (APEX2) allowed us to precisely determine the localisation of viperin at the ultrastructural level by EM. We identified that in the presence of exogenous HCV non-structural protein expression (and hence RC formation), viperin alters the formation of convoluted membranes that in-turn could have an impact on the establishment of replication complex formation that is crucial for HCV replication.

In addition to viperin binding the HCV NS5A protein, it can also bind to host proteins (FPPS, VAP-A, TRAF6, and IRAK1) to modulate cellular function such as lipid metabolism and innate immune signalling. We hypothesised that viperin exerts such a diverse range of functions through interaction with as yet unidentified cellular proteins and we employed a yeast two-hybrid screen to identify novel interacting partners. The peroxisomal biogenesis factor 19 (PEX19) was identified as a genuine viperin interaction partner and furthermore showed that expression of viperin not only co-localised with peroxisomes but redirected them to a perinuclear localisation and association with lipid droplets. The reason for this is not immediately clear, however peroxisomes have recently been shown to be a scaffold for the innate immune adaptor molecule MAVS and are now recognised as important organelles in activation of the host cellular response to viral infection. Using a combination of deconvolution and super-resolution microscopy and EM using APEX2 tagged viperin we show that viperin localises to the LD in association with peroxisomes and the mitochondria. It is, therefore, possible that viperin may direct MAVS+ve peroxisomes to sites of innate immune signalling. Consistent with this hypothesis we have shown that viperin augments IFN-β production for MAVS localised selectively on both mitochondria and the peroxisome, but not for each organelle individually. This implies that viperin may act as linker molecule for MAVS signalling from both organelles.

In conclusion, we propose that viperin localises within the HCV replication complex to impart its antiviral effect. Furthermore, viperin interacts with PEX19 and recruits peroxisomes to an “innate immune synapse” to augment innate immune signalling to

restrict viral infection. The work of this thesis contributes our understanding of the host-virus relationship in control of HCV and the possibility of the development of innate immune agonists as therapeutics for viral disease.

Declaration

I certify that this work contains no material which has been accepted for the award of any other degree or diploma in my name, in any university or other tertiary institution and, to the best of my knowledge and belief, contains no material previously published or written by another person, except where due reference has been made in the text. In addition, I certify that no part of this work will, in the future, be used in a submission in my name, for any other degree or diploma in any university or other tertiary institution without the prior approval of the University of Adelaide and where applicable, any partner institution responsible for the joint-award of this degree.

I give permission for the digital version of my thesis to be made available on the web, via the University's digital research repository, the Library Search and also through web search engines, unless permission has been granted by the University to restrict access for a period of time.

Onruedee Khantisitthiporn

October 17th, 2017

Acknowledgements

I would like to thank my supervisor Associate Professor Michael Beard for giving me the great opportunity to conduct my PhD in his laboratory, and for his continued support throughout my PhD.

I offer my sincerest gratitude to my co-supervisors Dr. Karla Helbig and Dr. Nicholas Eyre for their excellent teaching, support and technical guidance during my PhD.

I would like to thank all members of the Viral Pathogenesis Research Laboratory both past and present, especially Dr. Kylie Van der Hoek, Dr Amanda Aloia, Byron Shue, Chuan Kok Lim and Catherine Scougall.

I would also like to thank the Department of Molecular and Cellular Biology for the great opportunity to undertake a PhD and Thammasat University, Thailand for providing me a scholarship to conduct my PhD in Adelaide.

Finally, I would like to thank my parents, especially my mother who passed away during the last year of my PhD and my family for their continued love, support, and encouragement from Thailand.

Presentations and publications arising from this PhD

Presentations

Khantisitthiporn, O., Helbig, K.J., Eyre, N.S. and Beard, M.B. The novel interacting partners of viperin and their role in establishing a host antiviral state. 8th Australasian Virology Society Meeting and 11th Annual Meeting of the Australian Centre for Hepatitis & HIV Virology Meeting, Hunter Valley, Australia, 2015. (oral presentation)

Khantisitthiporn, O., Helbig, K.J., Eyre, N.S. and Beard, M.B. The novel interacting partners of viperin and their role in establishing a host antiviral state. Infectious and Immunity Conference, Lorne, Australia, 2016. (oral presentation)

Khantisitthiporn, O., Helbig, K.J., Eyre, N.S. and Beard, M.B. The ISG viperin interacts with peroxisomes to modulate antiviral innate immune signalling. Positive-Strand RNA Viruses meeting, Texas USA 2016. (poster presentation)

Khantisitthiporn, O., Helbig, K.J., Eyre, N.S. and Beard, M.B. The ISG viperin interacts with peroxisomes to modulate antiviral innate immune signalling. Viruses & Cells Gordon Research Conference, Lucca (Barga), Italy 2016. (poster presentation)

Van der Hoek KH, Eyre NS, Shue B, **Khantisitthiporn O**, Glab-ampai K, Jankovic-Karasoulos T, Roberts CT, Jolly LA, Carr JM, Helbig KJ, Beard MR. Attenuation of the innate response to Zika virus in placental trophoblasts and neural progenitor cells. Infectious and Immunity Conference, Lorne, Australia, 2017. (poster presentation)

Publication

Khantisitthiporn, O., Helbig, K.J., Eyre, N.S. and Beard, M.B. The interaction of viperin and peroxisomes via its novel interacting partner; *PEX19,* augments innate immune signalling. (Manuscript in preparation)

Publication (unrelated to the main part of this thesis)

Van Der Hoek, K. H., Eyre, N. S., Shue, B., **Khantisitthiporn, O.**, Glab-Ampi, K., Carr, J. M., Gartner, M. J., Jolly, L. A., Thomas, P. Q., Adikusuma, F., Jankovic-Karasoulos, T., Roberts, C. T., Helbig, K. J. & Beard, M. R. 2017. Viperin is an important host restriction factor in control of Zika virus infection. *Sci Rep,* 7**,** 4475.

Materials Providers

Abcam	Cambridge, UK
Addgene	Massachusetts, USA
Ambion	Texas, USA
Amersham Pharmacia Biotech	Birminghamshire, UK
Applied Biosystems	Massachusetts, USA
Beckman Coulter	Miami, FL, USA
Bioline	Sydney, Australia
BioRad Laboratories	California, USA
Cell Signaling	Massachusetts, USA
Clontech	California, USA
Corning	New York, USA
Eppendorf	Hamburg, Germany
GeneWorks	Adelaide, SA, Australia
Invitrogen	California, USA
Macherey Nagel	Düren, Germany
Merck	Darmstadt, Germany
Molecular Probes	Oregon, USA
Nalge Nunc International	New York, USA
New England Biolabs	Massachusetts, USA
Nikon	Tokyo, Japan
Olympus	Tokyo, Japan
Perkin Elmer	Massachusetts, USA
Promega	Wisconsin, USA
QIAgen	Hilden, Germany
Roche	Indiana, USA
Rockland	Pennsylvania, USA
Santa Cruz Biotechnology	Texas, USA
Sigma Aldrich	Missouri, USA
Stratagene	California, USA

Thermo Scientific	Massachusetts, USA
UVP Inc	California, USA

Abbreviations used

Abbreviation or symbol	Term
× *g*	Acceleration gravity
°C	Degree(s) Celsius
μg	Microgram(s)
μl	Microliter(s)
μm	Micrometer(s)
A	Adenine
aa	Amino acids
ATP	Adenosine triphosphate
bp	Base pair(s)
BSA	Bovine serum albumin
C	Cytosine
cDNA	Complementary deoxyribonucleic acid
CHC	Chronic hepatitis C
CLDN	Claudin
CMV	Cytomegalovirus
DAA	Direct acting antiviral
DAPI	4', 6-Diamidino-2-pheylinodole
dATP	Deoxyadenosine triphosphate
dCTP	Deoxycytosine tripshosphate
DDW	Deionized distilled water
DEPC	Diethyl pyrocarbonate
dGTP	Deoxyguanosine triphosphate
dH_2O	Deionised water
DMEM	Dulbecco's Modified Eagle Medium with HEPES
DMSO	Dimethyl sulfoxide
DMV	Double-membrane vesicle
DNA	Deoxyribonucleic acid

dNTP	Deoxynucleotide triphosphate
dsRNA	Double stranded RNA
DTT	Dithiothreitol
dTTP	Deoxythymidine triphosphate
EMCV	Encephalomyocarditis virus
EDTA	Ethylenediamine tetraacetic acid
ER	Endoplasmic reticulum
FACS	Fluorescence-activated cell sorting
FCS	Foetal calf serum
FDA	Food and Drug Administration
ffu	Focus forming units
G	Guanosine
g	Gram(s)
GAG	Glycosaminoglycan
GFP	Green fluorescent protein
HCC	Hepatocellular carcinoma
HCMV	Human cytomegalovirus
HCV	Hepatitis C virus
HCVcc	Cell-culture propagated hepatitis C virus
HEPES	4-(2-hydroxyethyl)-1-piperazineethanesulfonic acid
HIV	Human immunodeficiency virus
hr	Hour(s)
HRP	Horse radish peroxidase
Huh	Human hepatoma
IFN-γ	Interferon gamma
IFN-α	Interferon alpha
IFN-β	Interferon beta
IFN-λ	Interferon lambda
Ig	Immunoglobulin(s)
IRES	Internal ribosome entry site
ISRE	Interferon stimulated response element

JAK	Janus kinase
kb	Kilobase
kDa	Kilodalton(s)
kg(s)	Kilogram(s)
KO	Knock out
L-Agar	LB + agar
LB	Luria Bertani broth
LD	Lipid droplet
LDL	Low density lipoproteins
LDLR	Low density lipoprotein receptor
Luc	Luciferase
LVP	Lipoviral particle
M	Mole
mA	Milliampere(s)
MAVS	Mitochondrial antiviral-signalling protein
MCS	multiple cloning site
MEM	Minimum Essential Medium
mg	Milligram(s)
min	Minute(s)
ml	Milliliter(s)
mM	Millimolar(s)
MMV	Multi-membrane vesicle
MOI	Multiplicity of infection
mRNA	Messenger ribonucleic acid
MW	Molecular weight
N/A	Not applicable
NANBH	Nnon-A, non-B hepatitis
ng	Nanogram(s)
nM	Nanomolar
NPC1L1	Niemann-Pick C1 like 1
NS	Non-structural

nt (s)	Nucleotide (s)
OCLN	Occludin
OD	Optical density
ORF	Open reading frame
OSBP	Oxysterol-binding protein
PBS	Phosphate buffered saline
PCR	Polymerase chain reaction
PEG	Polyethylene glycol
pg	Picograms
pH	Negative logarithm of hydrogen ion activity
PI4KIIIα	Phosphatidylinositol 4-kinase III alpha
PI4P	Phosphatidylinositol 4-phosphate
pmol	Picomolar
RC	Replication complex
RdRp	RNA-dependent RNA polymerase
RNA	Ribonucleic acid
RNase	Ribonuclease
rpm	Revolutions per minute
RT	Room temperature
RT-PCR	Reverse transcriptase polymerase chain reaction
SDS	Sodium dodecyl sulfate
SDS-PAGE	Sodium dodecyl sulfate polyacrylamide gel electrophoresis
sec	Second(s)
SMV	Single-membrane vesicle
SOC	Super optimal broth with catabolite repression
SRB1	Scavenger receptor class B1
ss	Single stranded
STAT	Signal transducer and activator of transcription
SVR	Sustained virologic response
T	Thymidine

TAE	Tris, acetic acid, EDTA (TAE) buffer
TBEV	Tick-borne encephalitis virus
TEMED	N,N,N’,N’-tetramethylethylenediamine
TYK2	Tyrosine kinase 2
U/μl	Unit(s) per microliter
UTR	Untranslated region
UV	Ultraviolet
V	Volt(s)
v/v	Volume per volume
VAPA	Vesicle-associated membrane protein-associated protein A
VLDL	Very low density lipoprotein
w/v	Weight per volume
WHO	World Health Organization
WT	Wild-type
x g	Acceleration gravity
X-α-gal	5-bromo-4-chloro-3-indolyl-α-D-galactopyranoside

Chapter 1

Introduction

1.1 Hepatitis C Virus

1.1.1 Discovery and Epidemiology

Hepatitis C Virus (HCV) infection is a leading cause of acute and chronic liver disease worldwide. HCV was first categorised as non-A and non-B hepatitis virus (NANBH) (Feinstone et al., 1975) until the viral genome was isolated using molecular methods from NANBH plasma in 1989 (Choo et al., 1989). It is estimated that over 170 million people worldwide are infected with HCV (Organisation, 2014, Thomas, 2013). One of the major problems of HCV-infected patients is that approximately 80% of infected individuals will develop progressive chronic liver diseases such as fibrosis, liver cirrhosis, hepatic failure and/or hepatocellular carcinoma (Zhong et al., 2005). The World Health Organisation (WHO), estimates about 500,000 people die from HCV-related liver disease every year. In Australia, the prevalence of HCV infection has been estimated at 264,000 individuals and it is the most common cause of clinically significant liver disease (Razali et al., 2009, Razali et al., 2007). Approximately 8,000 new cases of HCV infection emerge each year (Razavi et al., 2014) resulting in increasing numbers of individuals with HCV-related chronic liver disease, which places a significant burden on the public health system (Thomas, 2013, Razavi et al., 2014, Davis et al., 2010).

1.1.2 Transmission

HCV is a blood-borne virus and prior to 1992, the most common transmission route was blood transfusion or organ transplantation. However, the improvement of screening techniques in blood banks in 1992, effectively eliminated HCV infection via this route, although this type of transmission remains in developing countries due to the limitation of screening methods, un-screened blood components, or other inappropriate medical procedures (Sievert et al., 2011). Injecting drug use (IDU) with needle and syringe sharing is the major mode of transmission of HCV in developed countries. Other modes of HCV transmission include tattooing, piercing, sexual intercourse or vertical transmission from mother to baby, although the latter two are rare (Thomas, 2013, Dore et al., 2003, Mohan et al., 2010).

1.1.3 Pathogenesis

HCV is a noncytopathic virus, and therefore liver disease, particularly in the chronic liver phase is a result of both innate and adaptive immune responses to HCV infected hepatocytes such as immune-mediated cytolysis. The hepatocyte is the primary and main target of HCV replication. However, HCV infection is not restricted to hepatocytes as HCV RNA has been reported in a small percentage of different cell types including mononuclear cells such as macrophages, monocytes, dendritic cells (Goutagny et al., 2003, Bouffard et al., 1992, Bain et al., 2001), B-cells (Sung et al., 2003), and gastric mucosa-associated lymphoid tissue (Tursi et al., 2002). The role of HCV replication at these extrahepatic sites, if at all, remains unknown and is the source of significant debate.

Acute HCV infection in most individuals often goes unrecognised as symptoms are usually absent or result in mild illness. Following acute infection, 20% of individuals successfully eliminate the virus, whereas the remaining 80% of patients will fail to develop an effective host antiviral response and subsequently will develop a chronic lifelong infection. Of those individuals who develop chronic infection, approximately 20% will have progressive liver disease over a period of 25-30 years (Figure 1.1) (Freeman et al., 2001), culminating in liver cirrhosis, with 2% of individuals progressing to hepatocellular carcinoma (HCC) (Alter, 1995). The host immune response to HCV infection results in chronic hepatic inflammation including liver fibrosis and cirrhosis. Cirrhosis is the most progressive form of liver disease which occurs after long-term damage of the liver and is characterised by the replacement of normal liver tissue by extensive scarring. Alcohol consumption and co-infection with other viruses such as human immunodeficiency virus (HIV) and hepatitis B virus (HBV) are co-factors which impact the rate of progression to advanced liver disease.

1.1.4 Treatment

Initial treatment for chronic hepatitis (CHC) was interferon-α (IFN-α) which became available in 1991; however response rates were poor with only 10-20% of individuals clearing the virus. IFN-α is a cytokine which is able to induce an antiviral response. Using IFN-α in combination with the guanine nucleotide analogue ribavirin improved the response rates to 40% (Foster, 2010). HCV treatment was revolutionised in 2001 by the conjugation of a polyethylene glycol group to IFN-α (pegylated IFN-α, PegIFN-α) which

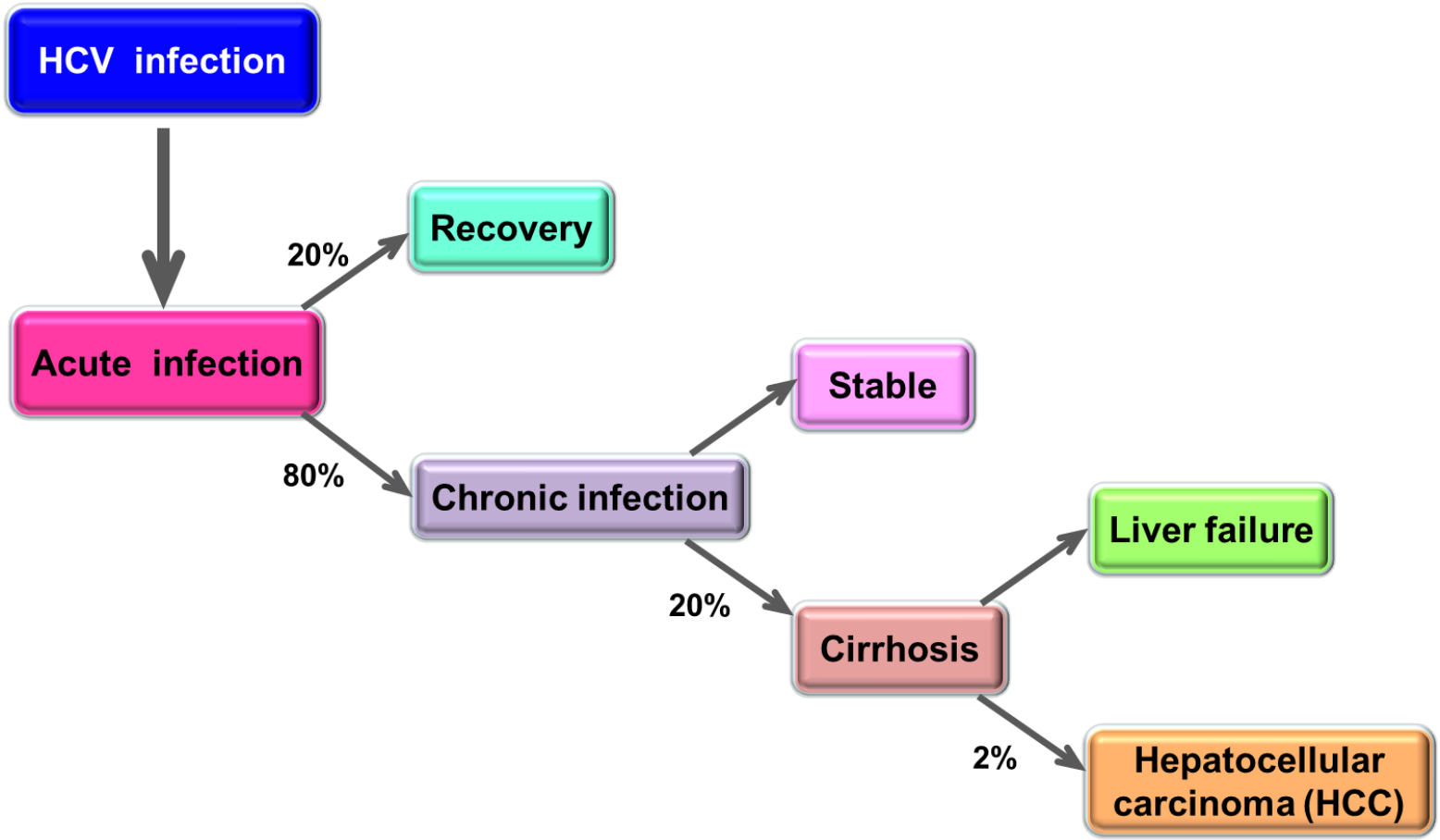

Figure 1.1: Clinical progression of HCV infection.

enhanced the half-life of IFN-α and resulted in increased antiviral activity (Glue et al., 2000). With a combination of PegIFN-α and ribavirin, a sustained virologic response (SVR, defined as undetectable HCV RNA in serum 6 months post-treatment) increased to an average of 40-50% in genotype 1 and 75-85% for genotype 2 and 3 infection (Manns et al., 2001, Fried et al., 2002, Hadziyannis et al., 2004). Such SVRs remain unsatisfactory especially in genotype 1 infected-individuals, which represents the most widely distributed genotype worldwide (Le Guillou-Guillemette et al., 2007). Another complicating factor for treatment decision is interleukin 28B (IL28B) genetic polymorphisms that are associated with HCV genotype 1. Genome-wide association studies (GWAS) identified IL28B polymorphism (on chromosome 19) as the most important factor in predicting interferon-based treatment response in HCV genotype 1 (Ge et al., 2009, Tanaka et al., 2009, Rauch et al., 2010). The favourable homozygous SNP rs12979860 (C/C genotype) is also associated with higher spontaneous HCV clearance rates (Ge et al., 2009, Thomas et al., 2009).

Interferon-based therapy is usually administered as a response-guided therapy for 24- or 48- weeks depending on viral loads, genotypes, IL28B polymorphism and presence/absence of cirrhosis. Such prolonged therapy is associated with numerous side effects such as flu-like symptoms, fatigue, insomnia, rash, anorexia, weight loss and haemolytic anaemia (Feld and Hoofnagle, 2005, Sharma, 2010). However, most the concerning side effects of all are liver decompensation and significant depression leading to suicides, thus excluding many patients from treatment. Complicating this, SVRs can be significantly reduced in patients with advanced liver fibrosis, African ethnicity, insulin

resistance, obesity, heavy alcohol consumption and HIV co-infection (Thomas, 2013). These limitations redirected researchers to focus on the development of second generation anti-HCV drugs known as the direct-acting antivirals (DAAs).

Direct-acting antiviral (DAAs) compounds are able to directly interfere with specific HCV viral proteins, thus arresting the viral life cycle (Gao et al., 2010, Jensen, 2011, Targett-Adams et al., 2011). The first generation DAAs approved by the US Food and Drug Administration (FDA) in 2011 were NS3/4A serine protease inhibitors [Boceprevir (Merck) and Telaprevir (Vertex Pharmaceuticals/ Johnson-Johnson)] for treatment of HCV genotype 1. These DAAs still require combination with pegylated IFN-α and ribavirin to yield satisfactory response (SVR rates to 70-80%) (Marks and Jacobson, 2012) with lower SVRs reported from treatment-experienced or cirrhotic patients. IFN-α remains a key component owing to the development of antiviral resistance to DAAs when used in monotherapy (Aloia et al., 2012, Calle Serrano and Manns, 2012). Arrival of the NS5B polymerase inhibitor (Sofosbuvir, Gilead Sciences) and the second generation NS3-4A protease inhibitors (Simeprevir, Johnson & Johnson) in combination with pegylated IFN-α and ribavirin has significantly improved the SVRs for HCV genotype 1 (Keating, 2015) but has also seen HCV genotype 2 as the most resistant genotype to DAAs. To avoid the complications of interferon-based therapy, Sofosbuvir has now been used in combination with other NS5A inhibitors such as Ledipasvir (Harvoni), Daclatasvir and Velpatasvir (Epclusa). These DAAs have completely changed the landscape of HCV treatment, particularly with Epclusa, showing excellent pan-genotypic effect (including genotype 4 and 6), promising SVRs in cirrhotic patients and a

very low level of drug resistance. The focus has now been shifted to improve the response rates in traditionally difficult to treat patients such as HIV co-infected and cirrhotic patients, with various combinations such as PrOD (Paritaprevir/ ritonavir/ ombitasvir/ dasabuvir) and elbasvir/grazoprevir (Zepatier).

1.1.5 Classification and genotypes

HCV is in the genus *Hepacivirus*, family *Flaviviridae*. The virus has now been classified into seven major genotypes (genotype 1-7) with numerous subtypes based on the phylogeny and the similarity of nucleotide sequence of the viral genome. The genotypes differ in nucleotide sequence by 30-35% from each other and subtypes differ from others by 15-25% (Simmonds et al., 2005, Smith et al., 2014). A worldwide distribution of HCV genotypes varies in geographical area (Figure 1.2). Genotypes 1-3, particularly 1a, 1b, 2a and 3a are widely distributed across the world including Australia (Dore et al., 2003). While genotypes 4-6 are mainly endemic to specific areas in Central Africa, the Middle East, South Africa and Asia (Bowden and Berzsenyi, 2006). HCV genetic diversity across the world has likely been influenced by historical and human migration.

1.1.6 HCV genome and proteins

HCV genome: HCV is a small-enveloped virus with a single-stranded, positive-sense RNA genome and as mentioned previously is a *Hepacivirus* within the *Flaviviridae* family. The HCV genome size is approximately 9.6 kb and comprises of a single open reading frame which encodes for a single polyprotein about 3,000 amino acids in length,

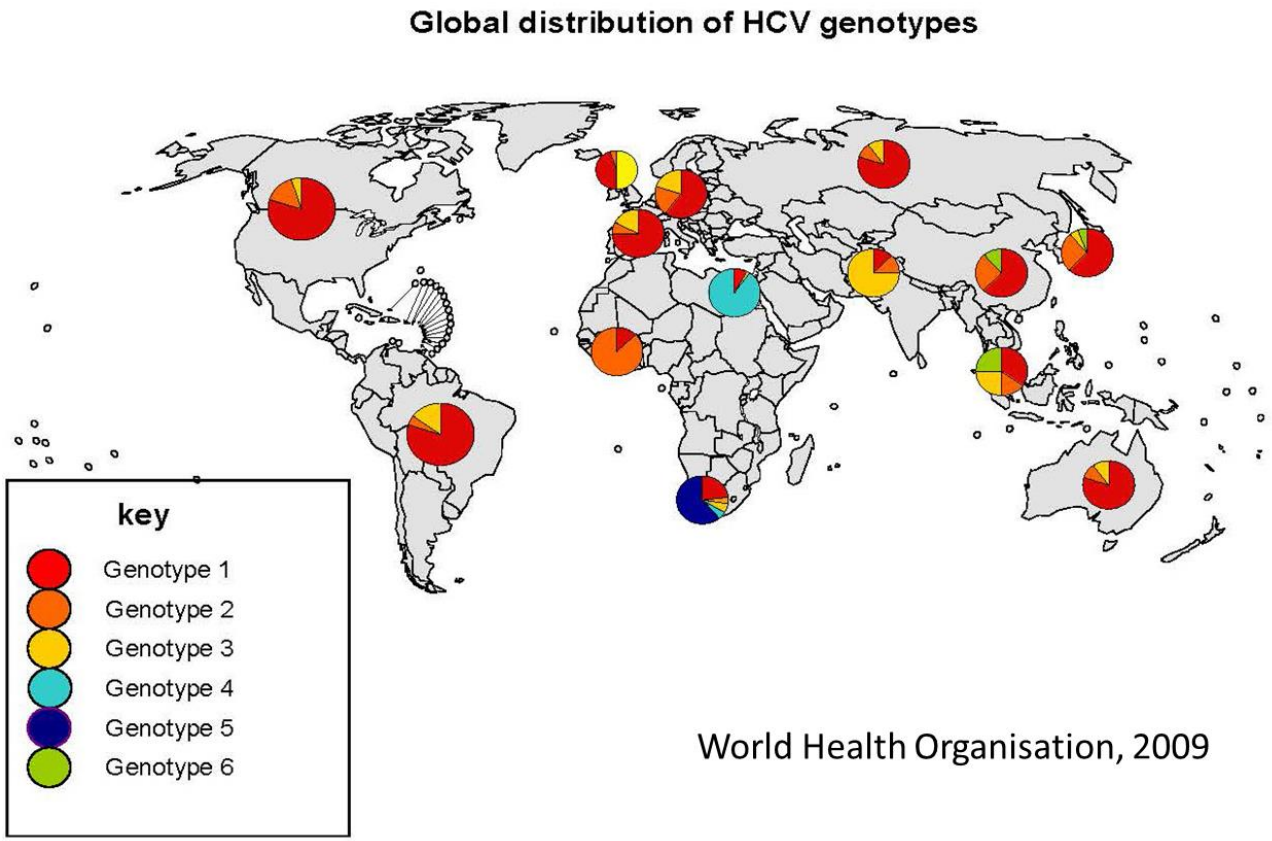

Figure 1.2: Global distribution of HCV genotypes.

and is flanked by two highly conserved untranslated regions (5'UTR and 3'UTR) (Figure 1.3) (Moradpour et al., 2007). The monocistronic plus-sense RNA genome of HCV is translated into a single polyprotein by host translational machinery using the HCV internal ribosomal entry site (IRES) in the 5' UTR. The 5' UTR contains 341 nucleotides; four highly structured domains and the internal ribosomal entry site (IRES) which controls the translation of the open reading frame into a single polyprotein. The IRES element mediates cap-independent translation initiation of HCV RNA by binding to the 40s ribosomal subunit to form a stable pre-initiation complex. The 3' UTR (approximately 225 nucleotides) which is essential for viral replication consists of three main regions including a variable region, a long polyuridine region (polyU/UC) and a highly conserved X region (Niepmann, 2013, Suzuki et al., 2007).

The polyprotein is post-translationally processed by host cellular and viral proteases to produce 10 viral proteins: 3 structural proteins (core, envelope glycoproteins E1 and E2), a transmembrane protein belonging to the virioporin family (p7), and 6 non-structural proteins (NS2, NS3, NS4A, NS4B, NS5A and NS5B) (Sharma, 2010, Sklan et al., 2009, Moradpour et al., 2007). A short summary of the function of HCV proteins is provided below.

Core: The HCV core protein which forms the viral capsid is present in various sizes (17 to 23 kDa) but the predominant form is the 21kDa form (Yasui et al., 1998). It is located at the N-terminus of the polyprotein and is cleaved by the endoplasmic reticulum (ER)

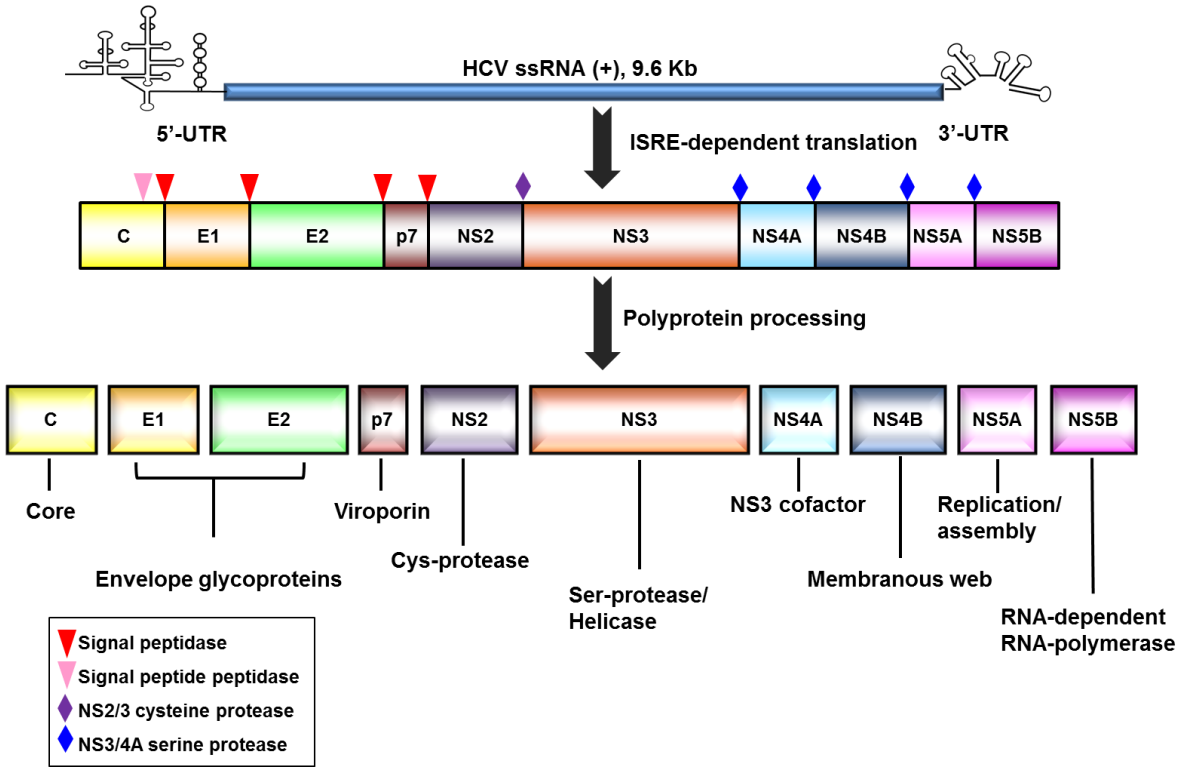

Figure 1.3: HCV genome organisation and polyprotein processing.
HCV is a 9.6 kb positive-strand RNA genome and consists of core and envelope glycoproteins E1 and E2; a transmembrane protein (p7); and non-structural proteins (NS2, NS3, NS4A, NS4B, NS5A and NS5B). The UTR at the 5' and 3' ends of the RNA are important to translation and replication of the viral RNA. Red arrowheads indicate cleavage sites of the HCV polyprotein precursor by signal peptidase. Pink arrowhead indicates C-terminal processing of the core protein by signal peptide peptidase. Diamonds represent the cleavage sites for NS2-3 and NS3-4A proteases.

signal peptidase (McLauchlan et al., 2002). It contains three distinct domains: an N-terminal hydrophilic domain, a C-terminal hydrophobic domain and a signal peptide for targeting the nascent HCV polyprotein to the endoplasmic reticulum (ER) and bringing the translocation of E1 to the ER lumen (Lo et al., 1995). The immature form of the core protein (p23) is processed by an intramembrane protease and the signal peptide peptidase (SPP) to be mature form of the core protein (p21) (Weihofen et al., 2002, McLauchlan et al., 2002). The mature core protein (p21) is responsible for viral nucleocapsid formation and subsequently viral RNA packaging (Yasui et al., 1998). Moreover, it has been shown to associate with the lipid droplet after releasing from the ER membrane (McLauchlan et al., 2002, Boulant et al., 2006, Miyanari et al., 2007). Additionally, it has been shown to impact HCV pathogenesis by promoting the formation of lipid droplets which may enhance steatosis formation and possibly the development of HCC (Barba et al., 1997, Moriya et al., 1997, Moriya et al., 1998, Asselah et al., 2006).

Envelope glycoproteins E1/E2: Both envelope proteins (E1 and E2) are highly glycosylated transmembrane proteins. E1 and E2 (30-35 kDa and 70-75 kDa, respectively) form non-covalent heterodimers which is the major integral component of the viral envelope (Goffard and Dubuisson, 2003). The E1 and E2 complex/heterodimer facilitates the attachment of the HCV virion to cell receptors which are necessary for HCV entry and fusion (Hsu et al., 2003, Moradpour et al., 2007, Suzuki et al., 2007).

p7: p7 is a small polypeptide (63 amino acids) which is an integral membrane protein and localises to the ER (Haqshenas et al., 2007). It contains two transmembrane domains

connected by a cytoplasmic loop (Carrere-Kremer et al., 2002). It belongs to the viroporin family and has been documented to act as a cation channel which allows calcium ion flow from the ER into the cytoplasm (Griffin et al., 2003, Pavlovic et al., 2003). The role of p7 in the virus life cycle is not well understood, but it is not required for viral replication (Jones et al., 2007, Steinmann et al., 2007). It has shown to be essential for infectivity (Sakai et al., 2003) and involved in viral particle assembly and release (Gentzsch et al., 2013). Although most of the researches up to date highlight the role of p7 in viral assembly and release, the molecular mechanism of p7 in the HCV life cycle is uncertain and remains to be clarified.

NS2: NS2 (23 kDa) localises to the ER and contains cysteine autoprotease activity (Grakoui et al., 1993, Hijikata et al., 1993, Lorenz et al., 2006) which is located at the C-terminal domain and cleaves NS2 from NS3 (Selby et al., 1994). It is dispensable for RNA replication and plays a central part but undefined role in viral particle assembly and possibly egress (Jirasko et al., 2008, Jones et al., 2007). It is demonstrated that NS2 interacts with structural and non-structural proteins; E1, E2, p7, NS3 and NS5A and directs envelope proteins to lipid droplets which are the site of viral assembly (Popescu et al., 2011a).

NS3/4A complex: NS3 is a multifunctional protein and contains seine protease activity at its N-terminus and a helicase/NTPase activity at the C-terminal domain (Yao et al., 1999). The serine protease of NS3 is essential for HCV polyprotein cleavage of the remaining downstream non-structural proteins; NS3/NS4A, NS4A/NS4B, NS4B/NS5A

and NS5A/NS5B. NS4A which forms a non-covalent complex with NS3 acts as a co-factor of protease activity by stabilising the NS3/4A complex and is essential for its membrane association (Brass et al., 2008, Morikawa et al., 2011). The localisation of the NS3/4A complex is primarily on the ER membrane and in the replication complex (RC) (Wolk et al., 2000). In addition to its role in the viral life cycle, it also facilitates viral immune evasion by cleaving of adaptor proteins essential for innate immune signalling, Toll/interleukin-1 receptor domain-containing adaptor-inducing interferon-β (TRIF) and MAM-localised mitochondrial antiviral signalling protein (MAVS) (Li et al., 2005b, Meylan et al., 2005, Horner et al., 2011). Accordingly, the NS3/4A serine protease is one of the most popular targets for anti-HCV treatment and has been used as a target of the first and the second generation of DAAs (Morikawa et al., 2011, Lin et al., 2009). The other function of NS3/4A complex which is the RNA helicase activity unwinds double-stranded RNA during viral replication in an ATP-dependent manner (Tai et al., 1996).

NS4B: NS4B is a conserved hydrophobic membrane protein (27 kDa) and localises to ER (Hugle et al., 2001, Lundin et al., 2003). It modifies ER membrane to induce the membranous web formation, which represents the site of HCV RNA replication (Egger et al., 2002, Gosert et al., 2003). NS4B is composed of four transmembrane domains, flanked by amphipathic N-terminal helix which is responsible for remodelling of the ER membrane (Hugle et al., 2001, Lundin et al., 2003, Yu et al., 2006). NS4B interacts with other HCV non-structural proteins and also has a function in viral assembly (Gouttenoire et al., 2010, Jones et al., 2009).

NS5A: NS5A is a phosphorylated zinc-metalloprotein without any enzymatic activity which plays a crucial role in viral replication and assembly (Blight et al., 2000, Lohmann et al., 2001, Appel et al., 2008, Tellinghuisen et al., 2008a). It is composed of 3 domains (Tellinghuisen et al., 2004): domain 1 (D1), and domain 2 (D2) have been linked with RNA replication, whereas domain 3 (D3) is critical for virion assembly (Appel et al., 2008, Tellinghuisen et al., 2008a, Tellinghuisen et al., 2008b, Kim et al., 2011). NS5A can be found in basally phosphorylated (p56) and hyperphosphorylated (p58) forms (Kaneko et al., 1994) and the phosphorylation status of NS5A affects the level of HCV replication (Appel et al., 2005, Appel et al., 2008, Blight et al., 2000). NS5A has been reported to interact with HCV RNA (Huang et al., 2005), and other HCV proteins such as core (Shimakami et al., 2004, Masaki et al., 2008) and interacts with a number of host cellular proteins such as Rab5a and the vesicle-associated membrane protein-associated protein A (VAP-A) (Coller et al., 2009, Hamamoto et al., 2005, Eyre et al., 2014). NS5A has shown to bind to the HCV core protein at the lipid droplet interface which may regulate HCV virus assembly (Shi et al., 2002, Goh et al., 2001). In addition, it was recently shown in live imaging studies that NS5A binds to HCV RNA and may facilitate the transfer of HCV from sites of replication to sites of virion assembly (Fiches et al., 2016). Due to its multiple functions, it is a target of a number of new DAAs in development.

NS5B: NS5B is an RNA-dependent RNA polymerase (RdRp) and has a central function in RNA synthesis of both positive and negative strand RNA (Behrens et al., 1996). Its C-terminal transmembrane domain is responsible for anchoring NS5B to the ER membrane

(Moradpour et al., 2004, Schmidt-Mende et al., 2001). NS5B is another target for the development of direct-acting antivirals (DAAs) (Di Marco et al., 2005, Pawlotsky, 2006).

1.1.7 HCV virion/particles

HCV viral particles are thought to be classical icosahedral symmetry and approximately 40-70 nm in diameter. The virion is composed of an HCV RNA genome, core and the envelope glycoproteins, E1 and E2 (Bartenschlager et al., 2011). The viral nucleocapsid which is core protein encapsulating the RNA genome is surrounded by a host-derived double-layer envelope containing the glycoproteins E1 and E2 (Bartosch et al., 2003, Nielsen et al., 2004). The association of HCV virions and various serum lipoproteins [low- and very-low-density lipoproteins (LDLs and VLDLs)] in circulation forms a complex of lipoviralparticles (LVP) and facilitates viral entry into hepatocytes (Thomssen et al., 1992, Andre et al., 2002).

1.1.8 HCV life cycle

The HCV life cycle consists of multiple steps such as HCV entry, translational polyprotein processing, viral replication and viral assembly and egress (Figure 1.4). A short summary of the each step of HCV life cycle is provided below.

HCV entry: HCV entry requires a set of essential host receptors on the hepatocyte surface. These include the low-density lipoprotein receptor (LDL-R) (Agnello et al., 1999, Monazahian et al., 1999), glycosaminoglycans (GAGs) (Barth et al., 2003),

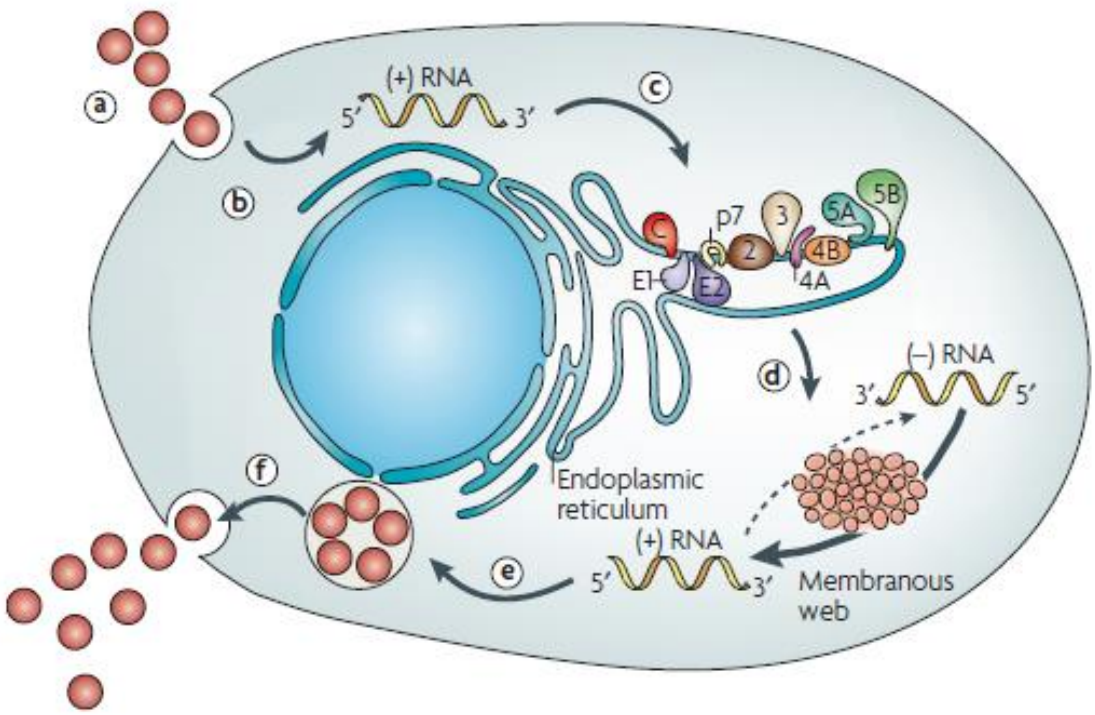

Figure 1.4: Schematic representation of HCV life cycle.

The multiple steps of HCV life cycle comprise of (a) virus-cell attachment and internalisation, (b) viral uncoating, (c) translation and polyprotein processing, (d) RNA replication and membranous web formation, (e) viral packaging and assembly, and (f) release of mature virions (Moradpour et al., 2007).

tetraspanin (CD81) (Pileri et al., 1998), scavenger receptor class B type I (SR-BI) (Scarselli et al., 2002), the tight junction component claudin-1 (CLDN1) (Evans et al., 2007) and occludin (OCLN) (Ploss et al., 2009) (Figure 1.5). The initial step of viral entry is an attachment of HCV particles to the hepatocyte cell surface via low-affinity interactions with LDL receptors and glycosaminoglycans (GAGs) (Agnello et al., 1999, Germi et al., 2002), subsequently leading to the high-affinity interaction of hypervariable region 1 (HVR1) of HCV glycoprotein E2 to the scavenger receptor class B type I (SR-BI) (Dao Thi et al., 2012, Scarselli et al., 2002). This binding induces the conformational change in E2 epitope and allows the high-affinity binding of the viral particle with CD81 (Bankwitz et al., 2010, Petracca et al., 2000). This CD81 and HCV E2 interaction results in the activation of the signal transduction which induces the lateral movement of CD81 and the HCV E2 complex towards the tight junction areas of the hepatocyte (Brazzoli et al., 2008), and subsequently results in an interaction with claudin-1 (CLDN1) (Evans et al., 2007, Harris et al., 2010). The interaction between CLDN1 and the CD81-bound HCV triggers clathrin-mediated endocytosis (Blanchard et al., 2006, Farquhar et al., 2012) which results in viral particle internalisation. Although OCLN is necessary for viral entry, its precise role remains unknown (Ploss et al., 2009, Sourisseau et al., 2013). Moreover, the cholesterol receptor Niemann-Pick C1-like 1 (NPC1L1) and transferrin 1 receptor have been reported to be essential co-factors for HCV entry, however the mechanism of these proteins are not yet understood (Sainz et al., 2012, Martin and Uprichard, 2013). Following internalisation, HCV particles are transported to Rab5a-

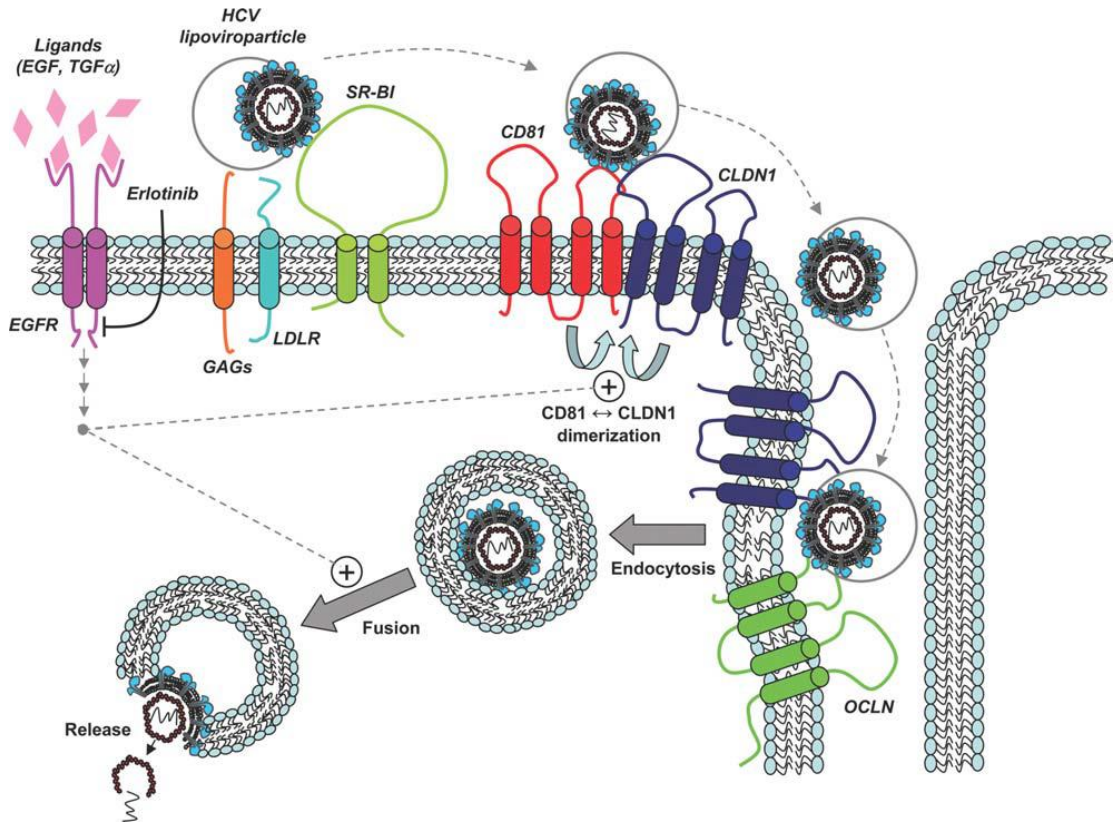

Figure 1.5: Schematic representation of HCV entry.

A set of essential host receptors including low-density lipoprotein receptor (LDL-R), glycosaminoglycans (GAGs), tetraspanin (CD81), scavenger receptor class B type I (SR-BI), claudin-1 (CLDN1) and occludin (OCLN) is required for HCV entry (McCartney et al., 2011).

containing early endosomes where the acidic pH inside induce the virus to uncoat (Coller et al., 2009, Farquhar et al., 2012) which results in the release of the viral genome into the cytosol to further undergo viral translation and replication processes (Niepmann, 2013).

HCV replication: Following entry, viral replication is initiated by translation of the single open reading frame from the positive sense RNA by host machinery using the HCV IRES. The single polyprotein is subsequently modified via post-translational process by host and viral proteases to produce the structural proteins (core, E1 and E2), a transmembrane protein p7 and non-structural proteins (NS2, NS3, NS4A, NS4B, NS5A and NS5B) (Sharma, 2010, Sklan et al., 2009, Moradpour et al., 2007). The membranous web which is the major site of viral RNA synthesis is then formed by the alteration of the cellular membrane, predominantly the endoplasmic reticulum (ER), which is driven primarily by the HCV non-structural protein NS4B, although other HCV non-structural proteins do play a role (Romero-Brey et al., 2012). The membranous web contains the HCV RC and is the site of HCV replication (Egger et al., 2002). The HCV RC comprises non-structural proteins, viral RNA and a number of cellular host factors (Gosert et al., 2003, Moradpour et al., 2003). Along with viral proteins, several host factors such as phosphatidylinositol 4-kinase III alpha (PI4IIIα), vesicle-associated membrane protein-associated protein A (VAP-A) and oxysterol-binding protein (OSBP) have been shown to contribute to the membranous web formation [reviewed in (Chukkapalli and Randall, 2014)]. The RNA dependent RNA polymerase, NS5B is responsible for the *de novo* synthesis of negative-strand RNA, which serves as the template for synthesising multiple copies of the HCV genome. The newly formed genomes are used for viral translation and

replication, and also utilised to form new virions through the association with core protein.

HCV assembly and egress: Following viral replication, the newly synthesised RNA is subsequently packaged into nucleocapsids to form the new virions. Although the precise mechanisms of HCV assembly and egress remain unclear, it is thought that the early steps of assembly of new virions occur on the cytosolic side of the ER membrane in close association with lipid droplets (LDs). The core protein is synthesised and matures at the ER membrane (Boulant et al., 2005) and subsequently migrates to the surface of LDs (Counihan et al., 2011) where RCs are recruited to this site via the interaction of core and NS5A associated with RCs (Miyanari et al., 2007, Masaki et al., 2008). The viral glycoproteins E1 and E2 are synthesised and translocated into the ER membrane (Duvet et al., 1998, Dubuisson et al., 1994), where the acquisition of a lipid envelope is required for the late stages of viral assembly. The immature virions subsequently undergo maturation through the cellular secretory pathway before releasing from the cell by exocytosis in a noncytolytic manner to complete the life cycle (Jones and McLauchlan, 2010, Bartenschlager et al., 2011, Popescu et al., 2011b, Lindenbach and Rice, 2013).

1.1.9 HCV model systems

Historically, studies of the molecular virology and viral pathogenesis of HCV were limited, due to the lack of a robust cell culture system that provided the complete viral life cycle. Furthermore, there was no small animal model system, with the chimpanzee being the only robust model to study HCV pathogenesis. A major breakthrough was

achieved in 1999 when the HCV subgenomic replicon system was developed (Lohmann et al., 1999), allowing autonomous replication of HCV RNA and expression of the non-structural proteins, although no progeny virions were produced due to the lack of structural proteins (Figure 1.6A). Variation to this replicon system subsequently emerged, including a full-length replicon and HCV replicons containing reporter constructs (Ikeda et al., 2002, Ikeda et al., 2005, Robinson et al., 2010, Beard et al., 1999). The HCV pseudo-particles (HCVpp) model (Figure 1.6B) which is a lentiviral or retroviral-based system was later generated and used for HCV entry studies (Bartosch et al., 2003, Hsu et al., 2003). In 2005, the infectious cell culture system (HCVcc) (Figure 1.6C) which enabled viral replication and the production of infectious virions, offered a complete viral life cycle in cell culture, and revolutionised *in vitro* HCV research (Lindenbach et al., 2005, Wakita et al., 2005, Zhong et al., 2005). In this study, we have utilised the HCV replicon and the infectious cell culture (HCVcc) systems, which will be described below.

1.1.9.1 HCV replicon systems

The HCV replicon system has been utilised extensively for the study of HCV replication, host-viral protein interactions, and for antiviral drug testing [reviewed in (Bartenschlager, 2002, Horscroft et al., 2005)]. The genomic (HCV structural and non-structural proteins) (Ikeda et al., 2002) and subgenomic (non-structural proteins) (Lohmann et al., 1999, Blight et al., 2000) replicons utilise the human hepatocellular cell line (Huh-7) for autonomous replication of the HCV genome under selective pressure (Figure 1.6A).

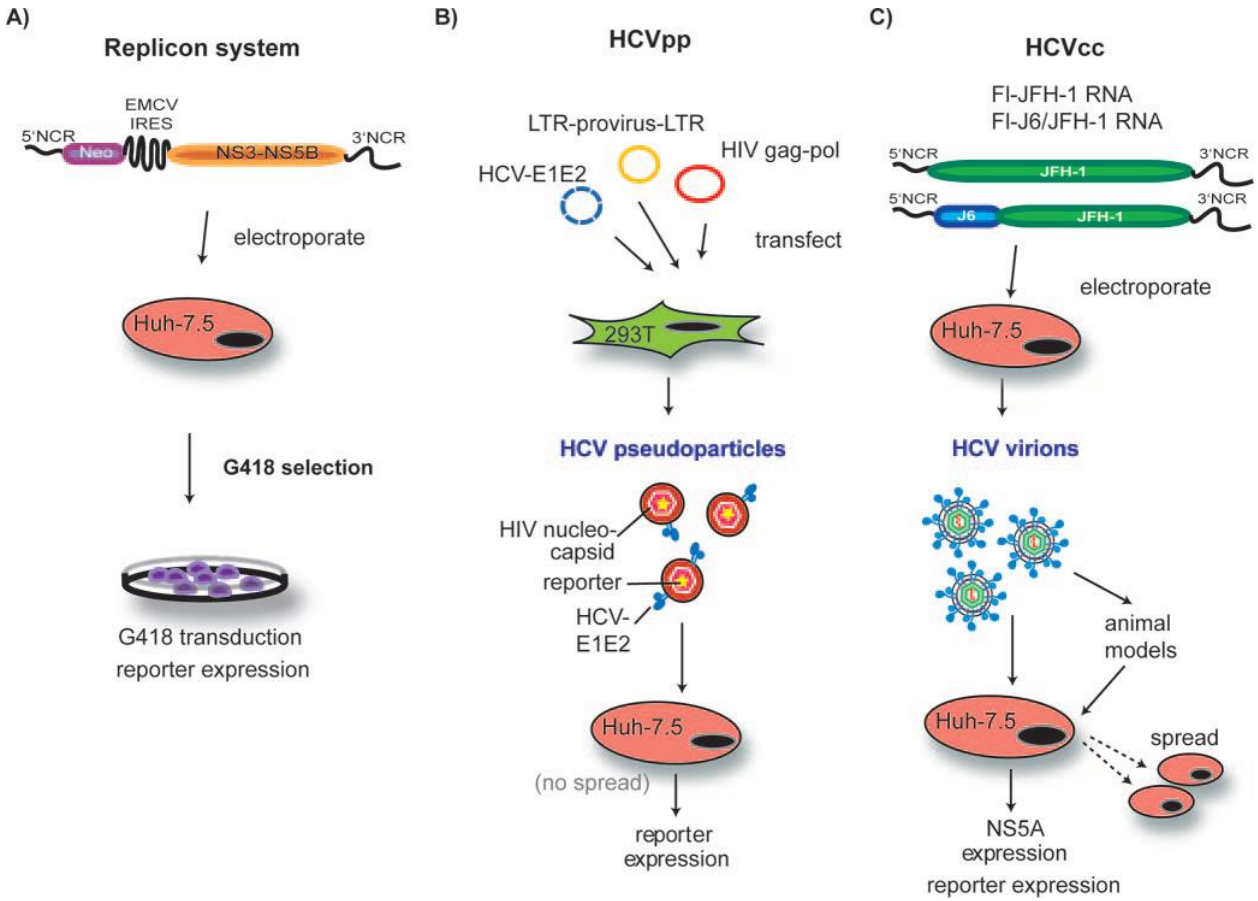

Figure 1.6: Schematic representation of cell culture-based HCV model.

Different systems for the study of HCV life cycle; **(A)** HCV replicon, **(B)** HCV pseudoparticles (HCVpp) and **(C)** HCV infectious cell culture (HCVcc) (Tellinghuisen et al., 2007).

Both the subgenomic and genomic replicons do not produce infectious HCV virions. The replicon systems are bicistronic and consist of two internal ribosomal entry sites (IRES). The HCV IRES in the first cistron controls the expression of a neomycin resistance gene, while the structural and non-structural proteins are under the control of an encephalomyocarditis virus (EMCV) IRES. Initially, HCV RNA is *in vitro* transcribed under the control of the T7 promoter and electroporated into Huh-7 cells and neomycin resistant clones are isolated and subsequently characterised to achieve efficient and autonomous HCV replication cell lines. The replicon systems do not allow for the complete study of HCV life cycle as they fail to produce infectious virus. These systems have been improved by the insertion of reporter genes such as fluorescent proteins and firefly luciferase which allow for high-throughput quantification of HCV replication, HCV live imaging (Schaller et al., 2007, Krieger et al., 2001, Ikeda et al., 2005).

1.1.9.2 Infectious cell culture model

A major development in understanding the HCV life cycle was generated in 2005 when a genotype 2a HCV cDNA isolated from a Japanese patient with fulminant hepatitis (JFH-1) was found to replicate efficiently and produce infectious viral particles in Huh-7 hepatocellular cell lines (Figure 1.6C). Infectious HCV particles in supernatants produced from cell culture-derived HCV JFH-1 (HCVcc) can be passaged *in vitro* on Huh-7 cells, as well as in animal models (chimpanzees and human liver chimeric mice) (Wakita et al., 2005, Zhong et al., 2005, Lindenbach et al., 2005, Lindenbach et al., 2006). HCV viral titres of this cell culture-derived HCV genotype 2a clone were initially low, however the viral titres were improved by the generation of chimeras of different genotypes such as

Jc1 (genotype 2a) (Pietschmann et al., 2006). This system provides the greatest advance in HCV research and has opened up the study of the full HCV life cycle. In addition, the HCVcc system has been improved by creation of luciferase and fluorescent protein-tagged viruses (Koutsoudakis et al., 2006, Schaller et al., 2007).

1.2. Innate immune response to viral infection

1.2.1 Overview

The innate immune response to pathogen infection is the first line of host defence to combat and eliminate pathogens including parasites, bacteria, fungus and viruses. This type of response is not specific to particular microorganisms and unlike the adaptive response, it does not provide a long-term host response, however it is rapid and required for the activation of the adaptive immune response. A series of conserved proteins or molecules of pathogens called "pathogen-associated molecular patterns, or PAMPs" are recognised by cellular receptors called "pattern recognition receptors or PRRs". PAMPs are conserved and shared by different pathogens such as proteoglycan, glycoproteins, lipopolysaccharide, and nucleic acids. PRRs are proteins expressed in a vast variety of different cell types and can be classified by their ligand specificity, function, and cellular localisation. The recognition of PAMPs and PRRs activates downstream signalling cascades which result in the production of immune products such as cytokines, chemokines and interferon. Induction of an antiviral immune response upon viral infection triggers the recognition of viral components by host PRRs and results in the activation of viral recognition pathways that ultimately induces the production of cytokines and interferon, particularly type I interferon (IFN-α and β) to limit viral

replication (Sen, 2001), and also induces type III IFN which is important in HCV infection [reviewed in (Bruening et al., 2017, Boisvert and Shoukry, 2016, Shin et al., 2016)].

1.2.2 Innate immune response to RNA virus infection

1.2.2.1 Cellular recognition of RNA viruses

The host innate immune response to RNA viral infection is initiated by the recognition of PAMPs by specific PRRs that can be broadly classified as cytoplasmic or membrane-bound PRRs. Toll-like receptors (TLRs) and RIG-I like receptors (RLRs) are the predominant PRRs in the detection of RNA virus infection. TLRs are membrane-bound receptors present on either the plasma membrane or in endosomes to sense the invading microorganism. The human TLRs consist of 10 members and among these receptors, the endosomal TLRs; TLR3, TLR7 and TLR8 have been shown to recognise nucleic acids of different types of RNA viruses (Table 1.1), whereas the endosomal TLR9 recognises unmethylated 2'-deoxyribo cytidine-phosphate-guanosine (CpG) DNA motif of bacterial and viral DNA (Hemmi et al., 2000). Additionally, TLR2 and TLR4 that are present on the cellular membrane have been reported to sense viral proteins such as HCV core and mouse mammary tumour virus (MMTV) or murine leukaemia virus envelope proteins (Dolganiuc et al., 2004, Rassa et al., 2002).

The TLR-independent mechanism of viral recognition, the RLR system, is an alternative pathway of virus sensing and plays a central role in the antiviral immune response (Yoneyama et al., 2004). RLRs are cytosolic proteins and are expressed in most

Table 1.1: Recognition of endosomal TLRs and RNA viruses

TLRs	Virus family	RNA virus	References
TLR3	*Flaviviridae*	Hepatitis C virus	(Li et al., 2005a)
		West Nile virus	(Daffis et al., 2008, Kawai and Akira, 2008, Wang et al., 2004)
	Picornaviridae	Coxsackievirus B3	(Negishi et al., 2008)
		Poliovirus	(Oshiumi et al., 2011)
		Rhinovirus	(Hewson et al., 2005)
	Reoviridae	Reovirus	(Kawai and Akira, 2008, Wang et al., 2004, Alexopoulou et al., 2001)
	*Pneumoviridae**	Respiratory syncytial virus	(Rudd et al., 2005)
	Orthomyxoviridae	Influenza A virus	(Guillot et al., 2005)
	Rhabdoviridae	Vesicular stomatitis virus	(Alexopoulou et al., 2001)
	Arenaviridae	Lymphocytic Choriomeningitis Virus (LCMV)	(Alexopoulou et al., 2001)
TLR7	*Orthomyxoviridae*	Influenza A virus	(Diebold et al., 2004, Lund et al., 2004)
	Flaviviridae	Hepatitis C virus	(Dolganiuc et al., 2006, Sato et al., 2007)
	*Pneumoviridae**	Respiratory syncytial virus	(Phipps et al., 2007)
	Rhabdoviridae	Vesicular stomatitis virus	(Lund et al., 2004)
	Retroviridae	Human immunodeficiency virus	(Beignon et al., 2005, Alter et al., 2007)
	Flaviviridae	Dengue virus	(Wang et al., 2006)
	Paramyxoviridae	Sendai virus	(Melchjorsen et al., 2005, Lee et al., 2007)
TLR7/8	*Retroviridae*	Human immunodeficiency virus	(Heil et al., 2004, Beignon et al., 2005, Alter et al., 2007)
	Flaviviridae	Hepatitis C virus	(Zhang et al., 2016)

* Taxonomy update, 2016 (Afonso et al., 2016).

mammalian cell types. RLRs belong to the family of aspartate-glutamate-any amino acid-aspartate/histidine (DExD/H)-box helicases and comprise of three classes: the retinoic acid-inducible gene I product (RIG-I), melanoma differentiation-associated antigen 5 (MDA5) and laboratory of genetics and physiology 2 (LGP2) (Kang et al., 2002, Yoneyama et al., 2004, Yoneyama et al., 2005, Yoneyama and Fujita, 2007). These three members of RLRs share a common structure including a central DExD/H box RNA helicase domain with an ATP-binding motif to hydrolyse ATP, and a C-terminal domain (CTD). RIG-I and MDA5, but not LGP2 also contain an N-terminal domain consisting of tandem caspase activation and recruitment domains (CARD) that is responsible for signalling (Figure 1.7) (Yoneyama et al., 2004, Yoneyama et al., 2005, Saito et al., 2007). RLRs are typically expressed at low levels in resting cells but are significantly increased upon viral infection and IFN stimulation (Kang et al., 2004, Yoneyama et al., 2004, Yoneyama et al., 2005, Imaizumi et al., 2005). In this chapter, we will focus on RLR signalling pathways upon viral infection.

1.2.2.1.1 Retinoic acid-inducible gene I (RIG-I)

RIG-I is a large protein (925 residues, 106 kDa) and highly conserved between vertebrates. Overexpression of RIG-I has been shown to limit replication of VSV and EMCV, and knockdown of RIG-I by siRNA reduces the production of type I IFN upon a variety of viral infections including Newcastle disease virus (NDV), Sendai virus (SeV) and EMCV (Yoneyama et al., 2004). Additionally, studies in RIG-I-deficient mice indicated that RLRs are essential for an innate immune response to viral infection in a

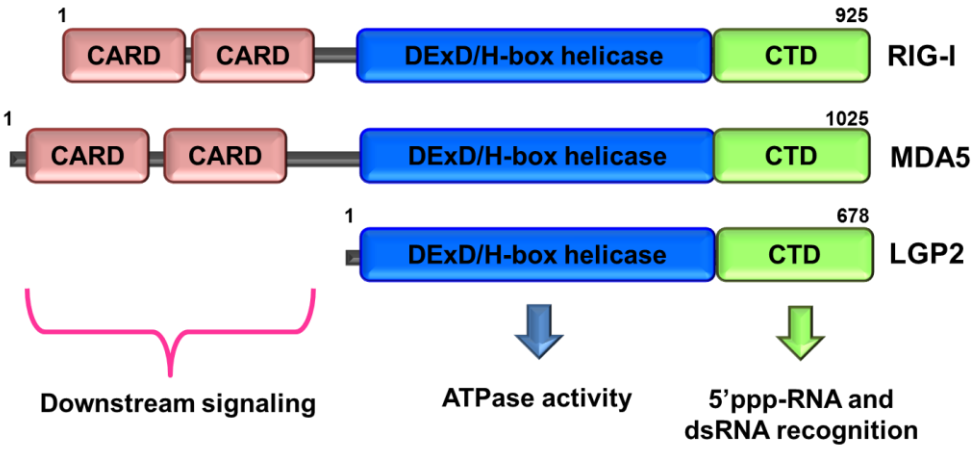

Figure 1.7: Schematic representation of the RLRs structural domains.

The three members of RLRs including RIG-I, MDA5 and LGP2 comprise the similar motifs of CARD domains (caspase activation and recruitment domain) which present on RIG-I and MDA5, but not in LGP2, a central DEAD box helicase and a C-terminal domain (CTD). Adapted from (Loo and Gale, 2011).

range of cell types, excepting plasmacytoid dendritic cells (pDCs) where TLRs preferentially sense RNA virus to stimulate an antiviral response (Kato et al., 2005). RIG-I is auto-repressed in the resting state to maintain low activity in the absence of RNA ligands. RIG-I senses short double-stranded RNA (dsRNA) or 5' triphosphate (5′ppp) uncapped ssRNA (Kato et al., 2006). Following binding to viral RNA components, RIG-I hydrolyses ATP to induce conformational change and subsequent releasing of CARD domains, allowing the interaction with the adaptor protein MAVS (Mitochondrial antiviral-signalling protein), to activate downstream signalling events that will be discussed in detail in subsequent sections (Kawai et al., 2005, Meylan et al., 2005, Jiang et al., 2011, Kowalinski et al., 2011).

1.2.2.1.2 Melanoma differentiation-associated antigen 5 (MDA5)

MDA5 displays the same overall domains as RIG-I and triggers signalling through CARD domains. MDA5 is essential to trigger the production of cytokine responses and crucial in the antiviral response. Overexpression of MDA5 increases type I IFN production and promotes antiviral activity against VSV and EMCV and knockdown of MDA5 gene has been shown to inhibit the type I IFN promoter (Yoneyama et al., 2005). Additionally, MDA5-deficient mice reduced type I IFN secretion in response to poly (I:C) stimulation and failed to develop an antiviral response against EMCV, which effectively escapes RIG-I sensing (Gitlin et al., 2006, Kato et al., 2006). A significant increase in morbidity and mortality and a reduction of an antiviral cytokine response were shown in $MDA5^{-/-}$ mice upon SeV infection (Gitlin et al., 2010). MDA5 has been shown to display an antiviral action itself or in cooperation with RIG-I against a number of viruses including West Nile virus (WNV) (Fredericksen et al., 2008b), rabies virus

(Faul et al., 2010), rotavirus (Sen et al., 2011), murine hepatitis virus (Roth-Cross et al., 2008) and murine norovirus 1 (McCartney et al., 2008). MDA5 typically recognises long dsRNA (at least 2 kb) (Kato et al., 2008), and initiates type I IFN production via CARD domains similar to RIG-I (Kang et al., 2002).

RIG-I and MDA5 do not respond to extracellular nucleic acid and have been shown to be essential in the activation of innate immune signalling against a board range of viruses. A list of RNA virus recognised by RIG-I and MDA5 are shown in Table 1.2.

1.2.2.1.3 Laboratory of genetics and physiology 2 (LGP2)

The third member of the RLRs, LGP2 is not well studied. LGP2 shares homology to RIG-I and MDA5, but lacks CARD domains and is thought to act as a negative regulator of RIG-I/MDA5 signalling. A study in LGP2-deficient cells has shown resistance to VSV infection and overexpression of LGP2 has been shown to inhibit SeV and NDV-induced ISRE activation (Venkataraman et al., 2007, Rothenfusser et al., 2005). In contrast, $LGP2^{-/-}$ mice exhibit impaired production of type I IFN in response to EMCV infection (Venkataraman et al., 2007). EMCV is specially sensed by MDA5, and this suggests a positive regulatory effect of LGP2 on MDA5.

1.2.2.2 RIG-I-like receptors (RLRs) downstream signalling cascade

The activation of RLR signalling is coordinated by several processes and requires the relevant adaptor molecules including Riplet, TRIM25, and MAVS to initiate signal transduction (Vazquez and Horner, 2015). The RIG-I signalling pathway is relatively

Table 1.2: Recognition of RLRs and RNA viruses.

RLR	Virus family	RNA virus	References
RIG-I	*Flaviviridae*	Hepatitis C virus	(Sumpter et al., 2005, Saito et al., 2007)
		West Nile virus	(Fredericksen et al., 2008b)
		Japanese encephalitis virus	(Kato et al., 2006)
		Dengue virus	(Loo et al., 2008)
	Arenaviridae	Lymphocytic Choriomeningitis Virus (LCMV)	(Zhou et al., 2010)
	Paramyxoviridae	Sendai virus	(Yoneyama et al., 2005, Kato et al., 2005)
		Newcastle disease virus	(Kato et al., 2005)
		Measles virus	(Plumet et al., 2007)
	*Pneumoviridae**	Respiratory syncytial virus	(Loo et al., 2008)
	Rhabdoviridae	Vesicular stomatitis virus	(Yoneyama et al., 2005, Kato et al., 2005)
		Rabies virus	(Faul et al., 2010)
	Orthomyxoviridae	Influenza A virus	(Kato et al., 2006)
	Reoviridae	Rotavirus	(Sen et al., 2011)
	Filoviridae	Ebola	(Cardenas et al., 2006)
	Bunyaviridae	Rift Valley fever virus (RVFV)	(Habjan et al., 2008)
		La Crosse virus (LACV)	(Habjan et al., 2008, Weber et al., 2013)
MDA5	*Flaviviridae*	Dengue virus	(Loo et al., 2008)
		West Nile virus	(Fredericksen et al., 2008b)
	Rhabdoviridae	Rabies virus	(Faul et al., 2010)
	Reoviridae	Rotavirus	(Sen et al., 2011)
	Paramyxoviridae	Sendai virus	(Gitlin et al., 2010)

* Taxonomy update, 2016 (Afonso et al., 2016).

well-characterised, while the mechanisms underlying MDA5 and LGP2 are not as well described. However, it is thought that sensing by both RIG-I and MDA5 activate the same signalling cascade which in turn induces the production of type I IFN and proinflammatory cytokine production (Yoneyama et al., 2005). In this chapter, we will focus on RIG-I downstream signalling that is depicted in Figure 1.8. RIG-I is present in the cytoplasm and is auto-inhibited and kept in a closed conformation in the resting state or in the absence of viral ligands. RIG-I is activated upon recognition with RNA ligands such as 5' di- or triphosphate dsRNA and undergoes the process of dephosphorylation and Lys (K) 63-polyubiquitination by the regulation of E3 ubiquitin ligase, Riplet and TRIM25. This results in conformational changes to open up the CARD domains and facilitates the association of RIG-I and the adaptor protein MAVS through a CARD-CARD domain interaction. This interaction induces the formation of the MAVS signalosome or innate immune synapse (Horner et al., 2011), which in turn activates the essential transcription factors in RLR signalling including interferon regulatory factor 3 (IRF3), IRF7 and NF-κB. IRF3/7 are phosphorylated through non-canonical IκB kinases IKKε or TBK1, while the activation of NF-κB requires the IKK complex (IKKα/β/γ). Phosphorylated IRF3 and IRF7 form homodimers and heterodimers which translocate to nucleus to activate the transcription of a specific set of genes involved in the innate antiviral response (Xu et al., 2005, Seth et al., 2005, Kawai et al., 2005, Meylan et al., 2005, Saha et al., 2006, Kumar et al., 2006). Activated IRF3/7 and NF-κB promote the transcription of proinflammatory cytokines and type I IFN, particularly IFN-β that can

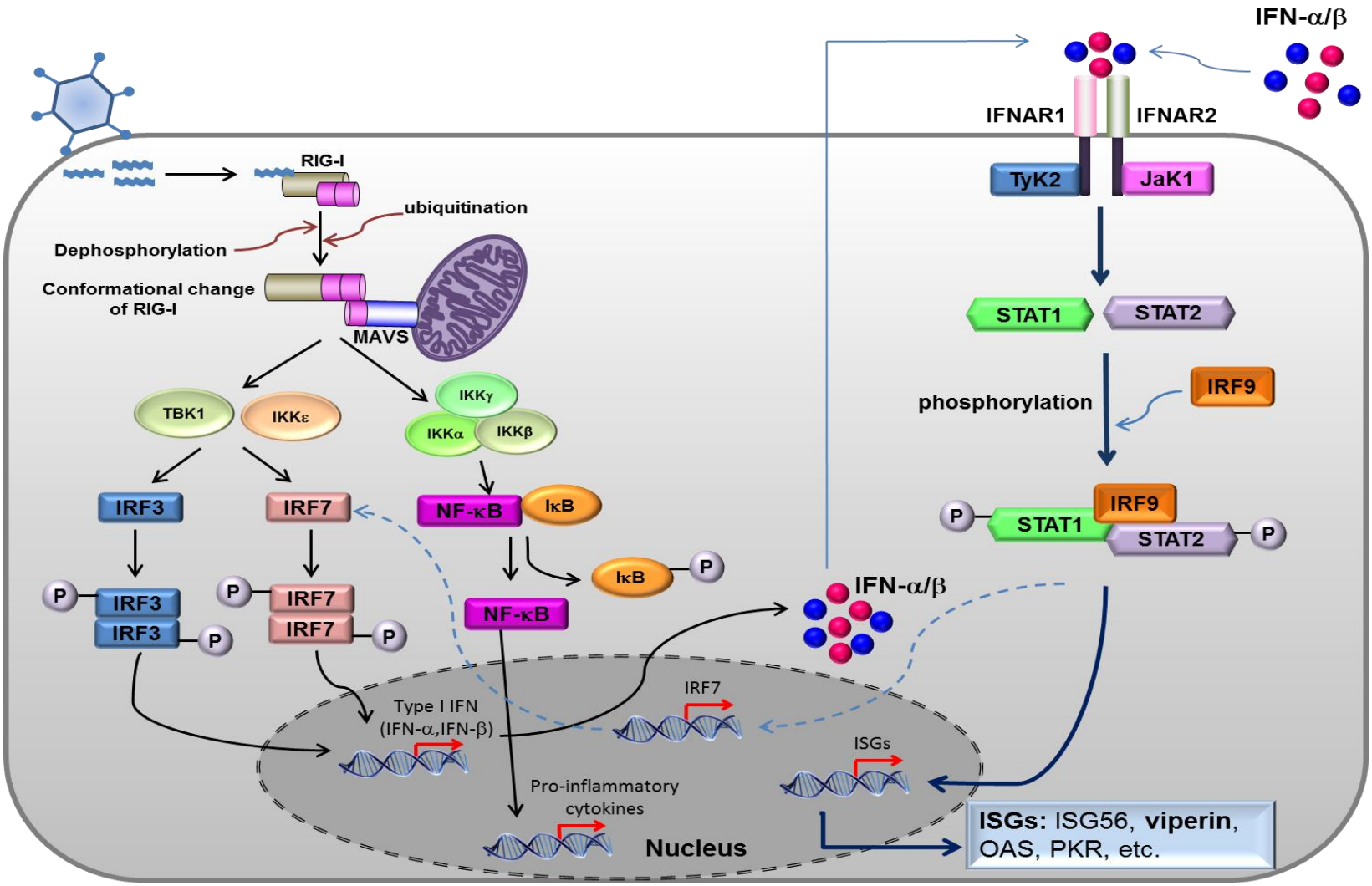

Figure 1.8: RIG-I downstream signalling pathway.

act in an autocrine and paracrine manner ultimately to induce the production of interferon-stimulated genes (ISGs). IRF3 is constitutively expressed in most cell types, whilst the expression of IRF7 is maintained at low level and is enhanced upon the production of IFN (Marie et al., 1998, Sato et al., 1998). Therefore, IRF3-dependent gene transcription is in many cases induced rapidly following RIG-I activation while IRF7 drives a delayed response.

Mitochondrial Antiviral-Signalling Protein (MAVS): MAVS is an adaptor protein that plays an essential role in the innate antiviral response. It is also called VISA (virus-induced signalling adapter), IPS-1 (IFN-β Promoter Stimulator 1) and Cardif (CARD Adaptor Inducing IFN-β). MAVS, a 540-amino-acid protein comprises a CARD domain at the N terminus, a proline-rich region, and a membrane-targeting transmembrane domain at the C-terminus for its localisation to various cellular compartments (Figure 1.9). Overexpression of MAVS increases the induction of type I IFN and ISGs, and knockdown of MAVS by siRNA inhibits this response upon VSV and NDV infection and in response to dsRNA stimulation (Kawai et al., 2005). Additionally, mouse embryonic fibroblasts (MEFs) from MAVS-deficient mice are susceptible to EMCV and VSV infection and have been shown to be severely impaired in the production of proinflammatory cytokines and type I IFN upon infection with a diverse RIG-I/MDA5-recognised RNA viruses. In contrast, MAVS was dispensable for type I IFN production following DNA virus infection (Kumar et al., 2006). This indicates a central role of MAVS in both RIG-I/MDA5-dependent signalling mechanism in response to infection with a variety of RNA viruses.

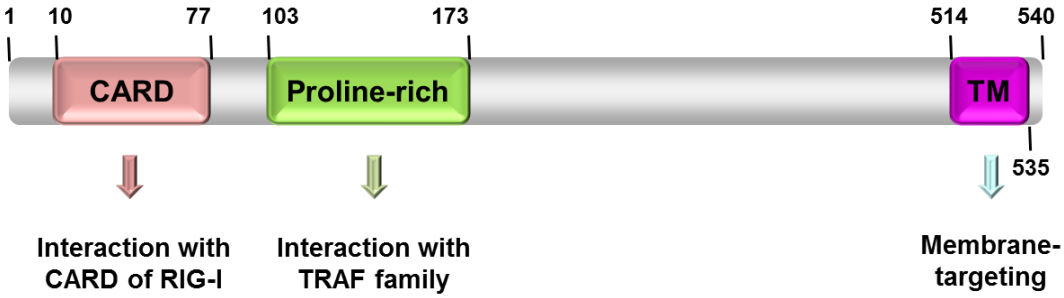

Figure 1.9: Schematic representation of MAVS structure.

MAVS (540 amino acids, 57 kDa) is composed of three distinct domains which are N-terminus CARD for interacting with CARD of RIG-I/MDA5, a proline-rich region containing TRAF-interacting motifs, and a transmembrane domain at C-terminus for outer membrane localisation at mitochondria, MAM and peroxisomes.

1.2.2.3 The interferon response to viral infection

Viral infection of mammalian cells results in the activation of viral recognition pathways triggered by replication intermediates and/or viral proteins (as described above) that ultimately induces an innate immune response to limit viral replication (Sen, 2001). Interferon (IFN), particularly type I interferon (IFN-α and β) is one of the essential components of innate immunity against the infection of the majority of viruses (DNA and RNA) including HCV infection. Interferons are glycoproteins and divided into three classes (I, II and III). Type I IFN was the first discovered family and composes of multiple members: IFN-α, IFN-β, IFN-ε, IFN-κ, IFN-δ, IFN-τ, and IFN-ω (Pestka et al., 2004, Perry et al., 2005, Sen, 2001, Sang et al., 2014). Type II IFN is composed of solely IFN-γ, while type III IFN family comprises IFN-λ1 (IL-29), IFN-λ2 (IL-28A), and IFN-λ3 (IL-28B) (Schneider et al., 2014, Pestka et al., 1987, Kotenko et al., 2003, Dornhoff et al., 2011). All IFNs share a common feature as antiviral agents, however type I IFNs are the most common type that are induced following viral infection; however type III IFN has also been shown to be critical in the innate antiviral response to HCV infection (Shin et al., 2016).

Type I IFN binds to its heterodimer receptor which is composed of IFN-α receptor 1 (IFNAR1) and IFNAR2 subunits, while type II IFN binds to an IFN-γ receptor complex (IFNGR) which consists of IFNGR1 and IFNGR2 subunits. Type III IFN signals through interleukin-10 receptor 2 (IL-10R2) and IFN-λ receptor 1 (IFNLR1). Binding of IFNs to their specific receptor triggers the expression of hundreds of interferon-stimulating genes (ISGs), many of which act to limit viral replication. The importance of this early IFN

response to viral infection is highlighted by the fact that most viruses have evolved strategies to combat either IFN production or IFN action (Katze et al., 2002). It was considered that a handful of ISGs was responsible for the direct antiviral process (i.e., MxA, PKR and 2,5-OAS) (Sen, 2001). However, it is now becoming apparent that many ISGs possess antiviral activity either directly or indirectly. The full repertoire of ISGs responsible for antiviral activity has not been revealed and the function of many ISGs remains to be clarified.

1.2.2.4 Interferon Transduction Pathway

Upon binding of IFNs to their specific receptors, there is activation of both the Janus kinase (JAK) and subsequently, signal transducer and activator of transcription (STAT) complexes (see Figure 1.8). Binding of both type I and III IFNs to their specific cell-surface receptors (IFNAR1/2 or IL-10R2/IFNLR1), initiates the activation of JAK family, specifically JAK1 and TYK2 (Silvennoinen et al., 1993). JAK1 and TYK2 undergo tyrosine phosphorylation on the intracellular domains of IFNAR and enable recruitment of the signal transducer and activator of transcription (STAT) 1 and STAT2. STAT1 and STAT2 are then phosphorylated at tyrosine residue 701 and 690 respectively. Phosphorylated STA1 and STAT2 dimerise and associate with interferon regulatory factor 9 (IRF9) to form the transcription factor complex, interferon-stimulated gene factor 3 (ISGF3). This ISGF3 multimeric molecule undergoes nuclear translocation and binds to the IFN-stimulated response element (ISRE) in the promoter to activate the transcription of hundreds of ISGs that display numerous biological functions, one of which is to control viral replication.

1.2.2.5 Interferon-stimulated genes (ISGs)

ISG expression, the product of stimulation of cells with IFNs, was first discovered more than 30 years ago (Knight and Korant, 1979) and since that initial report, more than 300 ISGs have been identified (de Veer et al., 2001). Originally it was thought that only a handful of ISGs existed, with classical ISG's such as PKR, OAS and Mx1, all displaying antiviral activity. However, mice and cells defective in one or more classical ISGs (PKR, OAS and Mx1) still retain antiviral function, suggesting the redundancy or the existence of several effectors that contribute to protection against viral infection (Zhou et al., 1999). It is increasingly clear that IFNs induce a diverse range of ISG expression upon viral infection and/or IFN stimulation. The ISG expression profile depends on cell type, type of viral infection, and dose/time point of IFN treatment. ISGs exert their antiviral functions at multiple stages of virus life cycle, however most ISGs remain to be characterised. Several ISG screening studies have aimed to identify antiviral ISGs and some of them have been well-characterised including the potent classical ISGs, PKR, Mx1, OAS and more recent discoveries such as ISG15, ISG20, ZAP, IFITM1-3, and viperin. A summary of antiviral ISGs has been reviewed in (Schoggins and Rice, 2011).

1.2.3 Innate immune recognition of HCV

1.2.3.1 Cellular recognition and downstream signalling events upon HCV infection

Like many +ve stranded RNA viruses, HCV infection of hepatocytes is recognised by RIG-I and endosomal TLRs, in particular TLR3. (Horner and Gale, 2013). RIG-I is the best-described PRR and is a key sensor for recognition of HCV RNA specifically 5' triphosphate (5'-ppp) RNA and the poly-U/UC region located within the 3' UTR (Saito et

al., 2008, Kato et al., 2008, Cui et al., 2008, Uzri and Gehrke, 2009). The RIG-I pathway is activated within hours after HCV infection and activation of RIG-I is sufficient to limit HCV replication (Loo et al., 2006, Sumpter et al., 2005).

Along with RLRs, HCV infection can be detected by TLRs. The endosomal TLR3 and TLR7 have been shown to induce a host anti-HCV response, although the precise mechanisms are not yet understood (Wang et al., 2009a, Li et al., 2012, Zhou et al., 2016, Zhang et al., 2009, Lee et al., 2006). TLR3 is highly expressed in primary hepatocytes derived from CHC patients, while there is no difference in the expression level of TLR2 and TLR7 between HCV-infected patients and controls (Tarantino et al., 2013). TLR3 activation has also been shown to block HCV replication (Wang et al., 2009a, Li et al., 2012), and this highlights the essential role of TLR3 in the host antiviral response against HCV infection. In addition to TLR3, TLR7 can recognise HCV RNA and induce the production of type I IFN in plasmacytoid dendritic cells (pDCs) (Takahashi et al., 2010). Recognition of HCV RNA by RIG-I and TLRs leads to the phosphorylation, dimerisation, and nuclear translocation of transcription factors IRF3/7 and NF-κB that culminate in the production of type I IFN and proinflammatory chemokines and cytokines.

1.2.3.2 ISGs targeting HCV

Prior to development of microarray technology, it was thought that only a handful of ISGs were expressed, however microarray studies of cells stimulated with IFN-α revealed that hundreds of genes are expressed following stimulation with IFN (de Veer et

al., 2001). Many of these ISGs have been shown to relate to antiviral activity and modulation of the immune responses, but others possess functions involved in lipid metabolism, apoptosis and protein degradation. A significant number of ISGs have been demonstrated to be upregulated in liver biopsies derived from acute or chronic HCV infection of chimpanzee or humans (Bigger et al., 2004, Sarasin-Filipowicz et al., 2008). Additionally, expression of 36 unique ISGs including IRF7, Mx1, OASL, OAS2, viperin and many ISGs with unknown function have been shown to increase in combination with a reduction in HCV viral titer (Brodsky et al., 2007). Collectively, this suggests that HCV infection can induce an innate antiviral response, however in many cases HCV can persist for reasons that are not completely understood.

Several discovery-based screens have been conducted in hepatoma cells to identify ISGs responsible for controlling HCV. A fluorescence-activated cell sorting (FACS)-based phenotypic screen was performed to determine the anti-HCV activity of 389 ISGs (Schoggins et al., 2011). In this approach, each ISG was inserted into the bicistronic lentiviral vector that also expressed the red fluorescent protein, TagRFP. Lentiviral transduction was used to express individual ISG and TagRFP following by challenging with HCV expressing a green fluorescent protein (GFP). A reduction of HCV reporter signal indicating the inhibition of viral replication within the ISG/TagRFP-positive cells was quantified using FACS. The strongest anti-HCV activity was observed in known key sensor and signalling molecules including RIG-I, MDA5, IRF1 and IRF7. Additionally, other ISGs (DDIT4, NT5C3, IFI44L, MAP3K14, IRF2, and OAS) were shown to impact HCV replication to a lesser degree. Given the fact that none of ISGs was sufficient to

inhibit HCV replication to a similar level as IFN-α stimulation, suggests that a single ISG is not responsible for control of HCV, but rather the combination of a number of ISGs.

In contrast to the ectopic study above, several groups have utilised RNA interference-based screens to identify ISGs. Using a whole-genome RNA interference-based screen, 93 genes were identified that mediate the suppression of HCV replication, and 23 of these genes were involved in mRNA processing and 9 genes involved in translation initiation (Zhao et al., 2012). The other group conducted an RNA interference (RNAi)-mediated gain-of-function screen and they identified several new genes including IFIT3, TRIM14, PLSCR1 and NOS2 that mediate anti-HCV activity. All of these ISGs identified in this study were induced by both IFN-α and IFN-γ, suggesting a substantial overlap of the effectors specific to HCV (Metz et al., 2012).

Several of these ISGs have been shown to play a role in the inhibition of HCV replication, i.e., the ISG 2'-5'-OAS has been shown to inhibit HCV replication through the RNase L pathway (Han and Barton, 2002). ISG6-16 can increase the anti-HCV activity of IFN-α (Zhu et al., 2003), while IFIT1 (also known as ISG56) has direct antiviral activity against HCV by suppressing of HCV IRES translation (Wang et al., 2003). Interestingly, enhanced expression of both ISG6-16 and ISG56 were observed in the liver biopsies from acute and chronic HCV-infected chimpanzees, suggesting that these ISGs may contribute to control HCV replication or spread (Su et al., 2002, Bigger et al., 2004). Additionally, PKR and the 3' to 5' exonuclease, ISG20, have been demonstrated to suppress HCV replication (Jiang et al., 2008, Zhou et al., 2011).

Moreover, viperin which belongs to the group of ISGs has been shown to be significantly expressed in HCV liver biopsies and has been reported to inhibit HCV replication via its interaction with non-structural protein 5A (NS5A) (Helbig et al., 2005, Helbig et al., 2011). The interferon-induced transmembrane (IFITM) family, in particular IFITM1-3 have been identified as important anti-HCV factors (Wilkins et al., 2013, Narayana et al., 2015). IFITM1 has been shown to impair HCV entry into hepatocytes by disturbing the binding of virus and host co-receptor, specifically CD81 and occludin (Wilkins et al., 2013), whilst IFITM2 and IFITM3 have recently been demonstrated to exert anti-HCV activity by interfering with the late stages of HCV entry, possible by directing the endocytosed HCV virion for degradation to the lysosome (Narayana et al., 2015). Although large-scale screens identified numerous ISGs that suppress HCV replication, the molecular mechanisms underlying the antiviral function remain to be characterised to expand our knowledge on the association of the host with HCV, and ultimately to improve antiviral therapy against HCV.

1.3. Viperin

Viperin, also known as RSAD2 (*r*adical *SA*M *d*omain-containing 2) and cig5 (cytomegalovirus inducible gene 5) was first identified in human cytomegalovirus (HCMV) infection of primary human fibroblasts, where two cDNA fragments termed cig5 and cig33 (cytomegalovirus inducible gene 5 and 33) were later found to form one transcript which was renamed as viperin (virus inhibitory protein, endoplasmic reticulum associated, interferon inducible) (Zhu et al., 1997, Chin and Cresswell, 2001).

1.3.1 Viperin protein structure and subcellular localisation

Human viperin is composed of 361 amino acids with a predicted molecular mass of approximately 42 kDa and belongs to the MoaA superfamily of radical S-adenosylmethionine (SAM) enzymes (Shaveta et al., 2010, Duschene and Broderick, 2010). It contains three distinct domains (Figure 1.10); 1) an N-terminal domain which varies between species and contains an amphipathic α-helix and a leucine zipper, 2) a highly conserved central domain that composes of three cysteine residues organized in a CxxxCxxC motif, and 3) a C-terminal domain that is highly conserved between species and has recently been shown to be an essential part of antiviral activity against a broad range of viruses. The N-terminal α-helix domain (residues 9-42) of viperin is responsible for anchoring within the endoplasmic reticulum (ER) membrane and is also associated with its ability to localise to lipid droplets (Hinson and Cresswell, 2009). The central domain (residues 71–182) contains motifs that are members of the 'Radical SAM' enzyme family, in which the CxxxCxxC motif is responsible for binding iron-sulfur clusters. The highly conserved C-terminal domain (residues 218-361) is important for the dimerisation of viperin and its role might be involved in protein-protein interactions and/or mediating an enzyme activity through substrate recognition. In addition, it has been reported that an aromatic amino acid residue at the C-terminus of viperin is required for its antiviral activity against HCV and DENV (Jiang et al., 2008, Helbig et al., 2011, Helbig et al., 2013).

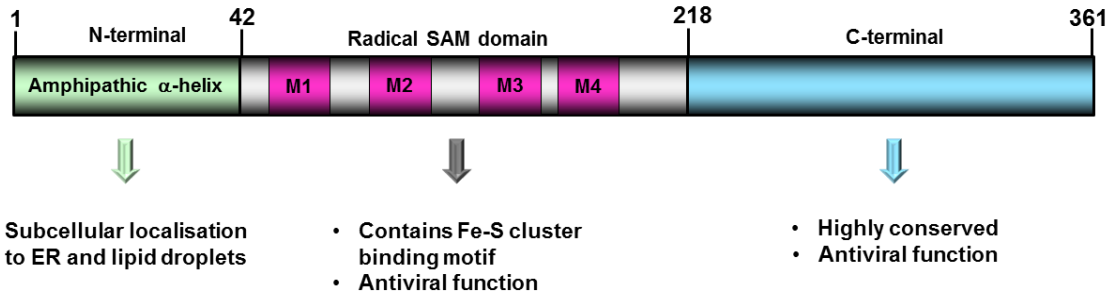

Figure 1.10: The structure of viperin.

Viperin composes of an N-terminal amphipathic α-helix for subcellular localisation, a number of conserved domains including the radical S-adenosyl methionine (SAM), a leucine zipper domain and a C-terminal region which has been reported as an antiviral activity domain against a broad of viruses.

1.3.2 Regulation of viperin expression

Viperin is induced in most cell types by type I IFN, type II IFN, type III IFN, double-stranded DNA, double-stranded RNA (dsRNA) analogues poly I:C, lipopolysaccharide (LPS) and infection with a number of viruses. Type I IFN (IFNα/β) is able to upregulate viperin expression in most cell types, whilst type II IFN (IFNγ) has shown to induce viperin expression in primary macrophages (Hinson et al., 2010). Expression of viperin is induced by the stimulants (mentioned above) through the classical IFN signalling pathways that activate the Jak/STAT pathway and culminates in the formation of the transcription factor complex ISGF3 (see section 2.4), which is able to bind the viperin promoter and induce its expression. Viperin expression has been shown to be regulated by ISGF3 complex, and counter-regulated by positive regulatory domain I-binding factor 1 (PRDI-BF1, also called BLIMP1) (Severa et al., 2006a). Promyelocytic leukaemia zinc finger (PLZF) has shown to be essential for the induction of a subset of antiviral ISGs including viperin. Additionally, PLZF-deficient mice defective in upregulation of the key antiviral ISGs and also viperin that are consequently more susceptible to viral infection (Xu et al., 2009).

A range of viruses including human cytomegalovirus (HCMV), vesicular stomatitis virus, Japanese encephalitis virus (JEV) and Chikungunya virus (CHIKV) can induce viperin independent of IFN production. (Chin and Cresswell, 2001, Boudinot et al., 2000, Chan et al., 2008, White et al., 2011). IFN-independent viperin expression is directly regulated by IRF1 or IRF3 (Grandvaux et al., 2002, DeFilippis et al., 2006, Stirnweiss et al., 2010). It is well-documented that MAVS is an essential adaptor protein that regulates the

production type I IFN and results in the transcription of ISGs. MAVS resides on mitochondria, MAM and recently has shown to localise on peroxisomes (Dixit et al., 2010). The peroxisomal MAVS activates IRF1 and IRF3 that results in the immediate and transient expression of a subset of ISGs including viperin, whilst the mitochondrial MAVS activates the induction of viperin and other IFNs that results in a stable antiviral effect (Dixit et al., 2010). Hence, IFN-mediated viperin expression is regulated by ISGF3 and PLZF, while IRF1 and IRF3 control IFN-independent viperin expression.

1.3.3 Antiviral functions of viperin

Viperin is expressed in a wide variety of species such as mammals and fish, and more recently has been found in reptiles (Milic et al., 2015). In addition, the expression of viperin is induced by a broad range of viruses, such as the *Flaviviridae* family; HCV (Helbig et al., 2005, Wang et al., 2012), Dengue virus (DENV) (Fink et al., 2007, Helbig et al., 2013), Japanese encephalitis virus (JEV) (Chan et al., 2008), West Nile virus (WNV) (Szretter et al., 2011), Tick-borne encephalitis virus (TBEV) (Upadhyay et al., 2014) and yellow fever virus (Khaiboullina et al., 2005); the *Togaviridae* family, Sindbis virus (SINV) (Chan et al., 2008, Zhang et al., 2007) and Chikungunya virus (CHIKV) (White et al., 2011); and others including Sendai virus (SeV) (Severa et al., 2006b), vesicular stomatitis virus (VSV) (Boudinot et al., 2000), pseudorabies virus (Boudinot et al., 2000), rhinovirus (Proud et al., 2008), lymphocytic choriomeningitis virus (LCMV) (Hinson et al., 2010), reovirus (Dixit et al., 2010), HIV (Nasr et al., 2012) and rabies virus (RABV) (Tang et al., 2016).

1.3.3.1 *In vitro* antiviral function

The antiviral effect of viperin was first demonstrated in HCMV infection. Constitutive expression of viperin in human fibroblasts significantly reduced the expression of proteins indispensable for HCMV maturation and assembly including gB, pp28 and pp65 (Chin and Cresswell, 2001). Subsequently, viperin has been shown to exert antiviral action against both DNA and RNA viruses (Chin and Cresswell, 2001, Helbig et al., 2005, Jiang et al., 2010, Wang et al., 2007, Upadhyay et al., 2014), however its mechanism is not fully understood. HeLa cells overexpressing viperin using a tetracycline-inducible system have been shown to block budding and release of influenza A virus by disrupting lipid rafts on the plasma membrane and increasing membrane fluidity (Wang et al., 2007, Tan et al., 2012). In this circumstance, viperin was found to bind and inhibit farnesyl diphosphate synthase (FPPS), a key enzyme involved in isoprenoid biosynthesis including cholesterol and sterol. Overexpression of FPPS reversed the effect of viperin on viral budding and restored normal membrane fluidity, however the precise mechanism by which viperin affects membrane fluidity and perturbs lipid rafts remains to be elucidated (Wang et al., 2007). Viperin was significantly upregulated by HIV-1 infection in monocyte-derived macrophages (MDMs) but is not induced in CD4+ T cells and monocyte-derived dendritic cells (MDDCs). Moreover, viperin overexpression in HEK293 cells directly inhibited HIV-1 production, and the radical SAM domain of viperin is responsible for this capability. Infection of HIV-1 in MDMs was also found to redistribute viperin to CD81 compartments, a marker for the site of HIV-1 assembly and egress. Interestingly, the addition of exogenous farnesol

significantly enhanced HIV-1 cDNA levels, indicating that viperin may interact with FPPS to inhibit HIV-1 viral egress (Nasr et al., 2012).

Viperin has been shown to inhibit a range of viruses in *Flaviviridae* family including HCV, DENV, WNV, and TBEV (Helbig et al., 2005, Jiang et al., 2008, Helbig et al., 2011, Jiang et al., 2010, Helbig et al., 2013, Szretter et al., 2011, Upadhyay et al., 2014). Expression of viperin in an inducible manner was shown to impede HCV replication in a HEK293 HCV replicon-based system. In this system, both of the radical SAM and the C-terminal domain were found to be important for anti-HCV activity (Jiang et al., 2008). Further work by our laboratory and other groups has demonstrated that the C-terminal domain of viperin is critical for limiting HCV replication in both an HCV replicon and infectious HCV culture system in hepatocyte cell lines, while the radical SAM domain was not required in this case. Additionally, viperin has been shown to interact with HCV NS5A and the proviral host factor, vesicle-associated membrane protein-associated protein A (VAP-A). It is postulated that viperin may impact the NS5A and VAP-A interaction within HCV RC to target a critical step for HCV replication (Helbig et al., 2011, Wang et al., 2012). Viperin has recently shown to inhibit DENV-2 in several cell types including Huh-7, A549 and primary human MDMs. In this instance, a C-terminal domain of viperin has shown once again to be crucial for anti-DENV-2 through the interaction with DENV2 NS3 protein, while the N-terminal amphipathic helix and the radical SAM domain is dispensable for this antiviral activity (Helbig et al., 2013). More recently, viperin was shown to exhibit a strong activity towards TBEV via its radical SAM domain. In addition, the C-terminal region of viperin has been shown to interact with CIAO1, a key component of the cytosolic iron-sulfur protein assembly (CIA)

machinery and this interaction is important for viperin stability and Fe-S cluster formation (Upadhyay et al., 2014). Thus, the radical SAM domain is indispensable for antiviral activity against TBEV, while the C-terminal domain is an indirect requirement for this response. Most recently, we have shown that ectopic expression of viperin significantly impaired Zika virus (ZIKV) replication and once again the C-terminal domain of viperin is required for this anti-ZIKV activity (Van der Hoek et al., 2017). In addition, ZIKV replication increased in mouse embryonic fibroblast cells (MEFs) isolated from CRISPR/Cas9 derived viperin null mice, reinforcing its antiviral role against ZIKV infection. Viperin is able to inhibit the replication of multiple viruses from the *Flaviviridae* family. The evidence to date suggesting that its antiviral function is achieved through different domains of the protein, however the C-terminal domain is crucial in mediating this action.

1.3.3.2 *In vivo* antiviral function

In vivo experiments have shown that viperin is able to restrict both WNV and CHIKV infection in a mouse model. WNV infected viperin knockout (KO) mice show increased lethality and enhanced viral replication in the CNS (Szretter et al., 2011), while CHIKV infected viperin KO mice show increased viral replication and joint pathology (Teng et al., 2012). In the case of influenza virus (IFV), there was no difference in the susceptibility of IFV infection, pulmonary damage and IFV titres between wild type (WT) and viperin KO mice (Tan et al., 2012). This result is in contrast to the study using ectopic viperin in an influenza culture system. This discrepancy may be owing to

redundancy of ISGs in innate immune response, and the production of other ISGs that can compensate for the effect of lacking viperin.

1.3.4 Evade and co-opt of viperin by viruses

It is increasingly clear that viperin is able to combat diverse viral infections, however this effect drives the evolution of the virus to evade or counteract the host immune response. JEV has been shown to circumvent the antiviral function of viperin (Chan et al., 2008), while HCMV utilises viperin to enhance infectivity (Seo et al., 2011). Overexpression of viperin or depletion of viperin by RNAi did not influence JEV replication. This is in direct contrast to the effect on other flaviviruses such as HCV, DENV and WNV. In addition, viperin has been shown to be degraded in JEV-infected cells through a proteasome-dependent mechanism suggesting that JEV evades the antiviral effect of viperin by negative regulation of viperin expression, however the mechanism of this degradation is unknown (Chan et al., 2008). To date, only one virus, HCMV has been shown to co-opt viperin to enhance viral infectivity. Previous studies have shown that viperin is induced in human fibroblasts following HCMV infection, in addition, 3 days post-infection, viperin redistributed from its normal localisation on the ER to Golgi apparatus and then to cytoplasmic vesicles containing the viral proteins, gB and pp28. (Chin and Cresswell, 2001). Further studies have shown that HCMV replication is impaired in shRNA mediated viperin knockdown cells. In this work, they found that HCMV infection transferred viperin to the mitochondria before transporting it to the Golgi and the HCMV assembly compartments. The interaction of viperin and HCMV viral protein, vMIA results in the relocation of viperin to the mitochondria, where it then

binds to the β subunit of the mitochondrial trifunctional protein (TFP), a protein that facilitates β-oxidation of fatty acids to generate adenosine triphosphate (ATP). This interaction inhibits TFP and subsequently results in a decrease of ATP levels which leads to a major disruption of the actin cytoskeleton that required for viral infection. Interestingly, replacing of the N-terminal amphipathic helix of viperin with a mitochondrial localisation sequence, either from vMIA or a host cellular mitochondrial protein, Tom70 had a similar effect, indicating the direct role of viperin in mediating actin cytoskeleton disruption independently of vMIA. Moreover, Fe-S binding cluster of the radical SAM domain has shown to be necessary for this effect but it is not required for binding to TFP (Seo et al., 2011).

Additionally, we have recently shown that overexpression of viperin is able to inhibit ZIKV replication, however ZIKV infection was found to attenuate the expression of a panel of ISGs, including viperin, IFIT1, IFITM1, ISG15, OAS1 and Mx1 in Huh-7 cells, placental (HTR8/SVNeo and JEG3) and neural progenitor derived cells (NPCs). This suggests that ZIKV perhaps evade the host innate immune response by impairing the ISG expression profile (Van der Hoek et al., 2017), and most likely through binding of ZIKV NS5 protein to STAT2 and prevention of downstream signalling (Kumar et al., 2016, Grant et al., 2016). The diversity of viperin activity as both anti- and pro-viral protein has been shown in Figure 1.11 (Helbig and Beard, 2014).

1.3.5 Roles of viperin in immune signalling

It is increasing clear that viperin exerts an antiviral response towards a number of viruses,

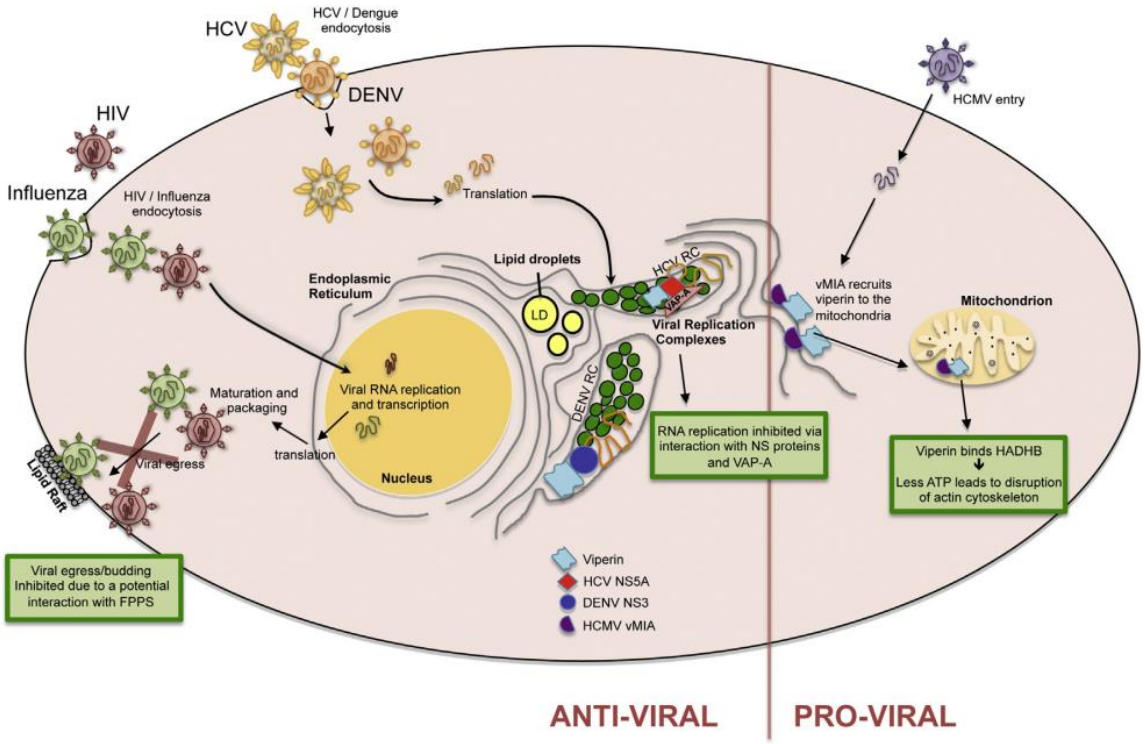

Figure 1.11: Viperin exerts a role in both antiviral and proviral host protein.

(Helbig and Beard, 2014)

however there is emerging evidence that viperin acts as a mediator in the immune signalling pathways. This role has been observed in viperin knockout mice (viperin$^{-/-}$) that were healthy and exhibited no obvious phenotypic change. Challenging of these knockout mice with ovalbumin (OVA) that induces a mixed of Th1 and Th2 response resulted in a significant decrease in OVA-specific IgG1, suggesting that viperin may possibly regulate the Th2 response (Qiu et al., 2009). This study has also shown that stimulation of CD4+ T cells derived from viperin$^{-/-}$ mice with anti-CD3 resulted in a significant reduction of Th2 cytokine expression (IL-4, IL-5 and IL-13), in association with a defect in the GATA-3 induction and a decrease of DNA binding activities of NF-κB and AP-1. This data suggests that viperin is involved in the adaptive immune response by promoting T-cell activation and differentiation.

Further work has demonstrated that pDCs derived from viperin-deficient mice show a defect in the production of type I IFN in response to TLR7/9 stimulation, suggesting the ability of viperin to modulate TLR7 and TLR9 signalling in pDCs to promote the production of type I IFN (Saitoh et al., 2011). The N-terminal amphipathic helix domain of viperin that targets to lipid droplet appeared to be responsible for this effect. In addition, viperin was found to interact and recruit the signalling adaptor proteins IRAK1 and TRAF6 to lipid droplets to facilitate ubiquitination of IRAK1, which in turn induces the nuclear translocation of IRF7 to stimulate the expression of type I IFN. Furthermore, it has recently been shown that siRNA-mediated knockdown of viperin in carcinoma cell lines (EJ) partially attenuated the CD40L-mediated upregulation of IFN-β and abrogated the recruitment of IRF7 to the nucleus resulting in a reduction of IFN-β production

(Moschonas et al., 2012). Taken together, it is becoming clear that viperin is able to orchestrate various aspects of innate immune signalling that may ultimately contribute to the antiviral response.

In contrast to the previous reports, recent work has shown that viperin and MAVS co-localised to the MAM that resulted in inhibition of the MAVS-dependent signalling pathway. It was revealed that bone marrow macrophages (BMM) derived from viperin KO mice could significantly increase their production of IFN-β in response to poly I:C stimulation. In addition, co-expression of viperin and MAVS reduced the expression of IFN-β in 293 cells when compared to MAVS expression alone, indicating that viperin negatively regulate MAVS-dependent signalling mechanism (Hee and Cresswell, 2017). The author explained that this conflicting result may be a result of the cell types used in this experiment.

The fact that viperin displays multiple biological functions including antiviral activity against both RNA and DNA viruses and has a role in innate immune signalling, along with the diversity of its capabilities as both an anti- and pro-viral protein, suggests that viperin is a critical protein in the host response to viral infection. These functions are most likely regulated by viperin ability to bind host and viral proteins. To date, viperin has been shown to interact with 6 host proteins (FPPS, TFP, IRAK1, VAP-A, TRAF6, MAVS and CIAO1) (Wang et al., 2007, Seo et al., 2011, Saitoh et al., 2011, Helbig et al., 2011, Wang et al., 2012, Hee and Cresswell, 2017, Upadhyay et al., 2014) and 3 viral proteins (HCV NS5A, DENV NS3, HCMV vMIA) (Helbig et al., 2011, Wang et al., 2012, Helbig et al., 2013, Seo et al., 2011). However, these viperin interactors do not

explain its diverse function and is likely that novel interacting partners remain to be discovered and characterised. This represents a major gap in our understanding of the biology and molecular mechanism of this important ISG viperin that mediates pro-/anti-viral responses or facilitates innate immune signalling, and will be a major topic of this thesis.

1.4 Peroxisomes and the antiviral response

1.4.1 Peroxisomes and their functions

Peroxisomes are essential dynamic and multifunctional organelles found in eukaryotic cells including yeast, plants, and mammals. They are a single membrane organelle with size ranging from 0.1-1.0 μm diameter. They are normally spherical but can change in their size, number, and shape depending on cell types and environment (Grabenbauer et al., 2000, Schrader et al., 2013). They contain catalase and oxidase enzymes that are indispensable for cell metabolism and also comprise at least 50 other enzymes depending on the cell type and organism (Wanders and Waterham, 2006). The metabolic function of peroxisomes is generally involved in lipid metabolisms such as biosynthesis of either phospholipids (plasmalogens), cholesterol, bile acids, and catabolism or decomposition of amino acid, fatty acids, hydrogen peroxide (H_2O_2) (Table 1.3) (Smith and Aitchison, 2013, Titorenko and Rachubinski, 2001). In addition, peroxisomes morphologically interact and communicate with other subcellular compartments such as ER, mitochondria and lipid droplets, although the precise role of how these organelles communicate and interact is poorly understood (Grabenbauer et al., 2000, Schrader, 2006, Beller et al., 2010).

Table 1.3: Metabolic functions of peroxisomes*.

Biosynthesis
Bile acids and cholesterol
Hormonal signalling molecules
Polyunsaturated fatty acids
Ether phospholipids (plasmalogens)
Pyrimidines
Purines
Degradation
Amino acids
Prostaglandin
Purine
Polyamine
Decomposition of H_2O_2 by catalase
α- and β-Oxidation of fatty acids
Superoxide radical destruction by superoxide dismutase
Other
Being as a platform in innate antiviral response

* Adapted from (Smith and Aitchison, 2013)

Peroxisomes require a set of proteins, called the peroxins that are encoded by the *PEX* gene in their formation and maintenance (Hettema et al., 1999, Smith and Aitchison, 2013). Peroxisomes can be formed through two mechanisms which are i) *de novo* generation in which pre-peroxisomal vesicles are derived from the ER and ii) growth and division (fission) (Figure 1.12). In *de novo* biogenesis, the ER contributes to the formation of pre-peroxisomes whereby peroxisomal membrane proteins (PMPs) are inserted into the ER membrane to form a new peroxisome, while the growth and division mechanism is responsible for the expansion of a number of peroxisomes. In this pathway, pre-existing peroxisomes undergo elongation, constriction, fission to produce daughter peroxisomes and subsequently growth and maturation to generate new peroxisomes.

1.4.2 Peroxisomes and RLR signalling

For many years the peroxisome was thought to only have a role in metabolic functions of the cell. However, most recently it is now emerging that peroxisomes are a platform for innate immune signalling. Several mitochondrial proteins such as Fis1 and Mff have been found to exist on peroxisomes, and more interestingly MAVS is similar in structure to these proteins. This led to a seminal study in which MAVS has been shown to reside on peroxisomes in addition to the mitochondria, and promote innate antiviral response from this organelle (Dixit et al., 2010). In this study, specific engineered localisation of MAVS to peroxisomes, mitochondria or the cytoplasm revealed that peroxisomal MAVS activated the immediate and transient IFN-independent signalling pathway to induce the expression of ISGs, while mitochondrial MAVS triggered a delayed IFN-dependent signalling pathway. Interestingly, a further study has shown that peroxisomes serve as a

De novo biogenesis

Growth and division

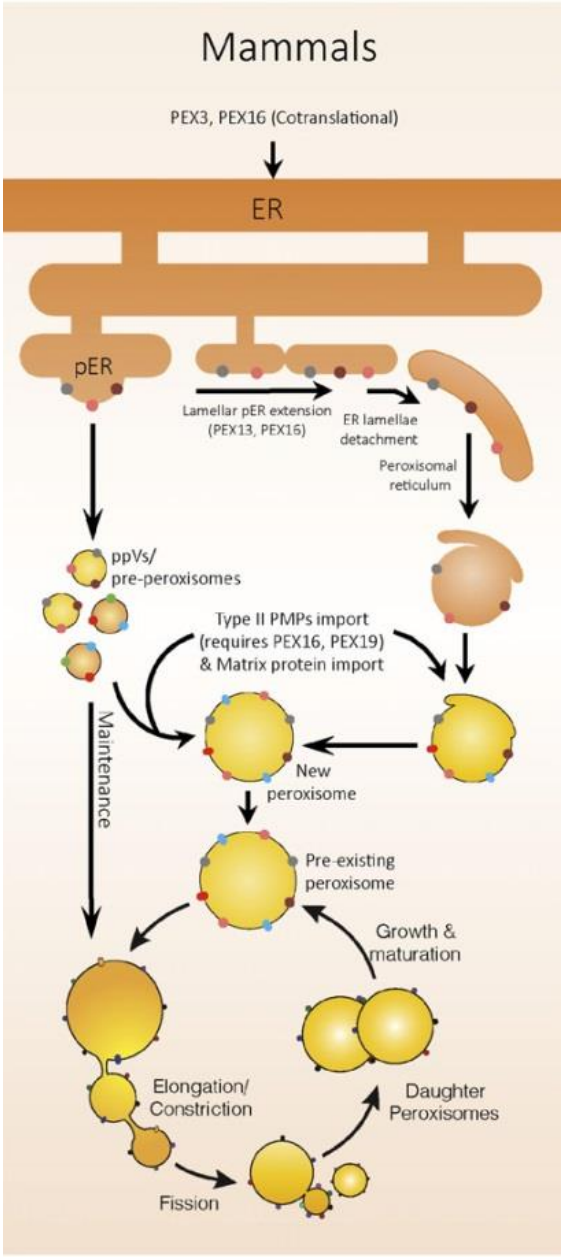

Figure 1.12: Two pathways of peroxisome biogenesis in mammals.

(Agrawal and Subramani, 2016)

primary site for induction of type III IFN (Odendall et al., 2014). This work has demonstrated that RLR signalling is able to induce the expression of type III IFNs (IFN-λ) upon sensing of RLR by a diverse range of pathogens including reovirus, Sendai virus (SeV), and Dengue virus (DENV), as well as the pathogenic bacteria, *Listeria monocytogenes* (Odendall et al., 2014). In addition, peroxisomal MAVS is required for the expression of IFN-λ1, but not IFN-β, whilst wild type and mitochondrial MAVS induced both types of IFNs upon SeV and DENV infection. Moreover, neutralisation of IFNλR following reovirus infection in T84 intestinal epithelial cells resulted in a strong reduction of the ISGs viperin and IFIT1, suggesting the role of type III IFNs in controlling the antiviral ISGs expression even in the presence of type I IFNs. Furthermore, disruption of mitochondrial function in primary human keratinocytes by treatment with protonophore carbonyl cyanide m-chlorophenylhyddrazone (CCCP) that does not impact peroxisome function resulted in the inhibition the production of IFN-β, while the expression of IFN-λ1 and viperin was enhanced, indicating that the RLR signalling pathway remain activate even in cells lacking mitochondrial function, and likely selectively induces from peroxisomes (Odendall et al., 2014). However, more recent work has shown that peroxisomal MAVS is able to activate the expression of both type I and III IFNs with the comparable level to mitochondrial MAVS following infection with various RNA viruses (Bender et al., 2015). Taken together, these observations indicate that peroxisomes act as a platform for the innate antiviral response. However, There is some controversy regarding the temporal and IFN-type induced via peroxisomal MAVS, with one report suggesting peroxisomal MAVS is activated early and induces IFN-independent gene expression while another suggests both IFN-α/β and

IFN-λ and equally expressed from peroxisomal MAVS. This discrepancy is most likely due to the different MAVS constructs and the sensitivity of assays that were used to measure type I IFN (Dixit et al., 2010, Odendall et al., 2014, Bender et al., 2015).

1.4.3 Peroxisome evasion by viruses

A number of viruses including HCMV, DENV, and WNV attempt to evade peroxisome-mediated antiviral responses, by inducing the degradation and fragmentation of the peroxisome (You et al., 2015, Magalhaes et al., 2016). This is further confirmation that the peroxisome plays a role in innate signalling. Flavivirus infection with DENV and WNV has been shown to mediate the degradation of peroxisomes in A549 cells that results in a decrease in peroxisome number and in catalase enzyme activity (You et al., 2015). In addition, the viral capsid protein of DENV and WNV was found to interact with peroxisomal membrane protein, PEX19, indicating that sequestration or degradation of peroxisomes may arise from the direct interaction of viral capsid and PEX19 (You et al., 2015). More recently, the HCMV vMIA protein (mitochondria-localized inhibitor of apoptosis) was found to reside on peroxisomes and induce their fragmentation. In addition, a reduction of IRF1 and viperin was found in the presence of vMIA, suggesting that vMIA disrupts the peroxisomal MAVS antiviral signalling. vMIA has also been shown to interact with PEX19 and specifically bind to peroxisomal MAVS, suggesting that the strategy of HCMV is to evade innate antiviral response by highjacking the peroxisomal membrane proteins (Magalhaes et al., 2016). Collectively, this confirms that the peroxisome is a significant organelle in innate immune signalling, however our understanding of the molecular and cellular details of this role is not fully understood.

1.5. Hypothesis and Aims

The overall aim of this thesis is to determine the anti-HCV mechanism of viperin at the cellular level. The first objective was to define how viperin displays anti-HCV activity and investigate how viperin interacts with or alters the HCV membranous web at the ultrastructural level. Viperin interacts with a number of cellular and viral proteins, however this interaction does not explain the diverse nature of viperin function. Subsequent aims were therefore focused on the identification and characterisation of novel viperin cellular interacting partners in the hope of defining the antiviral or innate immune modulatory function of viperin.

Hypothesis – Viperin localises to the HCV RC to impact HCV replication and furthermore novel viperin interacting partners remain to be discovered that will define the function of this multifunctional protein.

We specifically aim to:

1. Determine the anti-HCV mechanism of viperin at the level of the HCV RC.
2. Identify novel cellular interacting partners of viperin using a yeast two-hybrid system.
3. Characterise the novel interacting partners identified above to further define the role of viperin.

Chapter 2

Materials and methods

2.1 General Molecular Methods

2.1.1 Synthetic oligonucleotides (primers)

Synthetic oligonucleotides/primers in lyophilised form were ordered from GeneWorks at PCR/sequencing purity grade (see primer sequences in Appendix I). Stock of oligonucleotides was prepared by resuspending in MilliQ water to make up to a concentration of 20 μM. All oligonucleotides were stored at -20°C. The volume of MilliQ water to make up a 20 μM of stock oligonucleotides was determined using the following formula:

Volume of MilliQ water (ml) = number of nmoles of oligonucleotides/20

2.1.2 Bacterial transformation

The frozen α-Select Chemically Competent *E. coli* cells were purchased from Bioline™ for bacterial transformation. Competent cells were thawed on ice and 50 μl aliquots were placed in a pre-chilled microcentrifuge tube. Approximately 5-10 ng of plasmid DNA or 5 μl of ligation product was added to the cell suspension and the tube was gently mixed by tapping and incubated on ice for 30 min. The mixture was then heat shocked at 42°C for 45 sec and immediately placed on ice for 2 min. Then, 950 μl of SOC medium (see Appendix II) was added to the transformation reaction and incubated at 37°C with shaking at 200 rpm for 1 hr. To transform the ligation reaction, cells were centrifuged down to a pellet at 5000 × *g* for 5 min, 900 μl of SOC medium was discarded and pellets

were resuspended in the remaining SOC medium. The suspension was spread on LB-agar containing an appropriate antibiotic and incubated at 37°C overnight. For transformation of the plasmid DNA, 50-100 µl of the transformation reaction were plated on LB-agar containing an appropriate antibiotic and the plate was incubated at 37°C overnight.

2.1.3 Small scale plasmid DNA extraction (Mini-preparation)

A single transformed bacterial colony was inoculated into 5 ml of LB broth containing appropriate antibiotic and incubated with shaking at 200-250 rpm at 37°C overnight. The bacterial culture was pelleted by centrifugation at 5,000 × *g* for 5 min and supernatant was discarded. Plasmid DNA extraction was performed using a QIAprep Spin Miniprep Kit (Qiagen) as per manufacturer's instructions. In brief, cell pellets were resuspended in 250 µl of buffer P1 containing ribonuclease A (*RNase*A). 250 µl of buffer P2 was added and the preparation was gently mixed by inverting the tube. Then, 350 µl of buffer N3 was added and the mixture was centrifuged at 12,000 × *g* for 5 min. The supernatant was collected and put in the mini spin column and subsequently centrifuged at 12,000 × *g* for 5 min. The column was washed with 750 µl of PE buffer and then placed into the new collection tube. EB buffer (30-50 µl) was added the column and the column/tube was centrifuged for 1 min to elute the plasmid DNA.

2.1.4 Large scale plasmid DNA extraction (Maxi-preparation)

A single transformed bacterial colony was inoculated into 200 ml of LB broth containing appropriate antibiotic. The culture was incubated with shaking at 37°C overnight. The bacterial culture was pelleted by centrifugation at 5,000 × *g* for 15 min using an

AvantiTM J-25I Beckman Coulter centrifuge (JA10 rotor). Plasmid DNA extraction was performed using a NucleoBond® Xtra Maxi kit (Macherey-Nagel) as per manufacturer's instructions. In brief, cell pellets were resuspended in 12 ml of RES buffer containing ribonuclease A (*RNase*A). 12 ml of LYS buffer was added and the preparation was gently mixed by inverting the tube and incubated at room temperature (RT) for 5 min. Then, 12 ml of NEU buffer was added to the mixture and mixed by inverting 10-15 times before transferring to a pre-equilibrated NucleoBond Xtra column with filter. 15 ml of EQU buffer was added to the column with filter. The filter was then discarded and the column was washed with 25 ml of WASH buffer. Plasmid DNA was eluted with 15 ml of ELU buffer and subsequently precipitated with 10.5 ml of isopropanol. The precipitated plasmid DNA was pelleted by centrifugation at 15,000 × *g*, 4°C for 30 min using an AvantiTM J-25I Beckman Coulter centrifuge (JA25.50 rotor). The pellet was washed with 70% ethanol and resuspended with an appropriate volume of EB buffer.

2.1.5 Restriction endonuclease digestion

Restriction enzymes were obtained from New England Biolabs® Inc (NEB). Restriction enzyme digestions were performed in a 20 µl total volume, which contained 1 µg of plasmid DNA or 5 µl of ligation reaction (see section 2.1.7), 10 Units of restriction enzyme(s) and 1× appropriate NEBuffer. The digestion reactions were incubated at 37°C for 1-2 hr. The units of enzyme and appropriate buffer were provided on the NEB website. The digestion reaction was then visualised on a 1% agarose gel.

2.1.6 Agarose gel electrophoresis

Agarose gel electrophoresis was performed using 1-2% w/v agarose gel. The gels were prepared by dissolving molecular grade agarose (AppliChem) in 1× TAE buffer (see Appendix II). Gels were cast in a BioRad® Sub-Cell GT Minitank. DNA samples were mixed with 6× Loading dye (New England Biolabs) and loaded into wells on the agarose gel. Electrophoresis was performed at 100 Volts. To estimate the product size, 0.5 μg of 1 kb or 100 bp DNA markers (New England Biolabs) were run simultaneously. Following electrophoresis, gels were stained in 3× GelRed™ Nucleic Acid Gel Stain in DMSO (Biotium Inc) for 10-15 min. DNA bands were visualised under UV Transilluminator (BioDoc-ItTM Imaging System, UVP) using Quantity One® Version 4.6 Basic software (BioRad).

2.1.7 DNA ligation

Ligation reactions were performed using the Quick Ligation™ Kit (NEB). Ligation mixtures contained 50 ng of digested plasmid, a 3-fold molar excess of the similarly digested insert DNA, 10 μl of Quick Ligation Reaction Buffer (2×) and 1 μl of Quick T4 DNA Ligase (2,000 Units/μl) and dH_2O to a final volume 20 μl. The reaction was then mixed thoroughly and incubated at RT for 5 min and chilled on ice before being used in a transformation process or being stored at -20°C until use.

2.1.8 DNA purification from agarose gel

DNA bands were purified from agarose gels using a MinElute® Gel Extraction Kit (Qiagen®) according to the manufacturer's instructions. In brief, the DNA fragment was

excised from the gel with a clean, sharp scalpel and the gel slices were mixed with 3 volumes of QG buffer (100 mg of the gel slice was equal to 100 µl) and the agar was melted at 50°C for 5-10 min until the gel slice was completely dissolved. One gel volume of isopropanol was added to the mixture and then applied to the QIAquick column following by centrifugation at 12,000 × *g* for 1 min. The flow-through was discarded and the column was washed with 750 µl of PE buffer (centrifugation at 12,000 × *g* for 1 min). To elute the DNA from the column, the column was placed into a new 1.5 ml microcentrifuge tube and 30-50 µl of EB buffer (10 mM Tris-HCl, pH 8.5) was added to the column. After 1 min incubation at RT, the column/tube was centrifuged at 12,000 × *g* for 1 min.

2.1.9 DNA sequencing

DNA sequencing (Sanger sequencing) was performed by the Australian Genome Research Facility (AGRF, Australia). Samples were prepared according to the sample submission guidelines. The DNA sample consisted of 1µg of plasmid DNA, 9.6 pmol of an appropriate forward or reverse primer and adjusted to 12 µl with dH_2O. DNA sequencing results were analysed using FinchTV software (version 1.4.0) (Geospiza, Perkin Elmer®) and compared to known sequences in the Genbank database using the Basic Local Alignment Search Tool (BLAST) from the National Centre for Biotechnology Information website (http://www.ncbi.nlm.nih.gov/blast/Blast.cgi).

2.1.10 Total RNA extraction

Total cellular RNA was extracted using TRIzol® Reagent (Life technologies^{TM}). Cells grown in a monolayer in 6-well or 12-well culture trays (Corning Life Sciences) were washed with PBS once and directly lysed by adding 1 ml of TRIzol® Reagent per well of the 6-well tray. Cell lysates were transferred to RNase-Free 1.5 ml microcentrifuge tubes (Ambion). One-fifth volume of chloroform (0.2 ml for 1 ml of TRIzol) was added to the preparation, mixed thoroughly, incubated at 25°C for 2-3 min, and subsequently centrifuged at 12,000 × *g* at 4°C for 15 min. The top aqueous layer was transferred to a new tube. Total RNA was precipitated by adding 0.5 volume of cold isopropanol, mixed well and incubated at RT for 10 min. The RNA pellet was precipitated by centrifugation at 12,000 × *g* at 4°C for 10 min and washed with 1 volume of 75% (v/v) ethanol in RNase-free dH_2O. After centrifugation at 7,500 × *g* at 4°C for 5 min, the total RNA pellet was air-dried at RT. The RNA pellet was dissolved in 10-20 µl of RNase-free dH_2O. RNA samples were kept at -80°C until use.

2.1.11 Nucleic acid quantification

DNA or RNA samples were quantified using the Nanophotometer (Implen GmbH). The absorbance at 260 nm was read and concentrations of samples of were calculated using the following formula:

$$\text{Nucleic Acid (µg/ml)} = A_{260nm} \text{ x dilution factor x 50 (DNA) or 40 (RNA)}$$

The purity of nucleic acids was determined by measuring the ratio of the absorbance at 260 nm and 280 nm (A_{260nm}/A_{280nm}). The DNA and RNA preparations used in this study generally had an A_{260nm}/A_{280nm} of 1.8 and 2.0, respectively.

2.1.12 First-strand cDNA synthesis

First-strand cDNA was produced from the total RNA using M-MLV Reverse Transcriptase RNase H minus, point mutant (Promega). The reaction was performed in a pre-chilled RNase-free microcentrifuge tube containing 1 μg of total RNA, 1 μg of random hexamer primer (Geneworks) and RNase-free dH_2O to a final volume of 14 μl. The preparation was mixed gently and incubated at 70°C for 5 min. The tube was then cooled down at 4°C for a further 5 min and the following mixture of 5 μl of 5× M-MLV RT Reaction Buffer (Promega), 1.25 μl of 10 mM each dNTP mix (Promega), 0.5 μl of 40 Units/μl RNAsin® RNase Inhibitor (Promega), 1 μl of 200 Units M-MLV RT, RNase H (-) Point Mutant (Promega) and 3.25 μl dH_2O was added to the tube. Samples were mixed gently and incubated at RT for 10 min, then 42°C for 50 min. Finally, samples were diluted to a final volume of 100 μl with dH_2O and stored at -20°C.

2.1.13 Polymerase Chain Reaction (PCR)

PCR reactions were performed using a Thermal Cycler (S1000TM, BioRad®). Q5® High-Fidelity DNA polymerase enzymes were mainly used for cloning purposes. The reactions were prepared in a 0.2 ml PCR tube containing 25 μl of Q5 High-Fidelity 2× Master Mix, 1.25 μl each of 20 μM forward and reverse primers, 10 ng of DNA template and dH_2O to a final volume of 50 μl. PCR conditions consisted of initial denaturation at 98°C for 30 sec, followed by 30 cycles of 98°C for 10 sec, an appropriate annealing temperature for 30 sec, 72°C for 20-30 sec/kb and ended up with a final extension at 72°C for 2 min. The PCR reactions were visualised by agarose gel electrophoresis (see section 2.1.6) or stored at 4°C.

2.1.14 Real-Time Quantitative PCR (qPCR)

Quantitative PCR was used to determine relative levels of target RNA using the comparative CT method. qPCR reactions were performed using SYBR® Green PCR Master Mix (Applied Biosystems). The reactions consisted of 5 μl of cDNA, 10 μl of SYBR® Green PCR Master Mix and 300 nM each forward and reverse primer (see Appendix I). All samples were analysed in duplicate and also processed to quantify the RPLPO housekeeping gene in parallel to normalise input cDNA levels. An ABI StepOne Plus Real-Time PCR System (Applied Biosystems) coupled with the ABI PRISM 7000 SDS Software was used to control the reaction and comprised denaturation at 95°C for 10 min followed by 40 cycles of 95°C for 15 sec and 60°C for 1 min. A final step of 95°C for 15 sec, 60°C for 1 min, followed by increasing the temperature by 0.5°C increment up to 95°C was performed to facilitate the melting curve. Data were analysed using the StepOne^{TM} v2.2 software and the threshold was set at 0.2 for all experiments.

2.1.15 Extraction of cellular proteins

Total cellular proteins were extracted from 80-90% confluent cell monolayers in 6-well trays. Culture media was removed and cells were washed with PBS. Pre-chilled RIPA buffer or NP-40 buffer (200 μl) (see Appendix II) containing protease inhibitor cocktail (Sigma Aldrich) was added to the well. Cell lysate was then transferred to a 1.5 ml microcentrifuge tube and placed on ice for 20 min. The lysates were centrifuged at 12,000 × *g* at 4°C for 10 min. The supernatant protein fraction was collected and then used for further experiments or stored at -20°C.

2.1.16 SDS-PAGE and protein transfer

SDS-PAGE was performed as described by Laemmli (1970). Protein samples were prepared by boiling for 5 min with 1× SDS PAGE sample buffer (see Appendix II) before loading onto the gel (Mini Protean 4-15% Precast Gels, Biorad) alongside 7.5 µg Precision Plus Protein® Standards-Kaleidoscope (BioRad). Gels were run in SDS-PAGE running buffer at 100 Volts for 1-2 hr depending on protein size. Gels were then equilibrated in cold Transfer Buffer (see Appendix II) for 5-10 min. Nitrocellulose Blotting Membrane (Amersham ™ Hybond ECL) and filter papers were soaked in cold Transfer Buffer before assembling the Western Blot Transfer Apparatus (Mini Trans Blot Electrophoretic Transfer Cell, BioRad) as per manufacturer's instruction. Proteins were transferred onto the Nitrocellulose Blotting Membrane at 100 Volts for 90 min in a cold room.

2.1.17 Western blotting

Following protein transfer, membranes were blocked with 5% skim milk in 0.1% TBS-T for 1 hr with gentle agitation. Membranes were rinsed twice with 0.1% TBS-T (see Appendix II) and then incubated in the appropriate dilution of primary antibody in 1% skim milk (see Appendix III) overnight at 4°C. Thereafter, membranes were washed three times in 0.1% TBS-T for 5 min per wash with gentle agitation to remove unbound primary antibody. Membranes were then incubated with gentle agitation in the appropriate horseradish peroxidase-conjugated secondary antibody for 1 hr and washed as described before. Secondary antibody detection was carried out using the ECL Plus Western blotting detection reagent kit (Amersham Pharmacia Biotech) or the

Supersignal® West Femto Maximum Sensitivity Substrate detection kit (ThermoScientific) with chemiluminescent detection as per manufacturer's instructions. Protein bands were visualised by a Chemi DocTM MP Imaging System (BioRad) or by exposure to Kodak BioMax film with an appropriate exposure time depending on the signal intensity.

2.1.18 Co-immunoprecipitation

Whole Cell lysate preparation using NP-40 buffer as described in 2.1.15 were subjected to co-immunoprecipitation. All steps were performed at 4°C. Lysates were pre-cleared by incubation with 20 µl of protein A/G PLUS agarose (Santa Cruz Biotechnology) for 30 min. Samples were then centrifuged at 3,000 × *g* for 30 sec at 4°C, and supernatants were collected and incubated with 1 µg of the appropriate antibody for overnight. Protein A/G PLUS agarose beads (20 µl) were equilibrated with NP-40 lysis buffer and then added to each sample prior to incubation for 1 hr. Beads were then pelleted by centrifugation at 3,000 × *g* for 30 sec at 4°C and washed 5 times with 500 µl of NP-40 lysis buffer. Washed beads were resuspended in 30 µl of 2× SDS-PAGE sample buffer and boiled for 10 min followed by Western blot analysis.

2.1.19 Dual Renilla luciferase assay

Luciferase activity was measured using the Dual Luciferase Assay System (Promega). Cells were seeded at 5×10^4 cells/well in 12-well trays, cultured overnight and co-transfected with the plasmid of interest (500 ng), ISRE-luc or IFN-β-Luc (500 ng) and pRL-TK (10 ng). On the following day, cells were treated with IFN-α (for ISRE-luc) or

poly I:C (for IFN-β-Luc) for 8 hr and then washed once with PBS. 5× Passive Lysis Buffer (Promega) was diluted to 1× lysis buffer with MilliQ water, and 80 µl of working lysis buffer was added to each well followed by a single freeze-thaw to harvest the cell lysate. 20 µl of cell lysate was then added to an Opti-plate 96 (Perkin Elmer) and luciferase out-put was measured on a GloMax™ 96 Microplate Luminometer (Promega). Data were analysed using GraphPad Prism 6 software.

2.1.20 Duolink® In situ Proximity Ligation Assay

Cells were seeded at 7×10^4 cells/well in 12-well trays and cultured overnight prior to transient transfection. Cells were washed with 1x PBS and then trypsinised by adding 200 µl of trypsin and incubated for 2-5 min before adding 800 µl of complete media. 200 µl of cell suspension was then plated per well into 96-well trays. After cell attachment (24 hr), cells were fixed with cold Acetone:Methanol (1:1) for 5 min, then washed 3 times with PBS. Proximity ligation assays (PLA) were conducted using the Duolink® In situ kit (Olink® Biosciences) as per manufacturer's instructions. In more detail, fixed cells were blocked with 5% BSA in PBS for 1 hr at RT and then washed 3 times with PBS. A mixture of appropriate primary antibodies (different species such as mouse and rabbit) was added and the plate was incubated for 1 hr at RT, and then washed 5 times with PBS. An isotype control for each primary antibody species was used as a negative control. PLA probe mixture (anti-mouse minus and anti-rabbit plus) in 1% BSA was added to the wells and the plate was incubated at 37°C in a humidity chamber for 1 hr. Cells were then washed with wash buffer A (Olink® Biosciences) 2 times for 5 min each. The ligation solution was prepared by mixing 8 µl of 5× ligation stock, 31 µl of dH_2O and 1 µl of

ligase. 40 µl of ligation solution was added to wells and incubated at 37°C in humidity chamber for 30 min. The plate was washed 2 times with wash buffer A for 2 min each. An amplification step was performed by adding the mixture of 8 µl of 5× amplification stock, 31.5 µl of dH_2O and 0.5 µl of polymerase to the wells and incubating at 37°C in a humidity chamber for 1 hr. The reaction was washed 2 times with wash buffer B (Olink® Biosciences) for 10 min each, before a final wash with 0.01× wash buffer B for 1 min. Nuclear DAPI staining (described in section 2.6.5) was generally performed after proximity ligation assay. The cells were visualised by wide-field fluorescence microscopy and a red dot indicated a protein-protein interaction.

2.2 Yeast Two-Hybrid system

Yeast two-hybrid experiments were performed using the Matchmaker Gold Yeast Two-Hybrid system (Clontech) according to manufacturer's instructions. Briefly, yeast two-hybrid systems are tools for identifying and characterising novel protein-protein interactions. In a Matchmaker GAL4-based two-hybrid assay, a known protein of interest or bait protein (viperin in this study) is expressed as a fusion to the Gal4 DNA-binding domain (DNA-BD), while libraries of prey proteins derived from a cDNA library are expressed as fusions to the Gal4 activation domain (AD) (Fields and Song, 1989, Chien et al., 1991). When a bait protein interacts with a prey protein, the DNA-BD and AD are brought into close proximity to restore GAL4 function and subsequently activate transcription of four independent reporter genes (*AUR1-C*, *ADE2*, *HIS3*, and *MEL1*).

2.2.1 Competent yeast cell preparation

Competent yeast cells were prepared using a Yeastmaker Yeast Transformation System 2 (Clontech). Yeast cells from a frozen stock were streaked on YPDA agar plate (see Appendix IV). The plate was incubated at 30°C for 3-5 days until colonies appeared. One yeast colony (diameter 2–3 mm) was then inoculated into 3 ml YPDA medium in a sterile 15 ml culture tube and incubated at 30°C with shaking at 250 rpm for 8–12 hr. 5 µl of the culture were transferred to 50 ml of YPDA in a 250 ml flask and incubated with shaking until the OD_{600} reached 0.15–0.3 (16–20 hr). Yeast cells were pelleted by centrifugation at 700 g for 5 min at RT. The supernatant was discarded and the pellet was resuspended in 50 ml of fresh YPDA. Cells were incubated at 30°C with shaking until the OD_{600} reaches 0.4-0.5 (3-5 hr). Cells were pelleted at 700 g for 5 min at RT and washed in 30 ml sterile, dH_2O. The cell pellet was resuspended in 1.5 ml of 1.1xTE/LiAc, then transferred to a 1.5 ml microcentrifuge tube and centrifuged at 14,000 × *g* for 15 sec. The supernatant was discarded and the cell pellet was resuspended in 600 µl of 1.1xTE/LiAc. The cells were then ready to be transformed with plasmid DNA or stored on ice for a few hours.

2.2.2 Transformation

2.2.2.1 Small scale transformation

The transformation was performed in a pre-chilled 1.5 microcentrifuge tube. Plasmid DNA (100 ng) was combined with 5 µl of denatured-carrier DNA (10 µg/µl). Competent yeast cells (50 µl) were added to the mixture. PEG/LiAc (500 µl) was then added, gently mixed and incubated at 30°C for 30 min with gentle mixing every 10 min. DMSO (20 µl)

was added and the transformation mixture was incubated at 42°C for 15 min. Yeast cells were then pelleted by centrifugation for 15 sec at 14,000 × *g*. The supernatant was removed and cells were resuspended in 1 ml of YPD plus medium. Yeast cells were pelleted by 14,000 × *g* centrifugation and resuspended in 0.9% (w/v) NaCl solution. The cell suspension was diluted to 1/10 and 1/100 and 100 µl of each dilution was spread onto an appropriate SD selective medium.

2.2.2.2 Library scale co-transformation

The library scale co-transformation was performed in a pre-chilled 15 ml tube. Bait pDNA was combined with linearised prey plasmid and purified ds cDNA (see section 2.2.5.2.3) and then 20 µl of denatured-carrier DNA (10 µg/µl) was added. Competent yeast cells (600 µl) were added to the mixture. PEG/LiAc (2.5 ml) was then added, gently mixed and incubated at 30°C for 45 min with gentle mixing every 15 min. DMSO (160 µl) was added and the mixture was incubated at 42°C for 20 min. Yeast cells were then pelleted by centrifugation at 700 × *g* for 5 min. The supernatant was removed and cells were resuspended in 3 ml of YPD plus medium and incubated at 30°C with shaking for 90 min. Yeast cells were pelleted by centrifugation at 700 × *g* for 5 min and resuspended in 0.9% (w/v) NaCl solution. The cell suspension was diluted to 1/10 and 1/100 and 100 µl of each dilution was spread onto an appropriate SD selective medium.

2.2.3 Plasmid DNA extraction from yeast cells

A single colony was inoculated into an appropriate medium and incubated at 30°C with shaking overnight. Plasmid DNA was isolated from yeast cells using Easy Yeast Plasmid

Isolation Kit (Clontech) as per manufacturer's instructions. An overnight culture was pelleted by centrifugation and washed with 500 µl of 10 mM EDTA. The washed yeast cell pellet was then resuspended in 200 µl of ZYM buffer. Yeast cell walls were disrupted by adding 20 µl of Zymolase suspension and incubated with gentle shaking at 30°C for 1 hr. The spheroplasts (disruption of yeast cell walls) were pelleted by centrifugation at 2,000 × *g* for 10 min and then subjected to plasmid DNA extraction by SDS/alkaline lysis method. Briefly, the spheroplasts were resuspended in 250 µl of Y1 Buffer/RNase A solution and lysed by adding 250 µl of Y2 Lysis Buffer. Y3 Neutralization Buffer (300 µl) was then added and mixed gently by inverting the tube 6-8 times. The lysate was clarified by centrifuging at 11,000 × *g* for 5 min at RT. The supernatant was transferred to a Yeast Plasmid Spin Column inside a 2 ml collection tube and centrifuged at 11,000 × *g* for 1 min. The column flow-through was discarded and the spin column was washed with 450 µl of Y4 Wash Buffer. Plasmid DNA was eluted by adding 50 µl of YE Elution Buffer and incubated at RT for 1 min before centrifugation at 11, 000 × *g* for 1 min.

2.2.4 Construction and testing of the bait (viperin) protein expression plasmid

2.2.4.1 Cloning of pGBKT7-viperin

pLenti6-Viperin-Flag plasmid (Helbig et al., 2013) was diluted to 1 ng/µl and used as a template for viperin-coding DNA sequence amplification. Viperin was amplified using a Thermo Cycler (BioRad). The PCR reaction mixture (50 µl) consisted of 2 µl of template, 1.25 µl forward and reverse primers (Appendix I) (at 20 µM), 25 µl of Q5 High-Fidelity 2× Master Mix (New England Biolabs, USA), and made up to 50 µl with nuclease-free water. After 30 sec of an initial denaturation at 98°C, 30 cycles of PCR

(each cycle was 10 sec at 98°C, 30 sec at 50°C, and 1.15 min at 72°C) were performed and this was followed by 2 min at 72°C for the final extension. The PCR product was visualised on 1% agarose gel using electrophoresis, GelRed staining and a UV transilluminator. The PCR product was then purified using a PCR clean-up kit (Qiagen).

The bait plasmid (pGBKT7) (Clontech, see Appendix V) and purified-viperin amplicon were double digested with *Eco*RI-HF and *Bam*HI-HF at 37°C overnight. The double digested-products were subjected to 1% agarose gel electrophoresis and then purified from the agarose gel using MinElute® Gel Extraction Kit (Qiagen). The viperin amplicon was ligated with the linearised pGBKT7 plasmid. The ligation reaction was then transformed into α-Select Chemically Competent Cells (Bioline), plated on a LB-Kan plate and incubated at 37°C overnight. Five clones were randomly picked to screen the positive clones. They were individually inoculated into 5 ml of LB-Kan broth and incubated at 37°C with shaking at 200 rpm overnight. The cells were harvested by centrifugation at 4,000 × *g* for 5 min. The plasmids from each clone were extracted from *E. coli* cell pellets using a miniprep kit (Qiagen).

The recombinant plasmids were double digested with the *Eco*RI-HF and *Bam*HI-HF restriction endonucleases. The mixture was incubated at 37°C for 3 hr. The digested product was subjected to 1% agarose gel electrophoresis and GelRed staining in order to ensure that the plasmid contained the correct DNA insert. The recombinant plasmids that had an insert of the expected size for viperin were then sequenced and a clone that had no

undesired mutations was selected for large-scale plasmid DNA preparation (see section 2.1.4).

The recombinant pGBKT7-viperin plasmid was then transformed into competent *Saccharomyces cerevisiae* strain Y2H gold and plated on the SD/-Trp selective medium agar (see Appendix IV) and incubated at 30°C for 3-5 days. After incubation, five clones were randomly picked to check viperin insertion in pGBKT7 plasmid by colony PCR before being subjected to viperin expression analysis. Yeast colonies were resuspended in 20 µl of 20 mM NaOH, then boiled at 95°C for 10 min and 1 µl of the boiled yeast cells was used as a template for colony PCR.

2.2.4.2 Viperin expression

A colony of selected transformed yeast clones was inoculated into 2 ml of SD/-Trp broth (see Appendix IV) and the culture was grown at 30°C with shaking at 200-250 rpm overnight. 100 µl of the overnight culture was added into 10 ml of SD/-Trp broth. The preparation was incubated at 30°C with shaking at 200-250 rpm until the OD_{600} reached 0.4-0.6. Yeast cells were pelleted and resuspended in pre-warmed complete cracking buffer (see Appendix IV) containing a cocktail protease inhibitor. 100 µl of cracking buffer was used per 7.5 OD_{600} units of cells. The cell suspension was then transferred to a 1.5 ml microcentrifuge tube containing 80 µl of glass beads per 7.5 OD_{600} units of cells. Samples were heated at 70°C for 10 min and then vigorously vortexed for 1 min. Cell debris was pelleted by centrifugation at 14,000 × *g*, 4°C for 10 min and the supernatant was transferred to the new microcentrifuge tube and boiled for 5 min. The remaining cell

debris was pelleted by centrifugation at 14,000 × *g*, 4°C for 5 min and the supernatant was subjected to Western blot analysis to confirm the presence of viperin in the yeast cells using anti-cMyc clone 4A6 (Millipore) and specific anti-viperin antibody (Enzo life sciences).

2.2.4.3 Toxicity and auto-activation testing

One clone of yeast cells expressing viperin was selected for toxicity and auto-activation analysis. Yeast cells carrying pGBKT7-viperin or pGBKT7-empty (negative control) were plated onto the SD/-Trp, SD/-Trp/X and SD/-Trp/X/A agar plates (see Appendix IV) and grown at 30°C for 3-5 days. *Saccharomyces cerevisiae* strain Y2H gold carrying pGBKT7-53 was mated with *Saccharomyces cerevisiae* strain Y187 carrying pGADT7-T and plated on DDO/X/A (see Appendix IV) for use as a positive control for auto-activation testing. If the bait protein is not toxic to the yeast cell, the size of colonies containing bait plasmid are similar to colonies containing the empty plasmid on SD/-Trp. White colonies on SD/-Trp/XA plate represent non auto-activation of the bait protein. The expected results after 3-5 days of yeast cell growth on agar plates are shown in Table 2.1.

Table 2.1: Expected results of toxicity and auto-activation testing

Sample	Selective agar plate	2 mm colonies	Color
Viperin autoactivation test	SD/-Trp	Yes	White
Viperin autoactivation test	SD/-Trp/X	Yes	White
Viperin autoactivation test	SD/-Trp/X/A	No	No growth
Negative control	SD/-Trp	Yes	White
Positive control	DDO/X/A	Yes	Blue

2.2.5 Construction of the IFN-α-stimulated Huh-7 cDNA library

2.2.5.1 Optimisation of the concentration and time point of IFN-α for Huh-7 stimulation

Huh-7 were seeded at 7×10^4 cells/well in 12-well culture tray and subsequently treated with IFN-α-2A at 100, 250 and 1,000 Units/ml. Huh-7 cells were stimulated with IFN-α-2A at a concentration of 1,000 Units/well for 8, 16 and 24 hr (time course analysis). Each IFN-α-2A concentration and time point was assessed in triplicate. Cells were then collected for RNA extraction and cDNA synthesis with following analysis by real time RT-PCR.

2.2.5.2 IFN-α-stimulated Huh-7 cDNA library construction

The library was generated using Make Your Own "Mate & Plate" Library System (Clontech). The process to generate the library was described below.

2.2.5.2.1 Generating IFN-α-stimulated Huh-7 cell cDNA library

Huh-7 cells at 7×10^4 cells were stimulated with IFN-α-2A at the optimal concentration and time point (1000 Units/ml, 8 hr). Cells were harvested for RNA extraction using RNeasy Mini Kit (Qiagen). Total RNA was used as a template for generating the first strand cDNA using an oligo-dT primer. In brief, 1.5 μg (3μl) of total RNA was combined with CDS III (oligo-dT primer) and the mixture was incubated at 72°C for 2 min and immediately cooled on ice for 2 min. A master mix (9 μl) containing the following components; 2 μl of 5× First-Strand buffer, 1 μl of 100 mM DTT, 1 μl of 10 mM dNTP mix and 1 μl of SMART MMLV Reverse Transcriptase was prepared and added to the RNA mixture and subsequently incubated at 42°C for 10 min. Then, 1 μl of SMART III-

modified oligo was added to reaction mixture and incubated at 42°C for 10 min followed by 75°C for 10 min. After cooling down at RT, 1μl of RNase H (2 Units) was added and the reaction was incubated at 37°C for 20 min. The cDNA was used for long-distance PCR (LD-PCR) amplification.

2.2.5.2.2 Double-stranded cDNA (ds cDNA) synthesis by long-distance PCR

Double-stranded cDNA (ds cDNA) was amplified by long-distance PCR (LD-PCR) using Advantage 2 Polymerase Mix (Clontech). The LD-PCR reaction mixture was set up in 2 reactions. Each reaction (100 μl) consisted of 2 μl of first-strand cDNA (from 2.2.5.2.1), 70 μl of dH_2O, 10 μl of 10× Advantage 2 PCR buffer, 2 μl of 50× dNTP mix, 2 μl of 5'PCR primer, 2 μl of 3'PCR primer, 10 μl of 10× Melting solution and 2 μl of 50× Advantage 2 Polymerase Mix. The LD-PCR mixture was placed in a Thermo cycler (BioRad) and the cycler program was started at 95°C for 30 sec. Following incubation, 20 cycles (each cycle was 10 sec at 95°C, 6 min with increasing by 5 sec every cycle at 95°C) were performed, with a final step of 68°C for 5 min. The PCR products (7 μl) from two reactions were separately visualised by 1% agarose gel electrophoresis and GelRed staining using UV transilluminator. The LD-PCR product was subsequently purified as described in Section 2.2.5.2.3.

2.2.5.2.3 Double-stranded cDNA (ds cDNA) purification

The LD-PCR product was purified using CHROMA SPIN + TE 400 column (Clontech). Briefly, both samples (93 μl of each reaction) from 2.2.5.2.2 was applied separately to the centre of the prepared-spin column in a collection tube and subsequently centrifuged at

700 × g for 5 min. Two purified-samples were combined and cDNA precipitation was performed. One in ten volume of 3M sodium acetate was added and followed by 2.5 volumes of ice-cold 95-100% ethanol. The sample was placed at -20°C for 1 hr and then centrifuged at 14,000 rpm for 20 min at RT. The supernatant was discarded and the pellet was air-dried for 10 min. The cDNA pellet was resuspended in 20 μl dH_2O. This ds cDNA library was ready for the following screening process.

2.2.6 Screening viperin interacting partners by co-transformation method

pGBKT7-viperin plasmid (5 μg), purified-ds cDNA library (~5 μg, from section 2.2.5.2.3) and linearised pGADT7-Rec plasmid (3 μg) were combined in a pre-chilled microcentrifuge tube and transformed into competent *Saccharomyces cerevisiae* strain Y2H gold. The co-transformation reaction was performed according to section 2.2.2.2 and subsequently resuspended in 15 ml of 0.9% (W/V) NaCl in the last step before plating. The resuspended-cells were diluted to 1:10, 1:100, 1:1,000 and 1:10,000 and 100 μl of each dilution was plated on SD/-Trp, SD/-Leu and DDO plates (25mm dish) (see Appendix IV) to quantify the transformation efficiency. Two hundred microliters of the remainder were spread on DDO/X/A plate (100 mm dish) (see Appendix IV) for 50 plates and incubated at 30°C for 3-5 days.

2.2.7 Rescue plasmid from yeast cells

After incubation, all of the blue colonies that grew on DDO/X/A were streaked on a higher stringency QDO/X/A agar plate (see Appendix IV). All of the colonies that grew on QDO/X/A were streaked 2-3 times on DDO/X plate to get a pure single blue colony.

The mixture of bait and prey plasmids were rescued from yeast cells using Easy Yeast Plasmid Isolation Kit (Clontech) as described in section 2.2.3. All of the mixture plasmids were transformed into bacterial cells and plated on LB-Amp to select prey plasmids. The positive prey plasmids were identified by sequencing analysis using a T7 sequencing primer (see Appendix I). The positive interactions were confirmed by the co-transformation method. Candidate prey plasmid and pGBKT7-viperin or pGBKT7-empty plasmid were co-transformed into competent *Saccharomyces cerevisiae* strain Y2H gold and then plated onto DDO/X and DDO/X/A. The genuine and false positive interactions are shown in Table 2.2.

Table 2.2: Genuine and false positive interactions

Interactions	Sample	Selective agar plate	2 mm colonies	Color
Genuine positive	pGBKT7-viperin + candidate prey	DDO/X	Yes	Blue
		DDO/X/A	Yes	Blue
	pGBKT7 empty + candidate prey	DDO/X	Yes	White
		DDO/X/A	No	No growth
False positive	pGBKT7-viperin + candidate prey	DDO/X	Yes	Blue
		DDO/X/A	Yes	Blue
	pGBKT7 empty + candidate prey	DDO/X	Yes	Blue
		DDO/X/A	Yes	Blue

2.3 Tissue Culture Techniques

2.3.1 Tissue culture medium

Mammalian cell lines were maintained in Dulbecco's Modified Eagle Medium (DMEM) containing 4.5 g/L D-Glucose, 25 mM HEPES and 2 mM L-glutamine (Gibco BRL, Invitrogen). Standard DMEM was supplemented with 10% (w/v) foetal calf serum (FCS; Trace Biosciences), Penicillin (Invitrogen; 100 U/ml) and Streptomycin (Invitrogen; 100μg/ml). Blasticidin HCL 5 μg/ml (Invitrogen), Puromycin 3 μg/ml (Sigma-Aldrich) or Geneticin (G418) 800 μg/ml (Invitrogen) were added for selection and maintenance of stable cell lines in this study.

2.3.2 Cell maintenance

Cultured cell lines were maintained in sterile 0.2 μm vented tissue culture flasks (25 cm^2, 75 cm^2, or 175 cm^2), tissue culture dishes (3.5 cm^2, 6 cm^2 or 10 cm^2) or tissue culture trays (6, 12, 24, 48 or 96-well) (Corning Life Sciences). Near-confluent cells were passaged by removing culture medium, washing once with 1× PBS (see Appendix II), trypsinising with a small volume of Trypsin-EDTA (see Appendix II). Cells were then placed in the CO_2 incubator at 37°C for 3-5 min. Fresh culture medium was added to resuspend the cells. Cells were counted using a Neubauer Haemocytometer (Brand) with Trypan Blue (see section 2.3.3). Cells were grown at 37°C, 5% CO_2 in a humidified Panasonic CO_2 incubator (Panasonic Healthcare CO., Ltd). Cells were passaged every 2-3 days depending on cell types and confluency.

2.3.3 Trypan blue exclusion

Cells were counted using a Neubauer Haemocytometer (Brand) and Trypan Blue Stain solution (prepared by the Tissue Culture Service Unit). Typsinised cells were mixed with an equal volume of Trypan Blue and loaded into a haemocytometer. Cell concentration was then calculated using the following equation:

$$\text{Cell concentration (cells/ml)} = \text{cell count per grid} \times 2 \text{ (dilution factor)} \times 10^4$$

2.3.4 Cryopreservation of cells

Cells were cryopreserved in liquid nitrogen. 80% confluent of cells were trypsinised, resuspended in fresh culture media and centrifuged at 1,000 × *g* for 5 min. Culture media were removed and cell pellets were resuspended in fresh culture media. An equal volume of 2× freezing media [50% media, 30% FCS, 20% DMSO (Sigma)] was added to cell suspension and mixed gently. Cells were aliquoted (1 ml/vial) in sterile cryopreservation tubes (CryoTubeTM vials, NUNCTM). Cryotubes were transferred to a freezing chamber (Nalgene®) containing fresh isopropanol and placed in a -80°C freezer to achieve a cooling rate of -1°C/min. For long-term storage vials were stored in a liquid nitrogen based cryopreservation system, while stocks for short-term use (within 3 months) were kept in the -80°C freezer.

2.3.5 Resuscitation of frozen cells

Cryopreserved vials containing frozen cell lines were thawed quickly in a 37°C water bath and gently transferred to a T25 cm^2 or T75 cm^2 tissue culture flask containing pre-warmed standard tissue culture medium. Cells were incubated in the CO_2 incubator

overnight. Fresh tissue culture medium containing an appropriate antibiotic (if necessary) was replaced the next day.

2.3.6 Transient transfection of plasmid DNA

Mammalian cells were transiently transfected with expression plasmid DNA using Viafect (Promega) to achieve protein overexpression. Cells were seeded at 3×10^4 cells (24-well tray), 7×10^4 cells (12-well tray) and 2×10^5 cells (6-well tray) 24 hr prior to transfection such that the cells were 50-70% confluent at the time of transfection. ViaFect™ Transfection Reagent was used as per manufacturer's instruction. Briefly, ViaFect reagent was warmed up at RT for 10 min before use. Transfection complexes were prepared by mixing 100 µl of Opti-MEM® media (Life Technologies) with 3 µl of ViaFect reagent and 2 µg of DNA (for each transfection per well of a 6-well tray). Following 15-20 min incubation at RT, the mixture was added drop-wise to the cell monolayer. The plates were then gently swirled and returned to normal tissue culture condition (37ºC, 5% CO_2). Assays were performed 24-72 hr post transfection.

2.3.7 Generation of stable cell lines

Stable over-expressing cell lines were generated using a direct transfection method or an intermediate lentiviral or retroviral particle production method.

2.3.7.1 Direct transfection

Cells were transfected with plasmid DNA using the protocol as previously described in section 2.3.6. A specific antibiotic at an appropriate concentration (see section 2.3.1) for the selectable marker carried by the expression plasmid was added to culture media 3

days post-transfection. Untransfected cells treated with the same antibiotic were used a negative control. The cell line was considered as stable cells after the negative control culture was non-viable.

2.3.7.2 Lentiviral particle production

The lentiviral particles were produced in 293FT cell line. 293FT cells were seeded in a 6 well tray at a concentration of 2×10^5 cells/well to be transfected the following day. The total plasmid DNA was prepared by mixing an equal amount of target plasmid DNA with the lentiviral packaging plasmids psPAX2 (a packaging plasmid, Addgene plasmid # 12260), pMD2.G (VSV-G envelope expressing plasmid, Addgene plasmid # 12259) and pRSV-Rev (3rd generation lentiviral packaging plasmid, Addgene plasmid # 12260). The transfection mixture was prepared by mixing 100 µl of Opti-MEM® media (Life Technologies) with 3 µl of ViaFect reagent and 2 µg of total plasmid DNA and incubating for 15-20 min. The mixture was added to the cells before returning them to a standard CO_2 incubator. Culture media were changed the following day. The supernatants from 293FT cells were harvested at 48 and 72 hr post-transfection, then pooled, filtered through a 0.45 µm filter membrane, aliquoted into vials and stored at -80°C.

To generate the stable cells, the naïve cell lines or Huh-7 cells in this study were seeded at 2×10^5 cells/well in 6-well tray prior to lentiviral transduction. The lentiviral aliquot was rapidly thawed and then diluted 1:3 in complete media containing a final concentration of 8 µg/ml of polybrene (Millipore). The diluted lentiviral particles were then added to the target cells. Culture media were replaced 6 hr post-transduction and

cells were returned to the incubator. The antibiotic selection was started 3 days post-transduction (Blasticidin at 5 μg/ml for pLenti6/V5 derivatives, puromycin at 3 μg/ml for pTRIPz and GIPz shRNA derivatives). Treatment of non-transduced cells was used as a negative control. The polyclonal cell line was considered as stable cells when the negative control culture was non-viable.

2.3.7.3 Stable transduction of GIPz shRNA OSBP to generate OSBP knockdown cell lines

Six clones of plasmid DNA carrying shRNA targeting to OSBP were obtained from Open Biosystems (Thermo Scientific) in a pGIPz lentiviral construct encoding a green fluorescent protein. Lentiviral particles expressing OSBP shRNA were generated as described in section 2.3.7.2, and transduced Huh-7 cells were selected using 3 μg/ml puromycin (Invitrogen). Huh-7 cells were used as a negative control for puromycin selection. Non-targeting control (NTC) shRNA were also generated and used as a control for further experiments. The cells were considered as stable cell lines when the negative control culture was non-viable. Knockdown cells were tested by Western blot analysis using anti-OSBP (Proteintech).

2.3.7.4 Retroviral particles production

The process to generate the retroviral particles and make the stable cell lines by retroviral transduction was similar to the lentiviral particle production process as described in section 2.3.7.2. pCL-Ampho retroviral packaging plasmid (Novus Biologicals #NBP2-29541) was used instead of lentiviral packaging plasmids.

2.3.7.5 Generation of MAVS knockout (MAVS-KO) cell lines by CRISPR/Cas9 technology

20 nucleotides guide sequences (sgRNA) targeting to the gene of interest (MAVS) were designed on Benchling and generated with *Bsm*BI overhangs as complementary DNA primers (see Appendix I). These primers were annealed and ligated into *Bsm*BI digested LentiCRISPR v2 plasmid (Addgene). Following transformation into competent cells (see section 2.1.2) and mini-preparation (see section 2.1.3), a diagnostic *Bsm*BI digestion was performed to deduce which clones have the correct guide sequence. Lentivirus was generated as described previously in section 2.3.7.2. Huh-7 cells were transduced for 5 hr with lentivirus containing LentiCRISPR v2 encoding the MAVS sgRNA, and subsequently replaced with fresh complete media. Monoclonal populations of each potential knockout colony were obtained by dilution (1:100-1:200) onto 150 mm dishes to separate a single cell and once at a suitable size (approximately 4 weeks), colonies were isolated using a colony ring. Knockout cells were confirmed for MAVS-KO by immunofluorescence staining and Western blot analysis.

2.3.7.6 Generation of MAVS-KO Huh-7 expressing MAVS-WT, MAVS-pex or MAVS-mito stable cells

MAVS-WT (Addgene plasmid # 52135), MAVS-mito (Addgene plasmid # 44556) and MAVS-pex (Addgene plasmid # 44557) plasmids were gifts from Jonathan Kagan (Dixit et al., 2010). Retroviral particles containing each construct were produced and introduced into MAVS-KO Huh-7 cells by retroviral gene transfer (see section 2.3.7.4). MAVS

expressing cells were then enriched by cell sorting (BD FACSAria™ II) for higher GFP fluorescence signal compared to the background control.

2.4 Cell lines

2.4.1 HeLa

The HeLa cell line is derived from cervical cancer cells taken from Henrietta Lacks (Scherer et al., 1953).

2.4.2 293FT

The 293FT cell line (Thermo Scientific) is derived from human embryonal kidney (HEK) cells transformed with the SV40 large T antigen. It is fast-growing, highly transfectable and produces high viral titers.

2.4.3 Huh-7

The Huh-7 cell line is a human hepatocyte-derived carcinoma cell line, originally isolated from a 57-year-old Japanese male (Nakabayashi et al., 1982).

2.4.4 Huh-7.5

The Huh-7.5 cell line is derived from the Huh-7 cells which used to harbour replication of an HCV subgenomic replicon but were cured after IFN-α treatment. This cell line is highly permissive for HCV infection (Blight et al., 2002) as it has shown to be defective in RIG-I signalling (Sumpter et al., 2005). These cells were kindly provided by Charles Rice (Rockefeller University, New York, USA).

2.4.5 Huh-7+shControl

Huh-7 cells were stably transduced with lentiviral particles containing a pGIPz transgene cassette encoding a non-targeting control (NTC) shRNA and maintained under puromycin selection.

2.4.6 Huh-7+shOSBP

Huh-7+shOSBP cells are Huh-7 cells stably transduced with lentiviral particles expressing shRNA targeting to the OSBP gene and maintained under puromycin selection. This polyclonal stable cell line displayed knocked down OSBP expression.

2.4.7 Huh-7+T7

Huh-7+T7 cells are Huh-7 cells stably expressing T7 RNA polymerase and maintained under puromycin selection.

2.4.8 MAVS-KO Huh-7 cells

MAVS KO Huh-7 cells are Huh-7 cells that display a complete loss of MAVS function generated by CRISPR/Cas9 editing technology.

2.4.9 MAVS-KO Huh-7 stably expressing MAVS-WT, MAVS-mito or MAVS-pex cells

MAVS-KO Huh-7 stably expressing MAVS-WT, MAVS-mito or MAVS-pex cells were generated by retroviral gene transfer as described in section 2.3.7.6.

2.4.10 Subgenomic replicon

Huh-7.5 cells were transfected by electroporation with *in vitro* transcribed RNA generated from SGRm-JFH1 plasmid. The SGRmJFH1 plasmid was modified by removal of the RLuc-encoding sequence from SGRm-JFH1BlaRL plasmid, kindly provided by Kui Li (University of Tennessee Health Science Center) (Zhou et al., 2011). Individual blasticidin-resistant colonies harbouring replication of the SGRmJFH1 replicon were then expanded and screened. One clone (clone # 16) displaying homogenous NS5A staining was named "subgenomic replicon cells" and chosen for further experiments. This cell line was kindly provided by Nick Eyre (Eyre et al., 2016).

2.4.11 Mouse embryonic fibroblast cells (MEFs)

Viperin KO MEFs were derived from viperin deficient mice generated by CRISPR/Cas9 technology (Van der Hoek et al., 2017). Genomic analysis confirmed disruption of the viperin locus. Wild type MEFs from the original inbred C57BL/6 mouse strain were used as a control.

2.5 HCVcc Infectious System

2.5.1 Generation of HCVcc viral stocks

2.5.1.1 Preparation of HCV RNA

To generate the HCV Jc1 stock, 5 μg of plasmid containing HCV clone (pJc1) was digested with the *Mlu*I at 37°C overnight. HCV RNA was synthesised using a T7 High Yield RNA Synthesis Kit (New England Biolabs® Inc) as per manufacturer's instruction. The RNA synthesis mixture was prepared in a pre-chilled PCR tube and comprised of 2

µl of each ATP, CTP, GTP, UTP, 2 µl of 10× Reaction Buffer, 2 µl of T7 RNA polymerase enzyme and 1 µg of digested plasmid DNA in a total volume of 20 µl. The preparation was thoroughly mixed and incubated at 37°C for 3 hr. After incubation, samples were subsequently treated with 1 µl (2 Units) of TURBO DNAseTM (Ambion®) for 15 min at 37°C. Reactions were then transferred to a new pre-chilled RNAse free microcentrifuge tubes to perform RNA extraction using a standard protocol as previously described in section 2.1.10). The concentration of RNA was measured using a UV spectrophotometer Nanophotometer® (IMPLEN) and RNA integrity was checked by 1% agarose gel electrophoresis.

2.5.1.2 HCV RNA transfection

Huh-7.5 cells were cultured in two 175 cm^2 flasks until they were 80-90% confluent. Cells were harvested by trypsinisation and washed twice with 10 ml of Opti-MEM. Cells were then counted and resuspended in Opti-MEM at a concentration of 1×10^7 cells/ml. 0.4 ml of cell suspension was aliquoted per electroporation cuvette (Gene Pulser® cuvette), 10 µg of RNA was then added and the suspension was gently mixed. Electroporation was performed with a single pulse at 0.27 kV, 100 Ohms and 960 µF using a Gene Pulser XcellTM (BioRad). Electroporated-cells were then immediately plated into 175 cm^2 flasks containing 20 ml of fresh complete culture media. Cells were cultured for 2-10 days post-transfection and subcultured into new culture flasks when cells approached confluence. Virus-containing supernatants were collected at approximately 5 days post-transfection.

2.5.1.3 Concentration of HCV viral stocks using PEG precipitation

Virus-containing supernatants were transferred into 50 ml disposable centrifuge tube and adjusted to 40 ml with complete culture media. 10 ml of 40% (w/v) polyethylene glycol (PEG) in PBS (MW: 8000, Sigma) was added to give a final concentration of 8% (w/v). Tubes were then mixed well by inversion and incubated at 4°C overnight. Tubes were centrifuged at 3,900 × *g* for 30 min at 4°C and the supernatant was then discarded. The virus-containing pellets were resuspended in 1-2 ml complete media. Concentrated viral stocks were aliquoted into screw cap microcentrifuge tubes and stored at -80°C. Viral titres were calculated as described in 2.5.1.4.

2.5.1.4 Titration of infectious virus – Focus Forming Assay (FFA)

Infectious HCV stocks were titrated using focus forming assays. Huh-7 cells were seeded at 2×10^4 cells/well into 96-well trays. The next day, the PEG precipitated viral stock was serially diluted ten-fold in fresh culture media, to a final dilution of 1 in 10,000. Culture media were removed from near confluent Huh-7 cells and replaced with 40 μl of inoculum (in duplicate for each dilution). The cells were then cultured for 3 hr, washed once with PBS and replaced with fresh complete culture media. The cells were cultured for a further 3 days. At 3 days post-infection, cell monolayers were fixed with 100 μl of ice-cold Acetone:Methanol (1:1), incubated at 4°C for 15 min and subsequently labelled by immunostaining (see section 2.6.4) using anti-HCV antisera or purified antibody (prepared as previously described in (Eyre et al., 2009). HCV-positive cells were visualised by fluorescence microscopy (Nikon Eclipse *TiE* fluorescence inverted

microscope). The foci of HCV-positive cells were counted in each well (average duplicates). The viral titre was calculated using the following formula:

Titre [focus forming units (ffu/ml)] = Number of foci x dilution factor x 25

2.5.2 General protocol for HCVcc infection

Huh-7 cells were seeded at 7×10^4 cells in 12-well culture tray and subsequently infected with HCV Jc1 virus at MOI 0.1-1 in a 300 µl volume of complete media for 3 hr. Infected-cells were then washed twice with PBS and returned to the incubator for 24 hr before cells were harvested for mRNA quantification (real time RT-PCR) experiments or immunofluorescence analysis.

2.6 Fluorescence Microscopy

2.6.1 Coverslip preparation

Coverslips were used for high-resolution imaging. Coverslips were sterilised and then placed in 24-well tissue culture trays. Coverslips were then coated with 0.2% gelatin in PBS and incubated for 20 min, followed by washing once with PBS before seeding cells.

2.6.2 Acetone/Methanol fixation

To prepare Acetone:Methanol (1:1, v/v) fixative solution, an equal volume of Acetone (Ajax Finechem Pty Ltd) and analysis grade Methanol (Merck) were mixed well and stored at -20°C. Cell monolayers were washed with 1× PBS and then fixed with ice-cold acetone/methanol solution for 5-10 min at 4°C. Fixative solution was then discarded, and

cells were washed 3 times with PBS. Fixed cells were kept in PBS at 4°C before immunofluorescence labelling (see section 2.6.4).

2.6.3 4% Paraformaldehyde fixation

Cell monolayers in tissue culture trays were washed with 1× PBS and then fixed with ice-cold 4% paraformaldehyde (w/v) (see Appendix II) for 20 min at RT. The fixative solution was discarded and cells were then washed 3 times with 1× PBS. Cells were subsequently permeabilised by adding 0.1% Triton-X 100 (Sigma-Aldrich) in PBS followed by incubation at RT for 10 min.

2.6.4 Immunofluorescence labelling

Immunofluorescence labelling was performed after fixation (see section 2.6.2 and 2.6.3). Fixed cells were first blocked with 5% BSA in PBS (see Appendix II) for 1 hr at RT and then washed 3 times with PBS. Cells were labelled with primary antibody (see Appendix III) diluted in 1% BSA in PBS (see Appendix II) for 1 hr at RT. After washing 3 times with PBS, an appropriate dilution of fluorescence-conjugated secondary antibody (see Appendix III) was added to the wells and samples were incubated for 1 hr in the dark at RT. Following labelling, samples were washed 3 times with PBS. Where necessary, cells were also stained with the nuclear stain DAPI (see section 2.6.5) for 1 min in the dark. Cells were finally washed 3 times with PBS and samples were stored in PBS at 4°C or mounted on microscope glass slides (see section 2.6.6). Samples were visualised using a Nikon Eclipse *TiE* fluorescence inverted microscope and images were captured using NIS Elements software.

2.6.5 DAPI nuclear staining

DAPI nuclear staining was normally performed after immunofluorescence staining. The 4', 6-Diamidino-2-phenylindole (Sigma-Aldrich) stock solution (1 mg/ml) was diluted 1:1,000 in dH_2O to a final concentration of 1 μg/ml and added to the cells for 1 min. Cells were then washed 3 times with PBS. Samples were stored at 4°C prior to fluorescence microscopy visualisation.

2.6.6 Slide mounting

After staining, coverslips were mounted on glass slides using ProLong® Gold antifade reagent (Invitrogen) or the SlowFade® Antifade Kit (Invitrogen™, Life Technologies). A half-drop of antifade reagent was placed on a glass slide. Coverslips, coated in a cell monolayer, were placed cells down towards the mounting reagent on the glass slide. After leaving the mounting reagent to dry for approximately 15-20 min, coverslips were sealed using clear nail polish before visualising using a fluorescent microscope or storage at 4°C, in the dark.

2.6.7 Microscope specification

Immunofluorescent stained samples were visualised using a Nikon TiE inverted fluorescence microscope and images were captured using NIS Elements software.

2.6.8 Deconvolution

Deconvolution is a computationally intensive image processing technique for improving the contrast and resolution of immunofluorescence images captured using a fluorescence

microscope. Immunofluorescence images were initially acquired over a z-stack comprising 50 to 70 images (0.1-0.25 μm Z-steps), taking into consideration a medium background and a limited number of iterations (10). Deconvolution was performed after z-stacks using the NIS-A Blind Deconvolution WF module of NIS-Element Advanced Research v 3.22.14 software (Nikon).

2.7 Three Dimensional-Structured Illumination Microscopy (3D-SIM)

3D-SIM images were acquired at the Microbial Imaging Facility (The University of Technology Sydney). 3D-SIM was implemented using a V3 DeltaVision OMX 3D-SIM system fitted with a Blaze module (Applied Precision, GE Healthcare, Issaquah, USA). Solid-state multimode lasers provided wide-field illumination and multi-channel images were captured simultaneously using a × 60 1.4 numerical aperture UPlanSApo objective (Olympus, Toyko Japan), standard filter sets and a scientific CMOS 512 × 512 pixels 15-bit camera (pco.edge, PCO AG, Kelheim, Germany). Interference patterns were made by interfering light beams (Strauss et al., 2012). Specimens were sectioned using a 125-nm z-step and images were deconvolved using SoftWorX software (Applied Precision, GE Healthcare).

Image Analysis: Wide-field, deconvolved or f3D-SIM images were rendered and analysed using IMARIS software (v7.7 or above, Bitplane Scientific). Final images were processed using linear adjustments to signal contrast and brightness without alteration of gamma settings and prepared using Photoshop software (Adobe Systems, San Jose, CA, USA).

2.8 DAB staining of APEX2-tagged proteins for electron microscopy

Huh-7 cells were seeded at 5×10^6 cells in 150 mm cell culture dishes prior to transfection with 36 μg of APEX2-tagged expression plasmid. Cells were washed twice with cold 1× PBS before fixing with EM fixative (see Appendix II) for 30 min at 4°C with gentle agitation. The fixative reagent was discarded and cells were washed 5 times with cold PBS for 2 min each. Cells were incubated in cold PBS containing 20 mM glycine for 5 min to quench unreacted glutaraldehyde and then washed 5 times with cold PBS for 2 min per wash. SIGMAFAST DAB with Metal Enhance (Sigma-Aldrich) was prepared immediately prior to use by dissolving 1 DAB/Cobalt tablet and 1 Buffer/Urea Hydrogen Peroxide tablet in 5 ml of MilliQ water (scale up as required, ~5 ml/150 mm dish). PBS was removed from cells and replaced with DAB/H_2O_2 solution. Cells were incubated in DAB/H_2O_2 solution for 1-15 min depending on APEX2 expression levels and localisation. Dark colour development was monitored by eye or light microscopy. Following sufficient colour development, DAB/H_2O_2 solution was immediately removed from cells and cell monolayers were washed 5 times with cold PBS for 2 min each. Cells were carefully scraped from dishes and resuspended in cold PBS before transferring to 1.5 ml microcentrifuge tube. Cells were pelleted by centrifugation at 3,000 × *g* for 10 min at 4°C. At Adelaide Microscopy, cells were pelleted by centrifugation at 3,000 × *g* for 5 min, resuspended in 2% osmium tetroxide (Electron Microscopy Sciences) and incubated for 30 min on rotation. Cells were washed 5 times with ice-cold MilliQ water for 2 min each, then resuspended in ice-cold 2% aqueous uranyl acetate and incubated for 30 min with rotation. Samples were dehydrated in a series of cold graded ethanol (70%, 90%, 95% and 100%). Each step was performed twice for 10 min each. Pellets were washed

with anhydrous ethanol for 10 min at RT to avoid condensation, then infiltrated in anhydrous ethanol:resin (1:1) and incubated for 30 min with rotation. Supernatants were removed and pellets were incubated in 100% resin. 100% resin was changed 3 times for at least 1 hr each with one resin incubation step occurring overnight. The resin-embedded sample was polymerised in an oven at 70°C for at least 24 hr. Ultrathin (80 μm thick) sections were cut (Leica Ultracut UTC6) and mounted by a specialist at Adelaide Microscopy. Electron micrographs were acquired using a Tecnai G2 Spirit transmission electron microscope (Adelaide Microscopy, The University of Adelaide).

2.9 Data analysis

All data were statistically analysed using GraphPad Prism 6.

Chapter 3

Understanding the antiviral role of viperin against Hepatitis C virus

3.1 Introduction

The ISG, viperin (*RSAD2*) is a unique and highly conserved protein that is significantly expressed following viral infection. It is able to restrict replication of a broad range of RNA viruses including hepatitis C virus (HCV) (Helbig et al., 2005, Wang et al., 2012), dengue virus (DENV) (Fink et al., 2007, Helbig et al., 2013), Tick-borne encephalitis virus (TBEV) (Upadhyay et al., 2014), respiratory syncytial virus (RSV) (McGillivary et al., 2013), influenza virus (Tan et al., 2012, Wang et al., 2007) and HIV (Nasr et al., 2012). We previously reported that viperin interacts with the vesicle-associated membrane protein-associated protein subtype A (VAP-A), a host pro-viral cellular protein, and the HCV non-structural protein NS5A, a protein essential for HCV replication and virion assembly (Helbig et al., 2011). These interactions occur at sites of HCV replication within the HCV RC and at the lipid droplet (LD) interface, a site known to be important for the assembly of HCV virions. However, the ability of viperin to restrict HCV replication in the context of an HCV replicon strongly suggests that viperin exerts its antiviral effect at the level of RNA replication. Thus, while we have identified that HCV NS5A and the cellular protein VAP-A interact with viperin, our understanding of the precise molecular mechanism(s) of how viperin exerts its antiviral effect remains unknown. VAP-A is a known pro-viral host factor and also binds to the cholesterol recruiting protein oxysterol-binding protein (OSBP) (Wyles et al., 2002). OSBP also plays a role in HCV replication in that it is important for the enrichment of cholesterol in

HCV replication organelles. This raises the question of whether viperin interacts with VAP-A to perturb the function of OSBP in RC formation and ultimately HCV replication. Moreover, high-resolution analysis of viperin localisation at the ultrastructural level is required to better understand its influence on HCV replication organelle morphology and function. Therefore, the aim of this chapter was to determine if viperin's interaction with VAP-A can alter the interaction of VAP-A and OSBP and to investigate the localisation of viperin at the ultrastructural level by electron microscopy (EM) in the context of HCV RC formation.

3.2 Viperin does not require OSBP for its anti-HCV activity

3.2.1 Does viperin expression impact the interaction between VAP-A and OSBP?

Viperin has been shown by our laboratory to colocalise and interact with HCV NS5A and the host HCV pro-viral factor vesicle-membrane-protein-associated protein A (VAP-A) using immunofluorescence and fluorescence energy resonance transfer (FRET) analysis respectively (Helbig et al., 2011). VAP-A is a host protein that is involved in regulation of cholesterol exchange and trafficking (Weir et al., 2001) and has been shown to be important for HCV replication, likely via trafficking of cholesterol to the HCV RC (Tu et al., 1999, Evans et al., 2004, Gao et al., 2004). Moreover, another cholesterol recruiting protein, OSBP, also plays a role in HCV RC formation and integrity, and is recruited to the RC by association with phosphatidylinositol-4-phosphate (PI4P), a product of the activation of phosphatidylinositol 4-kinase III alpha (PI4KA) by HCV NS5A (Wang et al., 2014, Amako et al., 2009). It is thought that OSBP and VAP-A are recruited to emerging HCV replication sites via viral non-structural proteins including NS5A and

NS5B, that are not only involved in HCV replication, but also in the process of membrane remodelling. A summary of the viral and cellular proteins involved in this process are outlined in Figure 3.1 (Chukkapalli and Randall, 2014). Interestingly it was recently demonstrated that the antiviral effector protein, interferon-inducible transmembrane protein 3 (IFITM3), interacts with VAP-A that can, in turn, inhibit the interaction between VAP-A and OSBP leading to disruption of cholesterol homeostasis and inhibition of viral entry (Amini-Bavil-Olyaee et al., 2013). Furthermore, VAP-A and OSBP play an important role in controlling intracellular lipid and cholesterol homeostasis (Wyles et al., 2002, Raychaudhuri and Prinz, 2010), which is required for many viral infections such as influenza A virus (IAV), vesicular stomatitis virus (VSV) and herpes simplex virus (HSV) (Manes et al., 2003, Schroeder, 2010, Veit and Thaa, 2011, Wang et al., 2009b, Gianni and Campadelli-Fiume, 2012). Based on the above observations of an interaction of viperin with HCV NS5A and VAP-A, and the association of VAP-A and OSBP, it is possible that the interaction of viperin and VAP-A may block the association of VAP-A and OSBP to alter RC formation, and therefore impact HCV replication. We therefore investigated the impact of viperin expression on the association of VAP-A and OSBP.

To determine if the association between VAP-A and OSBP is retained in the presence of viperin, we generated a mammalian expression plasmid that contained the OSBP ORF

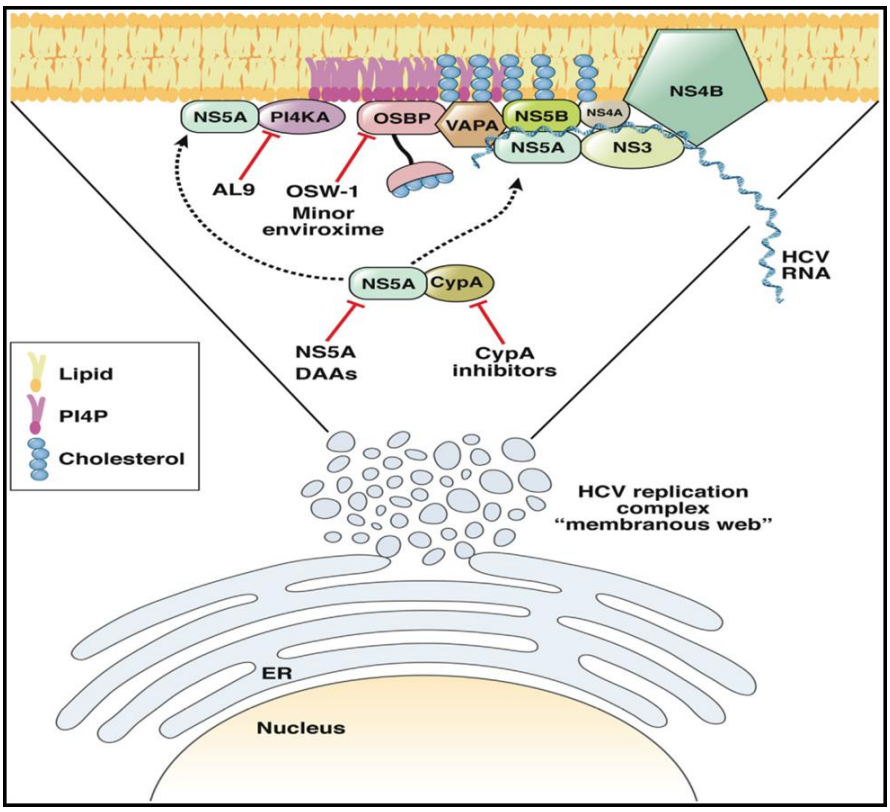

Figure 3.1: HCV membranous web formation.

HCV infection modifies the membrane of the endoplasmic reticulum to generate its replication compartment. HCV nonstructural proteins (NS3-NS5B) and several cellular host factors such as PI4KA, VAP-A and OSBP contribute to HCV RC and membranous web formation (Chukkapalli and Randall, 2014).

fused with a FLAG epitope tag at the N-terminus. The OSBP ORF including the FLAG tag was amplified from the plasmid OSBP-pOTB7 (Thermo Scientific) using specific primers (see Appendix I) and subsequently cloned into pLenti6/V5-D-TOPO. Recombinant plasmids were digested with *Bam*HI and *Mlu*I that revealed release of a ~2.4 kb band confirming generation of successful recombinant plasmids (Figure 3.2). The recombinant plasmids were sequenced and the results demonstrated 100% sequence identity to Homo sapiens OSBP (GenBank accession no. BC011581). Exogenous OSBP expression was confirmed following transfection of pLenti6-OSBP-FLAG into Huh-7 cells and immunostaining using an anti-FLAG antibody (Figure 3.3). As expected, FLAG-positive (and hence OSBP-positive) Huh-7 cells were clearly visible with a perinuclear staining pattern consistent with Golgi localisation, as has been previously described (Amako et al., 2009).

As discussed above, previous studies have shown that viperin associates with VAP-A and NS5A and moreover that VAP-A and NS5A associate with OSBP. Thus, to investigate the hypothesis that viperin may modify the association of VAP-A and OSBP, we transfected Huh-7 cells with various combinations of viperin, VAP-A and OSBP expression constructs to assess localisation/interaction of these proteins. Initially, we transfected Huh-7 cells with plasmids expressing VAP-A-mCherry and OSBP-FLAG, and visualised protein expression accordingly. As expected IF analysis of OSBP and VAP-A revealed significant overlap of fluorescent signals, suggesting co-localisation likely at the ER-Golgi contact sites (Mesmin et al., 2013). In contrast, viperin and OSBP do not co-localise, with the majority of viperin expression localised to the LD as we have

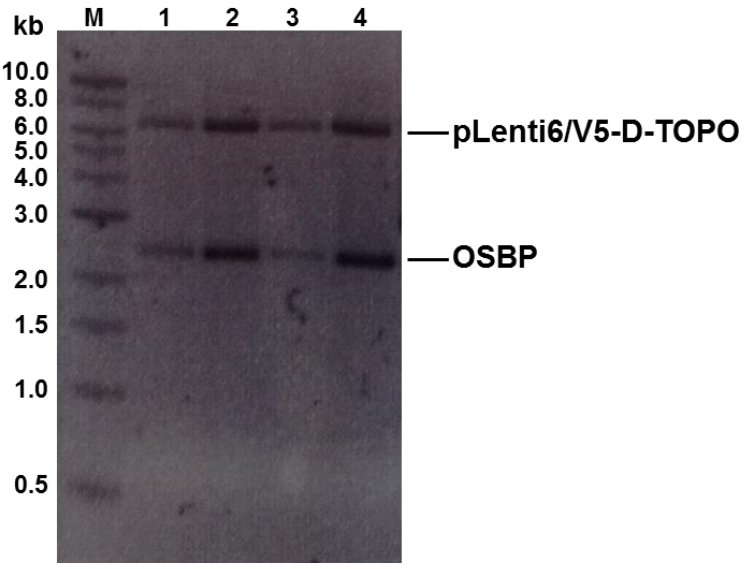

Figure 3.2: The OSBP gene was successfully cloned into pLenti6/V5-D-TOPO.

To confirm the positive clones, plasmid DNA was extracted from transformant clones and digested with *Bam*HI and *Mlu*I. Lane M, 1 kb DNA marker; lanes 1-4, a recombinant plasmid from clone no. 1-4, respectively.

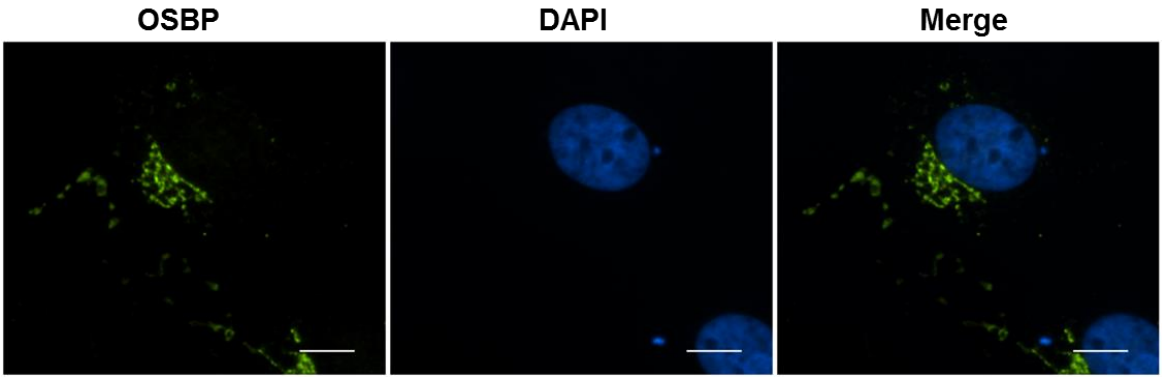

Figure 3.3: Exogenous OSBP expression in Huh-7 cells.

To investigate expression of OSBP-FLAG, Huh-7 cells were transiently transfected with a plasmid expressing OSBP-FLAG for 24 hr prior to immunostaining using mouse anti-FLAG (green) and Alexa Fluor 488-conjugated goat anti-mouse IgG secondary antibody (Ab). Nuclei were counterstained with DAPI (blue) and immunofluorescence images were visualised by immunofluorescence analysis using a Nikon TiE inverted fluorescent microscope (60x magnification). Scale bars are 10 μm.

shown previously (Hinson and Cresswell, 2009a, Helbig et al., 2011). Interestingly, expression of viperin and VAP-A results in co-localisation of the two proteins, that is marked by a significant redistribution of VAP-A from the ER to a perinuclear LD localisation (Figure 3.4). This suggests that while viperin does not interact with OSBP directly it is possible that the interaction of viperin with VAP-A may sequester VAP-A from OSBP to impact HCV replication.

To address this possibility, we transfected Huh-7 cells with plasmids expressing viperin, VAP-A and OSBP and assessed protein expression/co-localisation 24 hr post-transfection. Based on the strong co-localisation of viperin and VAP-A as seen above we hypothesised that viperin would sequester VAP-A from OSBP, however, this was not the case as while an interaction between viperin and VAP-A was evident there was also significant co-localisation of both VAP-A and OSBP. This data indicates that in the context of viperin, VAP-A and OSBP expression, viperin does not alter the interaction between VAP-A and OSBP (Figure 3.5).

3.2.2 Generation of stable OSBP knockdown cells

To further determine the role of OSBP in viperin's antiviral action, OSBP knockdown cell lines were created using a lentiviral vector encoding shRNAs targeting OSBP. 293FT cells were co-transfected with one of each of the 6 clones of pGIPZ OSBP-shRNA or pGIPZ non-targeting shRNA control (NTC) and the essential plasmids for lentiviral packaging. Huh-7 cells were then transduced with the resulting lentiviruses. The stable OSBP knockdown and control cell lines were selected with 3 μg/ml puromycin and

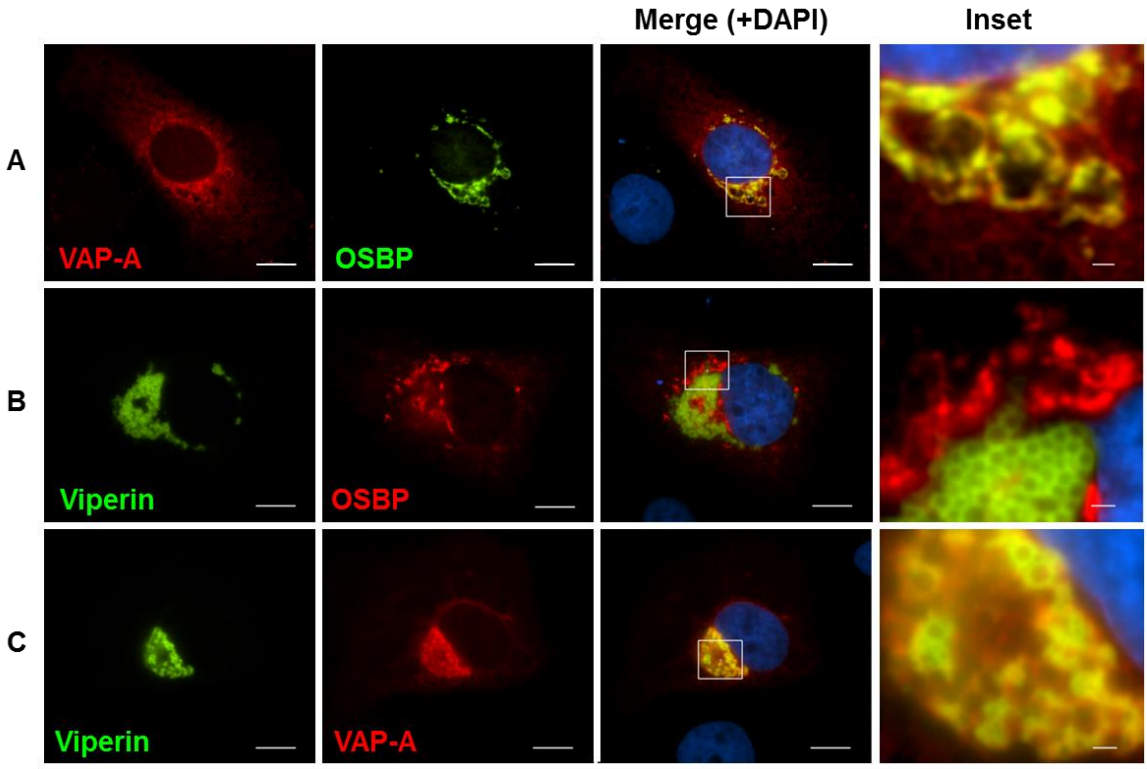

Figure 3.4: Co-localisation of VAP-A, OSBP and viperin.

To investigate the co-localisation of these proteins, Huh-7 cells were co-transfected with a pair of VAP-A-mCherry/viperin-GFP/OSBP-FLAG expression plasmids and returned to culture for 24 hr prior to staining with mouse anti-FLAG and **(A)** Alexa Fluor 488-conjugated goat anti-mouse IgG or **(B)** Alexa Fluor 555-conjugated goat anti-mouse IgG. Nuclei were counterstained with DAPI. Strong co-localisation of **(A)** VAP-A/OSBP and **(C)** VAP-A/viperin, but not **(B)** viperin/OSBP was observed by immunofluorescence analysis using a Nikon TiE inverted fluorescent microscope (60x magnification). Scale bars are 10 μm and 1 μm for main images and inset, respectively.

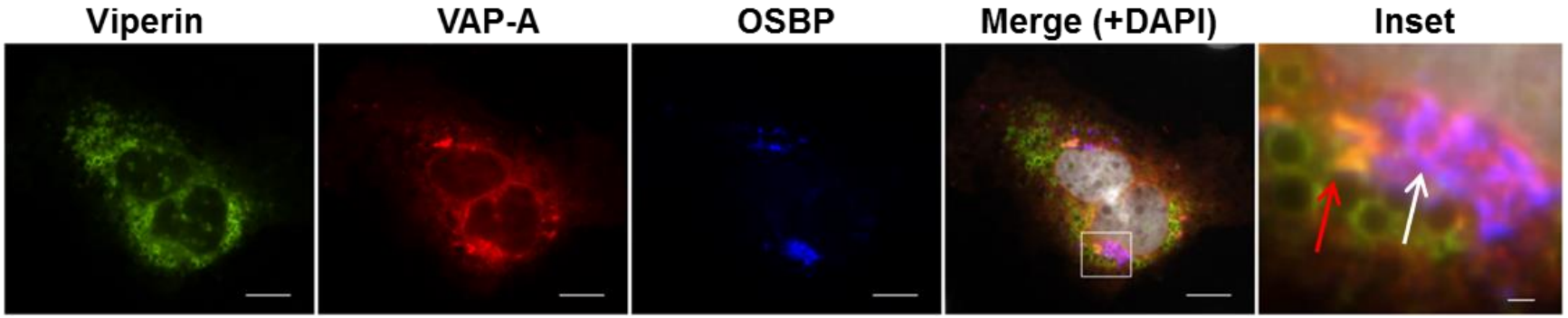

Figure 3.5: VAP-A colocalises with OSBP in the context of viperin expression.

To investigate whether viperin impedes the co-localisation of VAP-A and OSBP, Huh-7 cells were triple transfected with VAP-A-mCherry (red), viperin-GFP (green) and OSBP-FLAG (blue) for 24 hr prior to staining with mouse anti-FLAG and Cy5-conjugated goat anti-mouse IgG secondary Ab. Nuclei were counterstained with DAPI (white). Co-localisation of VAP-A/OSBP and VAP-A/viperin was observed by immunofluorescence analysis using a Nikon TiE inverted fluorescent microscope (60x magnification). Scale bars are 10 μm and 1 μm for main images and inset, respectively. Red and white arrows indicated the co-localisation of VAP-A/viperin and VAP-A/OSBP, respectively.

subjected to Western blot analysis to confirm the endogenous OSBP knockdown. Five clones of stable cell lines were obtained after puromycin selection. Clone no. 2 and 5 showed 82 and 74% knockdown of OSBP compared to the control (NTC) cell line (Figure 3.6).

To further confirm the involvement of OSBP in viral replication, the OSBP knockdown and control cell lines were infected with HCV and DENV, and the effects on viral replication were determined by real time RT-PCR. OSBP knockdown was found to limit HCV replication as shown in Figure 3.7, implying that OSBP is co-opted by HCV but not DENV. This result is consistent with previous reports which showed that OSBP has an impact on HCV replication but is not required for replication of DENV (Amako et al., 2009, Wang et al., 2014).

3.2.3 OSBP does not impact on viperin's antiviral activity.

The OSBP knockdown cell lines (both clones) were utilised to assess the effectiveness of viperin's ability to limit HCV replication in the absence of OSBP through viperin overexpression prior to HCV infection. OSBP knockdown and control cell lines were transfected with a plasmid expressing viperin-FLAG and an empty plasmid control, followed by real time RT-PCR quantification to assess HCV replication. Although, only a slight decrease in HCV replication was observed in the context of viperin overexpression, likely due to the lower transfection efficiency of about 25-30%, there was no difference in the levels of HCV replication in the context of viperin overexpression in OSBP knockdown cell lines (both clones) compared to that of each cell line transfected with

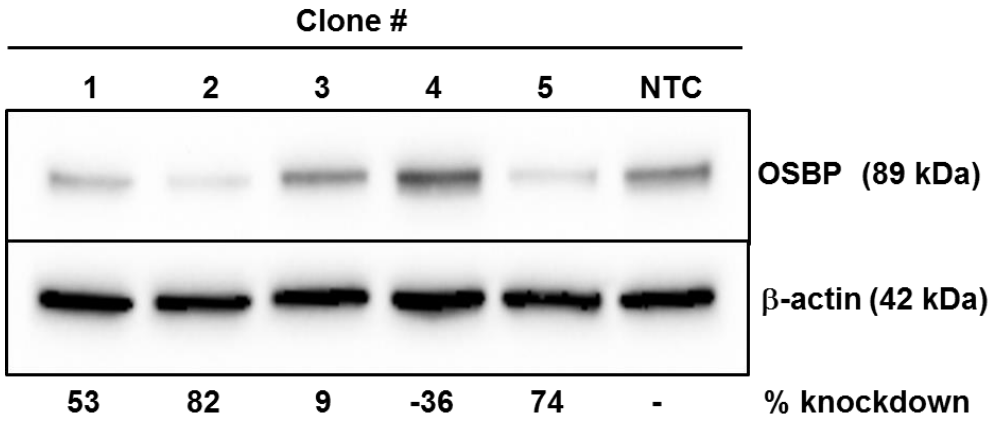

Figure 3.6: Stable OSBP knockdown cell lines.

To confirm knockdown of endogenous OSBP, whole cell lysates of 5 clones of OSBP knockdown cell lines and the non-targeting shRNA control (NTC) cell line were subjected to Western blot analysis using anti-OSBP and anti-β-actin (loading control) antibodies. Clone no. 2 and 5 displayed the strongest OSBP knockdown, with 82 and 74% knockdown efficiencies, respectively, compared to NTC control, following normalisation to the β-actin housekeeping gene control.

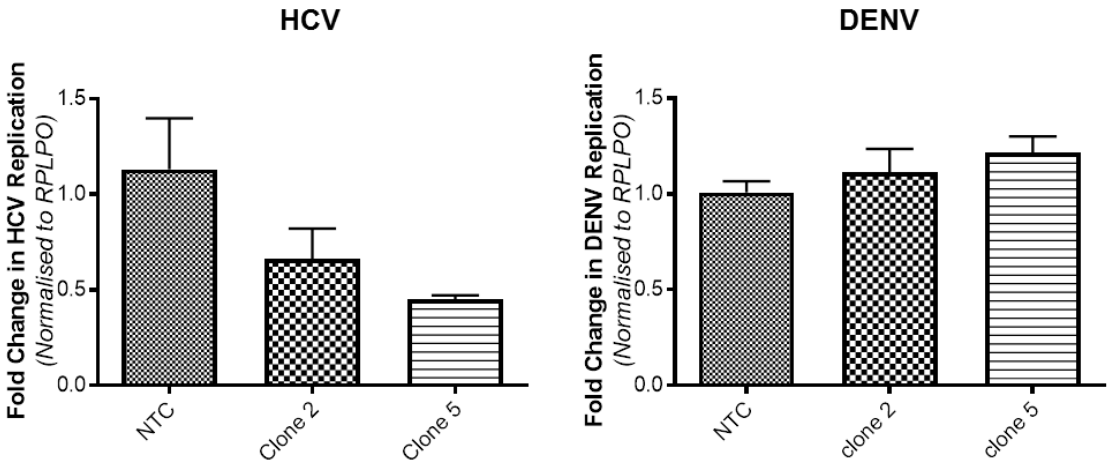

Figure 3.7: The involvement of OSBP in HCV and DENV replication.

To determine whether OSBP is required for HCV and DENV replication, OSBP knockdown (clones # 2 and 5) and control (NTC) cell lines were infected with HCV (1,000 ffu) and DENV (MOI 1) for 24 hr prior to real time RT-PCR analysis. OSBP knockdown resulted in a significant decrease of HCV replication (left bar graph), while there was no effect on DENV replication (right bar graph). Data are means ± SD (n=3).

the empty plasmid control (Figure 3.8). This suggests that OSBP is not required for the effectiveness of viperin in its anti-HCV activity, although further studies are required to definitely resolve whether viperin and OSBP impact on one another's function and the molecular mechanisms involved.

3.3 Visualisation of viperin by EM

3.3.1 Investigation of the cellular localisation of viperin and its impact on HCV membranous web formation.

Our results above suggest that viperin may not exert its antiviral effect through modulating the interaction of VAP-A and OSBP. However, it should be noted that the above interaction studies were performed in the absence of HCV replication. It is possible that in the context of HCV protein expression and the resulting alteration of cellular membranes, viperin, VAP-A and/or OSBP protein localisation may be altered. Given previous work from our laboratory showing an interaction between viperin and NS5A and VAP-A (also this thesis), we next investigated viperin protein localisation in the context of HCV-induced membranous web formation by transmission electron microscopy (TEM). While traditional methods to visualise protein localisation at the ultrastructural level such as immuno-EM have been used successfully to localise proteins to specific cellular compartments, these approaches are hampered by harsh tissue processing, which in many cases destroys fine cellular structures (Sosinsky et al., 2007, Schnell et al., 2012). As such, these approaches are time-consuming, technically challenging and often prone to false positive/negative results. However, this problem has in part been overcome by fusion of a genetically encoded APEX2 tag to the protein of

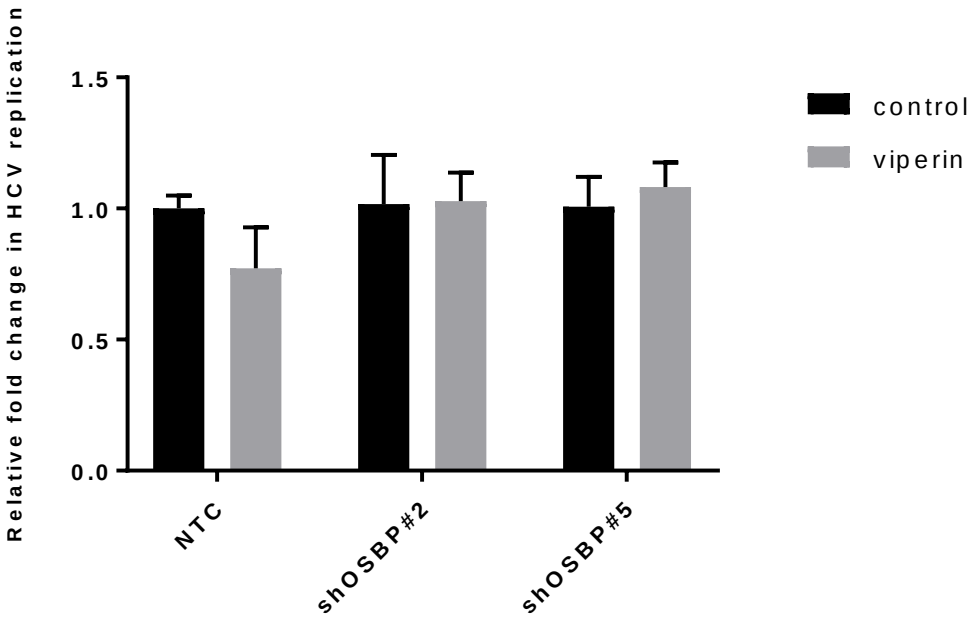

Figure 3.8: Viperin does not require OSBP for its anti-HCV activity.

To determine whether OSBP is required for viperin's ability to limit HCV replication, OSBP knockdown and control (NTC) cell lines were transiently transfected with pLenti6-viperin-FLAG or control plasmids for 24 hr followed by HCV infection (MOI~0.005) for 24 hr prior to real time RT-PCR analysis. The relative fold change of HCV replication in each cell line transfected with a plasmid expressing viperin-FLAG were expressed relative to that of each cell line transfected with the empty plasmid control. There was no significant difference in the relative fold change of HCV replication in the context of viperin expression compared to empty plasmid controls, suggesting that OSBP is not required for viperin's anti-HCV activity. Data are means ± SD (n=3).

interest (Martell et al., 2012). The APEX2 tag consists of a genetically engineered APEX2 peroxidase that can catalyse the conversion of DAB into an osmophilic polymer that can be visualised by TEM following staining with O_SO_4, allowing the location of the target protein with respect to cellular membranes. The insertion of an APEX2 tag allows for TEM studies to be performed using standard EM fixation protocols without the use of cryo-EM, hence resulting in significantly improved ultrastructural cellular morphology. Therefore, we generated a viperin expression construct with an APEX2 tag at the N-terminus that was used to explore the localisation of viperin at the ultrastructural level.

3.3.2 Generation of viperin-APEX2 tag

The APEX2-coding sequence was amplified using specific primers and pcDNA3 APEX2-NES plasmid (addgene # 49386) as a template and subsequently cloned into the pLenti6/V5-D-TOPO plasmid using *Bam*HI and *Xho*I restriction sites. An N-terminal FLAG tag was included to facilitate detection. Candidate clones were digested with *Bam*HI and *Xho*I to confirm the correct size of the inserted gene (813 bp) (Figure 3.9). This pLenti6-APEX2-FLAG plasmid was used as a control for further experiments. We next excised human viperin from pLenti6-viperin-mCherry using *Xho*I and *Sac*II (our laboratory construct) and ligated it into a linearised pLenti6-APEX2 plasmid. Positive transformants were confirmed by digestion with *Bam*HI and *Sac*II (Figure 3.10). The recombinant plasmids were confirmed by Sanger sequencing and showed 100% identities to Homo sapiens radical S-adenosyl methionine domain containing 2 or viperin (Accession no. NM_080657.4) and fused in frame with the APEX2 tag. For the remainder of the thesis, this plasmid will be referred to as pLenti6-viperin-APEX2.

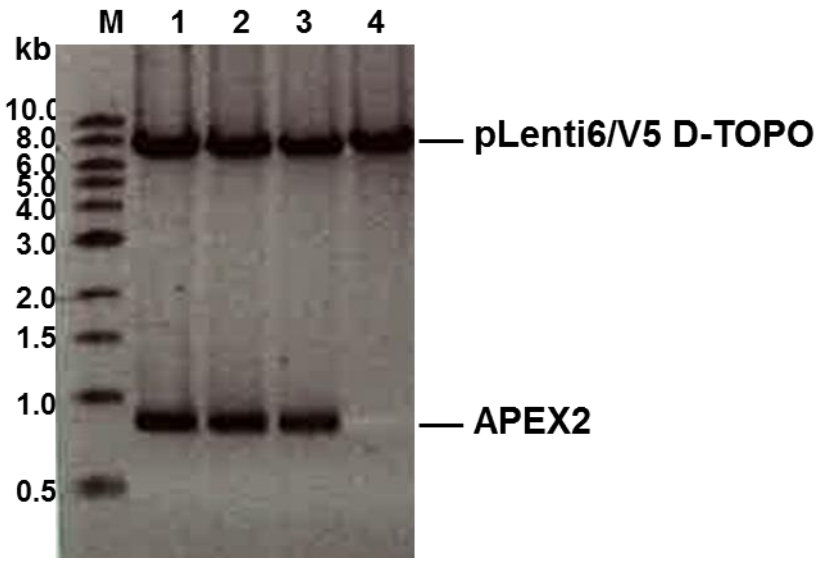

Figure 3.9: Patterns of *Bam*HI and *Xho*I digestion of APEX2 control plasmids.

To confirm the positive clones, plasmid DNA was extracted from transformant clones and digested with *Bam*HI and *Xho*I. Lane M, 1 kb DNA marker; lanes 1-3, a recombinant plasmid from clone no. 1-3, respectively; lane 4, pLenti6/V5-D-TOPO-empty plasmid.

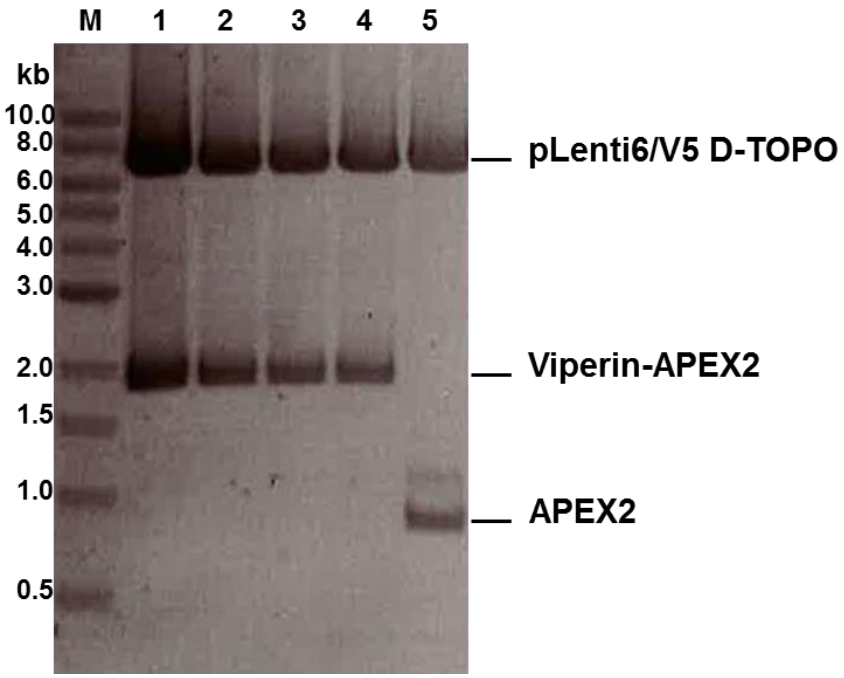

Figure 3.10: Patterns of *Bam*HI and *Sac*II digestion of viperin-APEX2 plasmids.
To confirm the positive clones, plasmid DNA was extracted from transformant clones and digested with *Bam*HI and *Sac*II. Lane M, 1 kb DNA marker; lanes 1-4, a recombinant plasmid from clone no. 1-4, respectively; lane 5, pLenti6-APEX2 control plasmid.

3.3.3 Expression of viperin-APEX2 tag in Huh-7 cells

To confirm expression of the viperin-APEX2 fusion protein, a plasmid expressing viperin-APEX2 was transfected into Huh-7 cells and 24 hr post-transfection cells were fixed, permeabilised and immunostained for the FLAG epitope. Huh-7 cells were also transfected with an expression plasmid expressing the APEX2 tag alone to control for APEX2 expression. As expected, both viperin fused with the APEX2 tag and APEX2 proteins were expressed and located in the cytoplasm as shown by immunofluorescence analysis (Figure 3.11). However, the expression patterns of the two proteins were very different with APEX2 alone revealing an amorphous cytoplasmic distribution, while viperin-APEX2 showed a staining pattern indistinguishable to that of FLAG-tagged viperin, in which viperin associated with the ER and LDs. This suggests that the insertion of an APEX2 tag does not impact the cellular localisation of viperin.

3.3.4 Viperin cellular localisation visualised by transmission electron microscopy (TEM)

APEX2 is a monomeric engineered plant peroxidase that enables simple and specific labelling of tagged proteins via its catalysis of H_2O_2-mediated polymerisation of 3'3'-diaminobenzidine (DAB) into a tightly localised precipitate that gives clear contrast following staining with O_SO_4. However, excessive polymerisation of DAB, and hence increased precipitate, can result in suboptimal resolution of protein localisation. It was therefore necessary to determine the optimal polymerisation time prior to TEM studies. This was achieved by transiently transfecting Huh-7 cells with a plasmid expressing viperin-APEX2 for 24 hr, after which cells were processed for APEX2 staining by

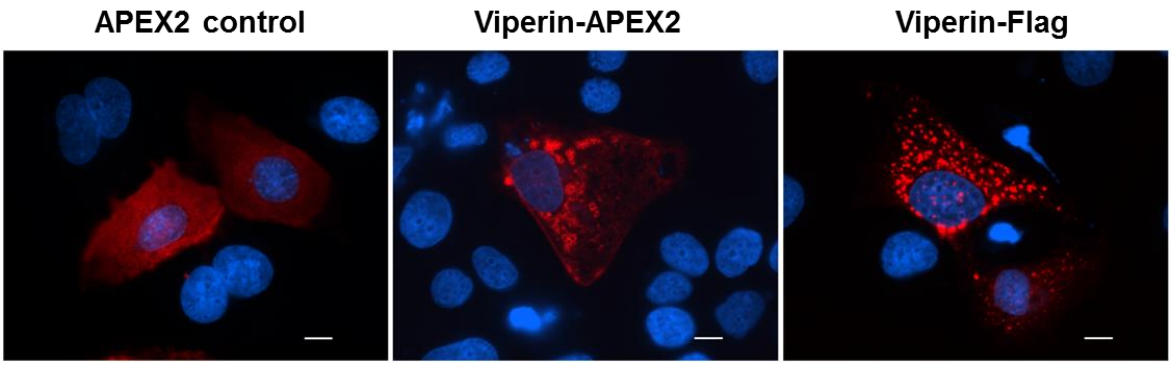

Figure 3.11: Viperin-APEX2 expression in Huh-7 cells.

To investigate the expression of viperin-APEX2 and APEX2 control, Huh-7 cells were transiently transfected with pLenti6-APEX2 control, pLenti6-viperin-APEX2 or pLenti6-viperin-FLAG for 24 hr and protein expression was analysed by immunostaining using mouse anti-FLAG and Alexa Fluor 555-conjugated goat anti-mouse IgG secondary Ab. Nuclei were counterstained with DAPI (blue). Viperin-APEX2 and APEX2 alone were expressed and localised in the cytoplasm. The expression and localisation pattern of viperin-APEX2 was similar to that of the viperin-FLAG (non-APEX2 tag) visualised by immunofluorescence analysis using a Nikon TiE inverted fluorescent microscope (60x magnification). Scale bars are 10 μm.

incubating with DAB for 2, 5, 7, 8, 10 and 12 min. Following this DAB precipitate was visualised by light microscopy. The objective here was to select a time post DAB treatment that allows for optimal EM resolution of DAB precipitates. As revealed in Figure 3.12, there was an appreciable increase in DAB precipitate over the given time course in viperin-APEX2 transfected cells, with 10 minutes determined to be the optimal exposure time for DAB staining.

To visualise the localisation of viperin in Huh-7 cells by TEM, a large scale transfection with pLenti6-viperin-APEX2 was performed in a 150 mm cell culture dish followed by sample preparation for TEM (see Chapter 2, section 2.7). The Huh-7 cell pellet was sectioned and processed by an EM specialist at Adelaide Microscopy. Electron micrographs of both transfected and untransfected cells were acquired using a Tecnai G2 Spirit transmission electron microscope (Adelaide Microscopy). Analysis of multiple fields of view revealed that there were cells positive for the DAB precipitate and thus positive for viperin expression (transfected with pLenti6-viperin-APEX2) and cells negative for DAB precipitate representing untransfected cells. In comparison to viperin negative cells, it was immediately apparent that there was an increase in the number of lipid droplets present within the cell. Furthermore, consistent with immunofluorescence data (Figure 3.13) where Huh-7 cells were transfected with plasmids expressing viperin-GFP and ADRP-mCherry (ADRP, lipid droplet marker), there was a significant localisation of viperin to the outer membrane of the lipid droplet and in some instances there was a strong association of viperin with the LD and the mitochondria (Figure 3.14, see additional EM figures in Appendix XI). This observation is specific for viperin-

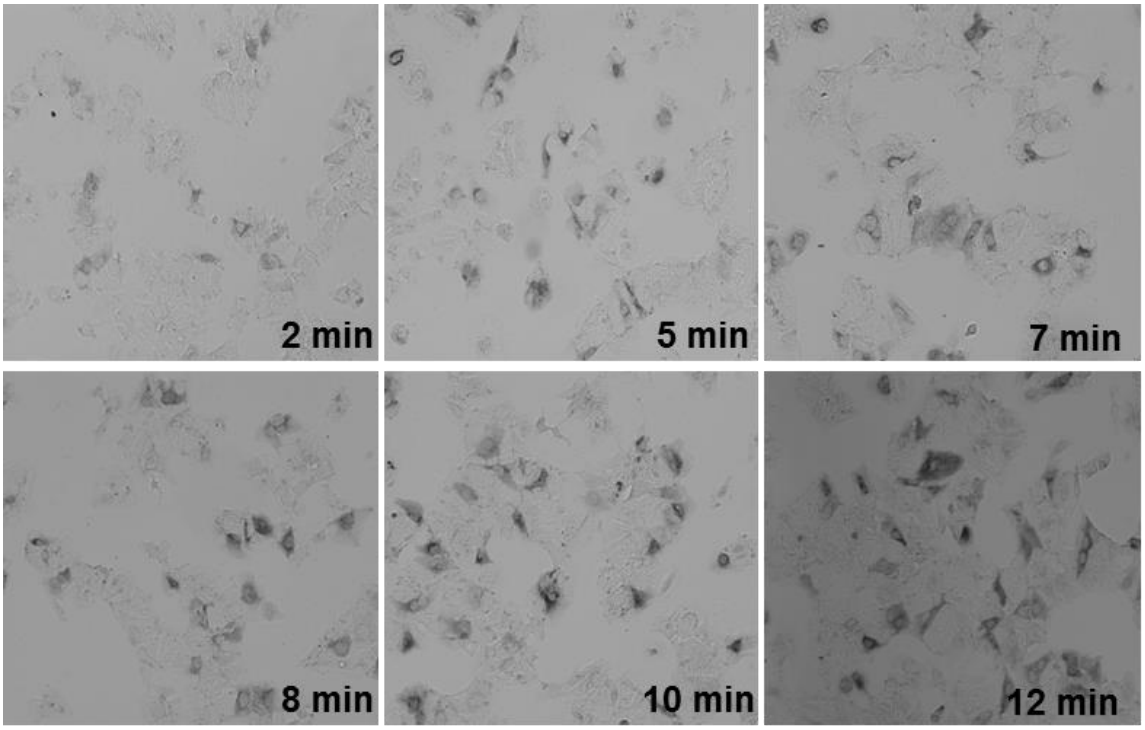

Figure 3.12: Optimisation of DAB staining for EM.

Huh-7 cells were transiently transfected with pLenti6-viperin-APEX2 and returned to culture for 24 hr followed by fixing with EM fixative reagent. Fixed cells were stained with DAB for various time points. Images were visualised by bright field fluorescence microscopy, using a Nikon TiE inverted fluorescent microscope (10x magnification). Note the development of DAB precipitate over time.

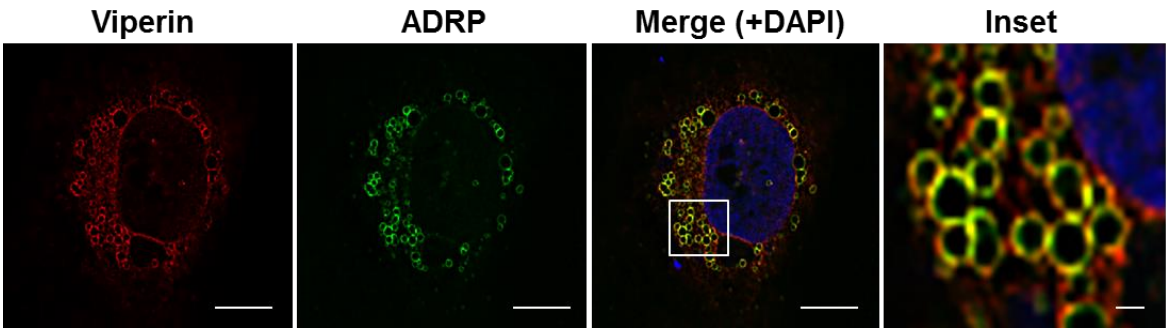

Figure 3.13: Localisation of viperin on LDs.

To investigate whether viperin localises to LDs, ADRP was used as an LD marker. Huh-7 cells were transiently transfected with pLenti6-viperin-mCherry (red) and ADRP-GFP (green), cultured for 24 hr and fixed prior to counterstaining of nuclei with DAPI (blue). Serial (0.25-μm) z-sections of immunofluorescence images were acquired using a Nikon TiE inverted fluorescent microscope and deconvoluted using the 3D AutoQuant Blind Deconvolution plug-in of NIS Elements Advanced Research v 3.22.14 software. Images are single representative z-sections. Strong co-localisation of viperin and the LD marker ADRP was observed using deconvolution fluorescence microscopy (60x magnification). Scale bars are 10 μm and 1 μm for main images and inset, respectively.

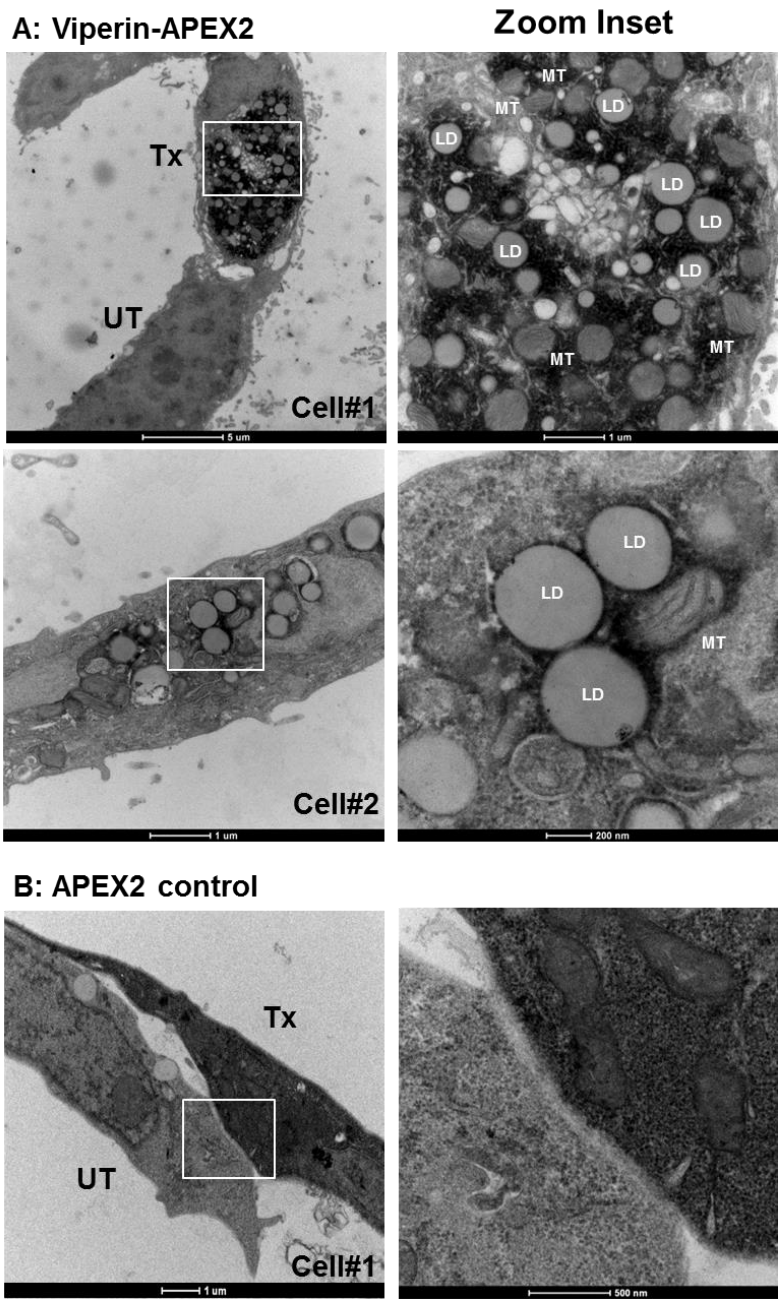

Figure 3.14: An ultrastructural view of viperin localisation.

Huh-7 cells were transiently transfected with viperin-APEX2 and APEX2 control, returned to culture for 24 hr and stained with DAB for 10 min followed by EM sample preparation. **(A)** Viperin-APEX2 and **(B)** APEX2 control were visualised using a Tecnai G2 Spirit transmission electron microscope. Tx, transfected cells; UT, untransfected cells; LD, lipid droplet; MT, mitochondria.

APEX2 expression, as APEX2 expression alone was distributed evenly throughout the cell and did not specifically localise to a specific compartment.

3.4 Viperin enhances lipid droplet accumulation

It was clearly evident in EM and IF images (see Figure 3.13 and 3.14) that in cells expressing viperin, there was a significant increase in the number of LDs. Indeed if the number of LDs increased in viperin expressing cells, we then assumed that neutral lipid would also be increased in the cell. With this assumption in mind, and to indirectly quantify the number of LDs in cells expressing viperin, Huh-7 cells were transfected with pLenti6-viperin-mCherry or pLenti6-mCherry control, and LDs were stained with BODIPY 493/503 prior to cell imaging using an Operetta high-content microscope in non-confocal mode (Perkin Elmer: CeSSA, Cell Screen SA). Image analysis was performed using Harmony software and DAPI staining to detect nuclei was used for cell counts. Approximately 4,000-5,000 cells were counted from each transfection experiment, and the mean of BODIPY 493/503 intensity was analysed per cell. Transfection efficiency derived from the transfection with pLenti6-viperin-mCherry and pLenti6-mCherry control was 25% and 48%, respectively (see raw data in Appendix X). The intensity of BODIPY 493/503 fluorescence per cell in viperin expressing cells was significantly higher compared to cells not expressing viperin. Furthermore, in cells expressing mCherry alone there was no increase in BODIPY 493/503 fluorescence, indicating that the effect was not an artefact of mCherry expression, or the transfection protocol (Figure 3.15). This result suggested that viperin promotes LD formation or accumulation, and may induce the close association of LDs with other organelles, such as

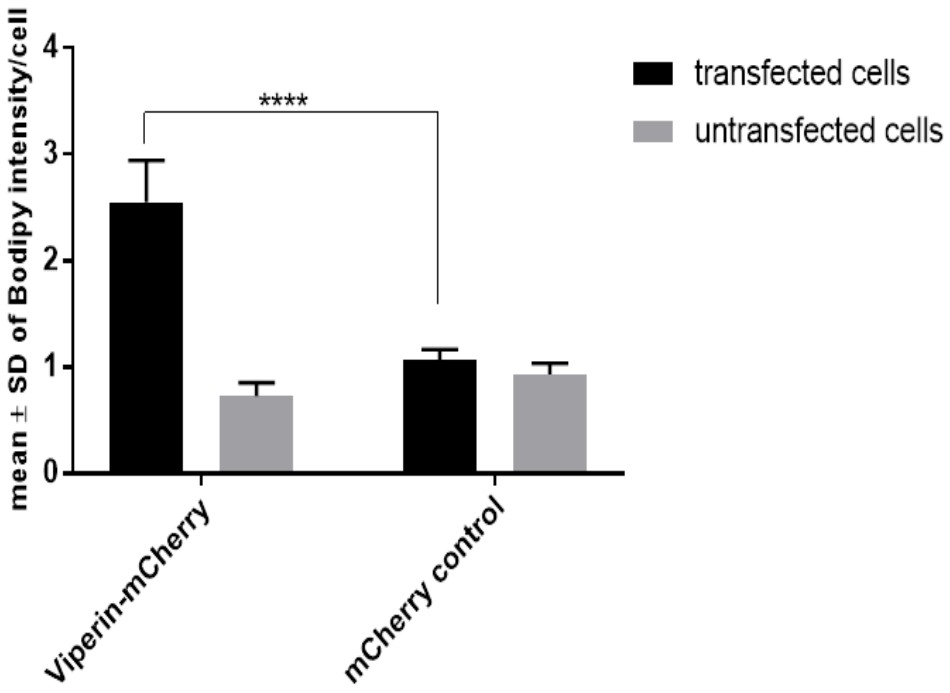

Figure 3.15: Viperin enhances LD accumulation.

To investigate whether viperin increased cellular LD content, Huh-7 cells were transfected with pLenti6-viperin-mCherry or pLenti6-mCherry control. LD staining was quantified following staining with BODIPY 493/503 via imaging using an Operetta high-content microscope in non-confocal mode. 25-fields were taken per well covering about 50% of the well in the central area. This equates to approximately 4,300 cells per analysis. 12 replicates were performed per condition and image analysis was performed using Harmony software. Cell counts were determined by enumeration of DAPI stained nuclei. The BODIPY 493/503 intensities of viperin-transfected cells were approximately two-fold higher than those of mCherry control-transfected cells. Data are means ± SD (n=12). 2-way ANOVA, ****$p<0.0001$

mitochondria. This may be of significance in viperin-mediated enhancement of innate immune signalling to combat viral infection.

3.5 Viperin restricts membranous web formation in a non-replicative model

Although several groups, including our laboratory, have reported that viperin displays its anti-HCV activity by limiting HCV RNA replication (Helbig et al., 2005, Wang et al., 2012), the molecular mechanism(s) that underpins this is poorly defined. As outlined above, the interaction of viperin with NS5A and VAP-A, both HCV RC components, suggests that viperin may alter RC formation and hence impact HCV replication. Therefore, viperin-APEX2 was utilised as a tool to determine the impact of viperin on HCV RC formation. The HCV replicon system provides efficient autonomous replication of HCV in cell culture, and has been used as a model for the molecular study of HCV RNA replication, viral-host interactions and membranous web formation (Blight and Norgard, 2006) and for all purposes would be a good model to study the interaction of viperin with host factors and the impact on viral replication and/or membranous web formation. However, HCV replicon cells are difficult to transfect and furthermore viperin is extremely potent in shutting down HCV replication, making these types of studies difficult in HCV replicon cell lines. Therefore, we adopted a non-replicative model of membranous web formation that is mediated by T7 RNA polymerase-driven NS3-5B polyprotein expression (Tai and Salloum, 2011).

3.5.1 A non-replicative model of HCV membranous web formation

The alteration of host membranes to establish the HCV RC can largely be attributed to expression of the HCV NS4B protein; however, most of the HCV non-structural proteins play some role in this process [reviewed in (Wang and Tai, 2016)]. Therefore it is possible to generate HCV membranous web formation by expressing the HCV non-structural proteins in the absence of HCV RNA replication. This can be achieved using T7 RNA polymerase (T7)-driven expression of the HCV NS3 to NS5B coding region that has been previously described by Tai, AW and Salloum, S (Tai and Salloum, 2011). In this model, a stable Huh-7 cell line expressing T7 RNA polymerase is transfected with a plasmid containing a T7 promoter driving expression of the HCV non-structural proteins. We were gifted two T7 based expression plasmids, one expressing NS3 to NS5B from an HCV genotype 2a [pTM1(NS3-5B)] construct and another that was essentially the same with the exception that the NS5A protein was fused with GFP to allow simple detection of the HCV non-structural proteins. A schematic of these plasmids is presented in Figure 3.16.

Initially, we generated a stable Huh-7 cell line expressing T7 RNA polymerase by retroviral transduction. Cells were selected with puromycin and expanded. To test expression of T7 polymerase, a T7 stable cell line was transiently transfected with pTM1(NS3-5B)/NS5A-GFP, and 24 hr post-transfection cells were visualised for GFP expression using fluorescence microscopy. Huh-7/T7 cell lines revealed GFP expression, indicating expression of T7 RNA polymerase and HCV non-structural protein expression (Figure 3.17). We then investigated the expression of HCV NS3 driven from the plasmid

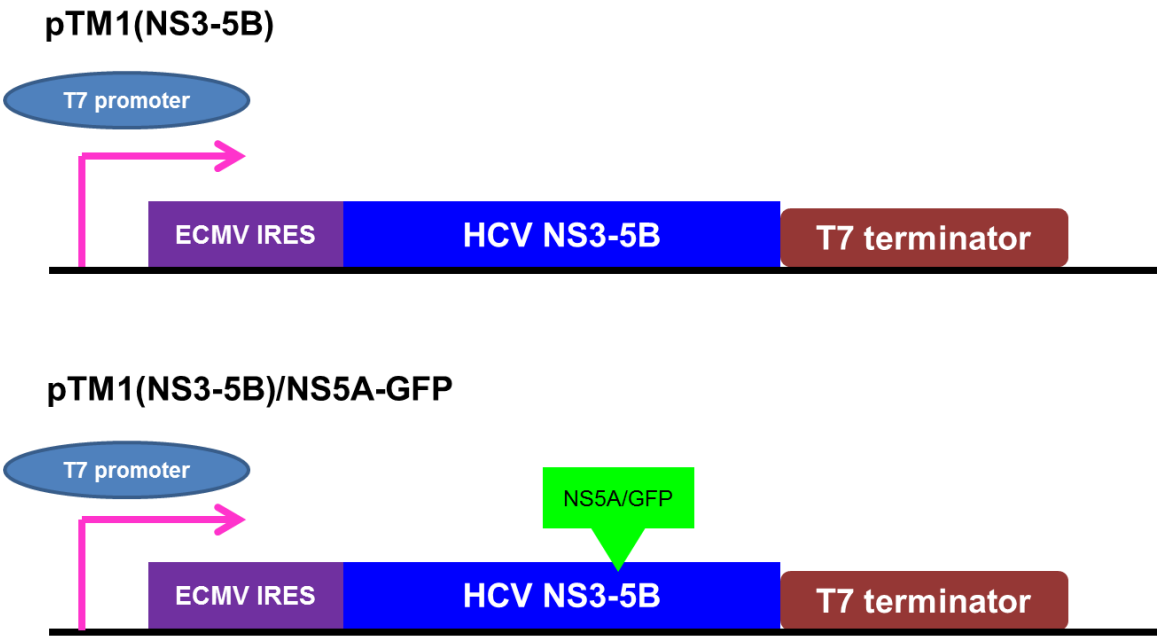

Figure 3.16: Schematic diagram of T7 driving the expression of HCV NS3-5B.
The pTM1(NS3-5B) and pTM1(NS3-5B)/NS5A-GFP constructs were kindly gifted by Tai, AW and Salloum, S (Tai and Salloum, 2011). Expression of subgenomic NS3-NS5B polyprotein with/without GFP insertion at domain III of NS5A is under the control of a T7 promoter.

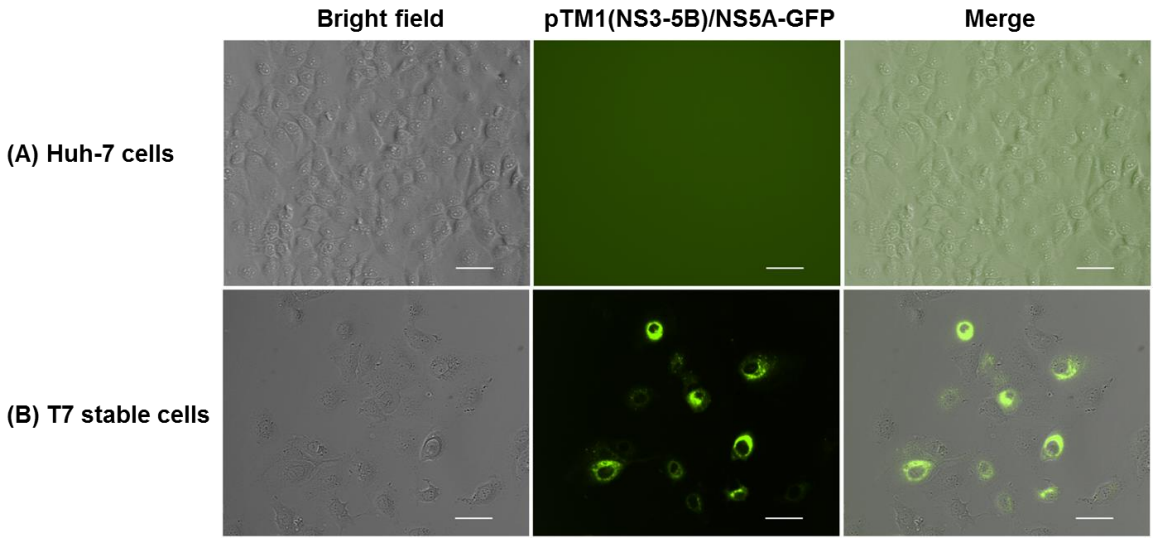

Figure 3.17: Expression of pTM1(NS3-5B)/NS5A-GFP in the T7 stable cell line.

To test if the T7 stable cell line carries T7 RNA polymerase enzyme integration, Huh-7 cells and the T7 stable cell line were transiently transfected with pTM1(NS3-5B)/NS5A-GFP. Strong GFP expression which indicates the presence of T7 RNA polymerase was observed in **(B)** the T7 stable cell line but not in **(A)** Huh-7 cells by fluorescence analysis using a Nikon TiE inverted fluorescent microscope (20x magnification). Scale bars are 50 μm.

pTM1(NS3-5B)/NS5A-GFP. Following transfection, NS3 was visualised by immunofluorescence microscopy using an antibody directed to NS3 (mouse monoclonal clone 2E3, BioFront Technologies). Clearly, NS3 was expressed and furthermore, there was co-localisation with NS5A (GFP tag) in large and small puncta that represent HCV RC (Figure 3.18) (Tai and Salloum, 2011). This system was to be employed in analysis of the impact of viperin expression on HCV-induced membrane rearrangements in the absence of potentially confounding effects of viperin on HCV RNA replication.

3.5.2 Viperin blocks formation of the altered cellular membranous web.

Previously published studies from our laboratory have shown that HCV NS5A interacts with viperin as determined by IF and FRET analysis. In a productive HCV replication system, this interaction occurred at the LD interface as well as the RC (Helbig et al., 2011). Therefore, prior to investigation of viperin localisation by EM in the context of membranous web formation, we evaluated the interaction of viperin with NS5A in the absence of RNA replication using the pTM1(NS3-5B)/NS5A-GFP system by immunofluorescence microscopy. Co-transfection of pLenti6-viperin-APEX2 and pTM1(NS3-5B)/NS5A-GFP into stable T7 expressing cell line and subsequent IF analysis revealed significant overlap of viperin and NS5A fluorescent signal indicating co-localisation of both viperin and NS5A (Figure 3.19).

To further investigate if viperin alters membranous web formation at the ultrastructural level, large-scale transient co-transfection of T7 stable cells with a plasmid expressing

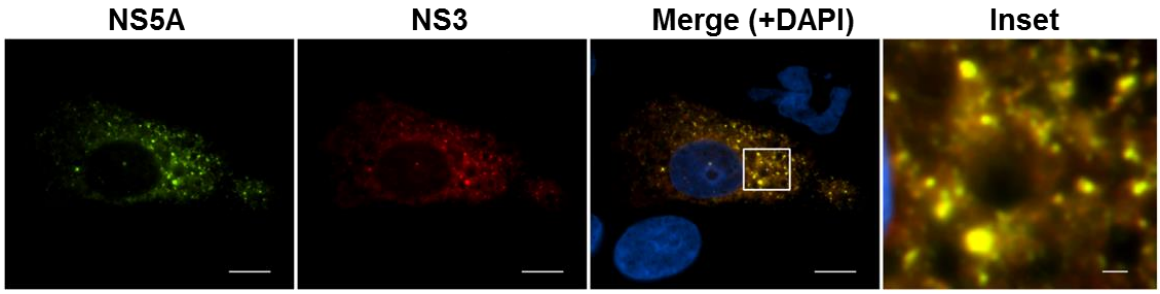

Figure 3.18: pTM1(NS3-5B)/NS5A-GFP expression results in NS3 and NS5A production.

To test that the non-replicative model is able to produce an essential polyprotein (NS3-NS5B) for membranous web formation, T7 stable cells were transiently transfected with pTM1(NS3-5B)/NS5A-GFP prior to staining with mouse anti-NS3 and Alexa Fluor 555-conjugated goat anti-mouse IgG secondary Ab. A strong co-localisation of NS5A and NS3 was observed by immunofluorescence analysis using a Nikon TiE inverted fluorescent microscope (60x magnification). Scale bars are 10 μm and 1 μm for main images and inset, respectively.

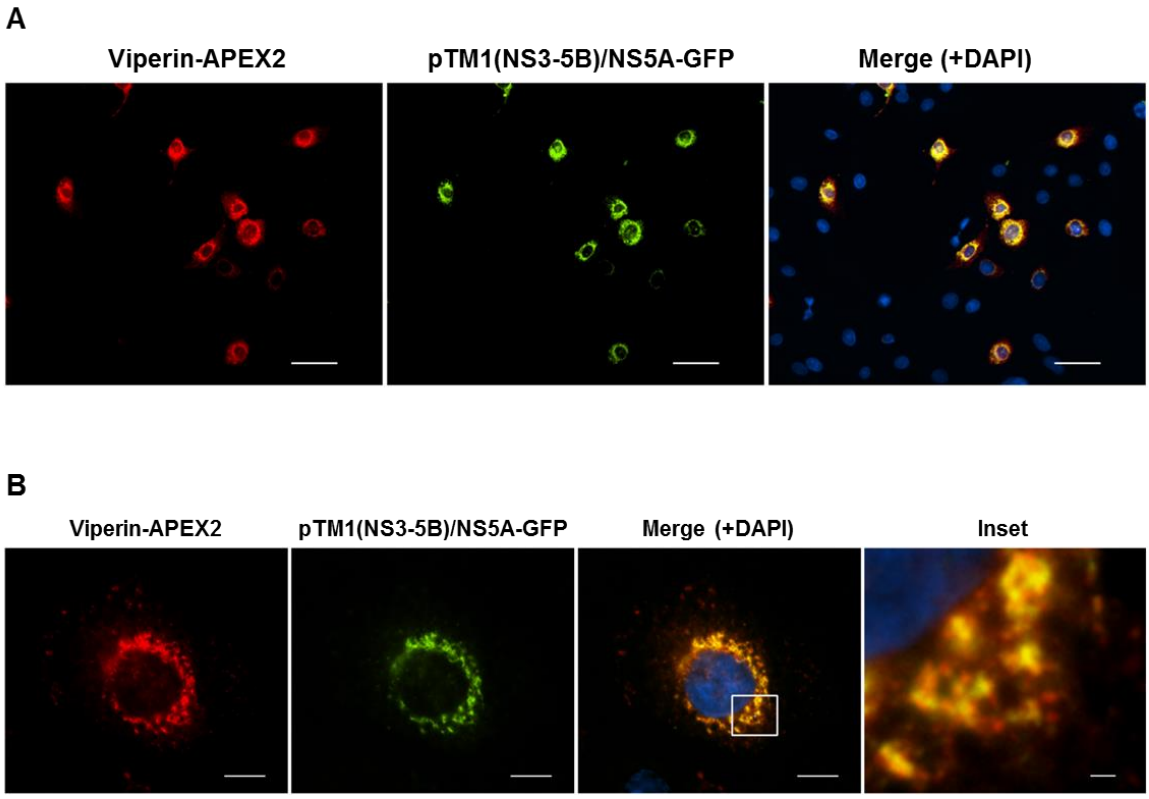

Figure 3.19: Co-localisation of viperin and NS5A.

To test that viperin colocalises with NS5A in the non-replicative model, T7 stable cells were co-transfected with pTM1(NS3-5B)/NS5A-GFP and viperin-APEX2 prior to staining with mouse anti-FLAG and Alexa Fluor 555-conjugated goat anti-mouse IgG secondary Ab. Co-localisation of viperin and NS5A was observed by immunofluorescence analysis using a Nikon TiE inverted fluorescent microscope. **(A)** 20x magnification and scale bars are 50 μm. **(B)** 60x magnification and scale bars are 10 μm and 1 μm for main images and inset, respectively.

viperin-APEX2 and pTM1(NS3-5B)/NS5A-GFP was performed in 150 mm dish prior to EM sample preparation as previously described in section 3.3.4. Co-transfection of a plasmid expressing APEX2 control and pTM1(NS3-5B)/NS5A-GFP was used as a control. As shown in Figure 3.20, no membranous web formation was observed in ectopic viperin-expressing cells, while single-, double- and multi-membrane vesicles (SMV, DMV, MMV) were observed in APEX2 control expressing cells. To confirm that no membranous web formation was present in viperin-transfected cells, all cells (~30 cells) in a grid EM sample were explored and there was no discernable membranous web formation in any cells. This indicates that viperin disrupts the formation of membranous webs, the sites of viral replication.

3.6 Discussion

HCV infection is a major health problem worldwide and there is currently no vaccine to protect from HCV infection. Although highly effective direct-acting antiviral drugs (DAAs) have been developed and approved, these therapies are costly and not available for all patients, particularly in developing countries. Therefore, many studies have attempted to understand the complete mechanisms of the viral life cycle and to investigate at the molecular level how host antiviral responses function to combat HCV infection. A more detailed understanding of host-virus interactions will facilitate development of improved anti-HCV agents that can be available for all patients and eventually reduce the burden of the disease. Since the ISG viperin was identified and shown to be a potent antiviral factor against a broad range of viruses (see section 3.1), we therefore aimed to investigate at the molecular level how viperin limits HCV infection.

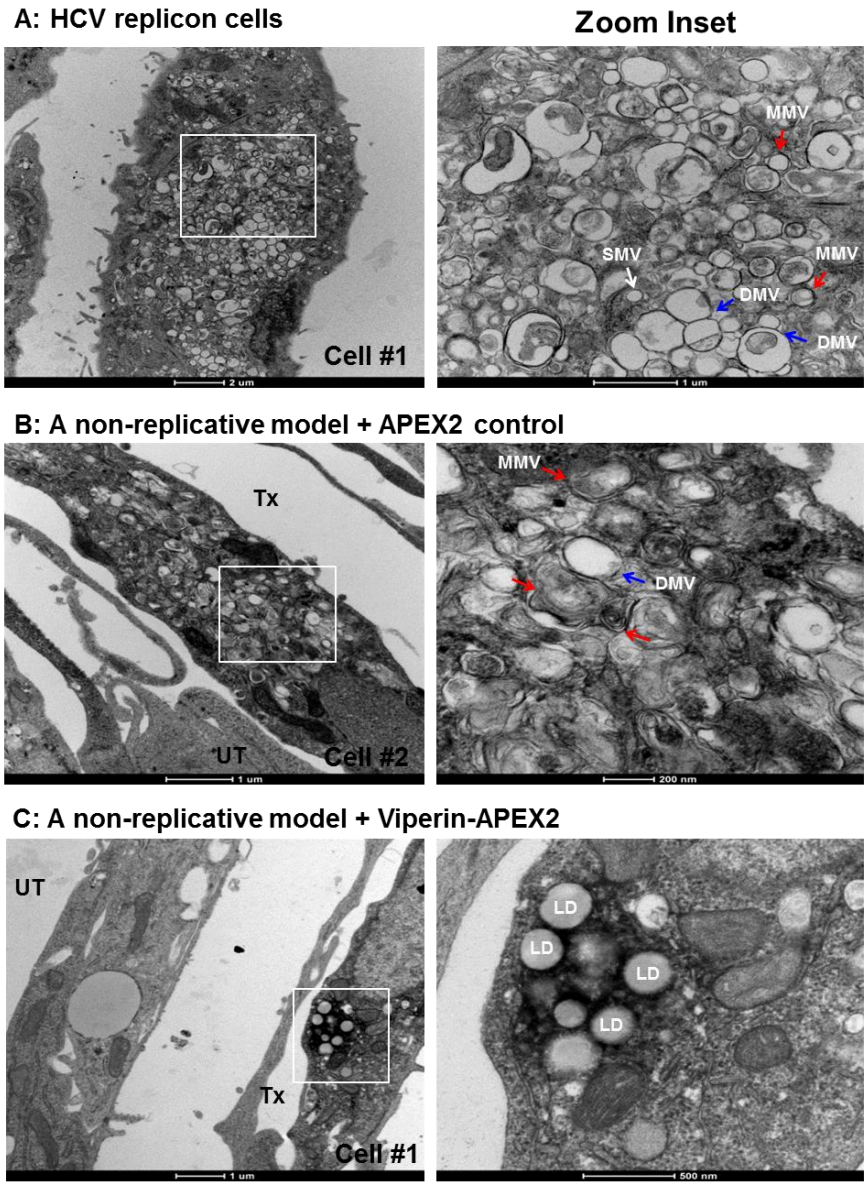

Figure 3.20: Viperin blocks membranous web formation.
To investigate whether viperin restricts the HCV RC, the presence of viperin in a non-replicative model was set up by co-transfecting T7 stable cells with viperin-APEX2 and pTM1(NS3-5B)/NS5A-GFP. Co-transfection of APEX2 control and pTM1(NS3-5B)/NS5A-GFP in T7 stable cells was used as a control. All samples were stained with DAB for 10 min followed by EM sample preparation. EM images of **(A)** HCV replicon cells, **(B)** non-replicative model +APEX2 control and **(C)** non-replicative model + viperin-APEX2 control were visualised using a Tecnai G2 Spirit transmission electron microscope at Adelaide Microscopy, The University of Adelaide. Tx, transfected cells; UT, untransfected cells; LD, lipid droplet. White, blue and red arrows indicate single, double and multiple membrane vesicles (SMVs, DMVs and MMVs) respectively.

Our laboratory has previously reported that viperin co-localises and interacts with the HCV NS5A protein, and a host pro-viral cellular protein (VAP-A) at HCV RC; the sites of HCV replication (Helbig et al., 2011). VAP-A is a well-characterised pro-HCV host factor that plays a role in lipid metabolism and traffic and has been shown to bind to the cholesterol recruiting protein, oxysterol-binding protein (OSBP) (Wyles et al., 2002). Several viral non-structural and host cellular proteins including VAP-A and OSBP have been shown to be important for HCV replication, which is summarised in Figure 3.1 (Chukkapalli and Randall, 2014). Moreover, it is interesting that binding of the antiviral effector protein, interferon-inducible transmembrane protein 3 (IFITM3) to VAP-A results in the inhibition of an interaction between VAP-A and OSBP, that ultimately culminates in the disruption of cholesterol homeostasis and blockade of viral entry (Amini-Bavil-Olyaee et al., 2013). Therefore, it is plausible that viperin may also block the interaction of VAP-A and OSBP to alter the formation of HCV RCs and hence inhibit HCV replication.

Initially, co-localisation of each protein was investigated, and we found that viperin did co-localise with VAP-A, but not OSBP, while as expected VAP-A co-localised with OSBP. It is well-documented that VAP-A is primarily localised to the ER (Skehel et al., 2000, Prosser et al., 2008), while OSBP localises to the Golgi (Amako et al., 2009). We also noted that the localisation pattern of VAP-A changed from ER localisation to viperin-positive LDs upon viperin expression. However, in the context of overexpression of viperin, VAP-A and OSBP in the same cells, we found that VAP-A retains its strong co-localisation with both viperin and OSBP, but note that their co-localisation presented

at different cellular compartments. Specifically, the co-localisation of viperin and VAP-A was strongest at the surface of LDs, while the association of VAP-A and OSBP seemed to be at ER and Golgi contact sites (Figure 3.5), which is consistent with the study of Wyles and colleagues (Wyles et al., 2002). Although VAP-A still co-localises with OSBP in the presence of viperin, this analysis was performed in the absence of HCV infection. Therefore, the interaction of VAP-A and OSBP may be altered in the context of HCV-induced cellular membrane rearrangements (Romero-Brey and Bartenschlager, 2014). Furthermore, VAP-A, along with OSBP has been shown to play roles in lipid metabolism and exchange from the ER to other organelles such as mitochondria, lipid droplets, and the plasma membrane (Raychaudhuri and Prinz, 2010). In addition, host lipids are important for many steps of HCV life cycle including replication, assembly and secretion (Ye, 2007). Consistent with its localisation to the ER and LDs, the antiviral activity of viperin against a diverse set of viruses may be reflective of viperin-mediated alteration of cholesterol/lipid homeostasis through an interaction with the host proviral protein, VAP-A. Viperin induced alteration in lipid raft fluidity has been shown in the case of influenza and HIV infection, in which viperin binding to the host farnesyl diphosphate synthase (FPPs) resulted in disruption of the plasma membrane through perturbing lipid rafts and hence inhibition of viral release from the plasma membrane (Wang et al., 2007, Nasr et al., 2012). Further studies are required to determine whether viperin-mediated alterations of HCV RC lipid content contributes to its antiviral activity against HCV.

To further investigate the potential involvement of OSBP in viperin's antiviral function, an OSBP knockdown cell line was created by shRNA targeting to OSBP. Two OSBP

knockdown cell lines (82 and 74% in clone no.2 and 5, respectively) were successfully generated (Figure 3.6). Infection of these two knockdown cell lines with HCV and DENV resulted in a reduction of HCV replication, while there was no effect on DENV replication. This suggests that OSBP plays a central role in the HCV, but not the DENV life cycle, and this result is consistent with studies by Wang and colleagues (Wang et al., 2014). To further investigate whether OSBP is required for the antiviral activity of viperin, HCV replication was determined in the context of viperin overexpression in OSBP knockdown cell lines. We found that ectopic expression of viperin in the context of depletion of OSBP did not impact HCV replication (Figure 3.8). These results supported the IF analysis in which viperin did not perturb the direct interaction of VAP-A and OSBP. An alternative explanation is that the small amount of remaining OSBP in the shRNA knockdown cells may be sufficient for viperin to exhibit its antiviral activity. Therefore, the association of these three cellular proteins (viperin, VAP-A and OSBP) will be of interest to further investigate in the context of HCV infection. Collectively, our results suggest that the molecular mechanism of viperin to restrict HCV replication is not through direct disruption of the interaction of VAP-A and OSBP. However, the fact that viperin binds to VAP-A and HCV NS5A, and viperin could interfere with the interaction of VAP-A and NS5A (Helbig et al., 2011, Wang et al., 2012), raises the possibility that viperin may instead disrupt the interaction of VAP-A and NS5A, which then, in turn, inhibits membranous web formation to ultimately impair HCV replication.

As previously discussed above, viperin could interrupt the binding of VAP-A and NS5A, leading us to determine the localisation of viperin in the context of HCV-induced membranous web formation and to determine how viperin alters the HCV RC formation

at the ultrastructural level by electron microscopy (EM). Given that specific immuno-labelling in the context of strong ultrastructural preservation is difficult to achieve using traditional immuno-EM approaches, we therefore generated a viperin expression construct with an APEX2 tag for EM purposes (Martell et al., 2012). We successfully created an expression plasmid encoding viperin-APEX2 and performed immunofluorescence analysis following transfection of this plasmid into Huh-7 cells, revealing that the APEX2 tag did not change the localisation of viperin on ER and LDs as the localisation pattern of viperin-APEX2 was similar to that of non-APEX2 tagged viperin (viperin-FLAG) (Figure 3.11). Visualisation of viperin-APEX2 following DAB staining by EM demonstrated that viperin induced LD accumulation. Interestingly it was also apparent that viperin frequently localised to the contact sites of LDs and mitochondria in a number of cells (Figure 3.14 and see additional EM image in Appendix XI). It is possible that viperin may contribute to the transfer of signals from these organelles to amplify innate antiviral responses, and this is further explored in chapters 5 and 6. Moreover, we also observed that viperin induced the formation of crystalloid ER, a specialised smooth ER that consists of multiple membrane tubules packed in a hexagonal form (see EM image of cell no. 8 and 9 in Appendix XI) and this result supports the study by the Cresswell group in which overexpression of viperin was also shown to induce crystalloid ER (Hinson and Cresswell, 2009b). However, to date, the function of crystalloid ER and the mechanism underlying the ability of viperin to induce this specialised structure of the ER is unknown.

Our results showed strong evidence that viperin increased the number of LDs in the context of viperin overexpression in Huh-7 cells (Figure 3.15), in addition to viperin's ability to induce LDs accumulation and enlargement suggested by our EM analysis (Figure 3.14). In contrast, the study by the Cresswell group (Hinson and Cresswell, 2009a) reported that viperin does not alter the number and size of LDs in bone marrow-derived macrophages (BMM) isolated from WT and viperin knockout mice following treatment with oleic acid overnight. However, there were several notable differences between our study and others: 1) different species of viperin, 2) differences in the experimental set-up and 3) different cell types. In our study, human viperin was overexpressed in Huh-7 cells, while the other study assessed the effect of viperin on lipid droplet formation in BMM cells derived from WT and viperin$^{-/-}$ mice. Although it is clear that viperin induced LD accumulation, dysfunction of LDs is associated with alterations in LD biogenesis (Wang and Sztalryd, 2011) which then may affect the viral life cycle. Therefore, the function of viperin-induced LD accumulation in the context of ectopically expressed viperin needs to be further investigated.

The viperin-APEX2 tag offers a useful tool to investigate, at the ultrastructural level, how viperin interacts/associates with HCV RCs. However, due to complications of transfection of plasmids expressing viperin into HCV replicon cells, the HCV membranous web formation without viral replication system (Tai and Salloum, 2011) was employed to investigate the ability of viperin to alter membranous web formation. It is interesting that ectopic expression of viperin completely blocks membranous web formation in the HCV non-replicative model and that LD accumulation was observed

once again in cells expressing viperin-APEX2, while typical virus-induced cellular membrane rearrangements to form membranous factories was clearly seen in cells expressing the APEX2 control (Figure 3.20). This suggests that viperin-induced LD accumulation may be a mechanism underlying antiviral activity. In addition, a previous report has shown that the C-terminus of viperin is a crucial domain that is responsible for its anti-HCV function (Helbig et al., 2011), therefore a series of viperin mutants, particularly C-terminal mutants, with an APEX2 tag would further enable investigation of which domain of viperin is responsible for inhibiting HCV RC/membranous web formation.

In conclusion, viperin displays its antiviral action by inhibiting the formation of the membranous web, pivotal sites of HCV replication. Although the mechanism underlying its antiviral function is likely not through the disruption of VAP-A and OSBP, as both of these factors are important for cholesterol and lipids biogenesis, this raises the possibility that viperin-induced LD accumulation may alter cholesterol and lipid homeostasis in a manner related to the regulated interaction of VAP-A and OSBP. Moreover, several studies have reported that many host pro-viral proteins can bind to viperin, thus we reasoned that a number of host proteins remain to be discovered and this hypothesis will be investigated and described in a subsequent chapter.

Chapter 4

Identification of novel interacting partners of viperin

4.1 Introduction

Viperin has been reported to be a restriction factor for a broad range of viruses, however the molecular mechanism(s) that underpin this restriction are diverse and in some cases are still unclear. As an example, the radical SAM domain is critical for viperin's anti-TBEV activity while this domain is dispensable for its anti-HCV activity (Upadhyay et al., 2014, Helbig et al., 2011). Viperin can bind to a number of host and viral proteins including the host lipid metabolising enzyme FPPS, and the innate immune adaptor molecules TRAF6 and IRAK1 that are key in TLR7 and 9 signalling, the adaptor protein MAVS, and the cytosolic Fe/S Assembly Component 1 (CIAO1) (Wang et al., 2007, Saitoh et al., 2011, Hee and Cresswell, 2017, Upadhyay et al., 2014). Viperin also interacts with viral proteins from HCV (NS5A), DENV (NS3) and HCMV (vMIA) (Helbig et al., 2011, Helbig et al., 2013, Seo et al., 2011). This clearly suggests that viperin has a wide diversity of interacting partners, although to date a systematic investigation of viperin cellular interacting partners has not been conducted. It is likely that many of the interacting partners of viperin remain to be discovered and characterised and this represents a major gap in our understanding of the biology of this important host-virus interaction. Therefore, the aim of this chapter was to identify and characterise novel cellular interacting partners of viperin.

In this study, the well-characterised yeast two-hybrid system (Y2H) was used to identify novel interacting partners of viperin. The Y2H system exploits the nature of the yeast Gal4 transcription factor. This Gal4 protein has 2 domains: a Gal4 DNA-binding domain (DNA-BD); and a Gal4 activation domain (AD). The Gal4 protein binds to an activating sequence (5' to the gene) leading to initiation of gene transcription. In the Y2H system, the 2 domains of the Gal4 protein are divided with the Gal4 DNA-BD fused to a known protein of interest or "bait protein" which, in this study, is viperin. The Gal4-AD is fused to "prey proteins", which are derived from a cDNA library of interest. When a bait protein (viperin-Gal4-BD) interacts with a prey protein (prey-Gal4-AD), the DNA-BD and AD are brought into close proximity that restores GAL4 activity and subsequently leads to transcriptional activation of a reporter gene (Figure 4.1) which in the case of the Y2H system is α-galactosidase that results in blue yeast colonies. As there are four independent reporter genes (*AUR1-C, ADE2, HIS3*, and *MEL1*) under the control of 3 promoters (G1, G2 and M1) in the Matchmaker Gold Yeast Two-Hybrid system (Clontech), the system generates significantly less false positives (Van Criekinge and Beyaert, 1999). Therefore, we used this Y2H system to identify novel interacting partners of viperin. A schematic of the main processes of the Y2H experiment at workflow is shown in Figure 4.2.

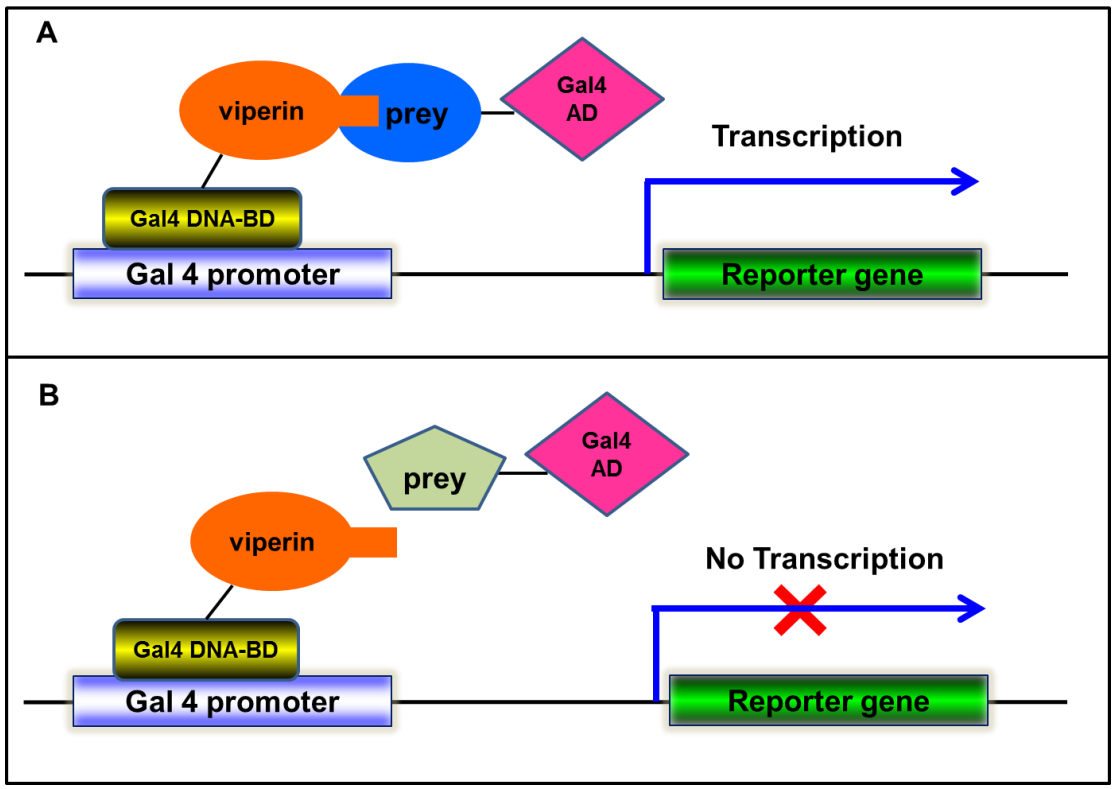

Figure 4.1: Schematic diagram of the yeast two-hybrid principle.

A bait protein (protein of interest; viperin in this study) and prey protein are expressed separately in fusion with Gal4 DNA-BD and Gal4-AD, respectively. (**A**) The interaction of bait and prey protein results in the expression of reporter genes, while (**B**) no interaction does not activate transcription of the reporter genes.

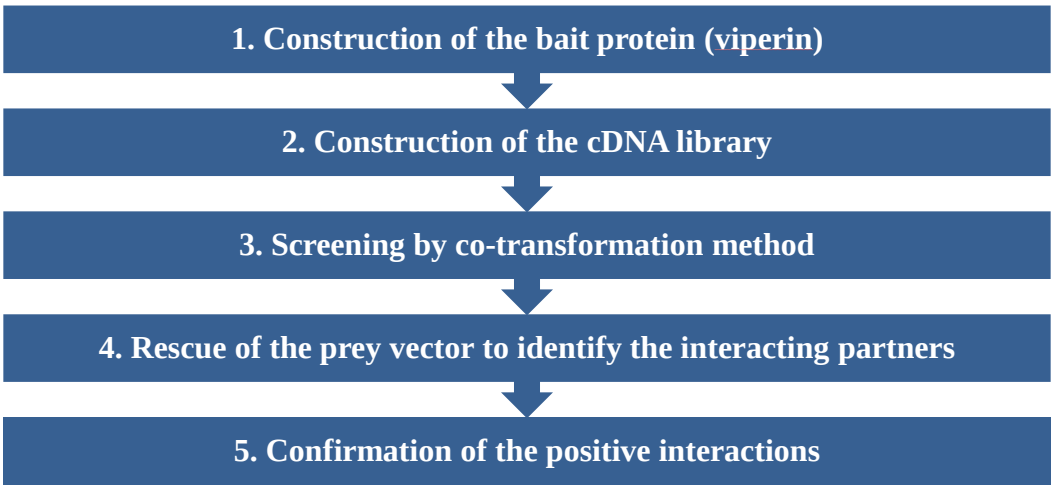

Figure 4.2: The main steps of Y2H experiments.

4.2 Construction and characterisation of the Y2H viperin bait plasmid (pGBKT7-viperin)

4.2.1 Cloning of viperin-coding cDNA sequence into a pGBKT7 plasmid

In order to screen for novel interacting partners of viperin, full-length human viperin (that will act as the bait) was cloned into the plasmid pGBKT7 (see Appendix V for plasmid map). To achieve this, the human viperin cDNA was amplified by PCR using specific primers (Appendix I) and the pLenti6-viperin-Flag plasmid (Helbig et al., 2011) as a template and the PCR amplicon was subsequently cloned into the plasmid pGBKT7. Five bacterial transformants were randomly picked and double digested with *Bam*HI and *Eco*RI to confirm the correct size of the inserted gene. The sizes of linear pGBKT7 plasmid and viperin gene fragments are ~7.3 kb and 1,086 bp, respectively as shown in Figure 4.3. The sequences of the recombinant plasmids were confirmed by Sanger sequencing and all gene-inserts showed 100% identity to Homo sapiens radical S-adenosyl methionine domain containing 2, or viperin, (Accession no. NM_080657.4). The pGBKT7-viperin plasmid was then transformed into competent *Saccharomyces cerevisiae* strain Y2H gold cells and plated on Tryptophan (Trp) dropout (SD/-Trp) selective medium to allow selection of Trp biosynthesis of transformant clones. Five colonies were randomly selected and lysed in 20 mM NaOH for further confirmation via colony PCR to verify the yeast cells contained the expected plasmid (pGBKT7-viperin). The results illustrated that all five clones contained viperin cDNA as shown in Figure 4.4.

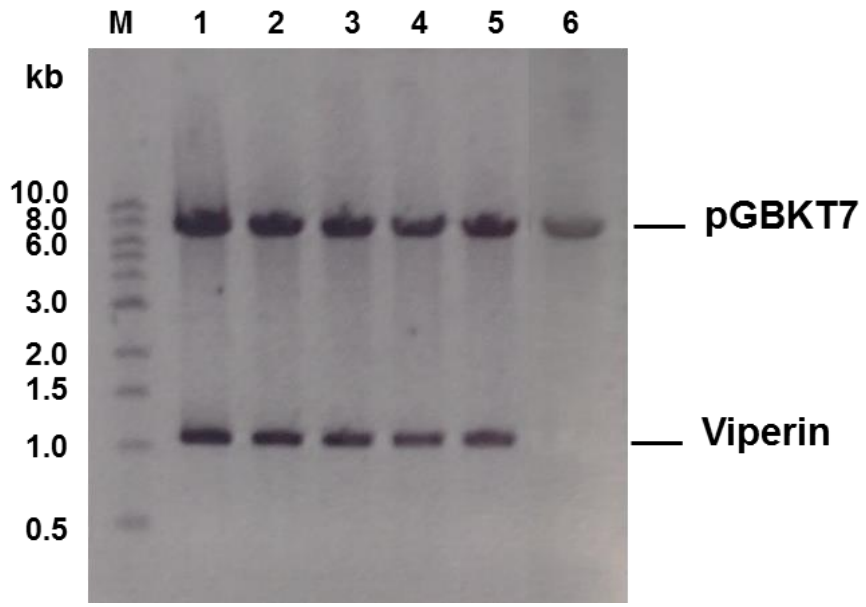

Figure 4.3: Viperin cDNA was successfully cloned into pGBKT7.

Insertion of the viperin cDNA into the plasmid pGBKT7 was confirmed by *Bam*HI/*Eco*RI digestion of plasmid DNA extracted from 5 bacterial transformants. Restriction digests were run on 1% agarose gel. Lane M, 1 kb DNA marker; lanes 1-5, a recombinant plasmid from clone no. 1-5, respectively; lane 6, pGBKT7-empty plasmid.

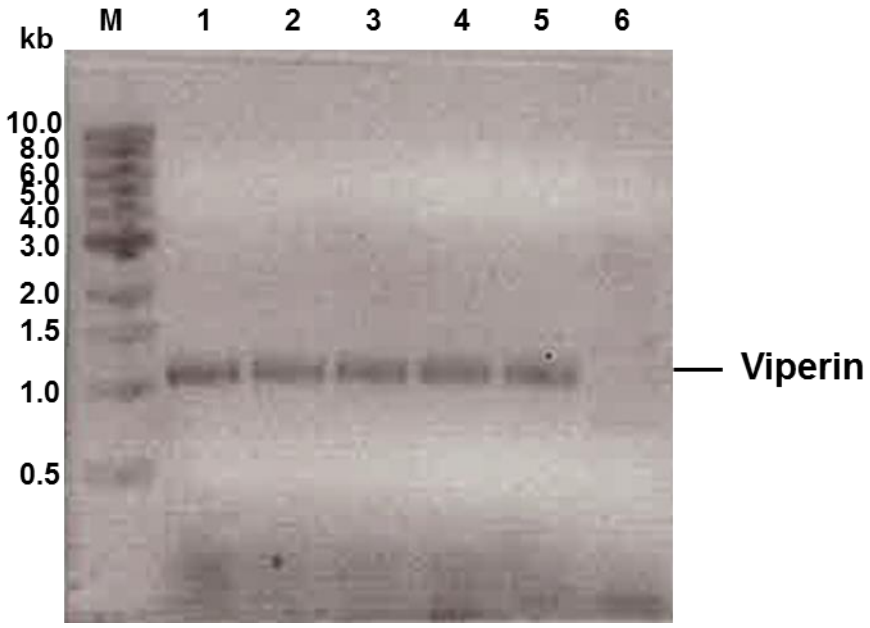

Figure 4.4: pGBKT7-viperin plasmid was successfully transformed into yeast cells. To test whether yeast cells (*Saccharomyces cerevisiae* strain Y2H Gold) contain the pGBKT7-viperin plasmid, five individual clones were randomly picked and lysed in 20 mM NaOH prior to colony PCR to detect viperin cDNA. Lane M, 1 kb DNA marker; Lane 1-5, yeast cells carrying pGBKT7-viperin clone no. 1-5, respectively; lane 6: yeast cells carrying pGBKT7-empty plasmid.

4.2.2 Viperin expression in *Saccharomyces cerevisiae* strain Y2H gold cells

Next, it was imperative to determine if viperin was expressed in transformed yeast cells. Five clones of the pGBKT7-viperin transformed *Saccharomyces cerevisiae* were grown to log-phase in SD/-Trp broth and whole cell protein lysates were extracted using cracking buffer (see section 2.2.4.2, Chapter 2). Viperin expression was detected by Western blot analysis using antibodies to Myc (Myc tag was incorporated in the original PCR cloning strategy) and viperin (Enzo life sciences). The result revealed that viperin was expressed in yeast cell transformants with a molecular mass of approximately 65 kDa that represents viperin fused with the DNA-binding domain (Figure 4.5). Variability was noted in the level of expression between yeast clones, however maximal viperin expression was observed for clone # 3. Clone #3 was further selected for analysis of bait toxicity, auto-activation and was used for further experiments in this study.

4.2.3 Toxicity and auto-activation testing of the bait protein

As a first stage before performing the Y2H screen, it is imperative to confirm that the bait protein (viperin) does not autonomously activate the reporter genes in *Saccharomyces cerevisiae* strain Y2H Gold, in the absence of a prey protein. Moreover, it is also necessary to verify that a bait protein is not toxic when expressed in yeast cells. If a bait protein is toxic, this can be observed by both solid and liquid cultures growing more slowly. To determine whether viperin was toxic or had auto-activation ability, *Saccharomyces cerevisiae* (strain Y2H gold) was transformed with pGBKT7-empty or pGBKT7-viperin plasmids and plated on the SD/-Trp selective medium for toxicity testing and on SDO/X medium for auto-activation testing. It was confirmed that viperin is

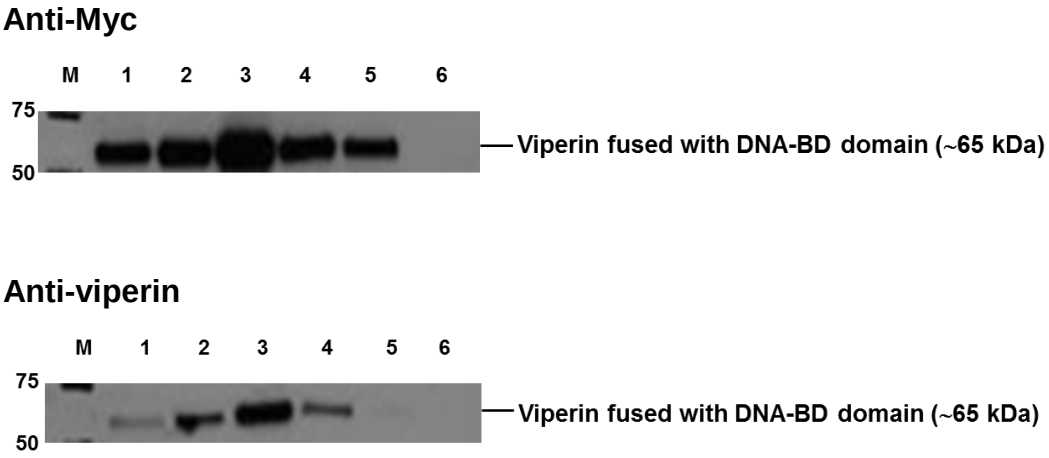

Figure 4.5: Viperin expression in *Saccharomyces cerevisiae* strain Y2H gold.

To investigate if viperin was expressed in yeast cells, clones were grown to log phase and whole cell lysates were extracted from yeast cells using a cracking buffer prior to Western blot analysis. (**A**) Viperin expression was detected by probing with anti-Myc (Millipore, clone 4A6) or (**B**) anti-viperin (Enzo life sciences) antibody. Lane 1-5: PGBKT7-viperin in Y2H gold clone 1-5, respectively, Lane 6: pGBKT7-empty in Y2H gold.

not toxic to the yeast cells as the size of yeast colonies transformed with the pGBKT7-viperin plasmid was similar to that of the yeast cells carrying pGBKT7-empty plasmid (Figure 4.6A). Furthermore, expression of viperin did not result in auto-activation of reporter genes, as demonstrated by red colonies on SDO/X selective medium (Figure 4.6B). Additionally, no colonies grew on the SDO/X/A medium indicating that viperin was not able to auto-activate the *MEL1* gene (encodes for α-galactosidase; enzyme for X-α-gal substrate) or the *AUR1-C* gene (encodes for aureobasidin A resistance). As expected, it was noticed that yeast colonies turned red when they were grown in medium containing a low concentration of adenine (SDO and DDO medium). The red pigment exhibited by *ADE2* mutants is a purine precursor which accumulates in yeast *ADE2* or *ADE1* strains, from which the Y2H gold strain is derived. Collectively these results indicate that viperin is not toxic when expressed in yeast and does not have auto-activation capacity.

4.3 Construction of the IFN-α-stimulated Huh-7 cell cDNA library

As viperin is an interferon-stimulated gene (ISG) that is upregulated following viral infection and IFN-α stimulation, we postulated that interacting partner of viperin may also fall into the class of ISGs or be associated with ISGs upregulation. Hence, we generated a cDNA library from Huh-7 cells stimulated with IFN-α for screening for interacting partners of viperin in the Y2H system.

A

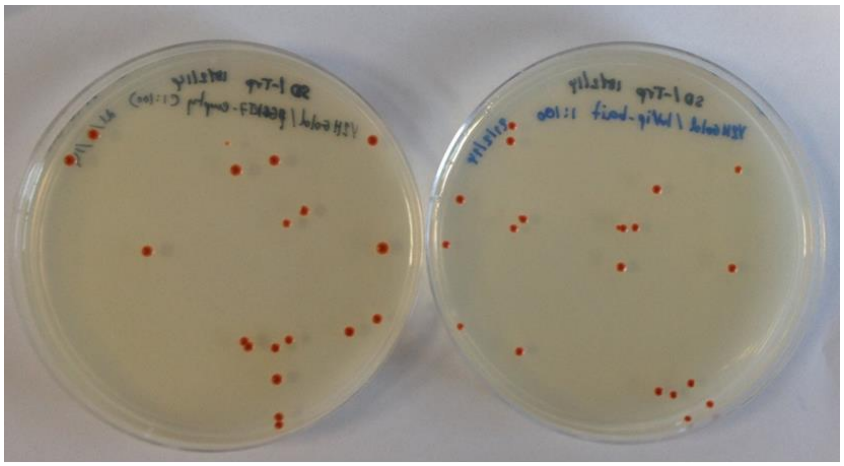

pGBKT7-empty pGBKT7-viperin

B

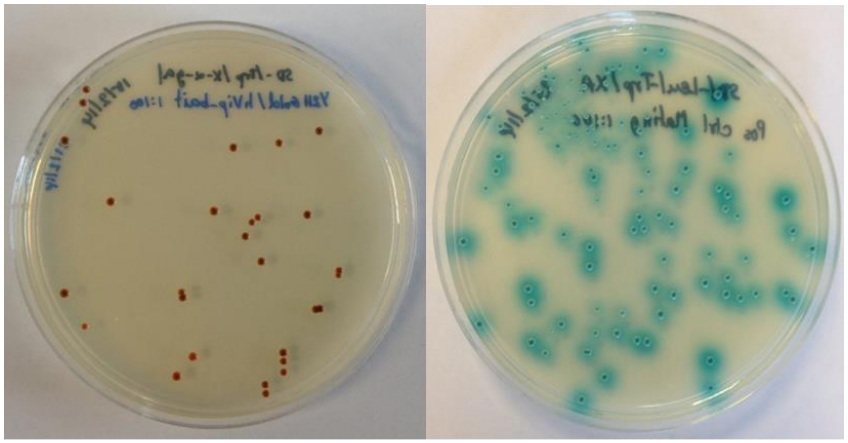

pGBKT7-viperin Positive control

Figure 4.6: Viperin expression in yeast is not an auto-activator and is not toxic.

To test if viperin expression in yeast is toxic or has auto-activator capability in the Y2H system, pGBKT7-empty and pGBKT7-viperin plasmids were introduced into *Saccharomyces cerevisiae* strain Y2H gold and plated on the SD/-Trp selective medium for (**A**) toxicity testing or (**B**) on SDO/X medium for auto-activation testing.

4.3.1 Determination of the IFN-α concentration and treatment time required for maximal viperin upregulation in Huh-7 cells.

Before generating the cDNA library from IFN-α-stimulated Huh-7 cells, we first determined the concentration of IFN-α and time post-stimulation that resulted in optimal viperin and other ISG mRNA expression levels. To determine the optimal concentration of IFN-α, Huh-7 cells were treated with IFN-α-2A (Peprotech) at 100, 250, 500 and 1,000 U/ml for 24 hr. Quantification of mRNA abundance (real time RT-PCR) demonstrated that viperin mRNA was upregulated by all treatment concentrations of IFN-α with maximum viperin mRNA levels being observed with 1,000 U/ml (Figure 4.7A). Moreover, viperin expression was maximal at 8 hr following IFN-α stimulation (1000 U/ml) of the Huh 7 cells (Figure 4.7B), after which mRNA rapidly declined.

4.3.2 Amplification of cDNA using long-distance PCR

Based on the results above (see Section 4.3.1), we next generated a cDNA library using the "Make Your Own "Mate & Plate" Library System" (Clontech) from Huh-7 cells treated with IFN-α at 1,000 U/ml for 8 hr. Following IFN-α stimulation, RNA was extracted from the Huh-7 cells and used for first strand cDNA synthesis using an oligo-dT primer and MMLV reverse transcriptase. Long-distance PCR was performed to prepare the library cDNAs (ds-cDNA) using Advantage® 2 Polymerase Mix (Clontech). Analysis of amplified cDNA on a 1% agarose gel revealed that the resulting cDNAs ranged from 100 bp to 10 kb representing good recovery of intact mRNA (Figure 4.8). cDNA of size >200 bp was purified using column chromatography and the final quantity of cDNA obtained was 6.3 μg and this was ready for the screening step.

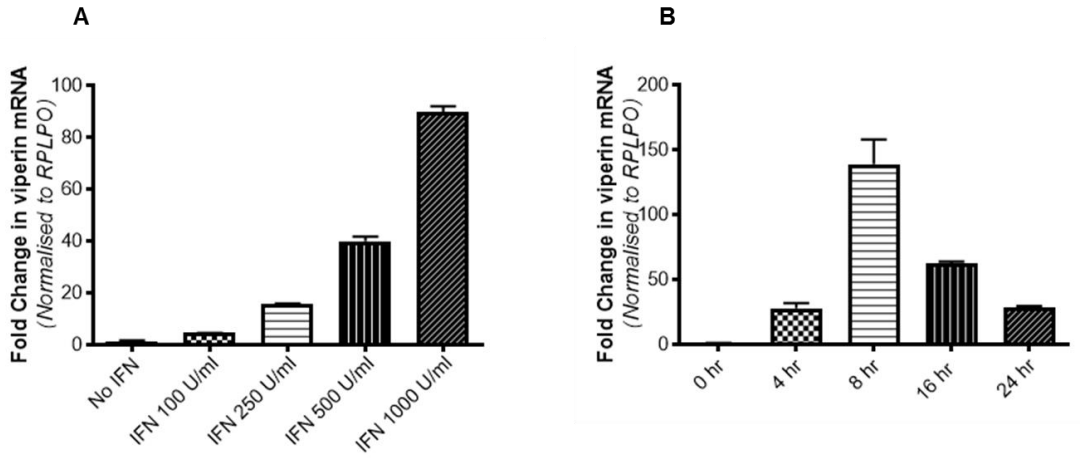

Figure 4.7: Dynamics of viperin mRNA expression in Huh-7 cells following IFN-α stimulation.

To assess viperin expression following IFN-α stimulation, **(A)** Huh-7 cells were treated with IFN-α at 100, 250, 500 and 1,000 U/ml. (**B**) Huh-7 cells were treated with IFN-α 1,000 U/ml for 4, 8, 16 and 24 hr for time course analysis of viperin upregulation. Viperin mRNA expression was analysed by real time RT-PCR and expressed as fold change to no IFN-α treatment.

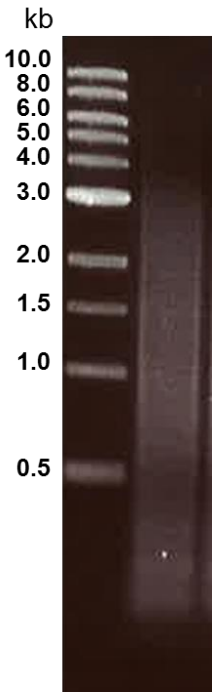

Figure 4.8: Long-distance PCR (ds cDNA) amplification.

ds-cDNA was amplified using Advantage® 2 Polymerase Mix (Clontech). The cDNAs (100 bp to 10 kb) were separated by electrophoresis on 1% agarose.

4.4 Proof of principle that the Y2H method can identify known interacting partners of viperin

The first attempt to screen for novel interacting partners of viperin using an IFN-α stimulated cDNA library (see Section 4.3) was unsuccessful, as screening more than 1 million independent clones resulted in no blue colonies. There are a number of possibilities that may explain this result. Firstly, a weak or transient interaction of viperin with interacting partners may result in an excess of aureobasidin A, which is toxic to the yeast cells. Secondly, it is possible that viperin interactions may not occur in the nucleus and hence result in no transactivation. To investigate if either of these possibilities were at play and to validate our Y2H approach, known interacting partners of viperin were constructed in prey plasmids. It has been reported by our laboratory using immunofluorescence and fluorescence resonance energy transfer (FRET) analysis that the host factor VAP-A and NS5A interact with viperin within the HCV RC (Helbig et al., 2011). Therefore, the interaction of viperin with VAP-A and HCV NS5A was assessed in yeast cells prior to conducting further screening experiments. VAP-A and NS5A were amplified using pLenti6-VAP-A-mCherry (Helbig et al., 2011) and pJc1 plasmid (Eyre et al., 2010) as templates (PCR products were of the expected size, as show in Figure 4.9), cloned into pGADT7 AD (prey) plasmid and transformed into α-Select Chemically Competent *E. coli* cells. Positive clones were tested by double digestion with *Nde*I and *Eco*RI (Figure 4.10) and confirmed by DNA sequencing. These plasmid constructs were then used to investigate the interaction of viperin with either VAP-A or NS5A in yeast cells and also used to titrate an appropriate concentration of aureobasidin A for screening of viperin's interacting proteins in the Y2H system. The

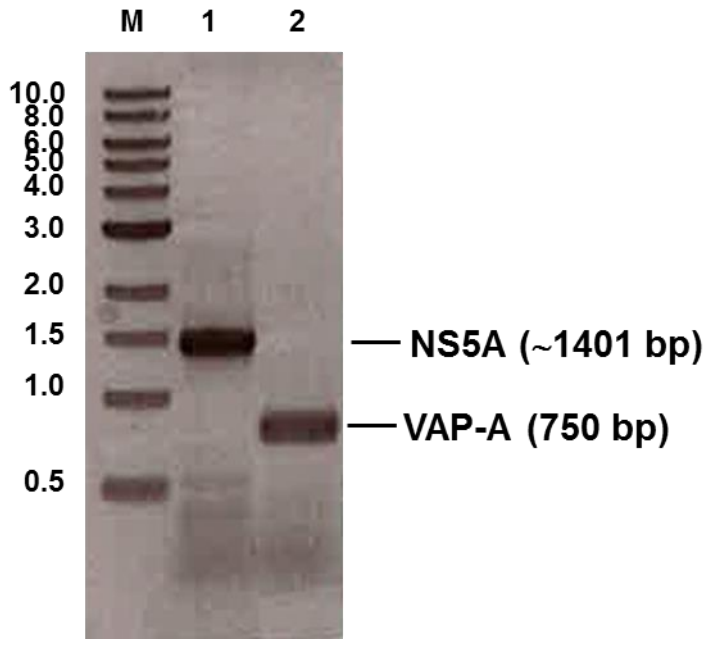

Figure 4.9: NS5A and VAP-A amplicons.

NS5A and VAP-A PCR products revealed by 1% agarose gel electrophoresis and Gel Red staining. Lane M, 1 kb DNA marker; lane 1, NS5A gene amplicon (1,401 bp) and lane 2, VAP-A gene amplicon (750 bp).

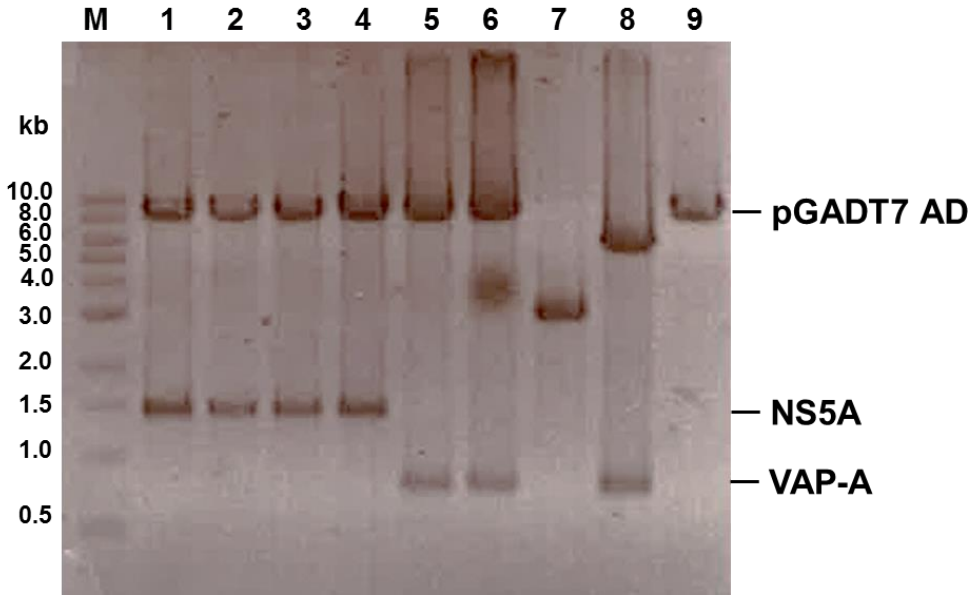

Figure 4.10: Patterns of *Nde*I and *Eco*RI double digestion of recombinant NS5A/VAP-A pGADT7 AD plasmids.

To confirm the positive clones, plasmid DNA was extracted from transformant clones and subjected to double digestion with *Nde*I *and Eco*RI. Lane M, 1 kb DNA marker; lanes 1-4, pGADT7 AD-NS5A recombinant plasmid clones no. 1-4, respectively; lanes 5-8, pGADT7 AD-VAP-A recombinant plasmid clones no. 1-4, respectively; lane 9, pGADT7 AD empty plasmid.

appropriate plasmids were co-transformed into competent *Saccharomyces cerevisiae* strain Y2H gold and various concentrations of aureobasidin A were used as outlined in Table 4.1. After 3-5 days of incubation of the transformed yeast cells, viperin was found to interact with VAP-A as determined by the emergence of blue colonies, but not with NS5A. We also found that low concentrations of aureobasidin A (< 50 ng/ml) were required to observe the interaction between viperin with VAP-A (Table 4.1). This low concentration of aureobasidin A together with pale blue colonies suggests that the interaction between viperin and VAP-A is weak or transient that results in low expression of the reporter gene (Figure 4.11). It is intriguing as to why we did not observe a viperin-NS5A interaction in our system. It is well-established that VAP-A interacts with NS5A and it may be possible that a prior VAP-A and NS5A interaction may be required to facilitate the interaction of viperin with NS5A. Alternatively, there may be other factors required for viperin-NS5A interaction that are not found in yeast cells (but are found in mammalian cells, where the interaction has been demonstrated). These experiments highlight one of the limitations of the Y2H system: the protein interactions that are observed in mammalian cells may not be observed in yeast cells (and *vice versa*). Nevertheless, we successfully identified that a viperin-protein interaction can occur in yeast cells verifying our approach.

4.5 A second screen for novel interacting partners of viperin by co-transformation method in the Y2H system.

In a second attempt to screen for novel interacting partners of viperin, pGBKT7-viperin (bait) plasmid, cDNA library (prepared from IFN-α-treated Huh-7 cells) and

Table 4.1: Aereobasidin A Titration

Co-transformation	DDO (SD/-Trp/-Leu)/X + aereobasidin A (ng/ml)						
	0	**25**	**50**	**75**	**100**	**150**	**200**
pGBKT7-Viperin + pGADT7 AD-VAP-A	+ (*)	+ (*)	+ (*)	-	-	-	-
pGBKT7-Viperin + pGADT7 AD-NS5A	+	+	+	-	-	-	-
pGBKT7-Viperin + pGADT7 AD-empty plasmid	+	+	+	-	-	-	-
pGADT7 AD-VAP-A + pGBKT7-empty plasmid	+	+	+	-	-	-	-
pGADT7 AD-NS5A + pGBKT7-empty plasmid	+	+	+	-	-	-	-

+ (*): Pale blue colonies

+ : White colonies

- : No growth

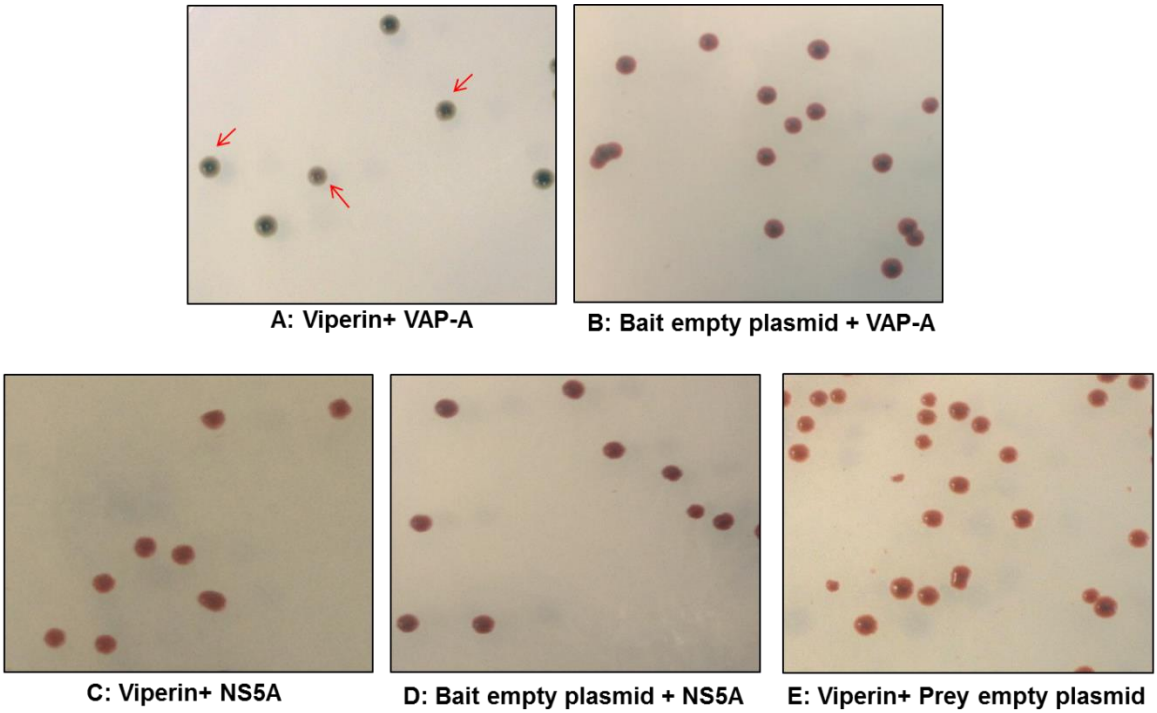

Figure 4.11: Viperin interacts with VAP-A but not HCV NS5A in a Y2H system.

To assess the interaction of known viperin interacting partners in the Y2H system, the plasmid pGBKT7-viperin was co-transfected with **(A)** pGADT7 AD-VAP-A or **(C)** pGADT7 AD-NS5A into competent *Saccharomyces cerevisiae* strain Y2H gold and incubated for 3-5 days. Note that blue colonies are present in **(A)** only. Co-transformation of pGBKT7-empty plasmid with **(B)** pGADT7 AD-VAP-A or **(D)** pGADT7 AD-NS5A and **(E)** pGBKT7-viperin with pGADT7 AD-empty plasmids were used as negative controls. Red arrows in **(A)** indicate pale blue colonies.

linearised pGADT7-Rec (prey) plasmid (Clontech) were combined and co-transformed into competent *Saccharomyces cerevisiae* strain Y2H Gold. The transformation reaction was spread onto 50 plates of DDO (SD/-Trp/-Leu)/XA medium (150 mm petri-dish size). After incubation for 3-5 days, 40 blue colonies were observed from 50 plates (Figure 4.12A). All blue colonies were picked and re-streaked on DDO/X medium to separate any contamination of blue and white colonies. This process was repeated three times until there were pure blue colonies (Figure 4.12B). Plasmid DNA representing the bait cDNA was rescued from all blue colonies and subsequently transformed into bacterial cells and plated onto LB-Amp plates to select bacteria harbouring the prey plasmid. All extracted prey plasmids (40 in total) were analysed by DNA sequencing and sequence compared to the NCBI GenBank database. Seven plasmids were identified that contained full-length or truncated open reading frames (ORF) fused in frame to the GAL4 AD sequence in the prey plasmid. The coding sequences from each of the 7 plasmids were translated to amino acid sequence and compared to known sequences in the GenBank databases using the Basic Local Alignment Search Tool (BLAST) from the National Centre for Biotechnology Information (NCBI) (Table 4.2). The identified sequence above from the Y2H screen was validated by co-transformation of each of the rescued-prey plasmids with pGBKT7-viperin. This validation screen identified that there were two genuine positive interacting partners of viperin: peroxisome biogenesis factor 19 (PEX19); and apolipoprotein A1 (ApoA1) (Figure 4.13).

A

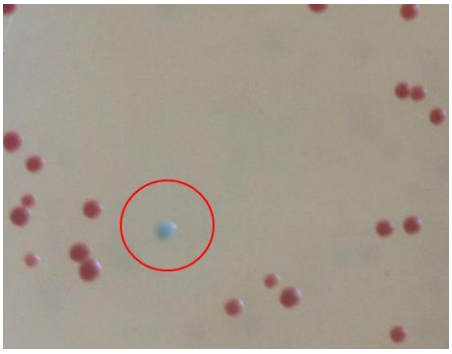

B

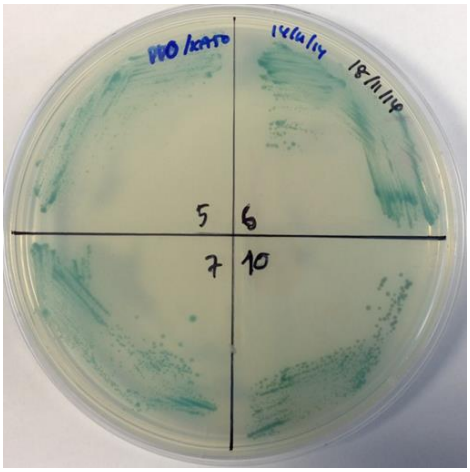

Figure 4.12: Screening of viperin's interacting partners by co-transformation method.

In order to screen the interacting partners of viperin, the pGBKT7-viperin (bait) plasmid, ds cDNA and linearised pGADT7-Rec plasmid were co-transformed into competent *Saccharomyces cerevisiae* strain Y2H Gold and spread onto 50 plates of DDO/XA medium. **(A)** Blue colonies were observed after 3-5 days incubation. **(B)** All blue colonies were re-streaked (x3) until pure blue colonies were present on selective medium (DDO/XA plate).

Table 4.2: Validation, by co-transformation method, of viperin interacting partners identified in the Y2H screen

Prey no.	Protein	Amino acid residues of a full-length protein from Genbank database	Amino acid residues of a candidate prey protein that fused in frame to the GAL4-AD sequence	Results from validation experiment
Prey#4,6,25	SUMO-conjugating enzyme (UBC9)	1-158	1-158	False positive
Prey#7	Protein phosphatase 1, catalytic subunit, alpha isoform	1-349	3-31	False positive
Prey#55	**Peroxisomal biogenesis factor 19 (PEX19)**	1-299	1- 272	**Genuine positive**
Prey#62	**Apolipoprotein A1**	1-267	104-267	**Genuine positive**
Prey#16	F-box and leucine-rich repeat protein 6, isoform CRA_d	1-300	19-300	False positive
Prey#3	FAM46A (HBV X-transactivated gene 11 protein)	1-442	337-442	False positive
Prey#57,70	Lectin, galactoside-binding	1-391	200-391	False positive

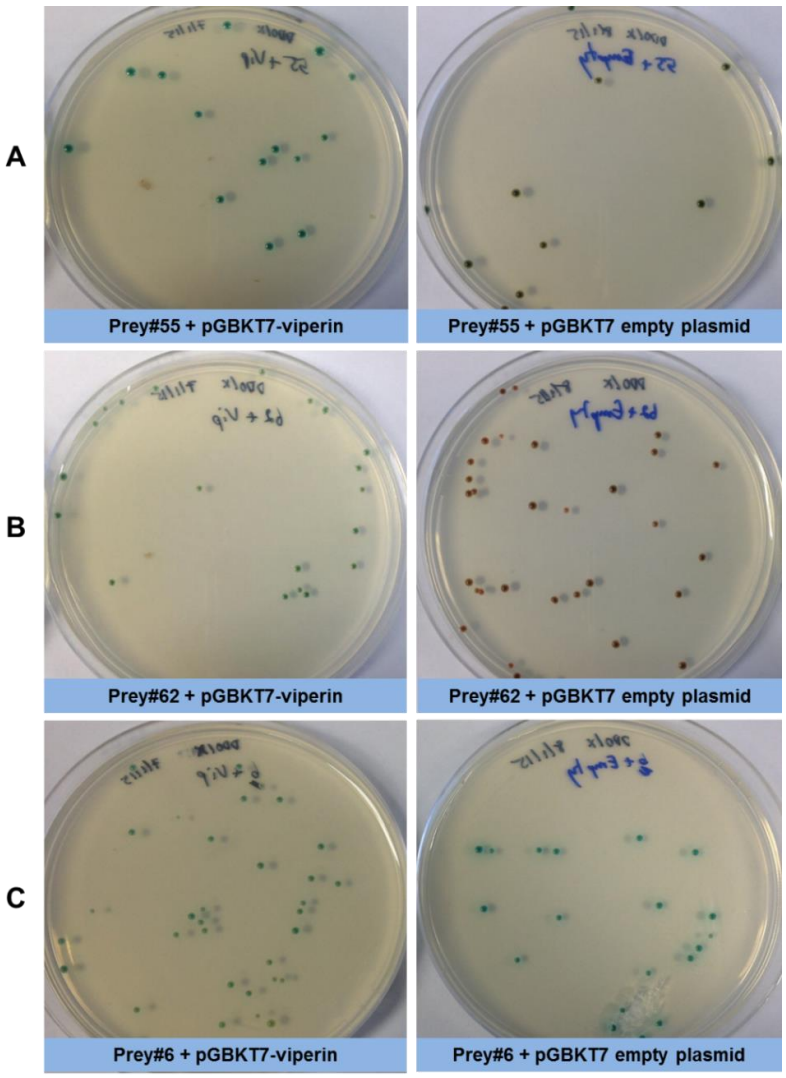

Figure 4.13: Validation of viperin interacting partners by co-transformation method.

To confirm the positive interaction of viperin and its novel interacting partners, pGBKT7-viperin and candidate prey plasmid were co-transformed into competent *Saccharomyces cerevisiae* strain Y2H gold and plated onto DDO/X and DDO/XA. The co-transformation of candidate prey plasmid and pGBKT7-empty plasmid was used as a control. **(A, B)** blue colonies appeared only for the co-transformation of the candidate prey plasmids and pGBKT7-viperin but not on the control plate representing a true positive interaction, **(C)** while blue colonies found on both plates indicated a false positive interaction**.**

4.6 Confirmation of viperin-interacting partners by other techniques

It was somewhat disappointing that only such few true positive interacting partners were identified in the Y2H screen. However, this alleviated the need to rationalise or prioritise target proteins for analysis. To investigate the interaction of viperin with hits identified above, expression plasmids encoding cDNA representing PEX19 (pCMV6-PEX19, catalogue number RC201756) and APO-A1 (pCMV6-ApoA1, catalogue number RC210762) were obtained from Origene. These plasmids contain the complete ORF downstream of the CMV promoter and are fused in frame to a Myc and FLAG tag at the C-terminus. These plasmids were subsequently used to confirm the interaction of viperin with PEX19 or ApoA1 using immunoprecipitation and proximity ligation assays.

4.6.1 Confirmation of viperin-interacting partners by proximity ligation assays

In order to assess the interaction of viperin with PEX19 and ApoA1 in eukaryotic cells, proximity ligation assay (PLA) was employed. In brief, proximity ligation assay enables detection and visualisation of subcellular localisation of protein-protein interactions using immunofluorescence microscopy. The interacting proteins are detected using primary antibodies raised in different species to the proteins in question. The appropriate secondary antibodies are conjugated with oligonucleotides (PLA probe MINUS and PLA probe PLUS) and following binding to corresponding primary antibodies results in a close proximity of the two probes if there is an interaction between the 2 proteins in question. The fluorescently labelled probe generates a fluorescent signal following ligation and amplification of the two oligonucleotides or probes. Initially, it was necessary to remove the FLAG tag from PEX19 and ApoA1 constructs while retaining

the Myc tag as at the time we did not have a reliable viperin antibody (for IF) and all viperin expression constructs were FLAG-tagged. We generated PEX19-Myc and ApoA1-Myc by removing the FLAG tag using *Eco*RV and *Pme*I double digestion and then re-ligation of the digested plasmid. Removal of the FLAG tag was confirmed by transfection of the modified plasmids into Huh-7 cells and staining with mouse anti-FLAG and mouse anti-Myc. As shown in Figure 4.14, the new constructs were stained by anti-Myc but not by anti-FLAG indicating the fusion of only the Myc tag for both constructs. Moreover, these plasmids were analysed by DNA sequencing and the results showed that they lacked the FLAG tag-coding sequence. These plasmids were further used in PLA.

To investigate the interaction of viperin and the candidate interacting partners by PLA, Huh-7 cells were co-transfected with pLenti6-viperin-FLAG and pCMV6-PEX19-Myc or pCMV6-ApoA1-Myc for 24 hr and then PLA was performed using mouse anti-FLAG and rabbit anti-Myc. A combination of mouse isotype control and rabbit anti-Myc was used as a control for the assay. A fluorescent signal represented a protein-protein interaction in cells as shown in Figure 4.15, implying that viperin interacts with PEX19 and ApoA1 in Huh-7 cells.

4.6.2 Confirmation of viperin-interacting partners by co-immunoprecipitation

The interaction of viperin and PEX19 and ApoA1 was next examined by co-immunoprecipitation (Co-IP). Huh-7 cells were transiently co-transfected with pLenti6-

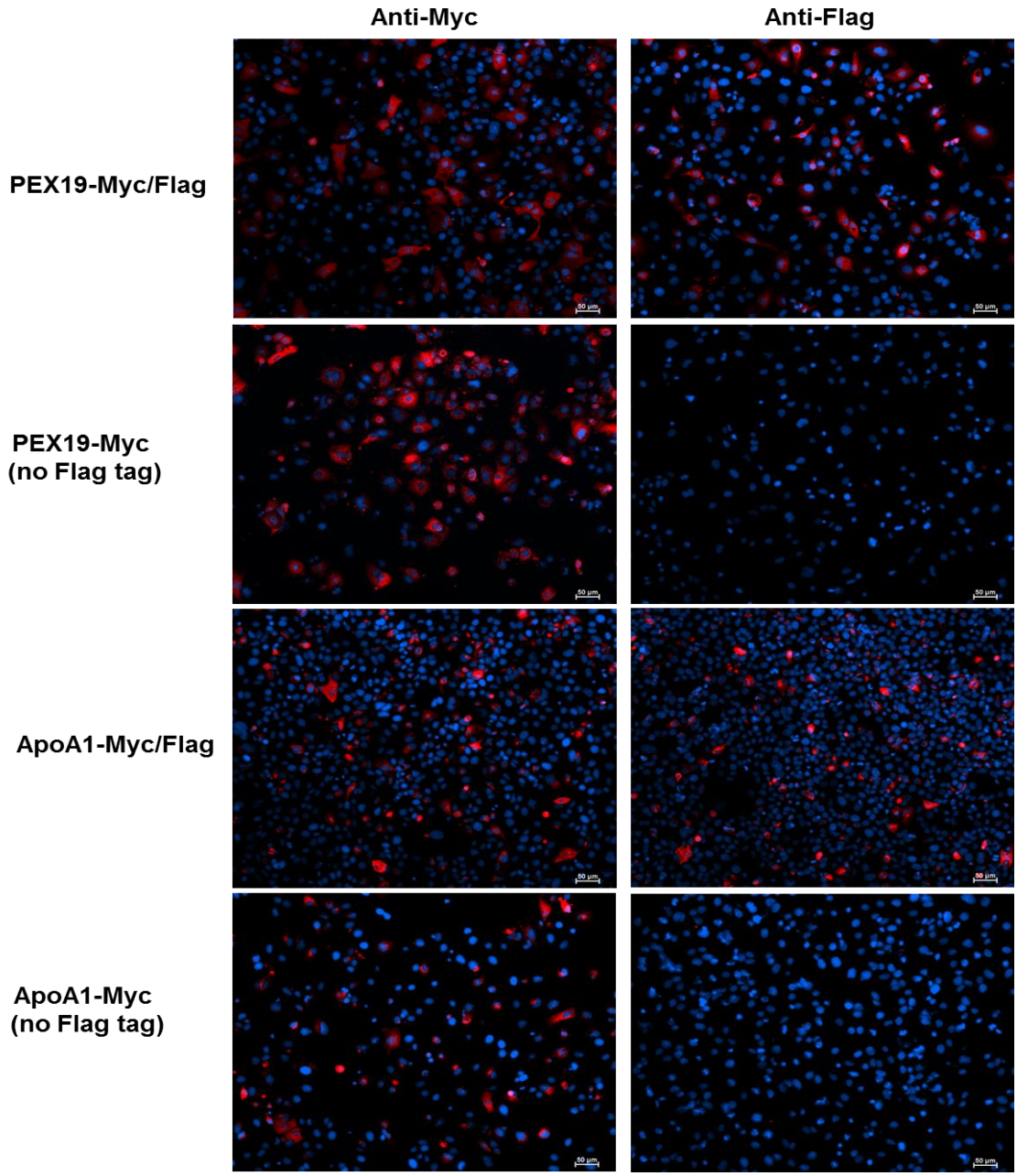

Figure 4.14: Generation of PEX19-Myc and ApoA1-Myc tag plasmids.

The Myc-tagged plasmids were confirmed by staining with mouse anti-FLAG/mouse anti-Myc, followed by an Alexa Fluor 555-conjugated goat anti-mouse IgG (Red). Nuclei were counterstained with DAPI (blue). Cells were visualised using a Nikon TiE inverted fluorescent microscope (10x magnification). Scale bars are 50 μm.

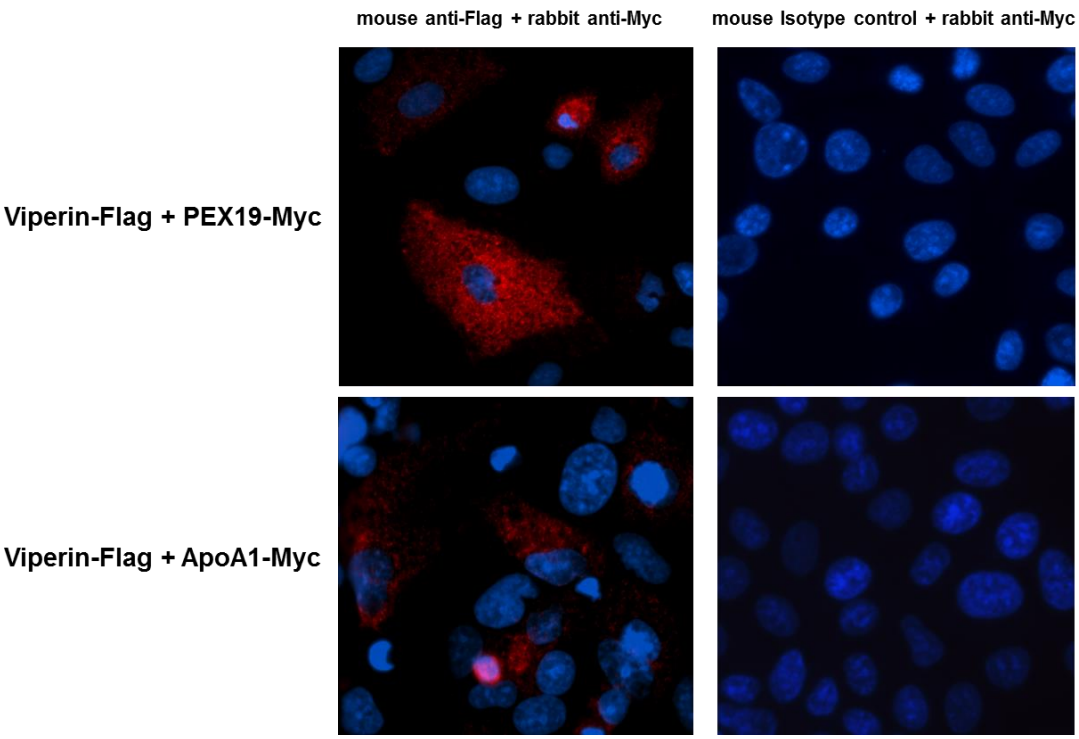

Figure 4.15: Viperin associates with PEX19 and ApoA1 as determined by proximity ligation assays (PLA).

To investigate whether viperin interacts with PEX19 and ApoA1, Huh-7 cells were transiently transfected with pLenti6-viperin-FLAG and pCMV6-PEX19-Myc or pCMV6-ApoA1-Myc and cultured for 24 hr. PLA was performed using mouse anti-FLAG (to detect viperin) and rabbit anti-Myc (to detect either PEX19 or ApoA1). A combination of mouse isotype control and rabbit anti-Myc was used as a negative control and nuclei were counterstained with DAPI (blue). Red dots in cells were visualised using a Nikon TiE inverted fluorescent microscope (20x magnification).

viperin-mCherry and pCMV6-PEX19-Myc/FLAG or pCMV6-ApoA1-Myc/FLAG, cultured for 24 hr and then a whole cell lysate was prepared. Viperin was immunoprecipitated from the cell lysate using anti-mCherry, while co-precipitation of PEX19 and ApoA1 with viperin was detected by Western blot analysis using anti-FLAG antibody. As shown in Figure 4.16, PEX19 co-precipitated with viperin and this was consistent with the PLA result indicating that PEX19 is an interacting partner of viperin. In contrast, ApoA1 was not detected by Co-IP with viperin. It is possible that the interaction of viperin with ApoA1 is weak or transient in nature, such that cell lysis may dissociate the interaction of these proteins, resulting in negative Co-IP results.

4.7 Discussion

It is clear from many published reports that viperin is a potent cellular antiviral factor against a broad range of viruses, however there is no unifying molecular mechanism that underpins this function. For example, the radical SAM domain is crucial for the antiviral function of viperin against TBEV but not HCV or DENV (Upadhyay et al., 2014, Helbig et al., 2011, Helbig et al., 2013). Moreover, viperin can bind to a number of host and viral proteins (see section 4.1). It has been shown to disrupt lipid rafts through its interaction with the host lipid metabolising enzyme farnesyl pyrophosphate synthase (FPPS), a mechanism that is specific for influenza and HIV (Wang et al., 2007, Nasr et al., 2012) and has also been shown to reduce cholesterol and sphingomyelin on cellular membranes, both of which are are the main components of lipid rafts and necessary for rabies virus infection (Tang et al., 2016). In addition, viperin can also impact HCV replication

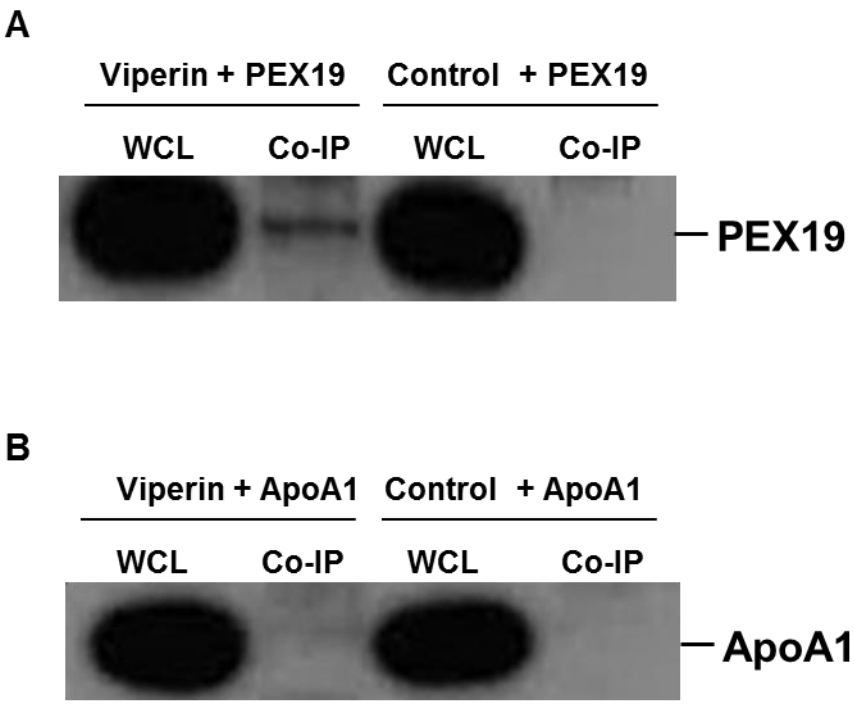

Figure 4.16: Confirmation of the interaction of viperin and PEX19 or ApoA1 by co-immunoprecipitation.

To determine whether viperin interacts with PEX19 and ApoA1, Huh-7 cells were transiently transfected with pLenti6-viperin-mCherry and pCMV6-PEX19-Myc/FLAG or pCMV6-ApoA1-Myc/FLAG for 24 hr. The co-transfection of pLenti6-mCherry plasmid and pCMV6-PEX19-Myc/FLAG or pCMV6-ApoA1-Myc/FLAG plasmids served as a negative control. Whole cell lysates were then extracted and viperin was immunoprecipitated using anti-mCherry. Viperin immunoprecipitates were analysed by Western blot analysis using anti-FLAG antibody to detect **(A)** PEX19 and **(B)** ApoA1, as indicated.

through interaction with the HCV NS5A protein and the HCV pro-viral cellular factor VAP-A. Furthermore, viperin seems to be involved in antiviral signalling as it was shown to be important in Toll-like receptor 7 (TLR7) and TLR9 signalling through its interaction with the adaptor molecules IRAK1 and TRAF6. Clearly, the domains of viperin cannot possibly account for its diverse range of biological functions and are most likely explained by its ability to interact with and modulate cellular protein function. While some host factors have been identified, they cannot account for the diverse nature of viperin function. We therefore hypothesise that cellular interacting partners of viperin remain to be discovered and characterised. This gap in knowledge led us to identify and characterise novel interacting partners of viperin in order to expand and fulfil our understanding of the diverse cellular biological functions of viperin.

There are a number of methods to identify protein-protein interactions and the recent explosion of proteomic techniques such as affinity purification coupled with mass spectrometry has revolutionised identification of protein interacting partners. Initially, we entertained the idea of using co-immunoprecipitation-coupled mass spectrometry (MS) to identify novel interacting partners of viperin. However, this approach required a specific antibody to viperin that could be used in immunoprecipitation experiments. We therefore evaluated a number of commercial monoclonal and polyclonal antibodies against viperin and found that these were not robust in Western blot analysis, and were ineffective in immunoprecipitation experiments of either endogenous (following IFN-α stimulation) or exogenous expression of viperin in multiple cell types (Huh-7, 293T and HeLa cells) Accordingly, antibody-based methods were not suitable. We therefore adopted a

transcription-based yeast two-hybrid (Y2H) experimental system that is a proven powerful method to identify of protein-protein interactions in living cells (yeast cells) that reflect an *in vivo* situation.

In this study, we utilised the "Matchmaker Gold Yeast Two-Hybrid system (Clontech)" to identify novel viperin interacting partners. This system has advantages over previous versions of Y2H systems in that it consists of 4 reporter genes under the control of 3 promoters which lead to reduce false positives. Initially, viperin cDNA (bait protein) was cloned into the bait vector (pGBKT7) and then toxicity and auto-activation of the reporter genes (*AUR1-C, ADE2, HIS3,* and *MEL1*) of the bait were tested. Viperin was clearly expressed in yeast cells with no effect on the viability of the yeast cells or auto-activation of the reporter genes. As previously described by our laboratory using immunofluorescence microscopy and FRET analysis it has been shown that viperin interacts with HCV NS5A protein and the pro-viral host factor VAP-A. This provided an excellent opportunity to not only confirm these observations by another method but to test the ability of viperin to interact with a viral or mammalian protein in the context of yeast cells. We therefore cloned HCV NS5A or VAP-A cDNA into the Y2H prey plasmid pGADT7 AD. Interestingly following transfection of the bait and prey plasmids into yeast and selection of tryptophan (Trp) and leucine (Leu) biosynthesis genes (provided in bait and prey plasmids, respectively) on DDO (SD/-Leu/-Trp)/XA selective medium, we noted transactivation of the 3 independent promoter (G1, G2, M1) only in the presence of VAP-A and not NS5A. The reasons why we see transactivation only in the presence of VAP-A is not immediately apparent. However, it is well-documented that

VAP-A interacts with NS5A and it may be that the association of viperin and NS5A may be solely mediated by the interaction between VAP-A and viperin at sites of HCV replication. Alternatively, as previously mentioned it is possible that the NS5A-viperin interaction is either too weak or transient to be identified in the Y2H assay. Clearly further studies are required to confirm or refute the NS5A viperin interaction. Nevertheless, the observation that VAP-A can interact with viperin in our Y2H system confirms the validity of the experimental system.

Similar to many interferon-stimulated genes, viperin mRNA expression is significantly induced following IFN-α stimulation often from a very low baseline expression. We therefore reasoned that possible viperin interacting partners may also fall within the ISG family. Therefore, the cDNA library to generate the prey library was subsequently generated from Huh-7 cells stimulated with IFN-α and cloned in the linearised pGADT7-Rec (prey) plasmid. Implementation of our Y2H screen using the above-mentioned plasmids revealed 40 blue colonies that represent a positive interaction between viperin and the prey protein, from a total of more than 1×10^6 transformants. However, analysis of all 40 cDNAs by Sanger sequencing revealed that only 7 of the candidate prey proteins were fused in frame with the linearised pGADT7-Rec (prey) plasmid (Table 4.2) and are possible authentic viperin interacting partners. This represents a limitation of Y2H approach in which the system is prone to the identification of false positives hits which are defined as physical interactions identified in the screen that cannot be reproduced using independent assays. False positives can arise for a number of reasons and include; 1) excessive expression of the bait and prey proteins, 2) protein interactions in a

physiological compartment that does not correspond to their natural environment, 3) incorrectly folded proteins can lead to non-specific interaction and 4) auto-activation [reviewed in (Bruckner et al., 2009)]. It is possible that a number of the 40 identified hits in our screen fall into this category especially for those ORFs that are not fused in frame that would lead to aberrant protein expression. It was also intriguing that only a small number of interaction partners were identified and none of the previously identified viperin interaction partners were identified. This can be explained by a further limitation of Y2H false negatives that are defined as protein-protein interactions that cannot be detected due to the limitations of the assay. As above false negatives arise for a host of reasons, for example, protein interactions involving membrane proteins are mostly undetectable while it is possible that in some instances the fusion of bait or prey proteins may cause steric hindrance and block interaction. Furthermore, interactions must occur in the nucleus while post-translational modifications may be lacking in yeast while weak or transient interactions may go unnoticed [reviewed in (Bruckner et al., 2009)]. It is likely that a number of these factors (false positive) were at play in our Y2H screen as following confirmation of the co-transformation experiments using viperin (bait) and positive candidate prey proteins, we could only detect 2 genuine positive interacting partners of viperin namely PEX19 and ApoA1. The other candidate prey proteins gave false positive interactions as they auto-activated the reporter gene when expressed alone in the absence of interaction with the bait protein (Figure 4.13C).

As indicated above, the propensity of Y2H screens to identify false positives means that subsequent biochemical assays are essential to confirm identified hits. To confirm the

interaction of novel viperin interacting partners PEX19 and ApoA1 we employed co-immunoprecipitation (Co-IP) and proximity ligation assay (PLA) techniques. Both of these approaches require robust specific antibodies to the protein in question, however as described above, available commercial antibodies to viperin were unable to immunoprecipitate ectopic expression of viperin. To overcome this limitation, we utilised exogenous viperin expression in which viperin was tagged with either the FLAG epitope or fused in frame with mCherry. Interestingly we could only immunoprecipitate viperin from transfected cell lysates using a specific Ab to mCherry and not the FLAG epitope for reasons that are not immediately apparent. Therefore, the plasmid, pLenti6/V5-D-TOPO expressing viperin-mCherry was used for Co-IP studies to confirm the interaction of viperin and its novel interacting partners.

Using Co-IP and PLA approaches, we confirmed our Y2H results and revealed an interaction of viperin and PEX19. Interestingly, during the course of this thesis, our Y2H studies identifying PEX19, were confirmed in a study using liquid chromatography coupled to tandem mass spectrometry (LC-MS/MS) to identify cellular viperin interacting partners (Vonderstein et al., 2017). However, this was not the case for ApoA1 in which we could only detect an interaction using PLA but not Co-IP. The reasons for this are not clear but could be related to a weak interaction between viperin and ApoA1 that may not have survived the immunoprecipitation protocol. However, the PLA results suggest that indeed viperin and ApoA1 interact or are least in close proximity as a positive PLA can only be obtained when the proteins are within 40 nm of each other. Clearly further studies are required to confirm the interaction of ApoA1 and viperin such

as repeating immunoprecipitation experiments coupled with a confocal microscopy approach to visualise protein-protein interactions in a cellular context. Nevertheless, both PEX19 and ApoA1 are novel viperin interacting partners that require further investigation and for reasons that will become apparent in the following chapters of this thesis, we chose to further investigate the viperin-PEX19 interaction.

It is interesting to speculate as to why using the Y2H system that we did not uncover more viperin interaction partners especially previously recognised partners such as FPPS, TFP, IRAK1, VAP-A, TRAF6, MAVS and CIAO1. This may be for a host of reasons, some of which have been alluded to above and may in part relate to weak or transient interactions with viperin and the possibility of interactions occurring in specific cell subsets as was noted for the interaction between viperin with TRAF6 and IRAK1 only in pDCs.

In conclusion, we have identified two novel interacting partners of viperin, PEX19 and ApoA1. PEX19 is a key biogenesis factor in the formation of peroxisomes and given that peroxisomes are emerging as a key organelle in the host antiviral response, we have focused our efforts in the remainder of this thesis to investigate the interaction of viperin and PEX19 and determine how this interaction may mediate the cellular antiviral response.

Chapter 5

Viperin alters peroxisome biogenesis and localisation to augment innate immune signalling

5.1 Introduction

Work in Chapter 4 established using a Y2H approach that the peroxisomal biogenesis factor 19 (PEX19) and Apolipoprotein A1 (ApoA1) were novel viperin interacting partners. We decided to pursue the interaction between viperin and PEX19 based on the following: 1) recent reports suggest that the peroxisome plays an important role in innate immune signalling (Dixit et al., 2010, Odendall et al., 2014); 2) preliminary data from our laboratory suggests that viperin can modulate innate immune signalling (Beard and Helbig unpublished data) and; 3) a number of viruses can interact with PEX19 and subvert innate immune signalling from peroxisomes (You et al., 2015, Magalhaes et al., 2016). Collectively, this suggests that peroxisomes play a role in the innate immune response to viral infection and a PEX19/viperin interaction may impact this response.

PEX19 is necessary for early peroxisome biogenesis and acts as a cytosolic chaperone to facilitate peroxisomal membrane protein (PMP) insertion into the peroxisome membrane. PEX19 shuttles between the cytoplasm and peroxisomes, although it is predominantly localised to the cytoplasm (Sacksteder et al., 2000, Jones et al., 2004) and PEX19 interacts with multiple peroxisome biogenesis factors/peroxins (PEX) and peroxisomal membrane proteins (PMPs), including PEX3, PEX10, PEX11A, PEX11B, PEX12, PEX13, PEX14, PEX16, PMP22, PMP24, PMP34, and PMP70 (Sacksteder et al., 2000).

Peroxisomes are cytoplasmic organelles involved in oxidative reactions and biochemical pathways and require a number of peroxisomal biogenesis factors or peroxin proteins (encoded by *PEX* gene) for their biogenesis. Mutation or deficiency of peroxins leads a defect of peroxisome biogenesis that results in a failure of peroxisomal metabolic function. Clinically, Zellweger syndrome (ZS) is the most severe type of peroxisome biogenesis disorder (PBD), and the related-PBD syndromes are groups of severe neurological disorders which can lead to life-threatening outcomes in childhood (Steinberg et al., 1993, Wanders, 2004). In addition to their metabolic function, several recent studies have suggested that peroxisomes promote MAVS-dependent innate immune signalling in response to viral infection (Odendall et al., 2014, Dixit et al., 2010, You et al., 2015). Further evidence highlighting the importance of peroxisomes in host antiviral responses comes from a recent study in which the *Flaviviruses*, DENV and WNV decreased the number of peroxisomes and altered peroxisome biogenesis through viral capsid protein-mediated PEX19 degradation and this may be a mechanism for which DENV and WNV evade the innate immune response (You et al., 2015). Furthermore, in human cytomegalovirus (HCMV) infection, the viral protein, vMIA, (mitochondria-localised inhibitor of apoptosis) induces peroxisome fragmentation and limits antiviral signalling from peroxisomes. HCMV also evades the host antiviral response through an interaction of vMIA with PEX19, which interferes with the transport machinery of peroxisomes (Magalhaes et al., 2016).

Collectively, the literature surrounding PEX19 and peroxisomes suggests that they are both important in the early innate immune response to viral infection, and it is possible

that viperin expression following viral infection is able to trigger a downstream signalling cascade through peroxisomes to perform a multifunctional role. Accordingly, the objective of this chapter is to define how viperin and PEX19 interaction initiates a role in the innate immune response via peroxisomes.

5.2. Co-localisation of viperin and PEX19

Previous work in Chapter 4 established that PEX19 and viperin interact as determined by Co-IP and PLA. To further determine this interaction, we investigated the cellular localisation of interaction between endogenous PEX19 and viperin. Initially, to investigate the normal cellular distribution of PEX19, we immuno-stained Huh-7 cells with rabbit anti-PEX19 (Abcam, ab95959) and visualised by IF analysis using Alexa Fluor 488-conjugated goat anti-rabbit IgG secondary antibody. However, this antibody displayed significant background staining during IF analysis (Figure 5.1). This led us to employ an alternative strategy in which we used a plasmid expressing PEX19 tagged with Myc/FLAG for further study. The localisation of exogenous PEX19 was first investigated by transfecting Huh-7 cells with pCMV6-PEX19-Myc/FLAG plasmid (Origene) and PEX19 was visualised using an anti-FLAG antibody. A staining pattern of PEX19 was observed as punctate intracellular compartments distributed throughout the cytoplasm of Huh-7 cells that represents peroxisomes (Figure 5.2). A weaker signal was also observed, most likely representing the cytoplasmic (and possibly ER) localisation of PEX19. This staining pattern result is consistent with previous studies (Jones et al., 2004), suggesting correct localisation of exogenous expressed PEX19.

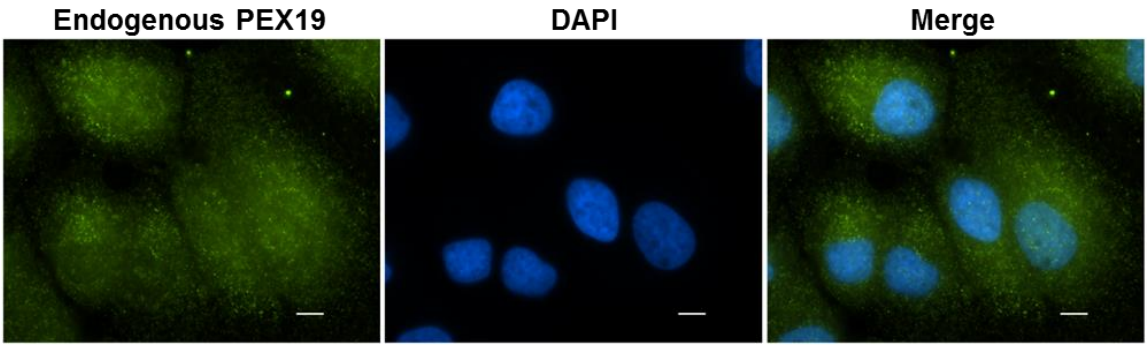

Figure 5.1: Endogenous PEX19 staining pattern.

To investigate the localisation of endogenous PEX19, Huh-7 cells were stained with rabbit anti-PEX19 (Abcam, ab95959) and Alexa Fluor 488-conjugated goat anti-rabbit IgG secondary antibody (Ab). Nuclei were counterstained with DAPI (blue). A significant background of staining using anti-PEX19 (green) was observed in the nucleus and cytoplasm by immunofluorescence analysis using a Nikon TiE inverted fluorescent microscope (60x magnification). Scale bars are 10 μm.

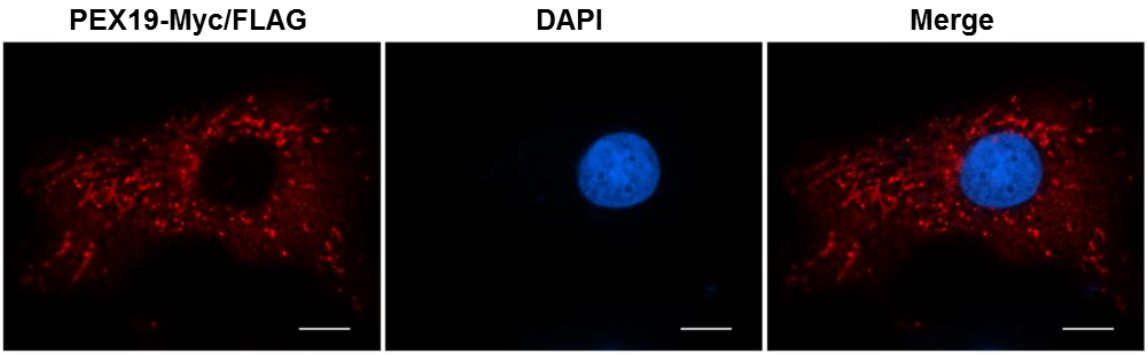

Figure 5.2: Exogenous expressed PEX19 localisation.

To investigate the localisation of PEX19 by exogenous means, Huh-7 cells were transiently transfected with pCMV6-PEX19-Myc/FLAG for 24 hr followed by staining with mouse anti-FLAG and Alexa Fluor 555-conjugated goat anti-mouse IgG secondary Ab. Nuclei were counterstained with DAPI (blue). The staining pattern of PEX19 (red) was observed by immunofluorescence analysis using a Nikon TiE inverted fluorescent microscope (60x magnification). Scale bars are 10 μm.

To further facilitate our studies of the PEX19 and viperin interaction, we generated a plasmid in which PEX19 was expressed with an N-terminal GFP tag. PEX19-encoding cDNA was amplified using pCMV6-PEX19-Myc/FLAG plasmid (Origene) as a template and cloned into pEGFP-C1 (Clontech). Positive clones were tested by double digestion with *Xho*I and *Sac*II and confirmed by DNA sequencing. To further identify peroxisomes, we used an expression plasmid encoding the resident peroxisome protein, PEX11B [pCMV6-PEX11B (Cat no.#RC202018, Origene)] containing the complete ORF fused to a Myc and FLAG tag at the C-terminus, while endogenous peroxisomes were visualised with mouse anti-PMP70 (Sigma-Aldrich, SAB4200181).

As mentioned previously PEX19 can shuttle between the cytoplasm and peroxisomes and therefore it was important to investigate whether PEX19 is present on peroxisomes or localised to the cytoplasm or both in Huh-7 cells. To investigate this, Huh-7 cells were co-transfected with a plasmid expressing PEX19-GFP and pCMV6-PEX11B-Myc/FLAG prior to staining with anti-FLAG. Additionally, localisation of PEX19 on native peroxisomes was also explored by transfecting Huh-7 cells with a plasmid expressing PEX19-GFP and staining with anti-PMP70. The majority of PEX19 distributed in the cytoplasm (and possibly ER), while a lesser proportion localised to peroxisomes as determined by co-localisation with peroxisome markers; PEX11B and PMP70 (Figure 5.3). This indicated that PEX19 localises to the cytoplasm and peroxisomes in hepatic cells.

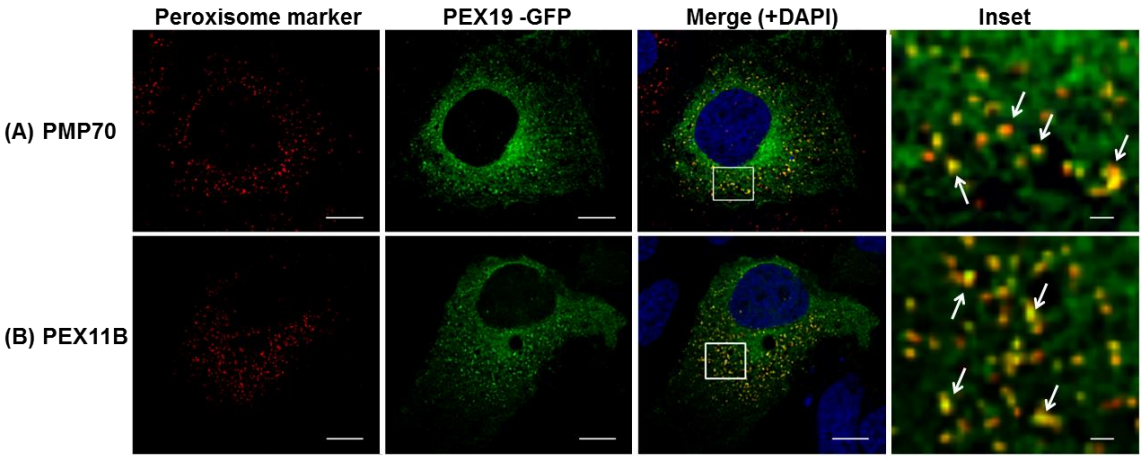

Figure 5.3: Localisation of PEX19 on peroxisomes.

To investigate the distribution of PEX19 between peroxisomes and the cytoplasm, exogenous PEX11B expressed from pCVM6-PEX11B-Myc/Flag and endogenous PMP70 were used as markers of the peroxisome. **(A)** Huh-7 cells were transiently transfected with a plasmid expressing PEX19-GFP for 24 hr prior to staining with mouse anti-PMP70 and Alexa Fluor 555-conjugated goat anti-mouse IgG secondary Ab. **(B)** Huh-7 cells were additionally transiently co-transfected with a plasmid expressing PEX19-GFP and PEX11B-Myc/FLAG for 24 hr prior to PEX11B staining with mouse anti-FLAG and Alexa Fluor 555-conjugated goat anti-mouse IgG secondary Ab. Nuclei were counterstained with DAPI (blue). Serial (0.25-μm) z-sections of immunofluorescence images were acquired using a Nikon TiE inverted fluorescent microscope and deconvoluted using the 3D AutoQuant Blind Deconvolution plug-in of NIS Elements Advanced Research v 3.22.14 software. Images are single representative z-sections. Colocalisation of PEX19 (green) and peroxisome marker PEX11B/PMP70 (red) was observed using deconvolution fluorescence microscopy (60x magnification). Scale bars are 10 μm and 1 μm for main images and insets, respectively. Arrows indicate co-localisation of PEX19 and PMP70/PEX11B.

The presence of PEX19 in both the cytoplasm and on peroxisomes raises the question as to the cellular sub-compartment where viperin interacts with PEX19. The co-localisation of viperin and PEX19 was therefore investigated by transiently transfecting Huh-7 cells with a plasmid expressing viperin-GFP and pCMV6-PEX19-Myc/FLAG prior to PEX19 staining with anti-FLAG. It was immediately apparent that there was a significant co-localisation between viperin and PEX19 (Figure 5.4). What was even more striking was the viperin-induced relocation of PEX19 from a homogenous cytoplasmic localisation to a region that surrounded circular structures with the cytoplasm (compare Figure 5.2 and 5.4) that are reminiscent of LDs. It is well-established that viperin can locate to the LD (Hinson and Cresswell, 2009a, Helbig et al., 2011), and it is possible that the PEX19 and viperin interaction may direct PEX19 to the LD. However, we first investigated the relationship between PEX19 and LDs in the absence of viperin. Transfection of Huh-7 cells with pCMV6-PEX19 Myc/FLAG and visualisation of PEX19 with anti-FLAG and LDs with the neutral lipid staining BODIPY 493/503 revealed no association of PEX19 with the LD (Figure 5.5). On the other hand, expression of viperin alone results in its localisation to the LD, as has been previously described (Hinson and Cresswell, 2009a, Helbig et al., 2011). To further confirm that viperin is able to redistribute PEX19 to LDs, co-localisation of viperin and PEX19 on LDs was observed using BODIPY 493/503 as a LD marker, and colocalisation was found on the LD surface, as expected (Figure 5.6).

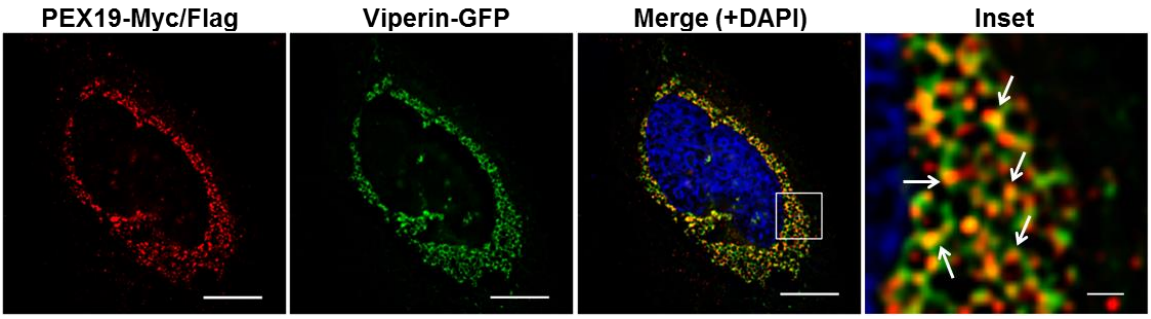

Figure 5.4: Co-localisation of viperin and PEX19.

To determine the cellular compartment in which viperin colocalises with PEX19, Huh-7 cells were transiently transfected with a plasmid expressing viperin-GFP and pCMV6-PEX19-Myc/FLAG for 24 hr followed by staining with mouse anti-FLAG and an Alexa Fluor 555-conjugated goat anti-mouse IgG secondary antibody. Nuclei were counterstained with DAPI (blue). Serial (0.25-μm) z-sections of immunofluorescence images were acquired using a Nikon TIE inverted microscope and deconvoluted using the 3D AutoQuant Blind Deconvolution plug-in of NIS Elements Advanced Research v 3.22.14 software. Images are single representative z-sections. Strong co-localisation of viperin (green) and PEX19 (red) was seen at circular structures within cytoplasm using deconvolution fluorescence microscopy (60x magnification). Scale bars are 10 μm and 1 μm for main images and the inset, respectively. Arrows indicate co-localisation of viperin and PEX19.

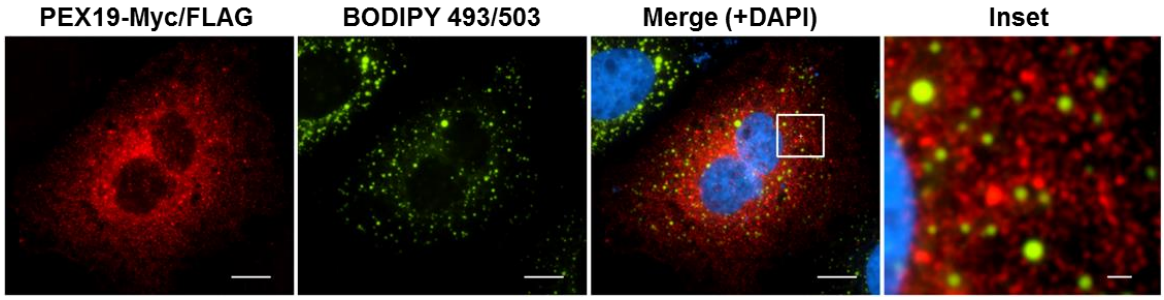

Figure 5.5: PEX19 does not localise to lipid droplets.

To determine the spatial localisation of PEX19 in relation to LDs in the absence of viperin, Huh-7 cells were transiently transfected with pCMV6-PEX19-Myc/FLAG for 24 hr prior to staining with mouse anti-FLAG and Alexa Fluor 555-conjugated goat anti-mouse IgG secondary antibody. LDs were detected by BODIPY 493/503 staining and nuclei were counterstained with DAPI (blue). No localisation of PEX19 (red) was observed on LDs (green) by immunofluorescence analysis using a Nikon TiE inverted fluorescent microscope (60x magnification). Scale bars are 10 μm and 1 μm for main images and the inset, respectively.

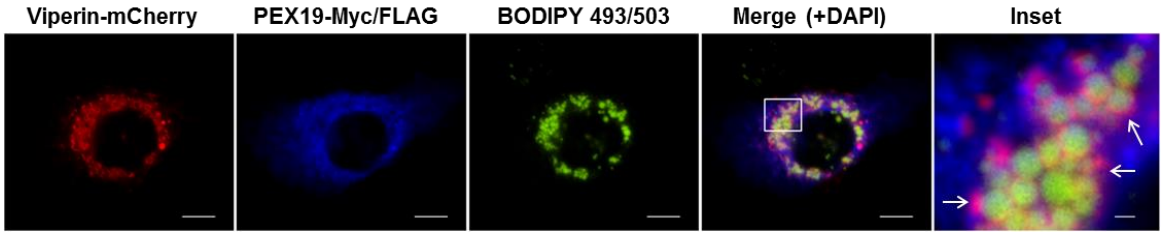

Figure 5.6: Localisation of viperin and PEX19 on lipid droplets.

To confirm that viperin and PEX19 interact at the LD interface, Huh-7 cells were transiently transfected with pLenti6-viperin-mCherry and pCMV6-PEX19-Myc/FLAG expression plasmids for 24 hr prior to staining with mouse anti-FLAG and Cy5-conjugated goat anti-mouse IgG secondary antibody. LDs were stained with BODIPY 493/503. Strong colocalisation of viperin (red) and PEX19 (blue) was observed (pink) in close proximity to LDs (green) by immunofluorescence analysis using a Nikon TiE inverted fluorescent microscope (60x magnification). Scale bars are 10 μm and 1 μm for main images and the inset, respectively. Arrows indicate the association with LDs.

5.3 Viperin redirects peroxisomes to lipid droplets.

Our previous results indicate that following the interaction between PEX19 and viperin, there is a change in localisation of PEX19 away from the cytoplasmic compartment to an association with the LDs. However, the fact that PEX19 can shuttle between the cytoplasm and peroxisomes raises the question; does viperin interact with cytoplasm- or peroxisomal-PEX19? We therefore investigated co-localisation of viperin and the peroxisome markers, PMP70 and PEX11B. Huh-7 cells were transfected with a plasmid expressing viperin-GFP and peroxisomes were either identified by PMP70 (anti-PMP70) or PEX11B that was expressed following co-transfection with plasmids expressing viperin-GFP and pCMV6-PEX11B-Myc/FLAG. Viperin associated with both peroxisome markers as shown in Figure 5.7. Interestingly, peroxisomes associated with viperin in a similar staining pattern to that of PEX19 (see Figure 5.4), indicating that viperin redirects peroxisomes to LDs in a significant number of cases. However, we also noted that viperin interacted with peroxisomes distant to LDs. Consistent with the PEX19 data in the absence of viperin, PMP70 (peroxisomes) did not localise in association with LDs (Figure 5.8), suggesting that this observation is mediated by an interaction of viperin with PEX19.

To increase our resolution of the interaction between viperin, LDs and peroxisomes, three dimensional-structured illumination microscopy (3D-SIM) super-resolution imaging was used. 3D-SIM is a wide-field imaging technique with 2-fold increases in the lateral and axial resolution and eliminates out of focus background fluorescence resulting in clear

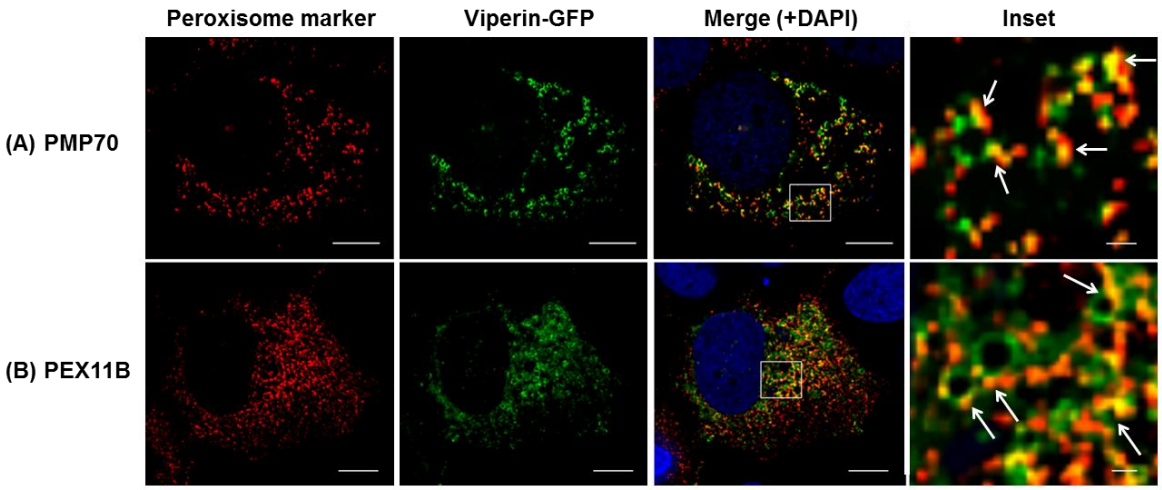

Figure 5.7: Redistribution of peroxisomes to LDs in the presence of viperin.

To determine whether viperin redirects peroxisomes to LDs, **(A)** Huh-7 cells were transiently transfected with viperin-GFP expression plasmid for 24 hr prior to staining with mouse anti-PMP70 followed by an Alexa Fluor 555-conjugated goat anti-mouse IgG secondary Ab to visualise peroxisomes. **(B)** In addition, Huh-7 cells were co-transfected with viperin-GFP and pCMV6-PEX11B-Myc/FLAG expression plasmids for 24 hr prior to PEX11B staining with mouse anti-FLAG and Alexa Fluor 555-conjugated goat anti-mouse IgG secondary Ab. Nuclei were counterstained with DAPI (blue). Serial (0.25-μm) z-sections of immunofluorescence images were acquired using a Nikon TiE inverted fluorescent microscope and deconvoluted using the 3D AutoQuant Blind Deconvolution plug-in of NIS Elements Advanced Research v 3.22.14 software. Images are single representative z-sections. Co-localisation of viperin (green) and the respective peroxisome markers PEX11B/PMP70 (red) was observed using deconvolution fluorescence microscopy (60x magnification). Note the significant co-localisation of viperin and the peroxisomes at the LD interface and at sites distant to the LD. Scale bars are 10 μm and 1 μm for main images and insets, respectively. Arrows indicate co-localisation of viperin and PMP70/PEX11B (peroxisomes).

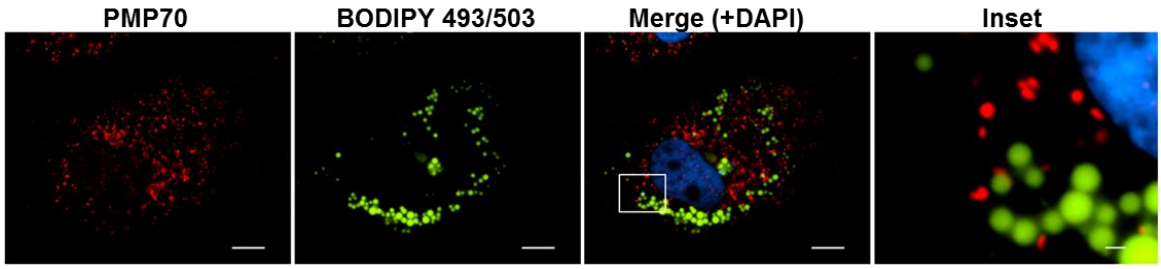

Figure 5.8: Localisation of peroxisomes with respect to LDs under resting conditions.

To determine whether peroxisomes localise to LDs in the absence of viperin, Huh-7 cells were stained with mouse anti-PMP70 and Alexa Fluor 555-conjugated goat anti-mouse IgG secondary antibody. LDs were stained with BODIPY 493/503 and nuclei were counterstained with DAPI (blue). Peroxisomes (red) were not observed to associate with LDs (green) by immunofluorescence analysis using a Nikon TiE inverted fluorescent microscope (60x magnification). Scale bars are 10 μm and 1 μm for main images and the inset, respectively.

contrast. 3D-SIM was performed at the Microbial Imaging Facility (The University of Technology Sydney, in association with Lynne Turnbull and Cynthia Whitchurch). We initially confirmed the localisation of viperin with the LD through the use of an expression plasmid expressing the resident LD membrane marker ADRP fused to mCherry, while viperin was expressed tagged with GFP. As expected viperin localised to the LD interface as determined by co-localisation between ADRP and viperin in addition to ER localisation of viperin. It was also apparent that viperin and PEX19 located to the LD interface and also most likely at the ER (Figure 5.9). Consistent with results in Figure 5.7, super-resolution 3D-SIM revealed that viperin presented at the LD in close association with peroxisomes (PMP70) (Figure 5.9). In some cases, viperin associated LDs are juxtaposed with the peroxisomes, while in some cases there was direct overlap of the signals. Collectively, this work suggests that viperin/PEX19 and the peroxisome interact in close association with the LD.

5.4 Viperin enhances the numbers of peroxisomes.

Given the nature of PEX19's ability to facilitate peroxisome biogenesis, we next investigated the impact of viperin on peroxisome numbers. A recent study has shown an association between the innate immune response to viral infection and the number of peroxisomes (Odendall et al., 2014). Given that viperin binds PEX19, it is possible that viperin augments innate immune signalling by increasing or altering peroxisome biogenesis and/or function. To quantify cellular peroxisome content in the presence of viperin we used an Operetta high-content microscope as previously described in Chapter 3. To specifically quantify cellular peroxisome content in the absence/presence of

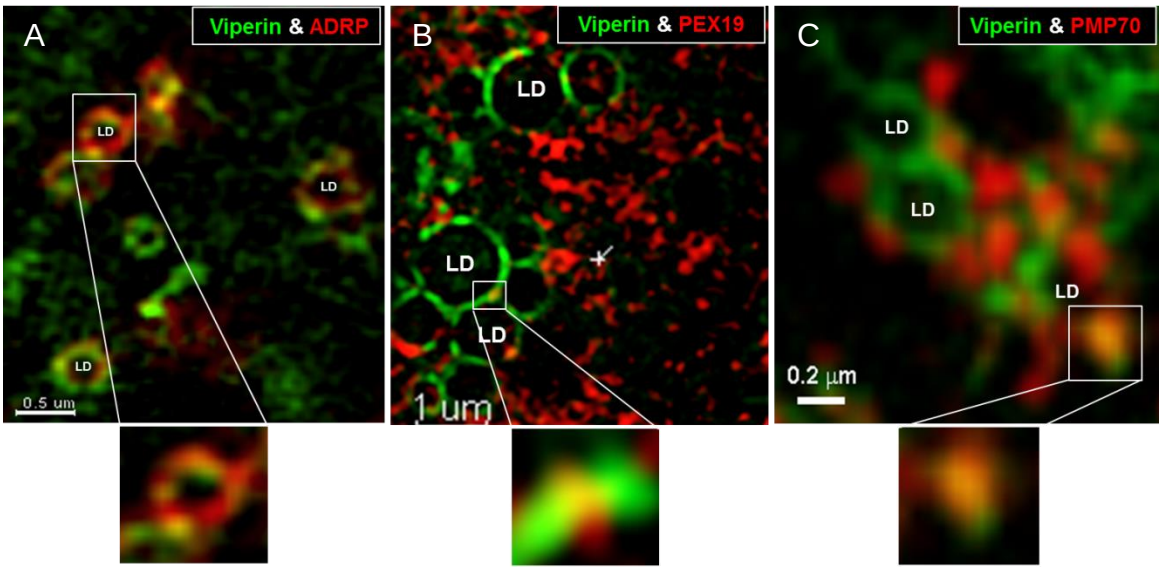

Figure 5.9: 3D-structured illumination microscopy (3D-SIM) super-resolution images.

3D-SIM was used to investigate the relationship/interaction between viperin and LDs (ADRP), PEX19 and peroxisomes (PMP70). **(A)** Huh-7 cells were transiently co-transfected with viperin-GFP and ADRP-mCherry expression plasmids which is LD marker. **(B)** Huh-7 cells were transiently co-transfected with viperin-GFP and PEX19-Myc/FLAG expression plasmids prior to staining with mouse anti-FLAG and Alexa Fluor 555-conjugated goat anti-mouse IgG. **(C)** Huh-7 cells were transiently transfected with a plasmid expressing viperin-GFP and stained with mouse anti-PMP70 and Alexa Fluor 555-conjugated goat anti-mouse IgG. 3D-super-resolution images were generated by 3D-structured illumination microscopy which performed with a V3 DeltaVision OMX 3D-SIM system fitted with a Blaze module (Applied Precision, GE Healthcare, USA). Images were deconvolved using SoftWorX software (Applied Precision, GE Healthcare) and rendered and presented using IMARIS software (v7.7 or above, Bitplane Scientific).

viperin, Huh-7 cells were transiently transfected with plasmids expressing viperin-GFP or GFP alone (as a control) prior to staining with mouse anti-PMP70 and Alexa Fluor 555-conjugated goat anti-mouse IgG. Images were obtained in non-confocal mode and analysed using Harmony software (Perkin Elmer) to quantitate absolute PMP70 positive fluorescence. Cells from each transfection experiment were counted and averaged, and the mean of Alexa Fluor 555 intensity (i.e. PMP70 content) was analysed per cell. A total number of approximately 4,000 cells was counted per group and transfection efficiency was approximately 34% and 55% for the transfection with viperin-GFP and GFP control, respectively (see raw data in Appendix X). The intensity of Alexa Fluor 555, an estimate of peroxisome content per cell was significantly higher in viperin expressing cells compared to GFP control-transfected cells, whereas no difference in Alexa Fluor 555 intensity was observed in the untransfected cell populations for samples transfection with viperin-GFP and GFP control plasmids (Figure 5.10).

Our results above suggest that the number of peroxisomes is increased in the presence of viperin expression. However, to confirm this observation, we investigated peroxisome biochemical activity through measurement of catalase enzyme levels. Peroxisomes contain catalase, an enzyme that converts hydrogen peroxide (H_2O_2) to H_2O and O_2 to protect against oxidative damage/stress. Consequently, to observe an alteration of peroxisome function induced by viperin, Huh-7 cells were transiently transfected with pLenti6-viperin-FLAG or an empty plasmid control, prior to catalase enzyme detection by Western blot analysis. The experiment was repeated twice with a representative shown

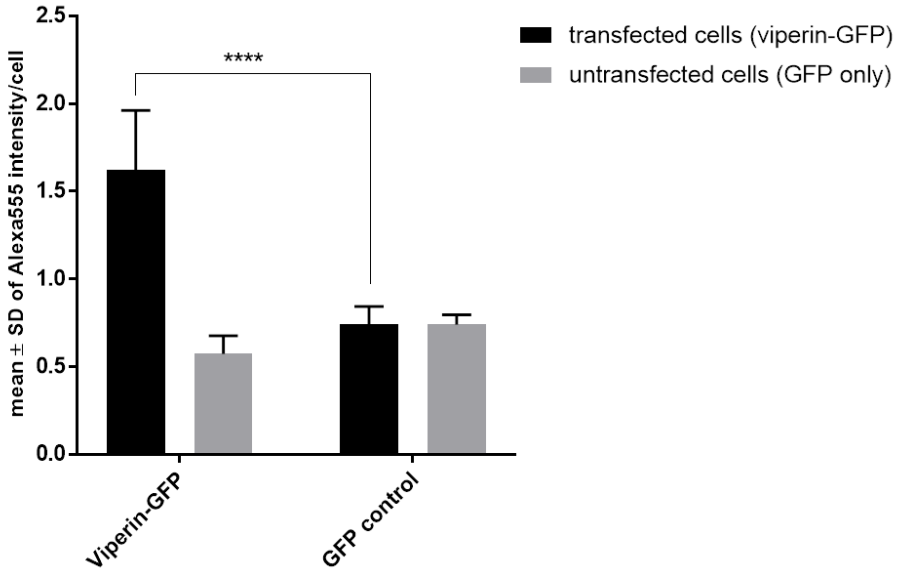

Figure 5.10: Viperin enhances peroxisome accumulation.

To investigate whether viperin enhances peroxisome accumulation, Huh-7 cells were transfected with plasmids expressing viperin-GFP or GFP alone (control), as indicated. Peroxisome content was quantified by staining with mouse anti-PMP70 and Alexa Fluor 555-conjugated goat anti-mouse IgG and cells were imaged using an Operetta high-content microscope in non-confocal mode. 25-fields were taken per well, covering approximately 50% of the well. 12 replicates were performed per condition and image analysis was performed using Harmony software. Cell counts were determined via automated enumeration of DAPI stained nuclei. Mean Alexa Fluor 555 intensity was determined for each cell. The Alexa Fluor 555 intensities of viperin-transfected cells were approximately two-fold higher when compared to GFP control-transfected cells. 2-way ANOVA, ****$p<0.0001$

in Figure 5.11A, there is an increase in catalase content of the cell in the presence of viperin. While only a modest increase in quantification of the immunoblot indicated an increase of catalase (approximately 35%) in the presence of viperin expression following normalisation to β–actin expression.

To further confirm an increase in catalase in the context of viperin, catalase enzyme detection using high-throughput microscopy (Operetta high-content microscope) was performed. Huh-7 cells were transiently transfected with plasmids expressing viperin-GFP or GFP control and were stained with goat anti-catalase prior to Alexa Fluor 555-conjugated rabbit anti-goat IgG. A total number of cells from each transfection condition were counted and averaged, and the mean of Alexa Fluor 555 intensity per cell was analysed using the Operetta high-content microscope and Harmony software as described above. Approximately 6,800 cells were analysed and approximately 32% and 57% transfection efficiencies were obtained for viperin-GFP and GFP control transfections, respectively (see raw data in Appendix X). The intensities of Alexa Fluor 555 labelling of catalase enzyme in viperin-transfected cells were significantly higher than those of GFP control-transfected cells, while there was no significant difference in the signal intensities of catalase staining in untransfected cells for both viperin-GFP and GFP control expressing cells (Figure 5.11B). These results suggest that viperin expression enhances the number of peroxisomes per cell.

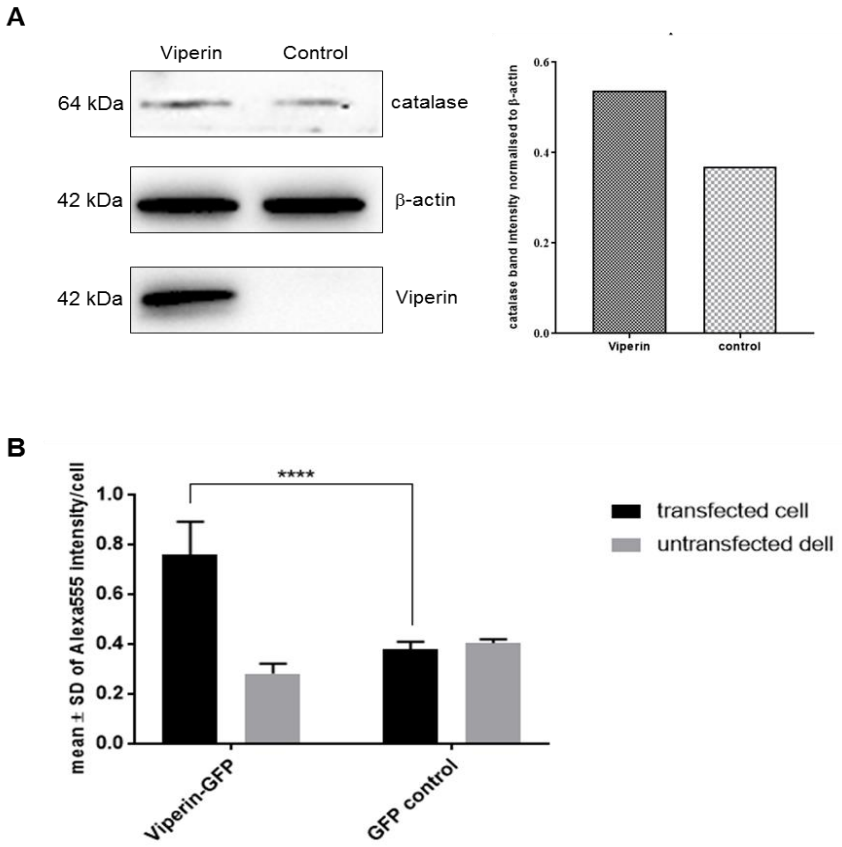

Figure 5.11: Viperin enhances peroxisome's catalase enzyme.

To investigate whether viperin enhances peroxisome's catalase enzyme, **(A)** Huh-7 cells were transfected with pLenti6-viperin-FLAG or empty plasmid control for 24 hr prior to cell harvesting and whole cell lysate preparation. Catalase enzyme was detected by Western blot analysis using goat anti-catalase. The band intensity of catalase enzyme was normalised to the internal control β-actin and represented in a bar graph. An approximately 35% increase in catalase was noted in the presence of viperin compared to control. **(B)** Huh-7 cells were transfected with plasmids expressing viperin-GFP or GFP alone (control), as indicated. The content of the peroxisomes was quantified by staining with goat anti-catalase and Alexa Fluor 555-conjugated rabbit anti-goat IgG and cells were imaged using an Operetta high-content microscope in non-confocal mode as described above. 6 replicates were performed per condition in this experiment. The Alexa Fluor 555 intensities of viperin-transfected cells were approximately double when compared to GFP control-transfected cells. 2-way ANOVA, ****$p<0.0001$

5.5 Viperin augments innate immune responses.

While a direct antiviral role of viperin against a diverse array of viruses is well-documented, it is also emerging that viperin can augment various aspects of innate immune signalling. There are a number of reports to suggest viperin controls both innate and adaptive immune responses. In viperin deficient mice (viperin$^{-/-}$), IgG1 levels were significantly decreased following challenge with ovalbumin, and the expression of Th2 cytokines IL-4, IL-5 and IL-13 were reduced in response to T cells stimulation with anti-CD3/CD28 (Qiu et al., 2009). This observation indicated that viperin may regulate Th2 response, although no mechanism underlying this investigation was proposed. In plasmacytoid dendritic cells (pDCs) deficient for viperin, type I IFN production was abrogated in response to TLR7 and TLR9 ligands (Saitoh et al., 2011). Moreover, knockdown of viperin resulted in a reduction of NF-κB in carcinoma cells and a decrease in IRF7-mediated induction of IFN-β gene expression (Moschonas et al., 2012). These results support a role for viperin in modulation of the immune response to pathogens, although further work is required to characterise this interaction.

Preliminary data from our laboratory also suggest that viperin can modulate the cellular response to poly I:C, a viral dsRNA mimic that activates RLR response in cells. To determine whether viperin modulates innate immune signalling, IFN-β mRNA abundance was observed in viperin$^{-/-}$ mouse embryonic fibroblast cells (MEFs) following activation of the RIG-I pathway by either poly I:C or Sendai virus (SeV) infection. MEFs were isolated from day 13.5-14.5 viperin$^{-/-}$ and WT C57BL/6 mouse embryos (Van der Hoek et al., 2017). IFN-β mRNA levels were significantly reduced in viperin$^{-/-}$ MEFs in response

to poly I:C stimulation and SeV infection (a well-known inducer of the cytoplasm RLR innate immune response) (Figure 5.12). To confirm a role for viperin in IFN-β production, we determined IFN-β promoter activity following transfection of Hela cells with the viperin expressing plasmid (pLenti6-viperin-FLAG) and a plasmid in which the luciferase reporter gene is driven by the IFN-β promoter. The ability of viperin to promote IFN-β production was considerably increased in response to poly I:C stimulation (Figure 5.13). These results suggest that viperin can augment innate immune signalling pathways.

5.6 A central domain of viperin is required for the interaction with PEX19.

5.6.1 Generation of a series of viperin mutants

Viperin is comprised of three distinct domains; an N-terminal domain that contains an amphipathic α-helix that is required for localisation to the ER and LDs (Hinson and Cresswell, 2009a, Helbig et al., 2011), a highly conserved central region that contains a radical SAM domain, and a C-terminal domain that contains no structural motifs but has been shown to be responsible for antiviral activity against a number of viruses (Helbig and Beard, 2014). A more comprehensive description of the domains of viperin is described in section 1.3.1, Chapter 1; we therefore investigated the domains responsible for the interaction with PEX19. A panel of viperin mutants (Figure 5.14) was created by PCR amplification and cloning into pLenti6/V5-D-TOPO with an N-terminal FLAG tag for detection. Positive clones were tested by double digestion with *Bam*HI and *Sac*II and confirmed by DNA sequencing. All of 5' and 3' viperin mutants were successfully constructed as shown in Figure 5.15 and 5.16. To investigate the localisation and

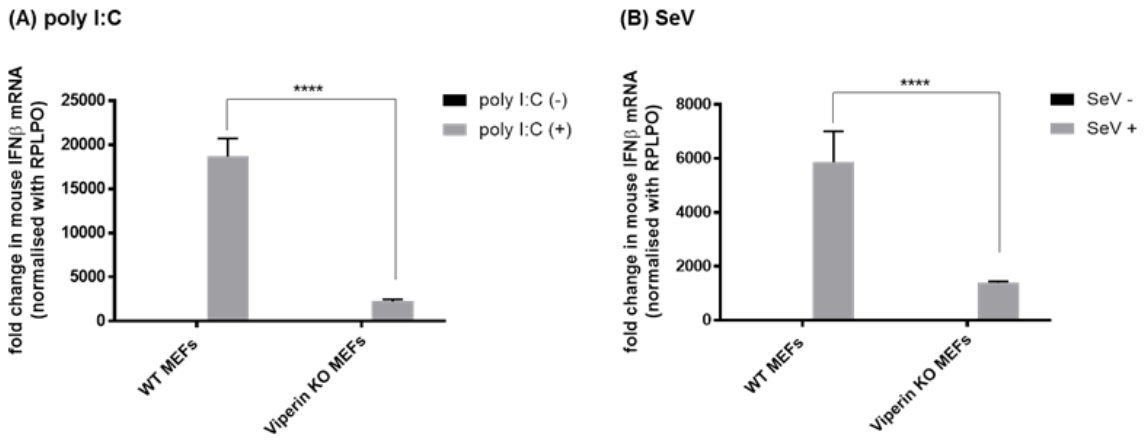

Figure 5.12: Viperin promotes IFN-β production in response to poly I:C and Sendai virus infection.

To assess the ability of viperin to regulate IFN-β production, WT and viperin$^{-/-}$ MEFs were **(A)** stimulated with poly I:C or **(B)** infected with SeV for 24 hr. IFN-β mRNA levels were quantified using real time RT-PCR. IFN-β message was significantly decreased in viperin$^{-/-}$ MEFs in response to poly I:C stimulation and SeV infection. 2-way ANOVA, ****$p<0.0001$.

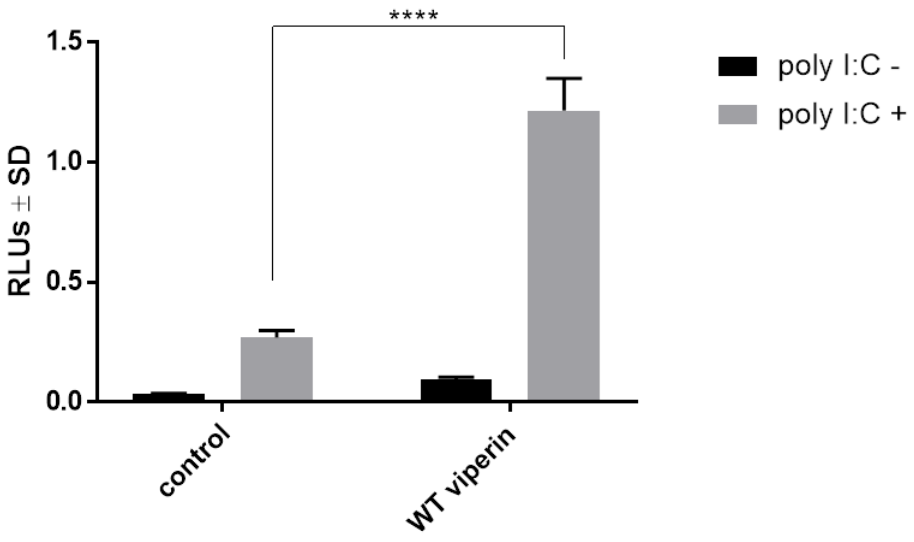

Figure 5.13: The ability of viperin to promote innate immune responses.

To investigate the ability of viperin to augment innate immune response by inducing the IFN-β production, HeLa cells were co-transfected with pLenti6-viperin-FLAG, IFN-β-luciferase and pRL-TK plasmids for 24 hr prior to stimulation with poly I:C for 24 hr. pLenti6/V5-empty plasmid was used as a control. Cell lysates were collected for luciferase activity by measuring on a GloMax^{TM} 96 Microplate Luminometer (Promega). Data were analysed using GraphPad Prism 7 software. Viperin is able to enhance poly I:C-induced IFN-β promotor activity. 2-way ANOVA, ****$p<0.0001$

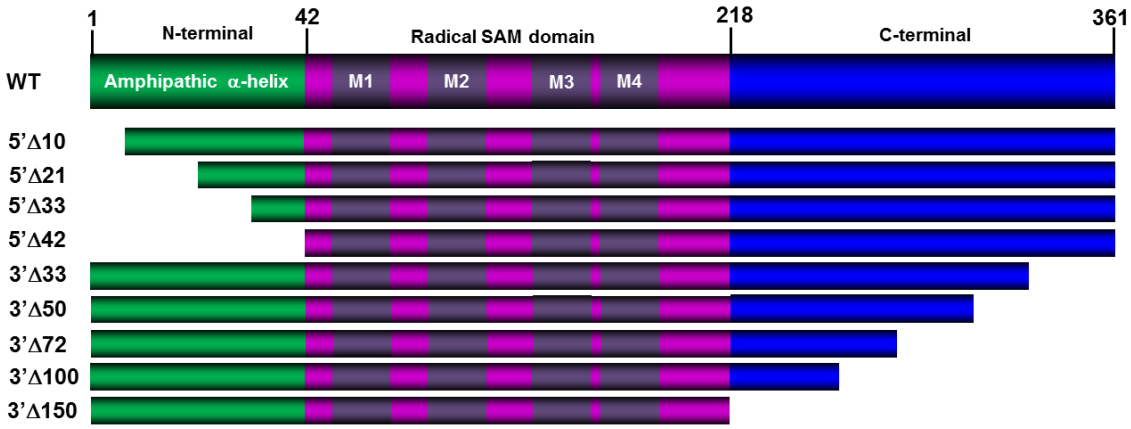

Figure 5.14: Schematic diagram of wild type (WT) viperin and a panel of mutant derivatives.

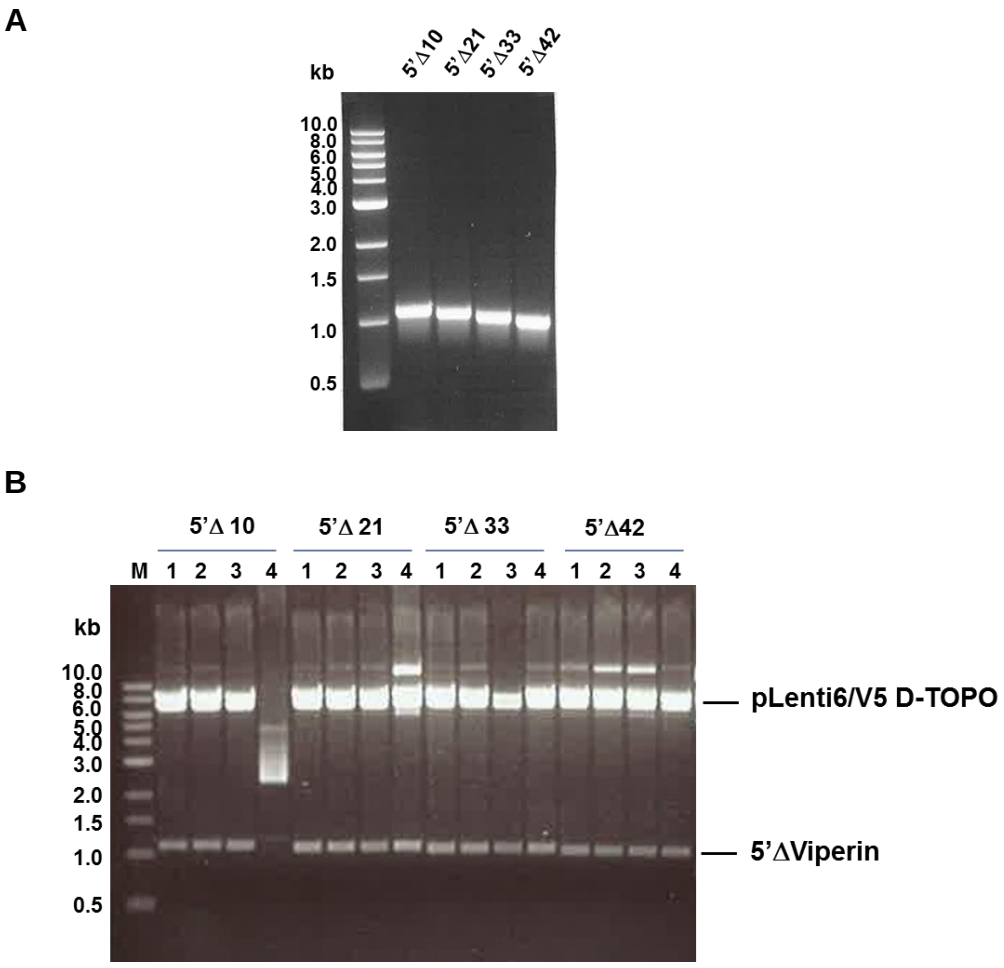

Figure 5.15: Construction of 5' viperin mutants.

To generate a series of 5' viperin mutants, **(A)** PCR products of each mutant were amplified with primers encoding a FLAG tag at the N-terminus and cloned into pLenti6/V5-D-TOPO. **(B)** To confirm the positive clones, plasmid DNA was extracted from transformant clones and subjected to double digestion with *Bam*HI and *Sac*II. Lane M, 1 kb DNA marker; 1-4, recombinant plasmids from clones no. 1-4, respectively.

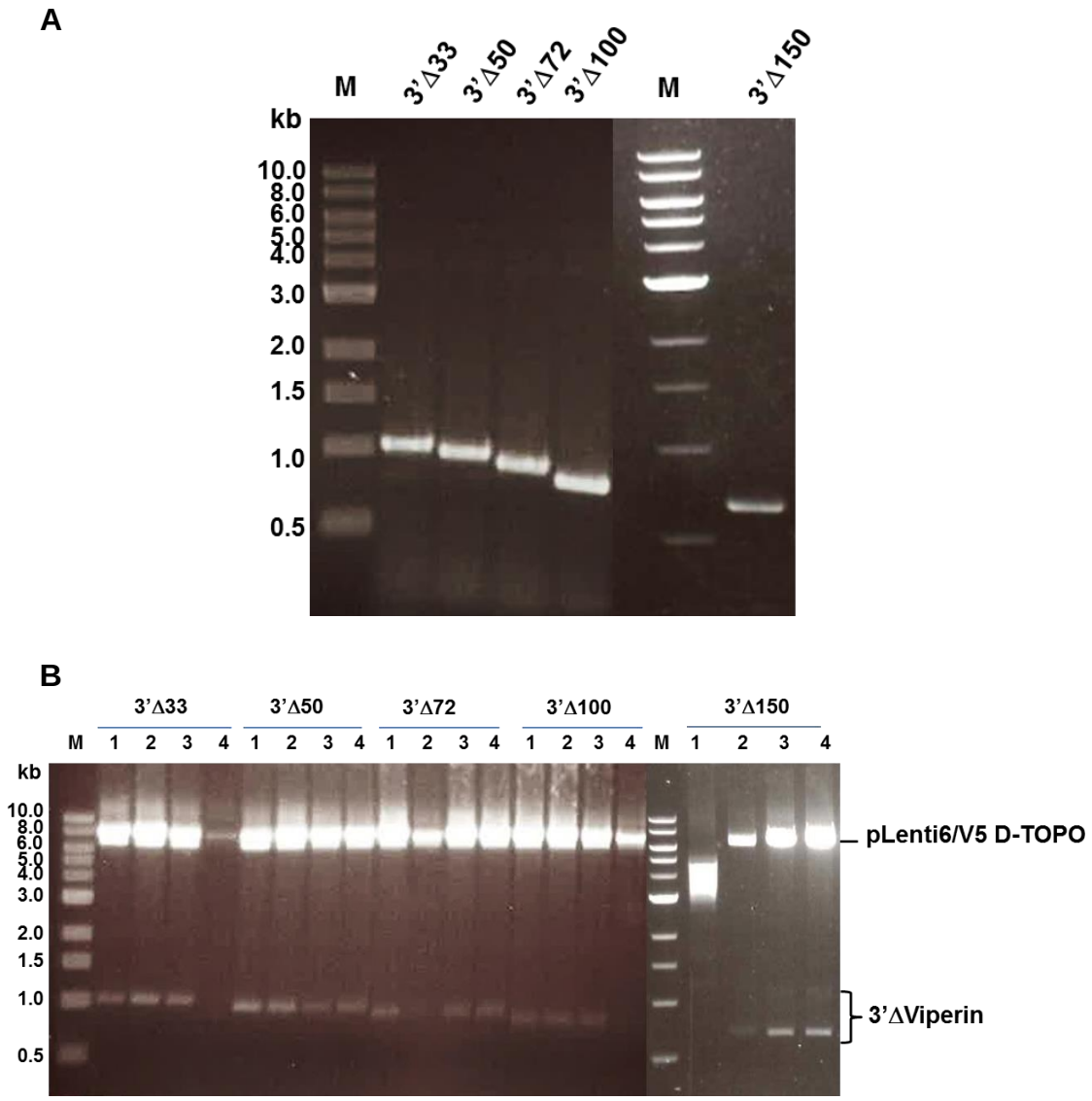

Figure 5.16: Construction of 3' viperin mutants.

To generate a series of 3' viperin mutants, **(A)** PCR products of each mutant were amplified with primers that encode FLAG tag at the N-terminus and cloned into pLenti6/V5-D-TOPO. **(B)** To confirm the positive clones, plasmid DNA was extracted from transformant clones and subjected to double digestion with *Bam*HI and *Sac*II. Lane M, 1 kb DNA marker; 1-4, recombinant plasmids from clones no. 1-4, respectively.

expression of viperin mutants, Huh-7 cells were transfected with a panel of mutants and stained with anti-FLAG and Alexa Fluor 555-conjugated goat anti-mouse IgG. Deletion of 33 amino acids from the N-terminal domain, resulted in viperin redistribution from the LDs and ER to a nuclear localisation and a homogeneous cytoplasmic pattern (Helbig et al., 2011, Hinson and Cresswell, 2009a). This was not surprising as the amphipathic-α helix at the N-terminal domain allows peripheral membrane proteins to embed into the ER and bind LD surfaces (Guo et al., 2009). However, all of 3' viperin mutants retain their localisation to the LD and ER, as is to be expected considering that these mutants retain their amphipathic-α-helix and their ability to localise to the LD (Figure 5.17).

5.6.2 The interaction of viperin mutants and PEX19

To determine which domain of viperin is required for binding to PEX19, Huh-7 cells were transiently co-transfected with each of the viperin mutants (FLAG-tagged) described previously and the PEX19-Myc expression plasmid (section 4.7.1, Chapter 4) prior to proximity ligation assay (PLA) analysis. PLA showed that all of the 3' and 5' viperin mutants were able to interact with viperin (Figure 5.18). This was certainly unexpected and suggests that the interaction is not dependent on viperin localisation. This is particularly evident in viperin mutants that contain a deletion of the N-terminal amphipathic-α-helix, that loose the ability to associate with the LD but still interact with PEX19. The ability of viperin to still bind to PEX19 in the absence of the 5' and 3' domains implies that a central radical-SAM domain may be responsible for PEX19 interaction. This observation was not pursued, but requires further investigation to determine the mechanism of interaction between viperin and PEX19.

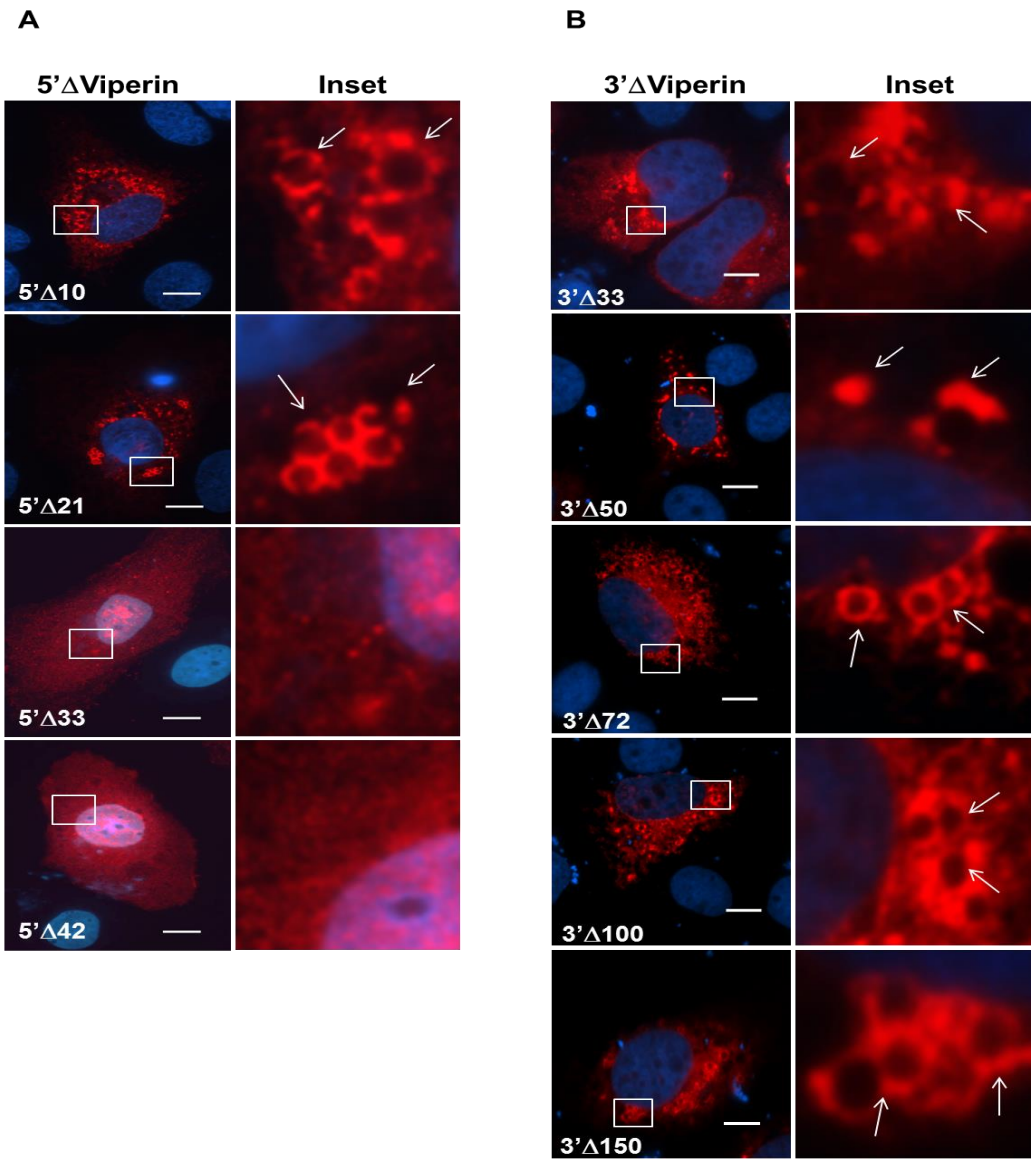

Figure 5.17: Viperin deletion mutants.

To determine the expression and localisation of viperin mutants, Huh-7 cells were transiently transfected with each of viperin mutant prior to staining with anti-FLAG and Alexa Fluor 555-conjugated goat anti-mouse IgG. Nuclei were counterstained with DAPI (blue). Expression and localisation of **(A)** 5'Δviperin and **(B)** 3'Δviperin (red) mutants were observed by immunofluorescence analysis using a Nikon TiE inverted fluorescent microscope (60x magnification). Scale bars are 10 μm. Arrows indicate putative LDs.

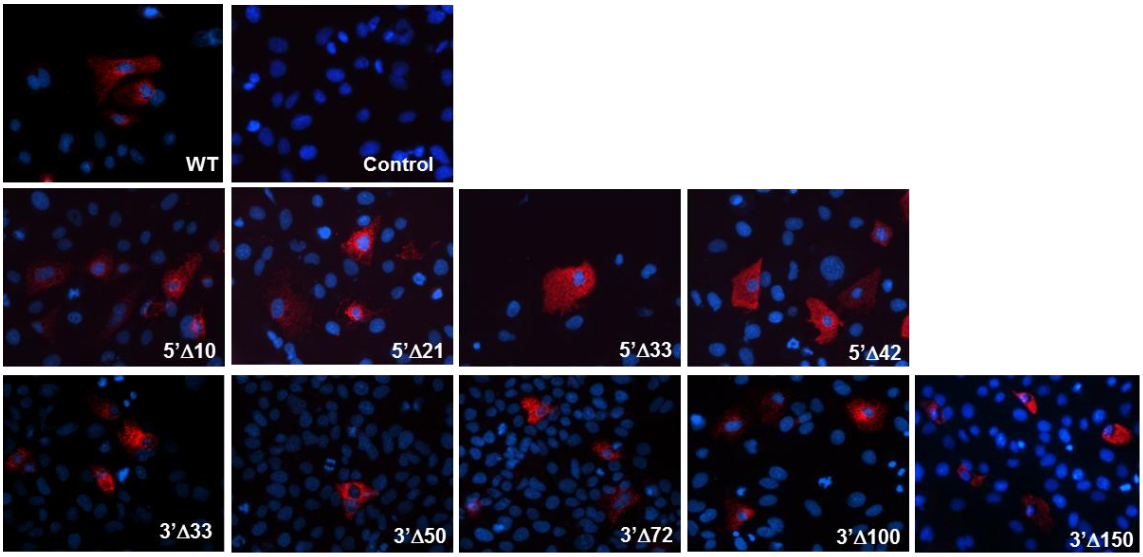

Figure 5.18: A panel of viperin deletion mutants associates with PEX19 as determined by proximity ligation assay (PLA).

To investigate whether viperin mutants interact with PEX19, Huh-7 cells were transiently transfected with pLenti6-viperin-FLAG (WT and mutants) and pCMV6-PEX19-Myc expression plasmids for 24 hr. PLA was performed using mouse anti-FLAG and rabbit anti-Myc. A combination of mouse isotype control and rabbit anti-Myc was used as a negative control and nuclei were counterstained with DAPI (blue). Red dots in cells were visualised using a Nikon TiE inverted fluorescent microscope (20x magnification).

5.7 Localisation on LDs and a C-terminal domain of viperin are required for viperin's ability to augment IFN-β promoter activity.

As described in section 5.5, viperin is able to promote a dsRNA (poly I:C)-induced innate response and we were therefore interested in the functional domains of viperin that may be responsible for their augmentation. To this end, we transfected Huh-7 cells with a plasmid in which the IFN-β promoter drives luciferase and a panel of plasmids that express viperin truncations as previously described. As expected WT viperin enhanced IFN-β promoter activity, however following deletion from the 5' terminus their enhancement progressively decreased. While the 5'Δ10 mutant showed a decrease trend, this was not significant compared to WT, and it was not until the 5'Δ21 that a statistical significant difference was observed. In contrast, none of the 3' deletion mutants retained their ability to augment the IFN-β promoter (Figure 5.19). This suggests that localisation of viperin to the LD (as determined by the 5'mutants) and the C-terminal domain are important in mediating this effect.

5.8 Viperin requires PEX19 for its ability to modulate innate immune signalling.

Our results above established that viperin promotes IFN-β promoter activity in response to dsRNA (see section 5.4). We, therefore, postulated that viperin requires the interaction with PEX19 and hence the peroxisome to enhance IFN-β promoter activation. To investigate this hypothesis, we required knockdown or knockout of PEX19. Initial attempts to delete the locus PEX19 using a CRISPR/Cas9 approach were unsuccessful. This is most likely due to the crucial requirement for peroxisomes in the cell and has been previously noted (Bender et al., 2015). We therefore used a transient knockdown

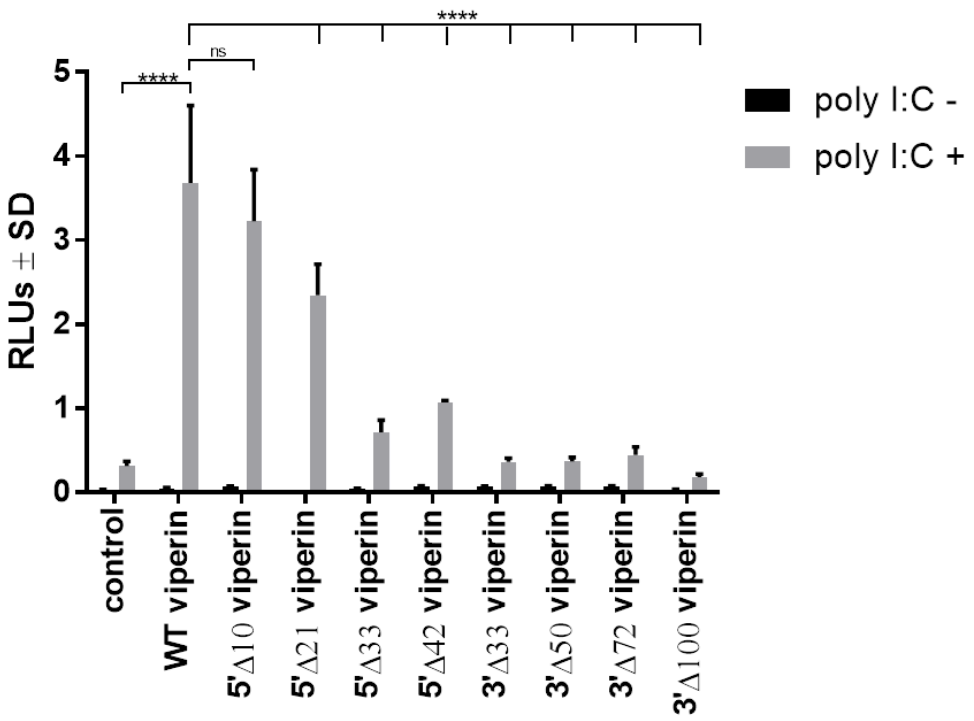

Figure 5.19: A critical domain is required for IFN-β production.

To investigate which domain is responsible for IFN-β production, HeLa cells were co-transfected with pLenti6-viperin-FLAG (WT and mutants), IFN-β-luciferase and pRL-TK plasmids for 24 hr prior to stimulation with poly I:C for 24 hr. pLenti6/V5-empty plasmid was used as a negative control. Cell lysates were collected for measurement of luciferase activity. Data are means ± SD (n=3). With the exception of 5'Δ10 and 5'Δ21, all viperin mutants abrogated IFN-β promotor activity.

approach of PEX19 using ON-TARGET plus SMART pool siRNA PEX19 (Dharmacon, GE Healthcare, USA) (see Appendix IX for target sequence). Huh-7 cells were transiently transfected with a pool of siRNAs directed to mRNA PEX19 for 48 hr prior to viperin expression for 24 hr and subsequent poly I:C stimulation for 24 hr. Knockdown of PEX19 was tested by Western blot analysis using rabbit anti-PEX19 that revealed an approximate 50% knockdown of PEX19 (Figure 5.20A). While not ideal, this degree of knockdown was the best that we could achieve. IFN-β mRNA levels were determined by real time RT-PCR analysis, and the result showed that in the presence of viperin expression and knockdown of PEX19, there was a trend in reduction of IFN-β mRNA compared to the siRNA control (Figure 5.20B). This indicated that viperin-PEX19 interaction facilitates/augments innate immune signalling in response to poly I:C.

5.9 Discussion

It is well-documented that viperin interacts with a broad range of host and viral proteins and our work in Chapter 4 using a Y2H approach now adds PEX19 to the list of viperin interacting partners. It is not immediately apparent as to the biological significance of viperin binding to PEX19. PEX19 is a cytosolic chaperone protein that plays a role in the early peroxisome biogenesis pathway by facilitating the insertion of peroxisomal membrane proteins (PMP) into the membrane of the peroxisome. Peroxisomes are significant dynamic organelles with a diverse function mainly in lipid metabolism and degradation of harmful hydrogen peroxide, however, most recently it is emerging that the peroxisome plays a key role in the innate antiviral response. While we have provided evidence for the interaction between viperin and PEX19, in this chapter we aimed to

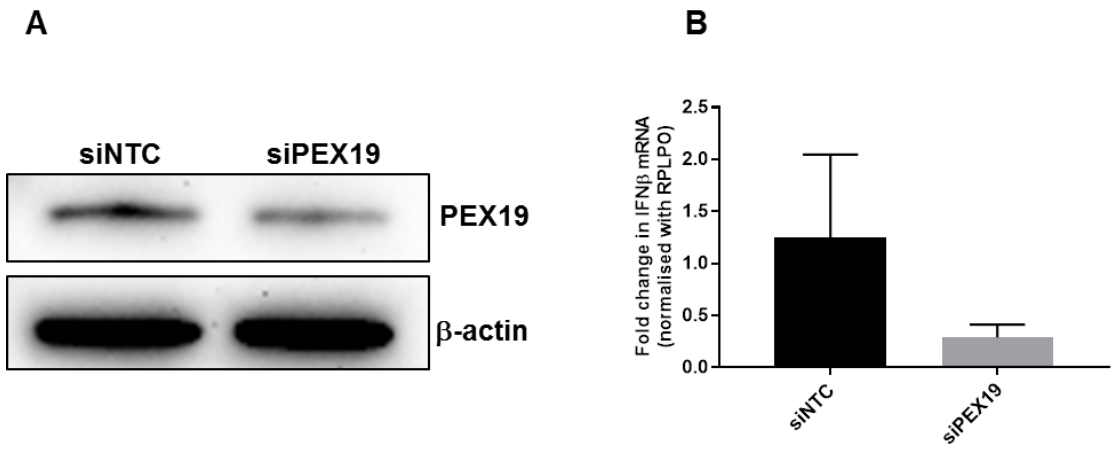

Figure 5.20: Interaction with PEX19 is required for the ability of viperin to augment innate immune signalling.

To test if viperin requires the interaction with PEX19 to modulate immune signalling, knockdown of PEX19 was achieved using a pool of siRNAs targeting PEX19 (Dharmacon). Huh-7 cells were transiently transfected with the PEX19-specific siRNA pool or non-targeting control (NTC) siRNA pool for 48 hr prior to viperin overexpression for 24 hr followed by poly I:C stimulation for 24 hr. **(A)** knockdown of PEX19 was analysed by Western blot analysis using rabbit anti-PEX19 and HRP-conjugated goat anti-rabbit. An approximately 50% knockdown of PEX19 was obtained using this approach. **(B)** IFN-β mRNA levels were determined by real time RT-PCR analysis and was reduced in response to poly I:C induction following viperin expression, in the absence of PEX19. A representative bar graph were from 2 independent experiments.

further characterise the PEX19-viperin interaction in a cellular context. PEX19 has been shown previously to shuttle between the ER and peroxisomes and in the process chaperones, proteins essential for peroxisome biogenesis and hence we were therefore interested in the cellular distribution of PEX19 in our Huh-7 cells (Sacksteder et al., 2000, Jones et al., 2004). We initially used an antibody directed toward PEX19 to observe endogenous PEX19 in Huh-7 cells, however this resulted in significant background fluorescence. To this end, we expressed exogenous PEX19 (GFP tagged) and visualised peroxisomes using an antibody directed towards PMP70 (resident peroxisomal marker) and expression of PEX11B (Flag-tagged, also a resident peroxisomal marker). As expected PEX19 localised to the peroxisome as determined by overlapping immunofluorescence for both PMP70 and PEX11B but was also localised independent of the peroxisome in what was presumed to be the ER (Figure 5.3). This distribution of PEX19 raises the question as to whether viperin interacts with PEX19 at the ER or the peroxisome. To answer this question we initially expressed viperin-GFP and PEX19-Myc/Flag and confirmed that not only do PEX19 and viperin co-localise but that the cellular distribution of PEX19 is significantly altered in the presence of viperin. This is evident in Figure 5.3 in which PEX19 is distributed homogenously throughout the cytoplasm at the ER and peroxisomes, while in Figure 5.4 in the presence of viperin, PEX19 assumes a more peri-nuclear localisation in association with viperin in what seems to be at the surface of circular structures. These circular structures are most likely to be lipid droplets as it is well-documented that viperin can localise to the surface of the LD via an interaction of its N-terminal amphipathic helix with the LD membrane. Interestingly, under normal conditions (i.e., no viperin) PEX19 does not interact with the

LD, however in the presence of viperin, PEX19 can be found in association with viperin at the LD interface. Most importantly we also show that this interaction occurs at the level of the peroxisome as there is a strong association between viperin and the peroxisomal markers PMP70 and PEX11B. To further resolve the interaction of viperin and PEX19 and the peroxisome we used 3D-SIM super-resolution imaging. 3D-SIM allows for the imaging of several cellular components and the mapping of their relative positions in macromolecular complexes, enabling the study of their spatial relationship within the cell over and above that of standard confocal microscopy. We confirmed our previous observation showing that viperin indeed interacts at the LD interface (ADRP positive) and that PEX19 also interacts with viperin at the same location. Interestingly, while we also noted direct overlap of signals suggesting an interaction between viperin and PMP70, we also observed PMP70 positive peroxisomes juxtaposed to viperin positive LDs. Collectively, this work provides evidence that viperin interacts with PEX19 at the peroxisome and recruits the peroxisome to a close association with the LD.

Preliminary data from our laboratory has shown that viperin can augment the innate immune response to RNA viral infection and poly I:C. Furthermore, the recent reports that MAVS is localised to and can signal from the peroxisome suggests that the ability of viperin to bind PEX19 and redistribute the peroxisome may somehow be linked to innate immune signalling from the peroxisome. As discussed above, the biogenesis of the peroxisome requires PEX19 and previous reports have linked peroxisome number with the innate response (Odendall et al., 2014).

It is therefore conceivable that viperin augments innate immune signalling by enhancing peroxisome biogenesis and/or function to maximise the antiviral response. Quantification of total cellular peroxisome content in the absence or presence of viperin using an operetta high content imager, found that peroxisome content (as determined by PMP70 accumulation) was significantly increased in the presence of viperin. Concomitant with this observation, we also found that the peroxisomal enzyme, catalase, was significantly enhanced in expression in the presence of viperin. Hence, the ability of viperin to increase peroxisome number or alter their localisation could possibly be a mechanism to augment the innate antiviral response. Interestingly, the capsid proteins of WNV and DENV can also bind PEX19, resulting in a significant loss of peroxisomes and corresponding IFN-λ production, that highlights the importance of the peroxisome in the host innate response to viral infection (You et al., 2015).

Preliminary data from our laboratory has implicated viperin expression in augmentation of the innate immune response to viral infection. To further explore this observation we made use of MEFs isolated from a viperin$^{-/-}$ KO mouse generated in our laboratory using CRISPR/Cas9 technology, and either transfected the MEFs (WT were used as a control) with poly I:C or infected them with SeV, both of which are well-documented to activate a RIG-I response. Consistent with our preliminary data, a lack of viperin resulted in a significant decrease in IFN-β mRNA, implicating viperin as a positive regulator of the innate response to viral infection. As we have outlined previously, viperin exerts its antiviral activity through a number of specific domains, however there is not a common mechanism, with viperin utilising different strategies to impact viral replication. For

example the radical SAM and C-terminal domains play a crucial role in viperin's anti-TBEV, while the N-terminal amphipathic helix is important for viperin's anti-DENV activity, and both the N- and the C-terminal domain are important for its anti-HCV activity (Helbig et al., 2011, Helbig et al., 2013, Upadhyay et al., 2014). We reasoned that similar domains of viperin would play a role in its ability to bind PEX19 and hence impact the innate immune response. We therefore used a panel of viperin mutants and firstly investigated their interaction with PEX19 using PLA (Figure 5.18). To our surprise, we noted that all viperin mutants, both N- and C- terminal, retained their ability to bind to PEX19 suggesting that either the central or the radical SAM domain may play a role in the interaction with PEX19. We did not investigate the role of the radical SAM domain through mutagenesis and it will be of interest to further investigate the role of this domain in the interaction with PEX19. The ability of all viperin mutants to bind to PEX19 suggests that viperin's capacity to augment innate immune signalling is most likely a function of the cellular localisation of viperin and not its ability to bind PEX19. This was certainly the case as viperin with a truncation of the first 21 AA retained the ability to augment innate immune signalling while truncation beyond this point and hence removal of the amphipathic helix and LD localisation significantly abrogated viperin's innate immune stimulation ability. Furthermore, all 3' deletion mutants significantly abrogated innate immune activation. Collectively, this work suggests that the ability of viperin to move to the LD is essential for its ability to modulate innate immune signalling and that the 3' terminal region of viperin is also important.

Our results to date have demonstrated that viperin expression can induce peroxisome accumulation and re-localisation that most likely underpins viperins' ability to augment the innate immune response. However, to conclusively determine the role of PEX19 in this process, we attempted to knockout PEX19 in Huh-7 cells using a CRISPR/Cas9 approach, however, this was unsuccessful. The fact that the peroxisome is an essential organelle to control and stabilise lipid metabolism and cellular homeostasis is most likely the reason as to why we could not create PEX19 knockout cells. This is consistent with the study from the Bartenschlager laboratory (Bender et al., 2015) in which similar studies were attempted. Accordingly, transient knockdown PEX19 was achieved through a siRNA approach in which Huh-7 cells were transfected with a Dharmacon smart pool targeting PEX19. Even though we could only achieve an approximately 50% decrease in PEX19 expression, these cells showed a decrease in viperin induced innate immune augmentation (Figure 5.20), implying that viperin requires PEX19/peroxisomes to trigger innate immune signalling. Obviously complete knockout of PEX19 would be ideal, however there are challenges associated with this approach as discussed above. However, a human fibroblast cell line defective in PEX19, isolated from a patient with Zellweger syndrome is available (Odendall et al., 2014) and could be used to further study the effectiveness of viperin to promote an innate immune response in the complete depletion of peroxisomes.

Previous studies demonstrated that the *Flaviviruses*, DENV and WNV have evolved a strategy to evade the MAVS-dependent innate antiviral response via degradation of peroxisomes (You et al., 2015). Infection with either DENV or WNV resulted in

reduction of peroxisome number, most likely through direct interactions of PEX19 and the DENV or WNV viral capsid proteins (You et al., 2015). Therefore, it is conceivable that the interaction of viperin and PEX19 may reverse the effect of virus-mediated degradation of peroxisome by either protecting peroxisomes from degradation or initiating peroxisome biogenesis. Clearly further studies are warranted.

In summary, viperin physically interacts with PEX19 and redirects peroxisomes to LDs, and it is possible that the radical SAM domain plays a principle role in this interaction. Moreover, PEX19, and hence peroxisomes are required for viperin to augment innate immune signalling in response to viral infection. A recent study has shown that viperin interacts with the innate immune adaptor protein MAVS (Hee and Cresswell, 2017) that is localised to the mitochondria, mitochondria-associated membrane (MAM) and peroxisomes and that maximal signalling requires the coming together of these organelles into an immune synapse (Dixit et al., 2010, Horner et al., 2011). This raises the question as to how viperin interacts with MAVS and the peroxisome to modulate an innate antiviral response in the formation of the immune synapse. The association of viperin, MAVS, and other cellular organelles (peroxisomes, LDs, mitochondria) will be investigated and described in the next chapter.

Chapter 6

Viperin augments innate immune response through the interaction with MAVS at mitochondria and peroxisomes

6.1 Introduction

It is well-established that mitochondrial antiviral signalling protein (MAVS), also named VISA/IPS-1/Cardif, is an indispensable adaptor protein for innate immune signalling. Anchoring of MAVS via its C-terminal domain to the outer membrane of mitochondria (Seth et al., 2005) engages and activates the downstream RLR signalling pathway that results in the expression of type I IFN (see Figure 1.8, Chapter 1). Localisation of MAVS to mitochondria is essential for innate immune signalling. MAVS engineered to a cytosolic localisation abrogates the innate antiviral signalling (Dixit et al., 2010) and moreover, cleavage of MAVS from the mitochondria by the HCV protease NS3/4a abolishes RIG-I signalling (Li et al., 2005b, Meylan et al., 2005, Foy et al., 2005). Recent studies have shown that in addition to the mitochondrial outer membrane, MAVS also localises to mitochondrial-associated membranes (MAM), a specialised subdomain that physically connects the ER to the mitochondria, and to peroxisomes (Horner et al., 2011, Dixit et al., 2010). Interestingly, in one study the selective localisation of MAVS to specific organelles such as mitochondria and peroxisomes generated a diverse and specific immune response upon viral infection (Odendall et al., 2014). However, this was not the case with studies from Bender *et al*. in which both mitochondrial and peroxisomal MAVS activated, the expression of type I and III IFNs with comparable efficiency upon infection with a range of RNA viruses (Bender et al., 2015). In addition, it has been

shown using a biochemical and microscopy approach that there is an interaction between mitochondria, peroxisomes and the MAM upon viral infection that constitutes the formation of a signalling innate "immune synapse" following RIG-I activation in response to viral infection (Horner et al., 2011, Vazquez and Horner, 2015). This suggests some sort of coordination of signalling from these organelles (Horner et al., 2011, Vazquez and Horner, 2015), however the spatial and temporal dynamics of these interactions are not understood.

Our previous results showing an interaction of viperin with the peroxisome, and subsequent shift in localisation of the peroxisome suggests that viperin (expressed in response to viral infection) may regulate the signalling of the immune synapse; at least from the peroxisome. Thus, we hypothesise that viperin is a regulator of innate immune signalling from the peroxisomes. Accordingly, the aim of this chapter is to define of how viperin controls MAVS signalling from different organelle compartments.

6.2 Viperin associates with MAVS, peroxisomes and lipid droplets.

Previous studies have identified the localisation of MAVS to the mitochondria, MAM and to peroxisomes (Horner et al., 2011, Dixit et al., 2010). However, to confirm localisation of MAVS to the mitochondria and peroxisomes in our culture model we investigated MAVS expression in association with various organelles in Huh-7 cells using a monoclonal Ab directed towards MAVS. Indirect immunofluorescence revealed as expected, a significant proportion of MAVS on the mitochondria (Mitotracker) and possibly the MAM, and to a lesser degree on peroxisomes (PMP70) (Figure 6.1). This

clearly indicated that MAVS localised to both the mitochondria, (and possibly MAM) and peroxisomes in Huh-7 cells.

Given our previous results showing viperin can interact with peroxisomes and the presence of MAVS on peroxisomes, we next investigated the association of viperin and MAVS. Spatial co-localisation of these proteins was investigated by transiently transfecting Huh-7 cells with a plasmid expressing viperin-GFP and staining with rabbit anti-MAVS followed by Alexa Fluor 555-conjugated goat anti-rabbit IgG. While there were areas of viperin that did not interact with MAVS, viperin-positive LDs were surrounded by MAVS positive mitochondria and in numerous instances there was an obvious overlap of fluorescent signal indicating possible interaction between viperin and MAVS (Figure 6.2). This result is consistent with a recent study that has shown an interaction of viperin and MAVS at the MAM (not mitochondria), however in this study interactions with the peroxisomes were not investigated (Hee and Cresswell, 2017).

As mentioned above, viperin interacts and directs peroxisomes in close proximity to LDs, and together with the data above that viperin does colocalise with MAVS, prompted us to investigate the association between viperin, the peroxisome and MAVS. The co-localisation of viperin, MAVS and peroxisomes was assessed by transiently transfecting Huh-7 cells with a plasmid expressing viperin-GFP prior to staining the endogenous MAVS (using rabbit anti-MAVS and Alexa Fluor 555-conjugated goat anti-rabbit) and peroxisomes (mouse anti-PMP70 and Cy5–conjugated goat anti-mouse).

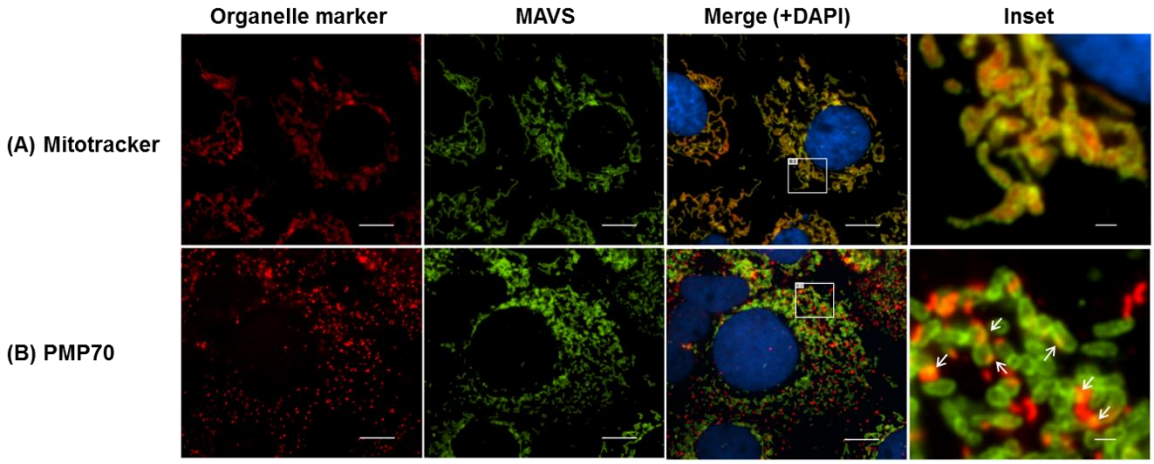

Figure 6.1: Localisation of MAVS to both mitochondria and peroxisomes.

To investigate MAVS localisation to mitochondria, Huh-7 cells were incubated with a permeable probe for mitochondrial labelling (MitoTracker® Red CMXRos, Cell Signalling Technology) for 30 min prior to staining with rabbit anti-MAVS and Alexa Fluor 488-conjugated goat anti-rabbit IgG secondary Ab. In addition, to observe the localisation of MAVS on peroxisomes, Huh-7 cells were stained with rabbit anti-MAVS and mouse anti-PMP70 followed by Alexa Fluor 488-conjugated goat anti-rabbit IgG and Alexa Fluor 555-conjugated goat anti-mouse IgG secondary Ab. Nuclei were counterstained with DAPI (blue). MAVS (green) is predominantly found on **(A)** mitochondria, with a lesser extent on **(B)** peroxisomes, which observed by immunofluorescence analysis using a Nikon TiE inverted fluorescent microscope (60x magnification). Scale bars are 10 μm and 1 μm for main images and insets, respectively. Arrows indicate the region of co-localisation.

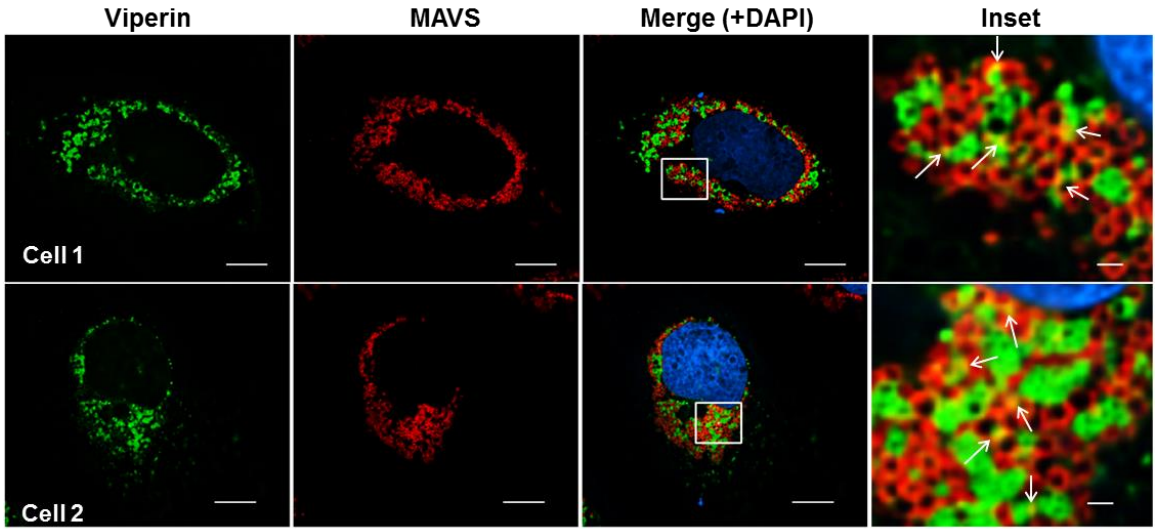

Figure 6.2: Co-localisation of viperin and MAVS.

To investigate if viperin does colocalise with MAVS, Huh-7 cells were transiently transfected with a plasmid expressing viperin-GFP prior to staining with rabbit anti-MAVS and Alexa Fluor 555-conjugated goat anti-rabbit IgG. Nuclei were counterstained with DAPI (blue). Serial (0.25-μm) z-sections of immunofluorescence images were acquired using a Nikon TiE inverted fluorescent microscope and deconvoluted using the 3D AutoQuant Blind Deconvolution plug-in of NIS Elements Advanced Research v 3.22.14 software. Images are single representative z-sections. Obviously co-localisation of viperin (green) and endogenous MAVS (red) was obviously seen using deconvolution immunofluorescence microscopy (60x magnification). Scale bars are 10 μm and 1 μm for main images and insets, respectively. Arrows indicate the co-localisation area.

Analysis of micrographs revealed that in Huh-7 cells not expressing viperin, there was some association of peroxisomes with MAVS (Figure 6.1), however as indicated above this was not a common occurrence. However, in the presence of viperin, we noted significant co-localisation between viperin (surrounding the LDs), MAVS and peroxisomes. In some cases, it seemed that viperin was acting as a connector or bridge between the peroxisomes and mitochondria (Figure 6.3). It has been suggested that the localisation of MAVS to the MAM-mitochondria interface is important for antiviral signalling function. However, how MAVS signalling from the peroxisome is orchestrated has not been addressed. These results suggest that at least in Huh-7 cells, viperin relocates MAVS positive peroxisomes in close proximity to MAVS present on mitochondria and the MAM to enhance antiviral signalling.

6.3 Differential localisation of MAVS creates a different innate immune signalling.

Selective localisation of MAVS on mitochondria/MAM or peroxisomes has established that peroxisomes are an important site of antiviral signal transduction. Studies from the Kagan laboratory revealed that peroxisomal-MAVS (MAVS-pex) induces a rapid interferon-independent antiviral effect, whereas mitochondrial-MAVS (MAVS-mito) activates the IFN dependent effect. Furthermore, MAVS-pex was responsible for type III IFN (IFN-λ) induction (Odendall et al., 2014). However, this is controversial as work from Bender *et al*. showed that MAVS-pex could equally induce both type I and III IFN expression (Bender et al., 2015). Nevertheless, peroxisomal localised MAVS is important for antiviral signalling. With this in mind and previously discussed data, we sought to

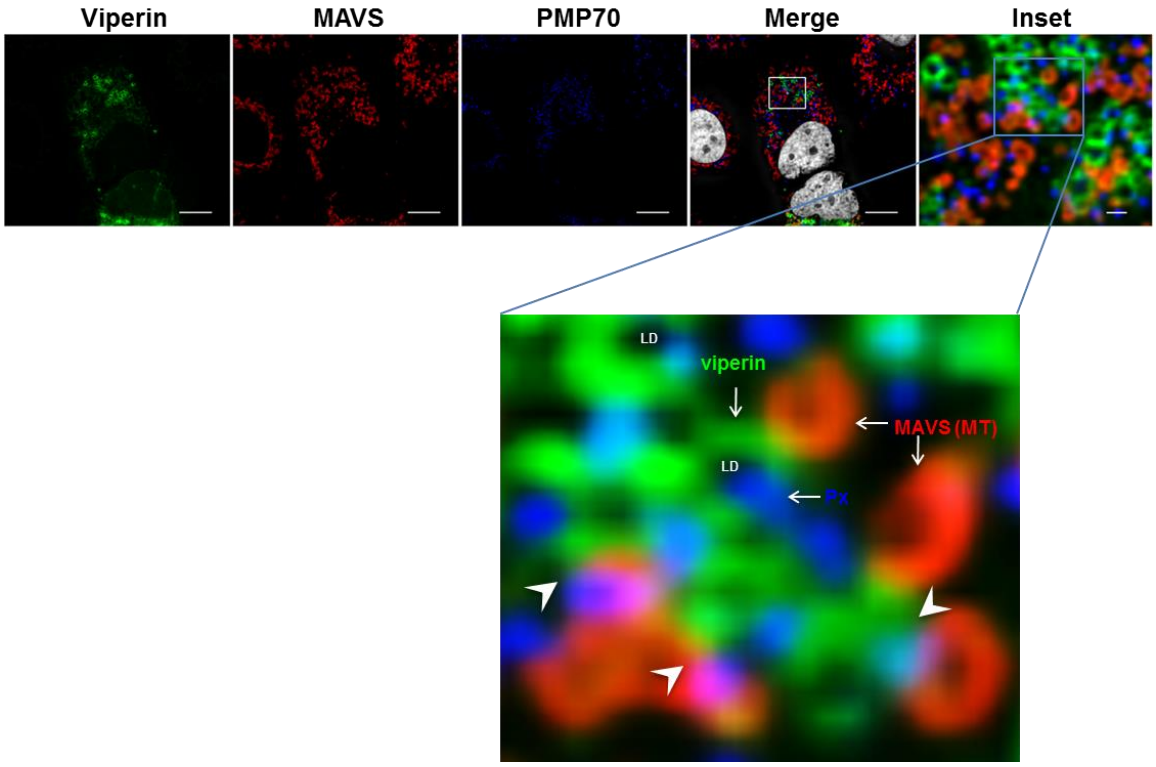

Figure 6.3: The association of viperin, MAVS, and peroxisomes.

To determine whether viperin is in close connection with MAVS and peroxisomes, Huh-7 cells were transiently transfected with a plasmid expressing viperin-GFP prior to staining with rabbit anti-MAVS and mouse anti-PMP70 following by a combination of an Alexa Fluor 555-conjugated goat anti-rabbit IgG and Cy5–conjugated goat anti-mouse IgG. Nuclei were counterstained with DAPI. Serial (0.25-μm) z-sections of immunofluorescence images were acquired using a Nikon TiE inverted fluorescent microscope and deconvoluted using the 3D AutoQuant Blind Deconvolution plug-in of NIS Elements Advanced Research v 3.22.14 software. Images are single representative z-sections. A close association between viperin (green), endogenous MAVS (red) and peroxisome/PMP70 (blue) was obviously seen using deconvolution immunofluorescence microscopy (60x magnification). Scale bars are 10 μm and 1 μm for main images and the inset, respectively. Arrows indicate viperin (on LDs), MAVS (mitochondria, MT) and PMP70 (peroxisomes, Px). Arrowhead indicates a close association area of the 3 proteins/organelles.

determine which MAVS subcellular compartment is under the regulation of viperin to augment antiviral innate immune signalling.

To address this experimentally, we adopted the approach of Dixit *et al*. in which MAVS was targeted to specific organelles by engineering specific organelle localisation signals to the C-terminus of MAVS. However, prior to generation of organelle specific MAVS cell lines, it was necessary to knockout endogenous MAVS in Huh-7 cells. MAVS knockout (MAVS-KO) in Huh-7 cells was successfully generated using CRISP/Cas9 technology (see section 2.3.7.5, Chapter 2) with immunofluorescence microscopy and Western blot analysis confirming deletion of the MAVS locus (Figure 6.4A, B). The functionality of these MAVS-KO cells to an innate immune response was tested by transfection of poly I:C, a known activator of the RIG-I pathway, followed by an assessment of the induction of IFN-β and IFN-λ1 mRNA by real time RT-PCR. As expected, IFN-β and IFN-λ1 mRNA levels were significantly reduced in MAVS-KO cells compared to the parental Huh-7 cells (Figure 6.4C), indicating successful knockout of MAVS and associated signalling.

To generate a stable Huh-7 cell line expressing MAVS with specific localisation to either the mitochondria, peroxisomes or both compartments, expression plasmids expressing MAVS-WT (addgene#52135), MAVS-pex (addgene#44557) and MAVS-mito (addgene #44556) were introduced into Huh-7 MAVS-KO cells using a retroviral transduction system (Dixit et al., 2010). In these plasmids, the MAVS transmembrane domain was

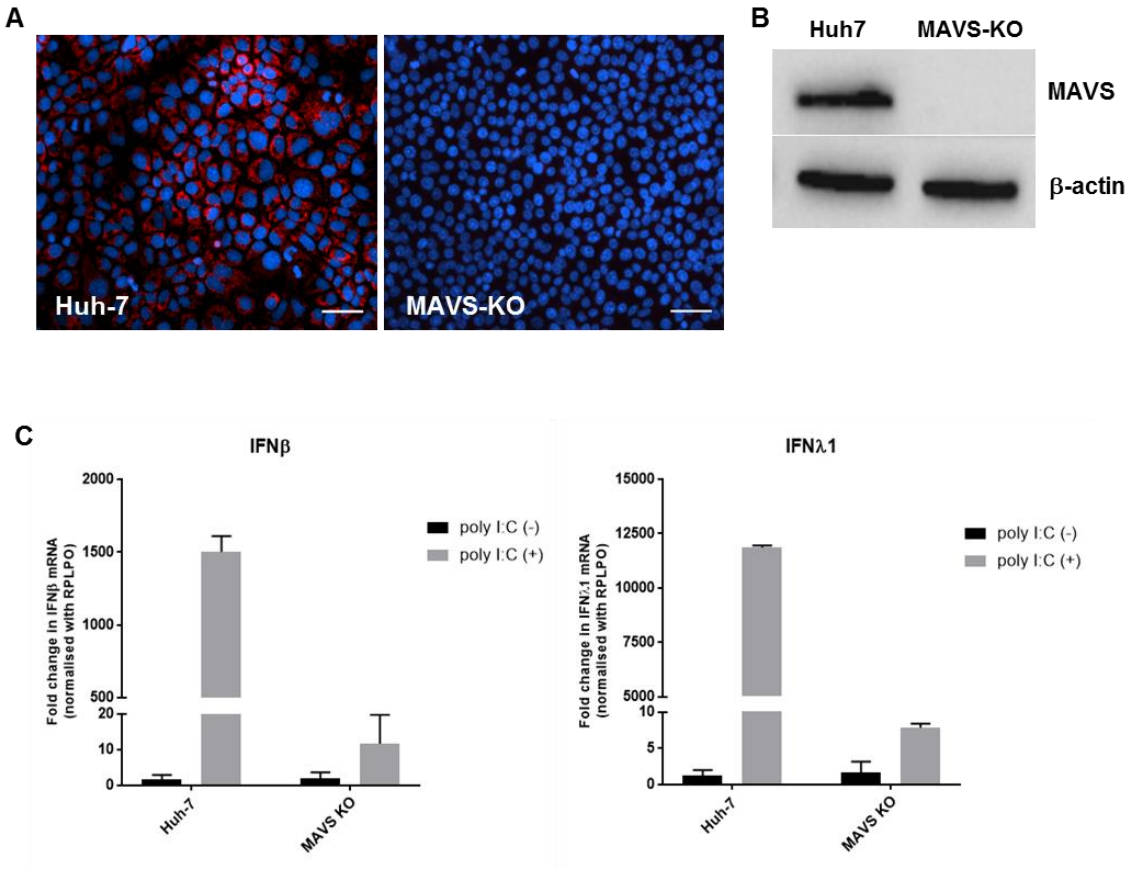

Figure 6.4: Generation of MAVS knockout (MAVS-KO).

To create MAVS-KO cells, Huh-7 cells were transduced with lentivirus containing LentiCRISPR v2 encoding the MAVS sgRNA for 5 hr and subsequently replaced with fresh complete media. A monoclonal population of each potential knockout colony was obtained under puromycin selection. MAVS-KO cells were tested by **(A)** immunofluorescence analysis using a Nikon TiE inverted fluorescent microscope (20x magnification, scale bars are 50 μm) and **(B)** Western blot analysis. **(C)** To determine the function of MAVS-KO cell line, this cell was stimulated with poly I:C for 24 hr, and IFN-β and IFN-λ1 mRNA level were assessed by real time RT-PCR. The IFN-β and IFN-λ1 mRNA were significantly decreased in MAVS-KO. Data are means ± SD (n=3).

replaced with a set of targeting sequences to direct MAVS to a single compartment (Figure 6.5). The plasmids also contain GFP that can be used to select for MAVS expressing cells. Following selection of GFP expressing cells by FACS at the single cell level, stable cell lines expressing MAVS were expanded and tested by immunoblotting and immunofluorescence microscopy analysis for MAVS expression and localisation (Figure 6.6). Expression levels between MAVS-WT and MAVS-mito were similar, however MAVS-pex expression was considerably lower and most likely reflects the differential localisation of MAVS expressed on peroxisomes compared to the mitochondria. Selectively expression of MAVS on distinct subcellular compartments was confirmed by immunofluorescence microscopy analysis using a specific marker of mitochondria (Mitotracker) and peroxisomes (PMP70). As expected, with parent Huh-7 cells, MAVS localised predominantly to the mitochondria with a lesser amount to the peroxisomes (Figure 6.7 and 6.8, respectively). MAVS-WT localised predominantly to mitochondria with a marginal amount on peroxisomes, while MAVS-mito and MAVS-pex are expressed on the specific subcellular compartments, mitochondria and peroxisomes respectively (Figure 6.7 and 6.8, respectively). For downstream studies, it was important to check that organelle specific MAVS still retained the capacity to signal. We therefore stimulated parent Huh-7 cells, Huh-7 MAVS-KO and organelle targeted MAVS cells with poly I:C (transfected) for 24 hr and assessed IFN-β and IFN-λ1 mRNA induction by real time RT-PCR. Stable cells expressing MAVS on both compartments i.e., Huh-7 (parent) and MAVS WT significantly induced expression of IFN-β and IFN-λ1 mRNA, while MAVS-pex and MAVS-mito cells resulted in an increase in IFN-β and

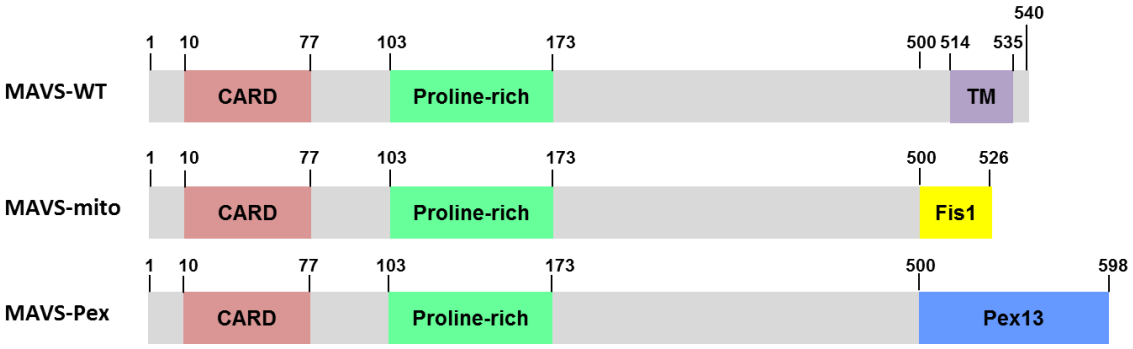

Figure 6.5: Schematic diagram of WT and engineered MAVS alleles targeting to a specific organelle.

The transmembrane domain (TM) of MAVS was replaced with Fis1 and Pex13 sequences to direct MAVS to mitochondria (MAVS-mito) and peroxisomes (MAVS-pex), respectively. Adapted from (Dixit et al., 2010).

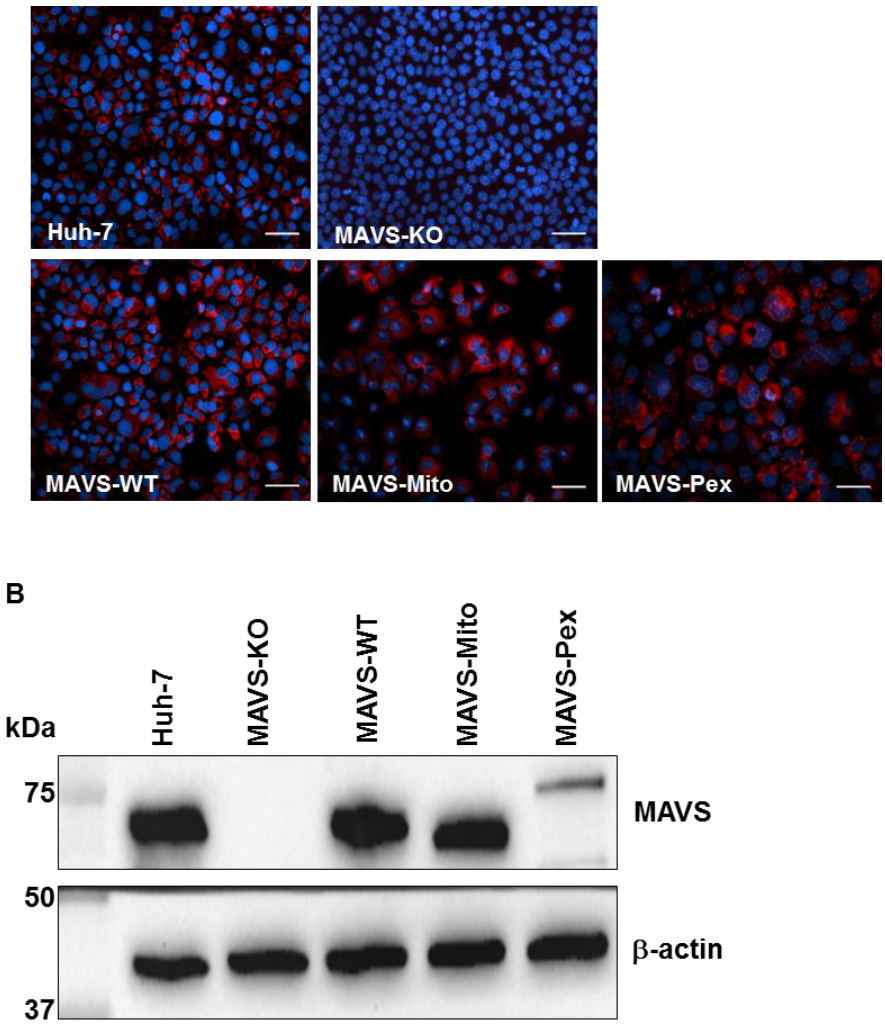

Figure 6.6: Generation of stable cell lines expressing MAVS allele.

To create stable cell lines expressing MAVS transgenes, MAVS-KO cells were transduced with retroviral containing MAVS alleles for 5 hr and subsequently replaced with fresh complete media for 3 days. A monoclonal stable cell expressing each MAVS allele was obtained by GFP positive cell sorting (BD FACSAria^{TM} II). The expression of MAVS in each stable cell lines was tested by **(A)** immunofluorescence analysis, using a Nikon TiE inverted fluorescent microscope (20x magnification, scale bars are 50 μm) and **(B)** Western blot analysis.

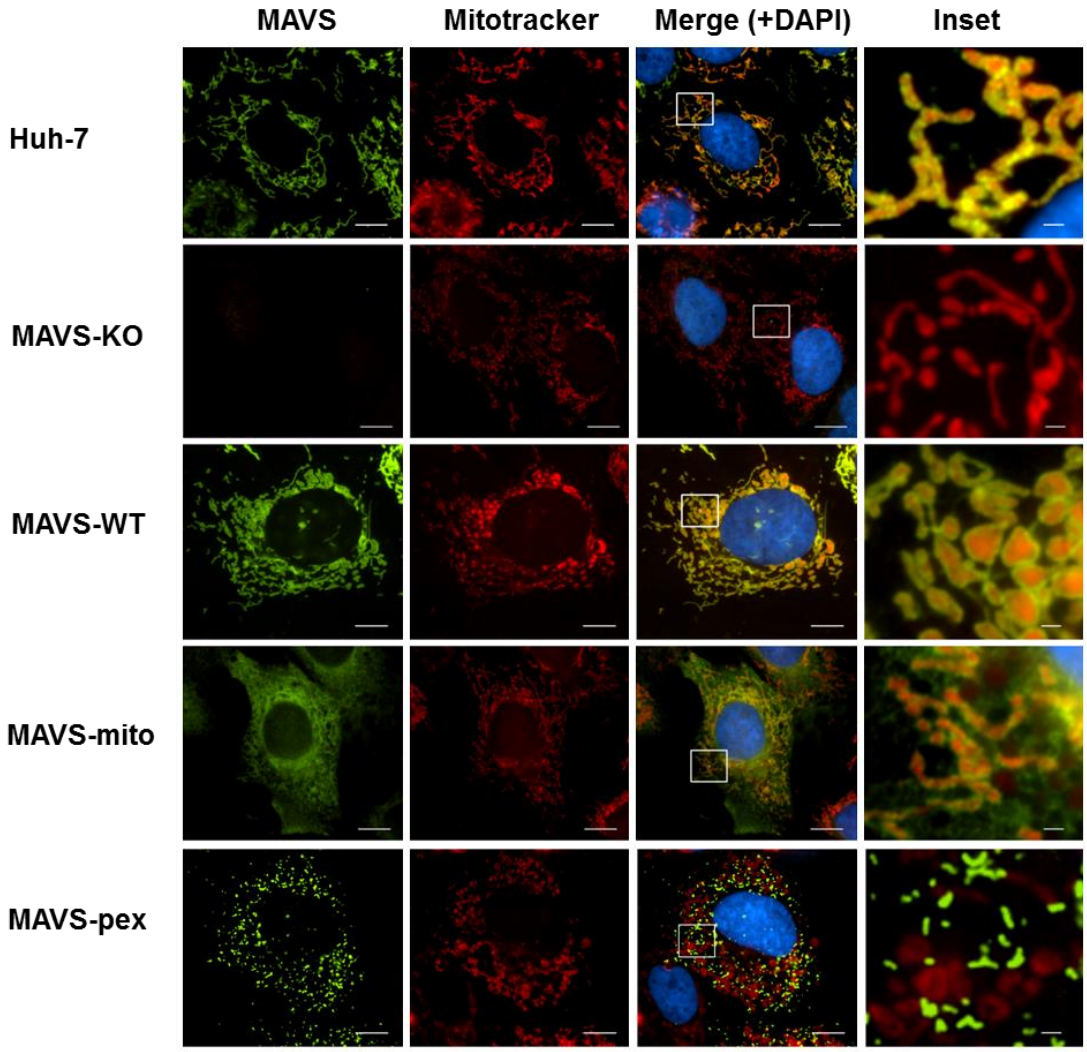

Figure 6.7: Stable cell lines expressing MAVS transgenes on mitochondria.

To determine the localisation of stable cell lines expressing MAVS transgenes on mitochondria, cell lines were incubated with permeable probes for mitochondrial labelling (MitoTracker® Red CMXRos, Cell Signalling Technology) for 30 min prior to cell fixation and staining with rabbit anti-MAVS antibody and Alexa Fluor 488-conjugated goat anti-rabbit IgG. Nuclei were counterstained with DAPI. Co-localisation of MAVS (green) and mitotracker (red) was obviously seen in Huh-7, MAVS-WT, MAVS-mito cell lines, whereas no co-localisation was found in MAVS-KO and MAVS-pex cell lines. All IF images were obtained by immunofluorescence analysis using a Nikon TiE inverted fluorescent microscope (60x magnification). Scale bars are 10 μm and 1 μm for main images and insets, respectively.

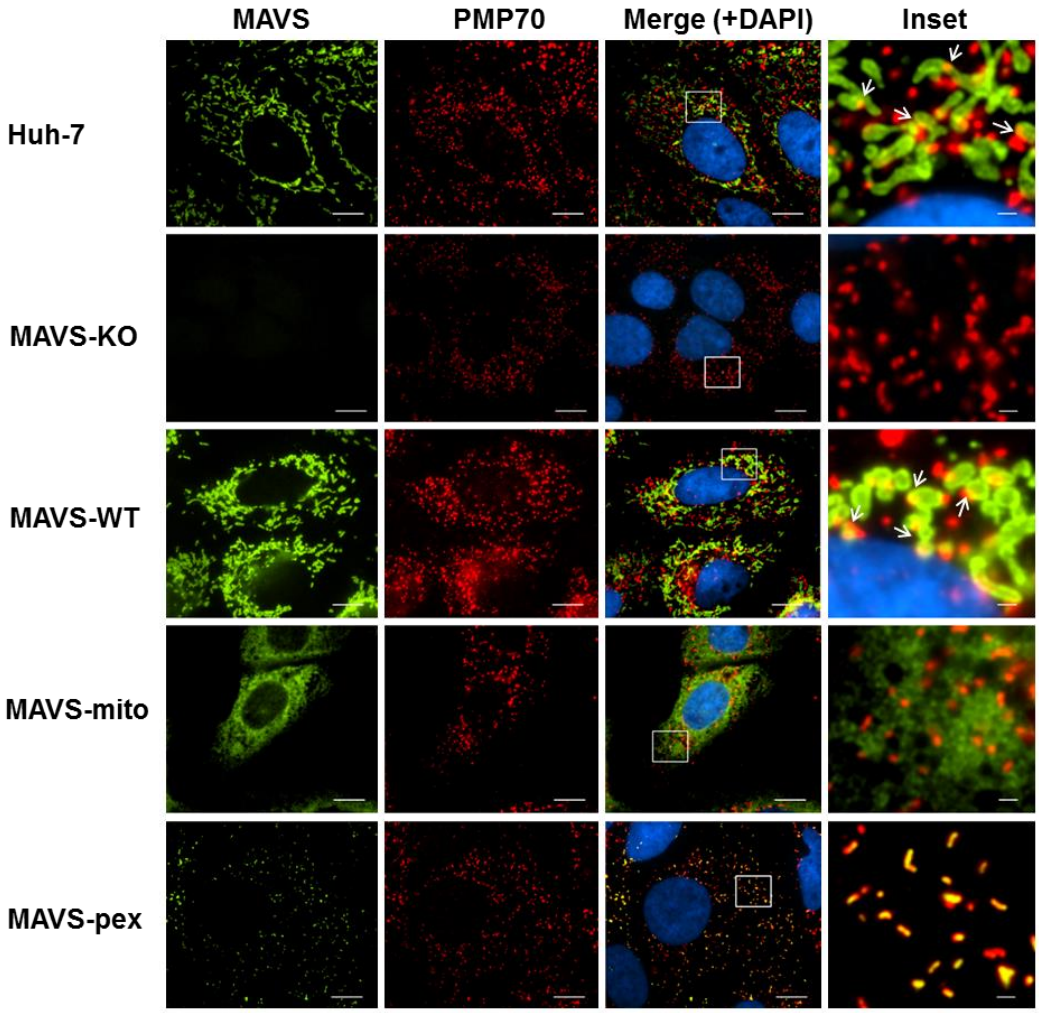

Figure 6.8: Stable cell lines expressing MAVS transgenes on peroxisomes.

To determine the localisation of stable cell lines expressing MAVS transgenes on peroxisomes, cell lines were stained with rabbit anti-MAVS antibody and mouse anti-PMP70 (peroxisome marker) prior to staining with a combination of Alexa Fluor 555-conjugated goat anti-mouse IgG and Alexa Fluor 488-conjugated goat anti-rabbit IgG. Nuclei were counterstained with DAPI. A partial co-localisation of MAVS (green) and peroxisomes (red) was observed in Huh-7, MAVS-WT, while a perfectly co-localisation was obviously seen in MAVS-pex cell lines. No co-localisation was found in MAVS-KO and MAVS-mito cell lines. All IF images were obtained by immunofluorescence analysis using a Nikon TiE inverted fluorescent microscope (60x magnification). Scale bars are 10 μm and 1 μm for main images and insets, respectively. Arrows indicate the localisation of MAVS on peroxisomes.

IFN-λ1 mRNA that was less than that for MAVS present on both compartments (Figure 6.9). This suggests that MAVS localisation to both organelles may be important for a maximal type I interferon response to viral infection.

6.4 Viperin mediates a MAVS signalling through mitochondria and peroxisome compartments.

Having established selective expression of MAVS on both the mitochondria and peroxisomes (MAVS-WT), mitochondria (MAVS-mito) and peroxisomes (MAVS-pex) and shown that these cell lines all respond to poly I:C, we are now in a position to investigate the impact of viperin on MAVS signalling from selected organelles. Selective MAVS expressing cell lines were transfected with a plasmid expressing viperin and 24 hr post-transfected cell were stimulated with poly I:C, and IFN-β and IFN-λ1 mRNA expression quantitated by real time RT-PCR.

As we have shown previously, expression of viperin in Huh-7 cells revealed a statistical increase in IFN-β and IFN-λ1 mRNA, while as expected, viperin or dsRNA (poly I:C) had no effect on mRNA expression in MAVS-KO cells. To our surprise, we noted no impact of viperin expression on IFN-β and IFN-λ1 expression in cells with selective expression of MAVS on either the mitochondria or peroxisomes. This was somewhat confusing as we anticipated that the trafficking of peroxisomes by viperin would be a contributing factor in innate immune augmentation. However, we did see a significant increase in both IFN-β and IFN-λ1 mRNA expression in MAVS-WT cells in which MAVS is expressed on both the mitochondria and peroxisomes. This increase was more

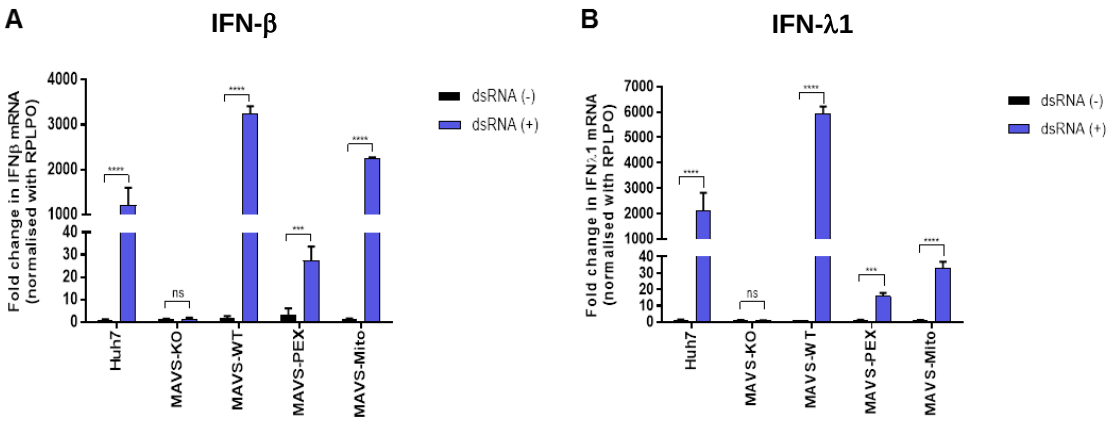

Figure 6.9: Induction of IFN-β and IFN-λ1 expression in a panel of stable cell lines expressing MAVS alleles.

To assess the signalling capacity of stable cell lines expressing MAVS alleles, all cell lines were stimulated with poly I:C for 24 hr prior to IFN-β and IFN-λ1 mRNA level quantification by real time RT-PCR. Selective MAVS expression on mitochondria and peroxisomes or both respond to poly I:C stimulation to produce **(A)** IFN-β and **(B)** IFN-λ1. Data are means ± SD (n=3). 2-way ANOVA, ****p<0.0001, *** p=0.0004.

marked with IFN-λ1 expression (Figure 6.10). This suggests that while MAVS can signal from either the mitochondria or peroxisomes, in the presence of viperin, optimal signalling occurs when MAVS is present on both the mitochondria and peroxisomes. It is not inconceivable to envisage that while signalling can occur from specific organelles, optimal signalling requires MAVS to be present on the mitochondria, peroxisomes and MAM to form the innate immune synapse, and that viperin may facilitate movement of the peroxisome to facilitate maximal innate immune induction.

6.5 Discussion

We have demonstrated previously in Chapter 5 that viperin promotes peroxisome biogenesis and positions peroxisomes in close association with LDs through an interaction with PEX19. However, the question remains as to what the biological significance of this interaction. It is possible that the ability of viperin to increase peroxisome numbers may facilitate innate immune signalling and downstream IFN and ISG expression as have been previously postulated. However, a second possibility is that the ability of viperin to redirect the peroxisome may help in the formation of the innate immune synapse to maximise innate immune signalling in response to infection. Elegant work by Horner *et al*. established that recognition of RIG-I following viral infection signals through MAVS that is present at the MAM-mitochondrial interface in what has been termed the "innate immune synapse", however in this model antiviral signalling from MAVS present on the peroxisome is not considered even though the literature strongly supports their role in the antiviral innate response (Horner et al., 2011). We postulate that viperin (expressed early following viral infection) interacts with PEX19 to

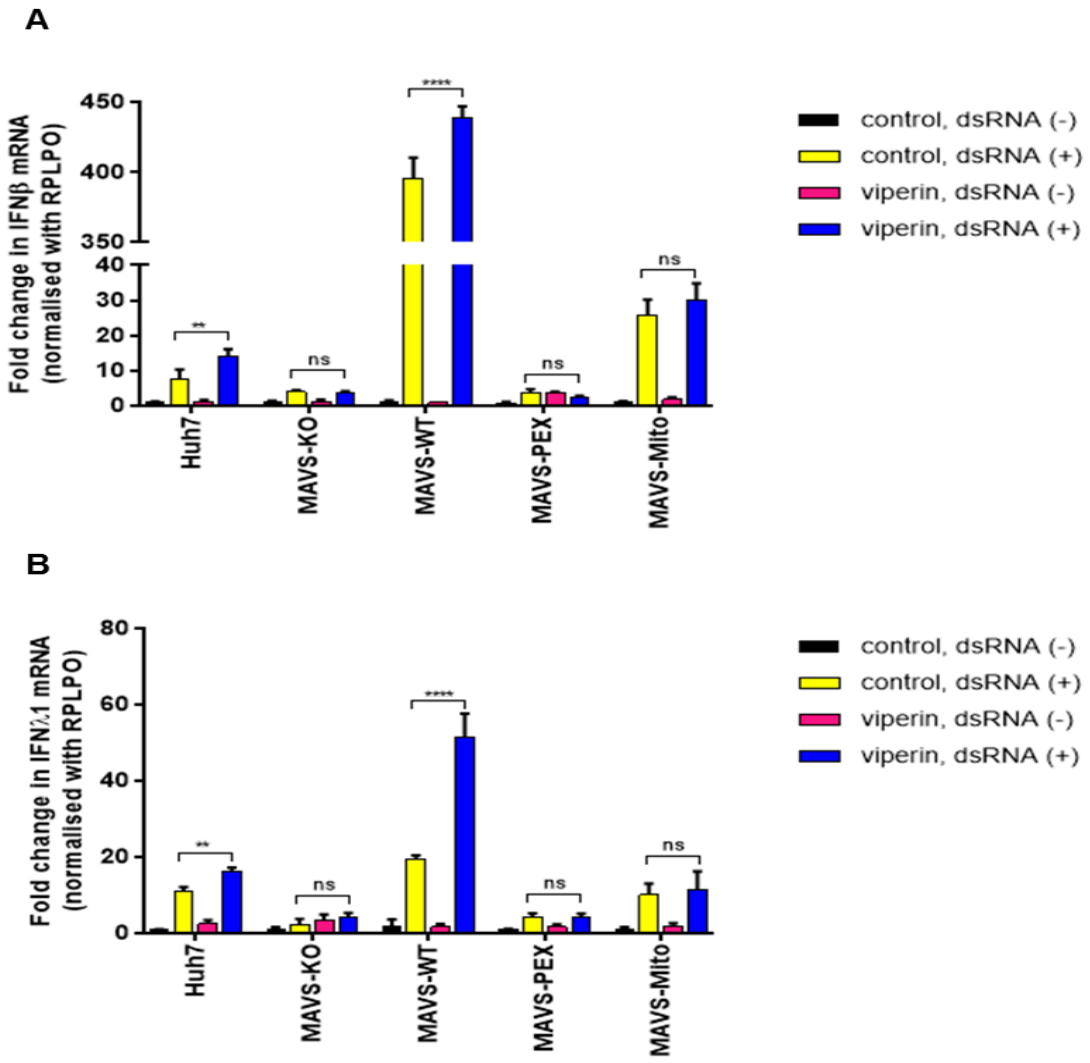

Figure 6.10: Viperin is required for MAVS signalling.

To determine the effectiveness of viperin to regulate MAVS signalling in the selectively MAVS localisation to mitochondrial and peroxisomes or both, all cell lines were transiently transfected with a plasmid expressing viperin-FLAG or plasmid control for 24 hr prior to poly I:C stimulation for 24 hr. IFN-β and IFN-λ1 mRNA level were quantified by real time RT-PCR. **(A)** IFN-β and **(B)** IFN-λ1 messages were drastically increased in MAVS-WT overexpressing of viperin in response to poly I:C stimulation while viperin is not able to enhance MAVS signalling in specific localisation of MAVS on mitochondria and peroxisomes. Data are means ± SD (n=3). 2-way ANOVA, ****p<0.0001.

drive the peroxisome in close association with the innate immune synapse to augment the cellular response to viral infection. With this in mind, we investigated the interaction of MAVS, viperin, peroxisomes and mitochondria at the cellular level and furthermore investigated the impact of viperin on activation of MAVS selectively expressed from either mitochondria, peroxisomes or both.

Initially, we assessed MAVS localisation to mitochondria and peroxisomes in our Huh-7 cells using immunofluorescence microscopy. Consistent with previous studies, we revealed that MAVS is primarily localised to mitochondria, while to a lesser extent on peroxisomes (Figure 6.1). This corroborates with the previous work from Bender and colleagues in which approximately 80% of MAVS was localised to the mitochondria and 20% to peroxisomes (Bender et al., 2015). As we established that viperin can bind to the peroxisome, the next logical step was to determine if there was an interaction between viperin and MAVS. As expected, immunofluorescence analysis in cells expressing viperin-GFP and stained for endogenous MAVS revealed an obvious co-localisation between the two proteins. It is unclear at this stage if there is a direct interaction between viperin and MAVS, however this co-localisation is most likely a function of the viperin-PEX19 interaction. Interestingly, this interaction seems to be at the interface between viperin present at the LD interface and MAVS positive mitochondria or peroxisomes, however from these images the role of the peroxisome cannot be deduced. To resolve this issue we further investigated the interaction between viperin, MAVS and the peroxisome using immunofluorescence microscopy. As in Chapter 5, in which we revealed an interaction between the LD, viperin and peroxisomes using super-resolution microscopy,

we now reveal an interaction between viperin, peroxisomes and MAVS in which it seems that viperin facilitates the interaction between the peroxisome and MAVS (Figure 6.3). While these images represent deconvolution microscopy of z-stacks, the resolution precludes detailed analysis. Future experiments should include super-resolution microscopy to further resolve these interactions. Interestingly, our viperin-APEX2 EM micrographs presented in Chapter 3 revealed viperin in close association with the LD and in many cases in close association with the mitochondria (Figure 3.14). Future experiments should extend these EM studies to identify the localisation of the peroxisome and possibly MAVS in this complex. The experiments outlined above clearly place viperin in association with the peroxisome at the mitochondrial interface (and possibly the MAM) and with the LD. This also suggests that the LD is also involved in playing a role as a scaffold in innate immune signalling. Together with the emerging evidence that the peroxisome is a platform for antiviral signalling (Dixit et al., 2010), we hypothesise that viperin interacts with the peroxisome to augment the innate antiviral response from this organelle.

To further investigate the role that viperin may have on innate signalling from the peroxisome we adopted an approach developed by the Kagan laboratory in which selective expression of MAVS to either the mitochondria, peroxisome or both, was achieved through engineering specific organelle targeting sequences to the carboxy terminal end of MAVS (Dixit et al., 2010). However, prior to generating selective localisation of MAVS, it was necessary to knockout endogenous MAVS (KO) expression. This was achieved using a CRISPR/Cas9 approach and as expected our Huh-

7 MAVS-KO cell line did not express MAVS as determined by immunoblot and immunofluorescence analysis. Furthermore, the production of IFN-β and IFN-λ1 mRNA was significantly reduced compared to the parental Huh-7 cells (Figure 6.4C), following stimulation with transfected poly I:C to activate cytosolic PRR recognition. This indicates that we have successfully generated a MAVS-KO cell line that is refractory to stimulation with poly I:C. We next generated stable Huh-7 cell lines expressing MAVS with specific localisation to either the mitochondria, peroxisomes or both compartments by retroviral delivery of MAVS cDNA expressing selective localisation of MAVS including MAVS-WT, MAVS-pex and MAVS-mito (Dixit et al., 2010). We successfully generated the selective expression of MAVS to distinct subcellular compartments, and as expected MAVS-WT localised predominantly to mitochondria (and possibly the MAM) with a lesser amount on peroxisomes, while MAVS-mito and MAVS-pex were selectively expressed on their target subcellular compartments, respectively (Figure 6.7 and 6.8). It was necessary to confirm that organelle specific MAVS maintained its capacity to signal. We found that following transfection of poly I:C, IFN-β and IFN-λ1 mRNA was significantly induced from all MAVS expressing lines, however the greatest expression was observed in MAVS-WT cells, followed by MAVS-mito and then MAVS-pex cells (Figure 6.9). This observation is consistent with that of Dixit *et al*., and may be reflective of lower expression of MAVS proteins in MAVS-pex cells (Figure 6.6B) (Dixit et al., 2010) or alternatively may reflect the fact that only a finite amount of MAVS can be loaded onto peroxisomes compared to the mitochondria. We attempted to select for clones of Huh-7 cells that expressed increased MAVS-pex by FACS, however all clones revealed similar levels of MAVS expression. Nevertheless, a significant induction of both

IFN-β and IFN-λ1 in MAVS-WT compared to MAVS-mito and -pex suggests that MAVS localised to both organelles is required for maximal innate immune activation. Although it is well-documented that MAVS can signal from both the mitochondria and the peroxisome, there is some controversy as to the relative roles of each organelle in this process. Studies from the Kagan laboratory indicated that peroxisomal MAVS activation triggers a rapid antiviral effect in an interferon-independent manner and is responsible for type III IFN (IFN-λ) production, while mitochondrial MAVS activates a late type I IFN dependent antiviral effect (Odendall et al., 2014). However, Bender *et al*. revealed that activation of peroxisomal MAVS could equally promote expression of type I and III IFN (Bender et al., 2015). There were a number of reasons for this discrepancy, the most significant being the use of different MAVS organelle targeting constructs and the sensitivity of read-out systems that used to measure IFN production. Bender *et al*. fused MAVS with the targeting sequences at aa 514, while the constructs engineered by Dixit *et al*. retained MAVS only up to aa 500, that may affect the signalling capacity of the MAVS fusion proteins. In our study, we have used the selective MAVS expression constructs from the Kagan laboratory and we found that activation of peroxisomal MAVS can result in expression of both IFN-β and IFN-λ1 mRNA. This contradicts the conclusions from the Kagan laboratory, and while we have only investigated mRNA expression, suggests that like the Bender *et al*. study, activation of peroxisomal MAVS can result in IFN-β and IFN-λ1 mRNA. This of course may be a moot point, as in a biological context, MAVS will always be expressed associated with mitochondria/MAM and the peroxisome.

Having established a system to evaluate MAVS activation in a selective manner we were now in a position to define the impact of viperin expression on MAVS signalling from the peroxisome, mitochondria or both. Given our previous data showing that viperin binds to the peroxisome (via PEX19) and alters its cellular localisation, we postulated that viperin would impact MAVS signalling from the peroxisome. However, to our surprise this was not the case. We noted that viperin did not augment MAVS-pex (or MAVS-mito) activation but unexpectedly did result in a significant increase in IFN-β and IFN-λ1 only when MAVS was present on both the peroxisome and mitochondria. This suggests that while it is possible for MAVS to signal from either mitochondria or peroxisomes alone, the enhancing function of viperin only occurs in the presence of MAVS on both organelles. However, our results were in contradiction to a recent study from Hee and Cresswell in which they demonstrated viperin mediates inhibition of the IFN response through physically interacting with MAVS specifically localised to the MAM (Hee and Cresswell, 2017). This discrepancy can be explained by the use of different cell lines (Hee and Cresswell used BMM) and possibly a different species of viperin as mouse viperin (not human as in this thesis) was utilised in the aforementioned report.

While it is well-established that MAVS localises to a diverse set of membranes, including at peroxisomes and mitochondria as well as the mitochondrial-associated membrane (MAM), the regulatory factors that mediate these different localisations are completely unknown. Furthermore, following viral infection the three intracellular membranes that contain MAVS (mentioned above) all interact with each other at the signalling synapse

during activation of the RIG-I pathway (Horner et al., 2011), suggesting that signalling from these organelles is co-regulated in a process that is also completely unknown. Based on evidence provided in this thesis it is not inconceivable to envisage that viperin expression following viral infection may indeed act in part to regulate MAVS-mediated antiviral signalling. In this model, recognition of viral RNA by RIG-I in the cytosol followed by RIG-I oligomerisation and RIG-I translocation to the MAM activates MAVS at the mitochondria and the MAM followed by recruitment of downstream signalling factors to form a MAVS signalling complex or the "innate immune synapse" (Horner et al., 2011, Vazquez and Horner, 2015). This early activation of the RIG-I pathway results in IRF3 independent gene expression, of which viperin is one, with viperin expression noted as early as 4 hours post infection (Dixit et al., 2010, Odendall et al., 2014). This viperin and PEX19/peroxisome interaction would function as a molecular chaperone in which it would help position peroxisomes via an interaction at the LD in close proximity to the innate immune synapse, resulting in an augmentation of innate immune signalling.

It should be noted in this study, we assessed the induction of both type I and III IFN mRNA in response to transfection of a synthetic dsRNA, poly I:C that is a potent activator of RIG-I. Future studies should confirm these observations at both the activation level and the cellular level using viral infection such as Sendai virus (SeV) or Newcastle disease virus (NDV) that are well-known activators of the RLR response. Interestingly it has been noted as mentioned above, that following viral infection (SeV) the known MAVS cellular compartments interact to maximise antiviral signalling. In addition, it would also be interesting to determine the role of viperin in modulation of MAVS

activation by MDA5, a PRR that is thought to be activated late in viral infection such as in WNV and Tulane virus infection (Fredericksen et al., 2008a, Errett et al., 2013, Chhabra et al., 2017).

In summary, our original hypothesis was that viperin would enhance innate immune signalling from the peroxisome using a selective model of MAVS expression to this organelle. However, this was not the case and we only noted an augmentation of the innate response when MAVS was present on both the peroxisome and the mitochondria, and possibly the MAM. This suggests that for the induction of a maximal innate response, MAVS is required at the peroxisome, mitochondria and the MAM and that viperin facilitates this activation by redirecting the peroxisome to the innate immune synapse. Clearly, MAVS expression at multiple sites within the cell is dynamic and must be coordinated to place all players in close vicinity for maximal expression. We therefore postulate that viperin is a strong candidate for augmenting the innate antiviral response from peroxisomal derived MAVS.

Chapter 7

Conclusions and Future Directions

Viral infection results in the activation of viral recognition pathways that trigger the induction of cytokines and predominately type I interferon (IFNs) expression to establish a host antiviral state (Sen, 2001). Binding of IFNs to their specific receptors initiates the production of hundreds of interferon-stimulated genes (ISGs). Many of these ISGs are uncharacterised, however there are a growing number that possess antiviral activity (Schoggins and Rice, 2011). One such ISG is viperin (*RSAD2*) that exerts a broad antiviral activity against a number of RNA viruses including hepatitis C virus (HCV) (Helbig et al., 2005, Wang et al., 2012), dengue virus (DENV) (Fink et al., 2007, Helbig et al., 2013), influenza virus (Tan et al., 2012, Wang et al., 2007), HIV (Nasr et al., 2012), respiratory syncytial virus (RSV) (McGillivary et al., 2013) and Tick-borne encephalitis virus (TBEV) (Upadhyay et al., 2014). The mechanisms responsible for its diverse antiviral activity are not well understood and seem to be specific for different viruses, including closely related viruses of the *Flaviviridae* family; HCV, DENV and TBEV. For example, the C-terminal domain plays a crucial role in antiviral activity against HCV and DENV, while the radical SAM domain is responsible for anti-TBEV activity (Helbig et al., 2011, Helbig et al., 2013, Upadhyay et al., 2014). This selective antiviral activity is in part related to well-conserved protein domains and the ability of viperin to bind and modulate several host factors. However, this does not fully explain viperin's diverse antiviral activity and molecular mechanisms that underpin its antiviral

activity. Furthermore, the full repertoires of the host interacting partners of viperin remain to be uncovered.

It has been reported that viperin interacts with VAP-A and the HCV non-structural protein NS5A, and could interfere with the interaction of VAP-A and NS5A at sites of HCV replication (Helbig et al., 2011, Wang et al., 2012). HCV can induce extensive intracellular membrane remodelling to form RC or membranous webs where RNA amplification takes place (Gosert et al., 2003, Ferraris et al., 2010, Romero-Brey et al., 2012). Several host and viral proteins are essential for the formation of membranous webs such as VAP-A, OSBP, PI4KA, NS4B, NS5A (Chukkapalli and Randall, 2014), however the precise molecular mechanism of host-virus interactions within the RC is not understood. The host pro-viral protein, VAP-A has been shown to bind to OSBP, the cholesterol recruiting protein oxysterol-binding protein that is essential for cholesterol traffic and exchange and as such plays a role in HCV replication by modification of intracellular membranes for the formation of the HCV RC (Wyles et al., 2002, Amako et al., 2009, Wang et al., 2014). Interestingly, the antiviral effector protein and also an ISG, interferon-inducible transmembrane protein 3 (IFITM3), has been shown to disturb the interaction of VAP-A and OSBP to inhibit viral entry (Amini-Bavil-Olyaee et al., 2013). Taken together, this raises the question of whether an association between viperin and VAP-A disrupts the interaction of VAP-A and OSBP to impact the function of OSBP in the formation of HCV RC to ultimately inhibit HCV replication. We therefore hypothesised that viperin binding to VAP-A can alter the interaction of VAP-A and OSBP and ultimately limit the formation of HCV RC.

To our surprise, our results in Chapter 3 revealed that viperin did not co-localise with OSBP and also did not disturb the interaction of VAP-A and OSBP as VAP-A maintained its co-localisation with OSBP. However, it is interesting that these interactions presented at different sites, with viperin interacting with VAP-A at LD interface, while the binding of VAP-A and OSBP is likely at the ER-Golgi contact sites**,** as expected (Amako et al., 2009). Our results also revealed that in the presence of viperin, the VAP-A localisation pattern was shifted from its typical ER localisation (Skehel et al., 2000, Prosser et al., 2008) to LDs where viperin accumulates, suggesting that viperin alters VAP-A localisation which may later impact HCV RC formation. However, as this was observed in uninfected cells, we therefore cannot rule out the possibility that extensive HCV-induced cellular membrane rearrangements to form membranous webs (Romero-Brey and Bartenschlager, 2014) may alter the localisation of host pro-viral proteins such as VAP-A and OSBP, such that altered interactions of viperin with these pro-viral factors can occur in the RC. Therefore, it will be of interest to further determine the association/interaction of these viral and host cellular proteins (HCV NS5A, viperin, VAP-A and OSBP) in the context of HCV-induced membrane rearrangements.

As indicated previously, the diverse functions of viperin cannot be explained by its intrinsic functions alone and it is likely that its effect is mediated at least in part through interaction with host proteins. While a number of viperin interacting partners have been identified including both viral (HCV NS5A, DENV NS3, HCMV vMIA) (Helbig et al., 2011, Wang et al., 2012, Helbig et al., 2013, Seo et al., 2011) and cellular proteins (FPPS,

TFP, IRAK1, VAP-A, TRAF6, MAVS and CIAO1) (Wang et al., 2007, Seo et al., 2011, Saitoh et al., 2011, Helbig et al., 2011, Wang et al., 2012, Hee and Cresswell, 2017, Upadhyay et al., 2014), we reasoned that more remain to be discovered. Understanding the repertoire of viperin interacting partners will help in elucidating the role of this enigmatic protein as an antiviral and in cellular functions. Therefore, a central aim of this thesis was to identify and characterise novel cellular interacting partners of viperin. In this thesis, a yeast two-hybrid approach was employed to identify novel interacting partners of viperin. As described in Chapter 4, we identified and confirmed that the peroxisomal biogenesis factor 19 (PEX19) and apolipoprotein A1 (ApoA1) are novel viperin interacting partners. Surprisingly, among 115 identified viperin interactomes using liquid chromatography coupled to tandem mass spectrometry (LC-MS/MS), PEX19 has been reported as a potential viperin interacting partner (Vonderstein et al., 2017), and thus confirms our findings. However, it was somewhat disappointing in that we could only reliably identify 2 viperin interaction partners. The reasons for this are outlined in Chapter 4 and highlight the limitations of the Y2H system for recovery of protein interaction partners. It is highly likely that the repertoire of viperin interaction partners extends beyond PEX19 and ApoA1 identified in this thesis and cellular and viral protein identified elsewhere. Therefore future experiments should use a more robust and sensitive system to recover interacting partners as such affinity purification coupled with Mass Spectrometry.

The significance of viperin binding to either of these proteins was not immediately apparent, however recent studies implicating the peroxisome as an important organelle in

innate immune signalling to RNA viral infection (Dixit et al., 2010, Odendall et al., 2014) and preliminary data from our laboratory implicating viperin in augmentation of innate immune signalling focused our efforts to investigate this interaction further. PEX19 is important for the peroxisome biogenesis pathway by facilitating the insertion of the peroxisomal membrane protein (PMP) into peroxisome membranes. Most importantly for this thesis is that recent work has implicated the peroxisome as a key organelle in innate immune sensing of viral RNA infection through the presence of the signalling adaptor protein MAVS on the peroxisome outer membrane in addition to its presence on mitochondria and mitochondrial-associated membranes (MAM) (Dixit et al., 2010). This raises important questions about the biological impact of the PEX19-viperin interaction on both peroxisome biology and innate immune signalling from peroxisomes. While the role of the peroxisome in innate immune signalling is in its infancy, the interaction of a number of viruses with peroxisomes provides evidence that peroxisomes are important organelles in the host innate response to viral infection (You et al., 2015, Magalhaes et al., 2016). Interestingly, a recent study has shown that WNV and DENV capsid proteins can bind and sequester PEX19 resulting in a significant loss of peroxisomes and a corresponding decrease in IFN-λ production (You et al., 2015). This could be a possible mechanism whereby the *flaviviruses*, WNV and DENV abrogate antiviral signalling from peroxisomes. Furthermore, the HCMV vMIA protein binds to PEX19 resulting in peroxisome fragmentation and downstream blockade of peroxisome-dependent antiviral signalling (Magalhaes et al., 2016). Collectively these observations in which viruses have evolved mechanisms to selectively evade peroxisomal MAVS-dependent antiviral signalling highlight the importance of these organelles in the cellular response to viral

infection. Clearly an improved understanding of the biology of innate immune signalling from peroxisomes and the cellular factors that dictate this is warranted.

The current model by Horner and colleagues regarding antiviral MAVS signalling postulates that upon RIG-I sensing of viral RNA in the cytosol and RIG-I oligomerisation, RIG-I translocates to the MAM-mitochondrial interface where MAVS becomes activated by CARD-CARD interactions between MAVS and RIG-I. This interaction results in MAVS oligomerisation for subsequent recruitment of downstream signalling factors to form the MAVS signalling complex that ultimately results in IRF3 phosphorylation and transcription of IFN-β and IRF3-dependent gene expression and initiation of the antiviral state. In this way, it is postulated that to initiate signalling there is formation of an innate immune synapse that brings together all relevant players at the MAM-mitochondrial interface (Horner et al., 2011, Vazquez and Horner, 2015). However, in this model the role of MAVS-dependent signalling from the peroxisome is neglected even though we know that the peroxisome plays an important role in the antiviral response. While some MAVS positive peroxisomes are in close proximity to the mitochondria as shown by others and us in this thesis, there is a significant proportion that is distant to the proposed innate immune synapse. This raises a question that to date has not been addressed or has been neglected; can MAVS positive peroxisomes signal independently of the innate immune synapse? This would seem somewhat counterintuitive, as this would require a complete complement of signalling and adaptor molecules including oligomerised RIG-I to assemble at the peroxisome. It is more likely

that following viral infection the peroxisome repositions itself to the innate immune synapse to initiate MAVS dependent peroxisome signalling.

How then do peroxisomes distant from the innate immune synapse position themselves in a context for maximal signalling? Based on the results from this thesis (Chapter 5), we propose that viperin acts as a chaperone to reposition the peroxisome at the innate immune synapse. This is supported by a number of lines of independent investigation. Firstly, the ability of viperin to interact with PEX19 and hence the peroxisome provides the first clue that viperin may play a role in peroxisome-mediated innate immune signalling. This is further reinforced by the fact that exogenous expression of viperin or the lack thereof in MEFs isolated from viperin$^{-/-}$ mice resulted in enhancement or suppression of the innate response to poly I:C or SeV infection, respectively. Clearly, viperin expression plays a role in modulation of the innate response to RNA viral infection. While the antiviral properties of viperin are well-documented, its ability to modulate innate immunity is less well understood. Work from Saitoh and colleagues reported that viperin promoted TLR7 and TLR9 mediated production of type I IFN in pDCs that was mediated by the interaction of viperin with the signal mediators IRAK1 and TRAF6 (Saitoh et al., 2011). Interestingly and relevant to this thesis, viperin recruited the adaptor molecules IRAK1 and TRAF6 to lipid droplets, that placed them in the correct environment for signalling. It is not surprising that viperin directed IRAK1 and TRAF6 to the lipid droplet as it is well-documented by our laboratory (including this thesis) and others that viperin can localise to the outer membrane of the lipid droplets, through a process mediated by its N-terminal amphipathic α-helix (Hinson and

Cresswell, 2009a, Helbig et al., 2011). Indeed, we also observed that viperin can also reposition peroxisomes in close association with lipid droplets. In the absence of viperin expression peroxisomes do not associate with the lipid droplets, however in contrast, in its presence, there was a close association of peroxisomes (PEX19, PMP70 and PEX11B positive foci) with lipid droplets as determined by wide-field immunofluorescence deconvolution microscopy. Super-resolution microscopy further defined this interaction revealing that peroxisomes are juxta-opposed to viperin-laden lipid droplets. Furthermore, using deconvolution microscopy we also demonstrated that there is significant co-localisation between viperin (present on the lipid droplets) and MAVS present on mitochondria and peroxisomes suggesting that viperin may redirect the peroxisomes in close proximity to the mitochondria and the MAM and hence the innate immune synapse. This raises the question as to the importance of the lipid droplet in this process. Mutational analysis of viperin in which the N-terminal amphipathic α-helix has been removed such that it can no longer locate to the lipid droplets also results in a significant decrease in viperin's ability to augment the cellular response to poly I:C. Interestingly, it is emerging that the lipid droplets can play a role in cellular signalling events and in unpublished results we have shown that in cells depleted of lipid droplets there is a significant decrease in the innate immune response to viral infection (Helbig K., unpublished data). In this regard, future studies should focus to determine if viperin can still augment the innate immune response to viral infection in the context of lipid droplet depletion. One could envisage that lipid droplet may not be essential for MAVS-dependent signalling from the mitochondria and the MAM but may impact signalling from peroxisomes.

Having established that viperin can augment innate immune signalling and its role in repositioning peroxisomes prompted us to investigate MAVS-dependent signalling from peroxisomes independent from that of the mitochondria and the MAM. This was achieved using a strategy developed by the Kagan laboratory in which selective expression of MAVS was achieved by first deleting endogenous MAVS from the cell followed by exogenous targeted MAVS expression to either the mitochondria, peroxisome or both (Dixit et al., 2010). In this way, we could investigate the impact of viperin expression on MAVS signalling from either the peroxisome or mitochondria or both. Given our previous data, we hypothesised that viperin would have the most impact on MAVS located on the peroxisome, however this was not the case as viperin expression had no impact on either MAVS signalling from the mitochondria or the peroxisome. However, we did see an enhancing effect of viperin on the expression of both IFN-β and IFN-λ mRNA when MAVS was expressed on both organelles. This suggests that viperin can only drive a maximal innate antiviral response when MAVS is present on the peroxisome and the mitochondria including the MAM. Based on our observations, we propose that following RNA virus infection recognition of RNA by RIG-I and subsequent activation of MAVS is achieved at the innate immune synapse that includes MAVS present on the outer mitochondrial membrane and the MAM. This results in IRF3 dependent gene expression and immediate expression of viperin. However, maximal signalling is not achieved until MAVS positive peroxisomes are redirected the innate immune synapse in a process that is facilitated by viperin interacting with PEX19 on the peroxisome. In this way all the appropriate adaptor molecules required for MAVS activation are in close proximity at the innate immune synapse for

efficient downstream signalling. This process is summarised in Figure 7.1. While all of our studies have relied on exogenous expression of viperin, it is pertinent to note that viperin expression is induced rapidly following viral infection by both IFN-independent and -dependent mechanisms (protein expression as early as 4 hr) that would result in a rapid enhancement of the antiviral response following viral infection (Dixit et al., 2010, Odendall et al., 2014). Furthermore, under interferon stimulation, viperin mRNA expression is tightly regulated with maximal expression at 8 hr post stimulation after which it rapidly declines (Figure 4.7). This suggests that viperin may be responsible for an early rapid enhancement of innate immune activation from MAVS present on peroxisomes that decreases over time as viperin expression is regulated. Ultimately a heightened innate response to viral infection would result in a more robust cellular antiviral response with the overall goal to control or limit viral replication.

In summary, we have demonstrated that PEX19 is a novel interacting partner of viperin and their interaction is crucial for recruiting peroxisomes to the lipid droplet surface and in a close proximity to mitochondria. In addition, the close association of viperin and MAVS at both mitochondria and peroxisomes augments the innate antiviral response. Collectively, the studies conducted in this thesis provide valuable insights into the association of viperin, MAVS and the peroxisomes for augmentation of the innate immune response and highlight a central role of viperin in both direct antiviral activity and acting as a molecular bridge within the innate immune synapse. Hence, an improved understanding of the molecular mechanisms involved in viperin's innate antiviral activity not only increase our understanding of the host response to viral infection but may also

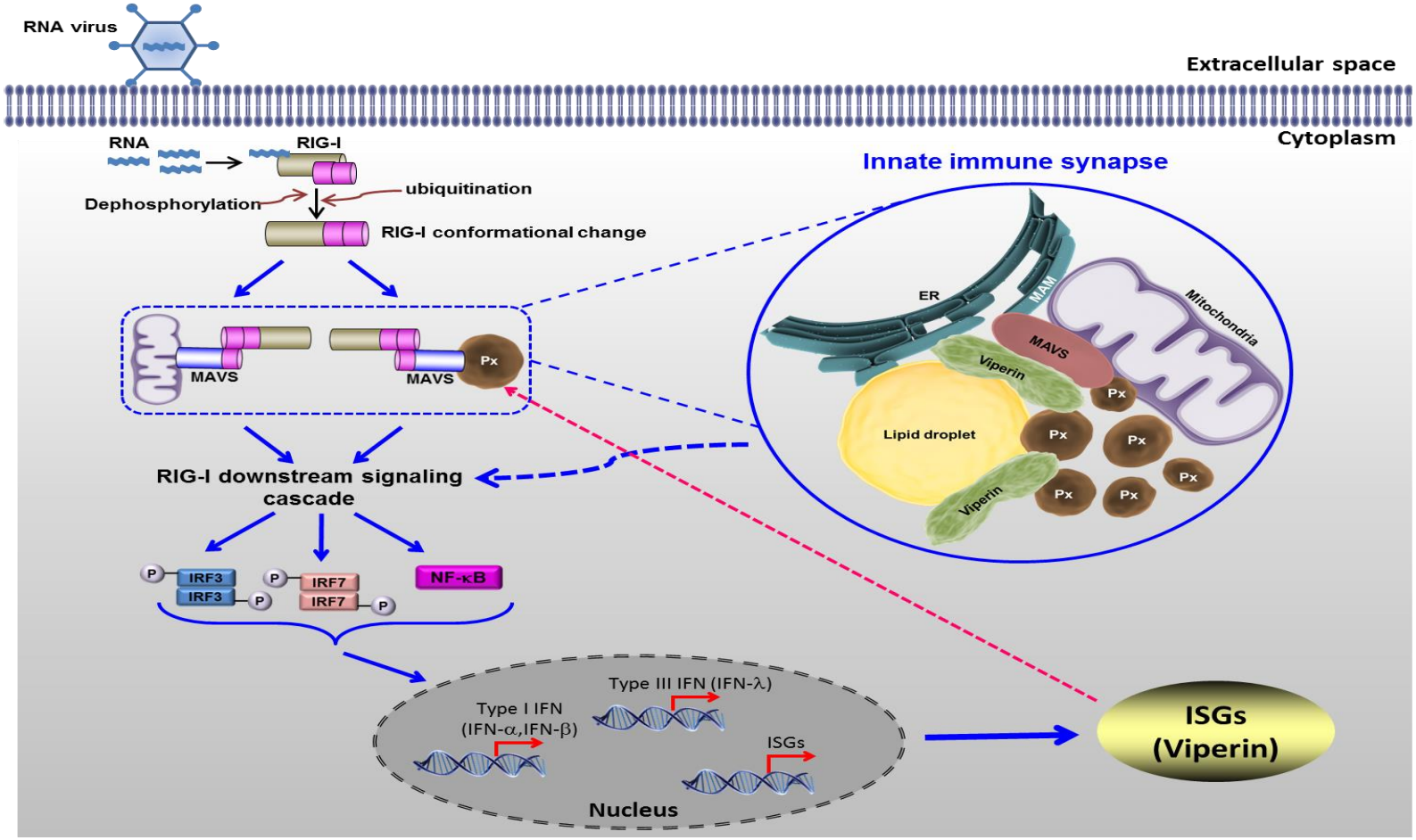

Figure 7.1: Schematic representation model of viperin interacting with MAVS in an innate immune synapse.
Upon RNA viral infection, activation of RIG-I signalling cascade results in the expression of viperin that subsequently interacts with PEX19 on peroxisomes and recruits peroxisomes in a close proximity to lipid droplets and mitochondria to form an innate immune synapse to augment innate immune signalling. Px, peroxisome; ER, endoplasmic reticulum.

be used for the development of pan-innate immune agonists as a therapeutics for viral infection.

Appendices

Appendix I: Primer sequences used in this study

Gene name	Forward primer (5' to 3')	Reverse primer (5' to 3')
Primers for cloning into mammalian expression plasmid		
OSBP (N-terminal Flag tag)	TTATGGATCCATGGACTACAAGGATGACGACGATAAGATGGCGGCGACGGAGCTGAGAG	AATAACGCGTTCAGAAAATGTCCGGGCATGAGCT
Human viperin (N-terminal Flag tag)	TTATGGATCCATGGACTACAAGGATGACGACGATAAGATGTGGGTGCTTACACCTGCTGCT*	CGCCGCGGCTACCAATCCAGCTTCAGATCA**
Human viperin 5'Δ10 (N-terminal Flag tag)	TTATGGATCCATGGACTACAAGGATGACGACGATAAGGGGAAGCTCTTGAGTGTGTTCAGG	Use **
Human viperin 5'Δ21 (N-terminal Flag tag)	TTATGGATCCATGGACTACAAGGATGACGACGATAAGAGCTCTCTGTGGAGGAGCCTGGTC	Use **
Human viperin 5'Δ33 (N-terminal Flag tag)	TTATGGATCCATGGACTACAAGGATGACGACGATAAGTGGCTGAGGGCAACCTTCTGGCTG	Use **
Human viperin 5'Δ42 (N-terminal Flag tag)	TTATGGATCCATGGACTACAAGGATGACGACGATAAGGCTACCAAGAGGAGAAAGCAGCAG	Use **
Human viperin 3'Δ33 (N-terminal Flag tag)	Use *	CGCCGCGGCTAACCAACATCCAGGATGGA
Human viperin 3'Δ50 (N-terminal Flag tag)	Use *	CGCCGCGGCTACAGAAAGCGCATATATTC
Human viperin 3'Δ72 (N-terminal Flag tag)	Use *	CGCCGCGGCTACAAGCAGGACACTTCTTT
Human viperin 3'Δ100 (N-terminal Flag tag)	Use *	CGCCGCGGCTAATCTTCTCCACAATTCTC
Human viperin (pTetOne system)	TTATGAATTCGCCGCCATGGACTACAAGGATGACGACGATAAGATGTGGGTGCTTACACCTGCTGCT	ATCTGGATCCCTACCAATCCAGCTTCAGATCA

Mouse viperin (N-terminal Flag tag)	TTATGGATCCATGGACTACAAGGATGACGACGATAAGATGGGGATGCTGGTGCCCACTG	AATACTCGAGTCACCAGTCCAGCTTCAGGTCAGC
Mouse viperin (N-terminal pEGFP tag)	AATAGGATCCTCACCAGTCCAGCTTCAGGTCAGC	TTATCTCGAGCGATGGGGATGCTGGTGCCCACTG
APEX2 (N-terminal Flag tag)	CCTGGATCCCATGGACTACAAGGATGACGAC	GGCTCGAGGGTCCAGGGTCAGGCGCTC
PEX19 (N-terminal GFP tag)	CCCTCGAGCGATGGCCGCCGCTGAGGAAGG	CGCCGCGGTCACATGATCAGACACTGTTC
Primers for cloning into yeast expression plasmid		
Human viperin (cloning into pGBKT7)	AATTGAATTCATGTGGGTGCTTACACCTGCTG	AATAGGATCCCTACCAATCCAGCTTCAGATCA
NS5A (cloning into pGADT7 AD)	CCTCATATGATGTCCGGATCCTGGCTCCGC	AGAGAATTCCTAGCAGCACACGGTGGTATCGTC
VAP-A (cloning into pGADT7 AD)	CCTCATATGATGGCGTCCGCCTCAGGGGCC	AGAGAATTCCTACAAGATGAATTTCCCTAG
Primers for cloning into LentiCRISPRv2 plasmid		
MAVS	CACCGCGCTGGAGGTCAGAGGGCTG	AAACCAGCCCTCTGACCTCCAGCGC
PEX19	CACCGTGCCTTCTCGAACTCCGCAG	AAACCTGCGGAGTTCGAGAAGGCAC
Real-time primers		
Human viperin	GTGAGCAATGGAAGCCTGATC	GCTGTCACAGGAGATAGCGAGAA
Murine viperin	TTGGGCAAGCTTGTGAGATTC	TGAACCATCTCTCCTGGATAAGG
HCV	TCTTCACGCAGAAAGCGTCTAG	GGTTCCGCAGACCACTATGG
RPLPO (36B4)	AGATGCAGCAGATCCGCAT	GGATGGCCTTGCGCA
PEX11B	GTCCTGAGATTCTGCATCACTGTT	CAGCCCACAGGACATTGTCA
PEX19	GCGTCATGTGCAAAATATGTGA	TCCAGCACCATCTCAAAACG
Human IFN-λ1	GGAAGAGTCACTCAAGCTGAAAA	AGAAGCCTCAGGTCCCAAT

	AC	TC
Murine IFN- β	AGAAAGGACGAACATTCGGAAA	CCGTCATCTCCATAGGGATC TT
Murine IFN-λ2	CCACATTGCTCAGTTCAAGTCTCT	TCCTTCTCAAGCAGCCTCTT CT
Sequencing primers(5' to 3')		
T7	TAATACGACTCACTATAGGGC	-
CMV	CGCAAATGGGCGGTAGGCGTG	-
V5 reverse	ACCGAGGAGAGGGTTAGGGAT	-
EGFP FP1	TACCTGAGCACCCAGTCC	-
DNA-BD	TTTTCGTTTTAAAACCTAAGAGTC	-
3' AD	AGATGGTGCACGATGCACAG	-

Appendix II: General Solutions and Buffers

The following solutions were obtained from the Central Services Unit (CSU) and Tissue Culture Services Unit (TSU), School of Biological Sciences, The University of Adelaide.

- 0.85% saline solution
- 10x GTS buffer
- 10x TBS buffer
- 1x and 20x PBS (phosphate buffered saline) solutions
- 20% Glucose solution
- 4M NaCl solution
- Ampicillin 1 mg/ml
- EDTA (different concentration and pH)
- Kanamycin 1 mg/ml
- L-Agar + ampicillin plates
- Luria agar plates
- Luria Broth
- SDS
- SOC media
- Tris solutions (different concentration and pH)
- G418
- Penicillin/streptomycin
- Trypan blue
- Trypsin-EDTA
- FCS (Foetal Calf Serum)
- 0.2 % (w/v) gelatin

Solution Components

Cell lysis RIPA Buffer (40 ml)	150mM NaCl (1.5ml of 4M NaCl) 0.5% deoxych = 0.2g 0.1% SDS (0.4ml of 10% SDS) 1% NP-40 (0.4 ml of NP-40) 50mM Tris (2 ml of 1M Tris) dH_2O 35.7 ml
Cell lysis NP-40 Buffer (40 ml)	50 mM Tris-HCL (2 ml of 1M Tris-HCL,pH8) 150mm NaCl (1.5 ml of 4M NaCl) 1% NP-40 (0.4 ml of NP-40) dH_2O 36.1 ml
5X Laemmli Buffer	5% β-Mercaptoethanol 0.02% Bromophenol blue 30% Glycerol 10% SDS 0.25 mM Tris-Cl (pH 6.8)
SDS PAGE Running Buffer	2.9% Trisma Base 14.14% glycine 1% SDS
SDS PAGE Transfer Buffer	0.3% Trisma Base 1.44% glycine 20% (v/v) methanol
TBS-T washing solution ***(Western blot)***	1x TBS buffer in dH_2O 0.1 % Tween® 20
Acetone:Methanol	50% acetone 50% methanol
4% Paraformaldehyde (100 ml)	4g of paraformaldehyde (PFA) 10ml of 10x PBS dH_2O up to a final volume of 100 ml
Gel-Red Solution	30 µl Gel-Red 2.5 ml 4M NaCl 100 ml dH_2O

Redsafe solution	5 µl Redsafe 100 ml of melted-agarose gel
1% Agarose	1g Agarose 100ml 1xTAE buffer
1% BSA	1 g of Bovine serum albumin (BSA) 100 ml of 1X PBS
5% BSA	5 g of BSA 100 ml of 1X PBS
EM fixative solution	4% paraformaldehyde 1.25% glutaraldehyde (EM grade) 4% sucrose (w/v) in PBS (pH 7.2)
2x Freezing medium (10 ml)	50% complete DMEM medium (5 ml) 30% FCS (3 ml) 20% DMSO (2 ml)

Competent Cells:

The *E.coli* α-Select Chemically Competent Cells used for bacterial transformation was:

*deoR endA*1 *recA*1 *relA*1 *gyrA*96 *hsdR*17($r_k^- m_k^+$) *supE*44 *thi*-1 Δ*(lacZYA-argFV*169) *Φ80δlacZ*ΔM15 F^- γ^-.

Appendix III: Antibodies

Antibody dilution for Western blot analysis

Primary antibody	Dilution	Incubation	Supplier
Mouse anti-FLAG	1:1,000	O/N, 4°C	Sigma Aldrich
Rabbit anti-FLAG	1:1,000	O/N, 4°C	Sigma Aldrich
Mouse anti-β-actin	1:10,000	O/N, 4°C	Sigma Aldrich
Rabbit anti-viperin	1:1,000	O/N, 4°C	Enzo life sciences
Rabbit anti-OSBP	1:1,000	O/N, 4°C	Proteintech
Rabbit anti-mCherry	1:1,000	O/N, 4°C	BioVision
Mouse anti-PMP70	1:1,000	O/N, 4°C	Sigma Aldrich
Rabbit anti-PEX19	1:1,000	O/N, 4°C	Abcam
Rabbit anti-MAVS	1:2,000	O/N, 4°C	Enzo Life Sciences
Goat anti-catalase	1:500	O/N, 4°C	Santa Cruz Biotechnology
Mouse anti-cMyc (clone 4A6)	1:1,000	O/N, 4°C	Millipore
Secondary Antibody			
Goat anti-mouse IgG (H+L), peroxidase conjugated	1:10,000	1 hr, RT	Thermo Fisher Scientific
Goat anti-rabbit IgG (H+L), peroxidase conjugated	1:10,000	1 hr, RT	Thermo Fisher Scientific
Rabbit anti-goat IgG (H+L), peroxidase conjugated	1:10,000	1 hr, RT	Thermo Fisher Scientific

Antibody dilution for Immunofluorescence labelling

Primary antibody	**Dilution**	**Incubation**	**Supplier**
Mouse anti-FLAG	1:200	1 hr, RT	Sigma Aldrich
Rabbit anti-FLAG	1:200	1 hr, RT	Sigma Aldrich
Mouse anti-PMP70	1:200	1 hr, RT	Sigma Aldrich
Rabbit anti-PEX19	1:200	1 hr, RT	Abcam
Rabbit anti-MAVS	1:200	1 hr, RT	Enzo Life Sciences
Goat anti-catalase	1:50	1 hr, O/N	Santa Cruz Biotechnology
HCV patient antisera	1:50	1 hr, RT	Pooled patient serum (genotype 2)
Secondary Antibody			
Anti-mouse/Alexa 488	1:200	1 hr, RT	Invitrogen
Anti-mouse/Alexa 555	1:200	1 hr, RT	Invitrogen
Anti-mouse/Cy5	1:200	1 hr, RT	Invitrogen
Anti-rabbit/Alexa 488	1:200	1 hr, RT	Invitrogen
Anti-rabbit/Alexa 555	1:200	1 hr, RT	Invitrogen
Anti-goat/Alexa 555	1:200	1 hr, RT	Abcam
BODIPY 493/503 (lipid droplet marker)	1:200	1 hr, RT	Invitrogen

Appendix IV: Media and reagents for yeast two-hybrid system

Table IV: Components of Yeast Media Set 2 & Yeast Media Set 2 Plus

Yeast Media Pouch	Volume of Media Each Pouch Makes
Rich Media (Routine Yeast Culturing)	
YPDA Broth	0.5 L
YPDA with Agar	0.5 L
Minimal Media Single Dropouts (SDO)	
SD/–Leu Broth	0.5 L
SD/–Leu with Agar	0.5 L
SD/–Trp Broth	0.5 L
SD/–Trp with Agar	0.5 L
Minimal Media Double Dropouts (DDO)	
SD–Leu/–Trp Broth	0.5 L
SD–Leu/–Trp with Agar	0.5 L
Minimal Media Quadruple Dropouts (QDO)	
SD–Ade/–His/–Leu/–Trp Broth	0.5 L
SD–Ade/–His/–Leu/–Trp with Agar	0.5 L
Additional Components in Yeast Media and other reagents	
X-alpha-Gal 250 mg	-
Aureobasidin A 1 mg	-
Cracking buffer stock solution (100 ml)	8 M Urea 5% w/v SDS 40 mM Tris-HCl [pH6.8] 0.1 mM EDTA 0.4 mg/ml Bromophenol blue dH_2O to a final volume of 100 ml
Complete cracking buffer (working solution)	1 ml of Cracking buffer stock solution 10 μl of β-mercaptoethanol 1 table of Protease cocktail inhibitor

Appendix V: Yeast plasmid maps

Yeast plasmids were provided in Matchmaker Gold Yeast Two-Hybrid System (Clontech, catalogue number 630489).

pGBKT7 Vector

pGBKT7 Vector Information PT3248-5

Cat. No. 630489
630443

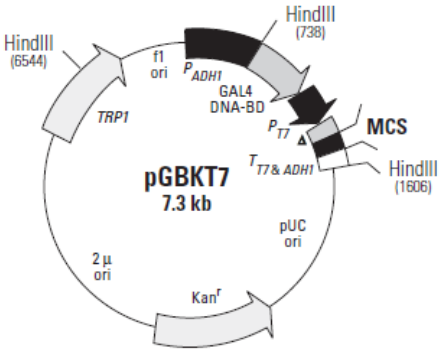

▲ c-Myc epitope tag

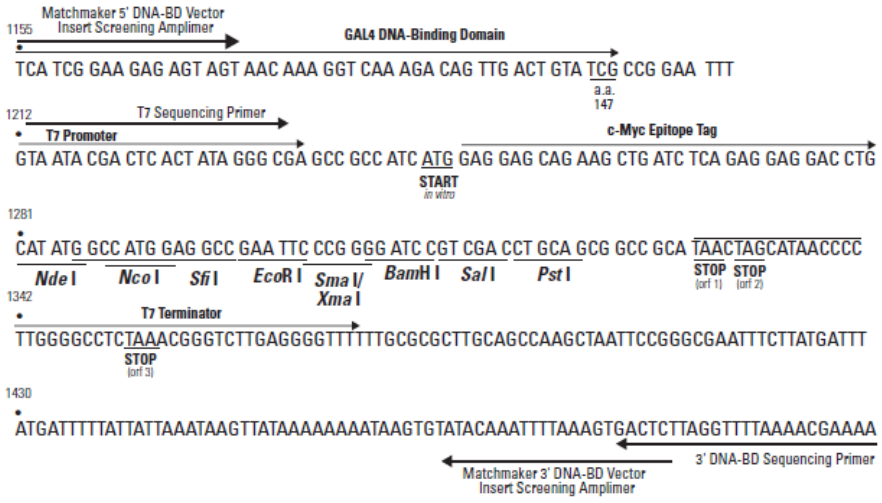

Restriction Map and Multiple Cloning Site (MCS) of pGBKT7. Unique restriction sites are in bold.

pGADT7 AD Vector

pGADT7 AD Vector Information PT3249-

Cat. Nos. 63044
63048
63049

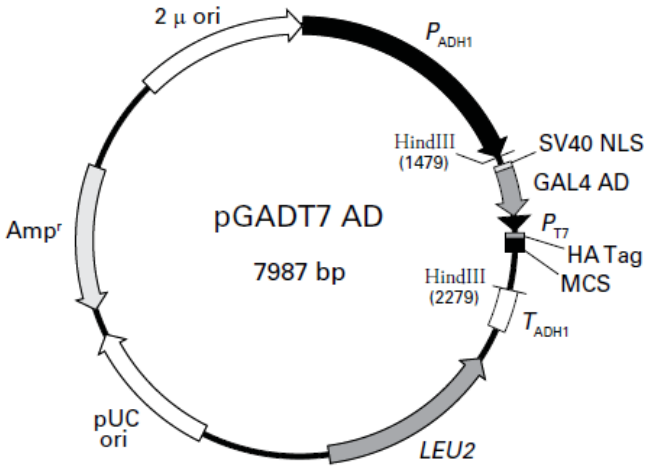

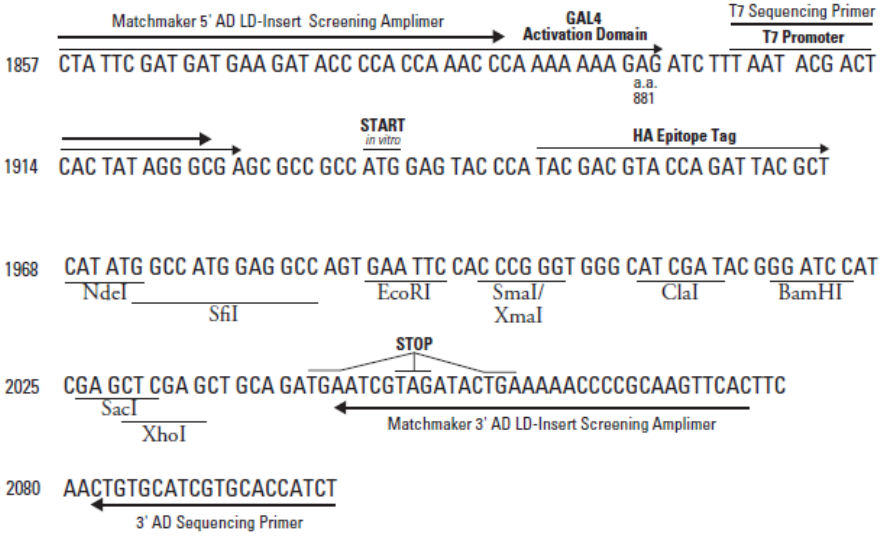

pGADT7 AD Vector Map and Multiple Cloning Site (MCS).

pGADT7-Rec Vector

pGADT7-Rec Vector Information PT3530-5

Sold as part of Cat. Nos. 630490 & 630491

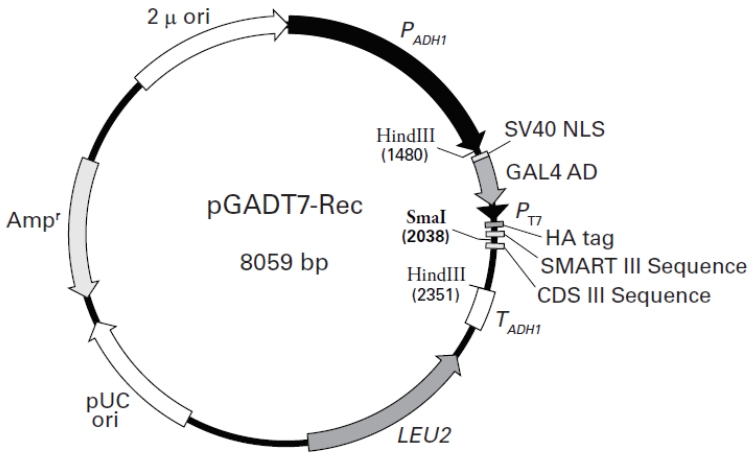

SMART™ III terminus

a.a. 881

MATCHMAKER 5' AD LD-Insert Screening Amplimer — GAL4 Activation Domain — T7 Sequencing Primer — T7 Promoter

1858 CTA TTC GAT GAT GAA GAT ACC CCA CCA AAC CCA AAA AAA GAG ATC TTT AAT ACG ACT

START *in vitro* — HA Epitope Tag

1915 CAC TAT AGG GCG AGC GCC GCC ATG GAG TAC CCA TAC GAC GTA CCA GAT TAC GCT

SMART III Oligonucleotide Sequence

1969 CAT ATG GCC ATG GAG GCC AGT GAA TTC CAC CCA AGC AGT GGT ATC AAC GCA GAG TGG

2026 CCA TTA TGG CCC

Partial SmaI site

CDS III terminus

CDS III Primer Sequence

2038 GGG AAA AAA CAT GTC GGC CGC CTC GGC CTC TAG AGG GTG GGC ATC GAT ACG GGA TCC

Partial SmaI site

STOP

2095 ATC GAG CTC GAG CTG CAG ATG AAT CGT AGA TAC TGA AAAACCCCGCAAGTTCACTTC

MATCHMAKER 3' AD LD-Insert Screening Amplimer

2152 AACTGTGCATCGTGCACCATCT

3' AD Sequencing Primer

Appendix VI: Mammalian expression plasmid maps

pLenti6/V5-D-TOPO Vector

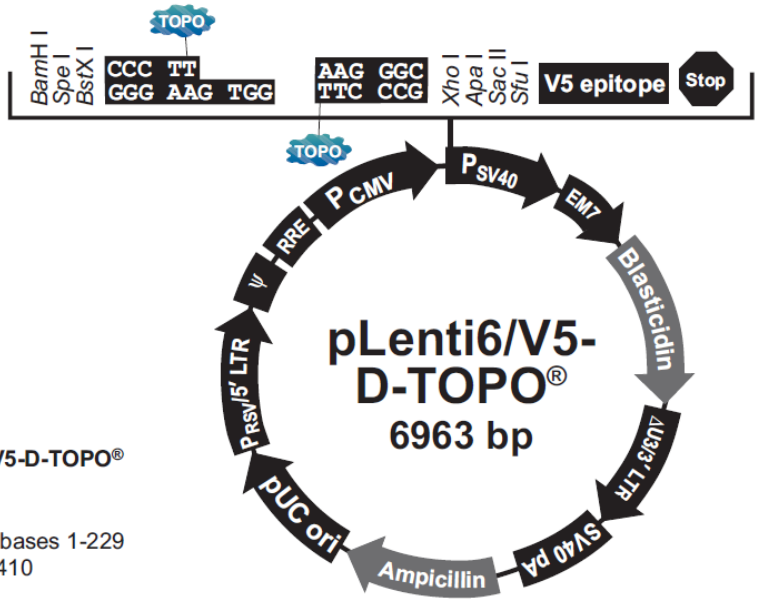

Comments for pLenti6/V5-D-TOPO®
6963 nucleotides

RSV enhancer/promoter: bases 1-229
HIV-1 5′ LTR: bases 230-410
5′ splice donor: base 520
HIV-1 psi (ψ) packaging sequence: bases 521-565
HIV-1 Rev response element (RRE): bases 1075-1308
3′ splice acceptor: base 1656
3′ splice acceptor: base 1684
CMV promoter: bases 1809-2392
CMV forward priming site: bases 2274-2294
Directional TOPO® site: bases 2431-2444
V5 epitope: bases 2473-2514
V5(C-term) reverse priming site: bases 2482-2502
SV40 early promoter and origin: bases 2569-2877
EM7 promoter: bases 2932-2998
Blasticidin resistance gene: bases 2999-3397
ΔU3/HIV-1 3′ LTR: bases 3484-3717
ΔU3: bases 3484-3536
Truncated HIV-1 3′ LTR: bases 3537-3717
SV40 polyadenylation signal: bases 3789-3920
bla promoter: bases 4779-4877
Ampicillin (*bla*) resistance gene: bases 4878-5738
pUC origin: bases 5883-6556

invitrogen™

pEGFP-c1 Vector

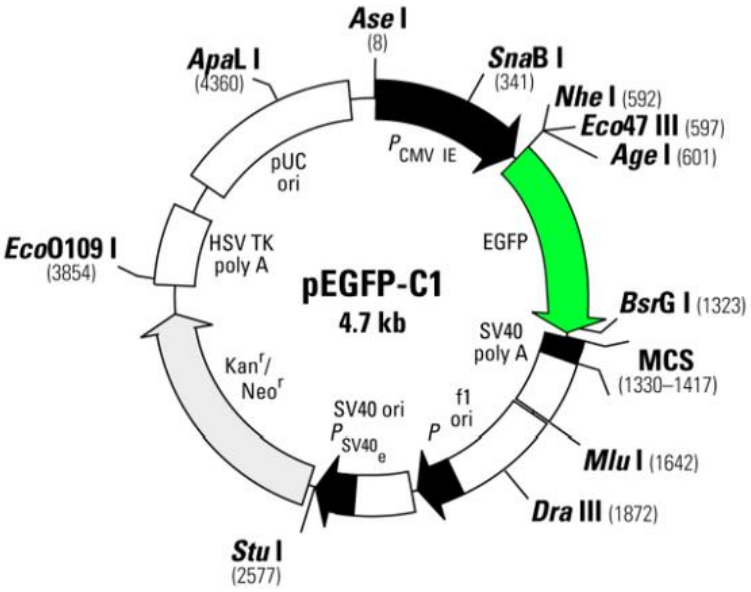

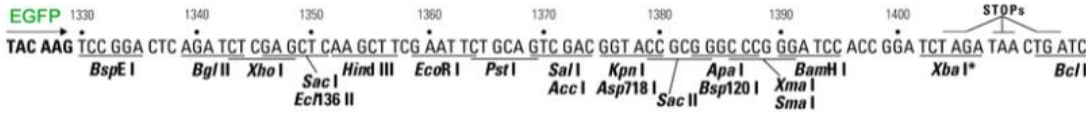

pcDNA3 APEX2-NES

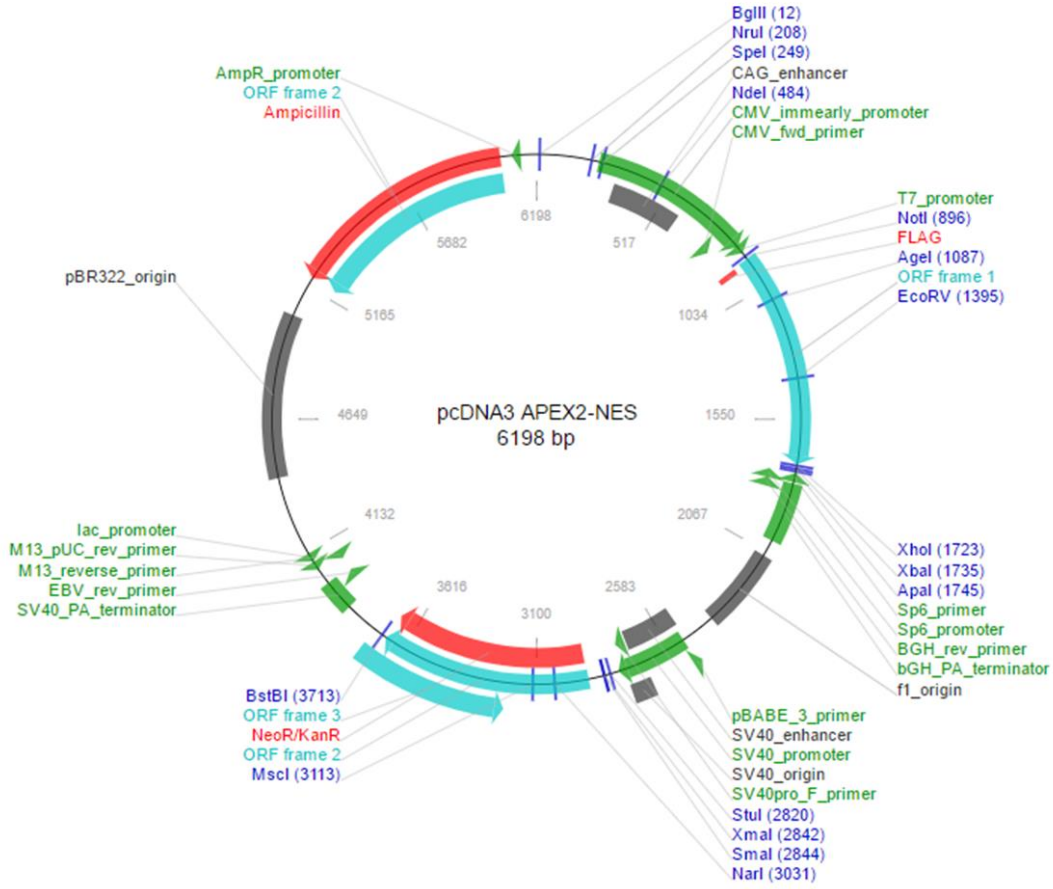

pcDNA3 APEX2-NES was a gift from Alice Ting (Addgene plasmid # 49386)

pCMV6-Entry-PEX19 (Origene, catalogue no. RC201756)

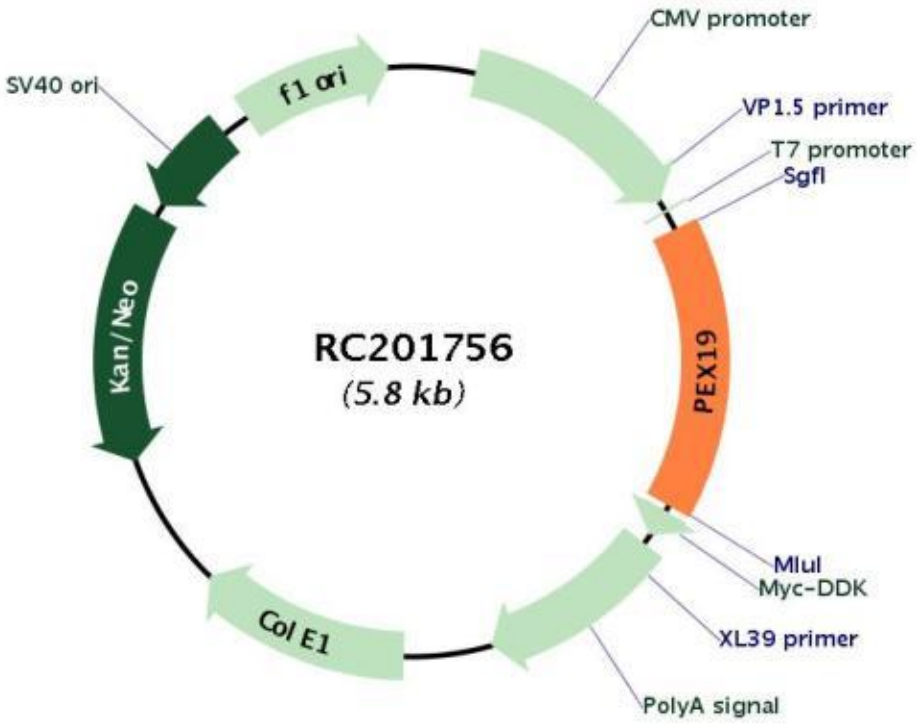

pCMV6-Entry-ApoA1 (Origene, catalogue no. RC210762)

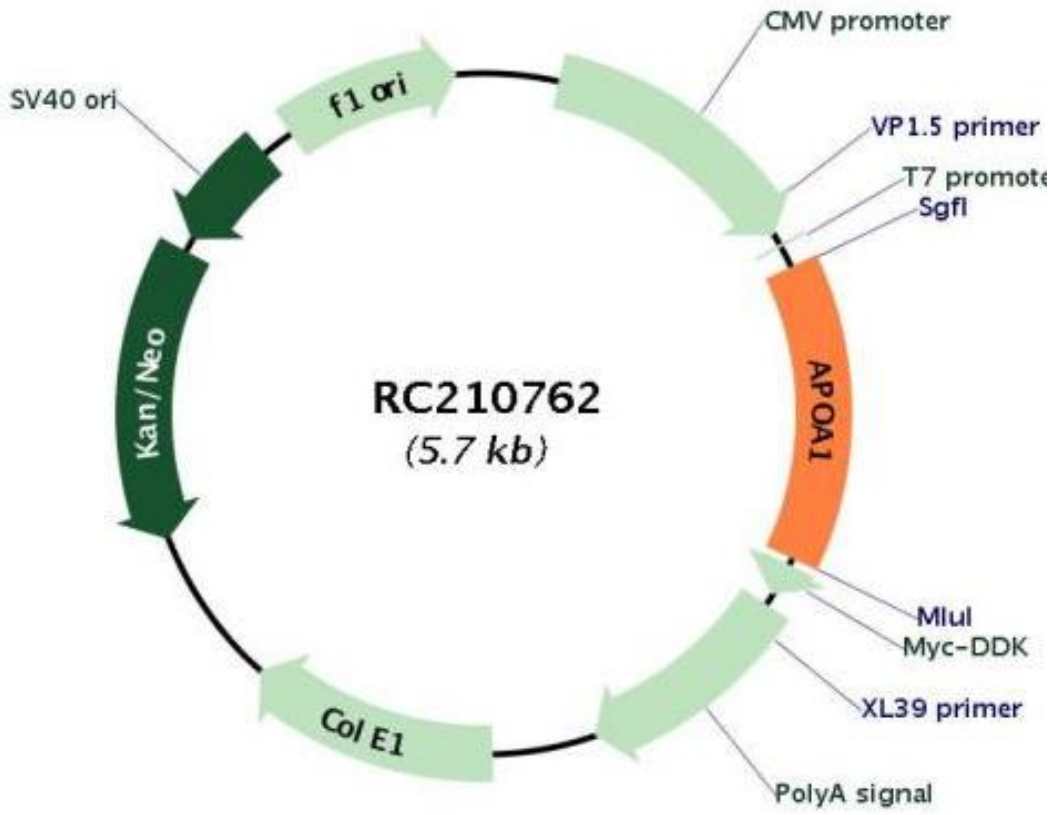

<u>Appendix VII</u>: Plasmid constructs in this study

Viperin and a panel of mutant derivatives

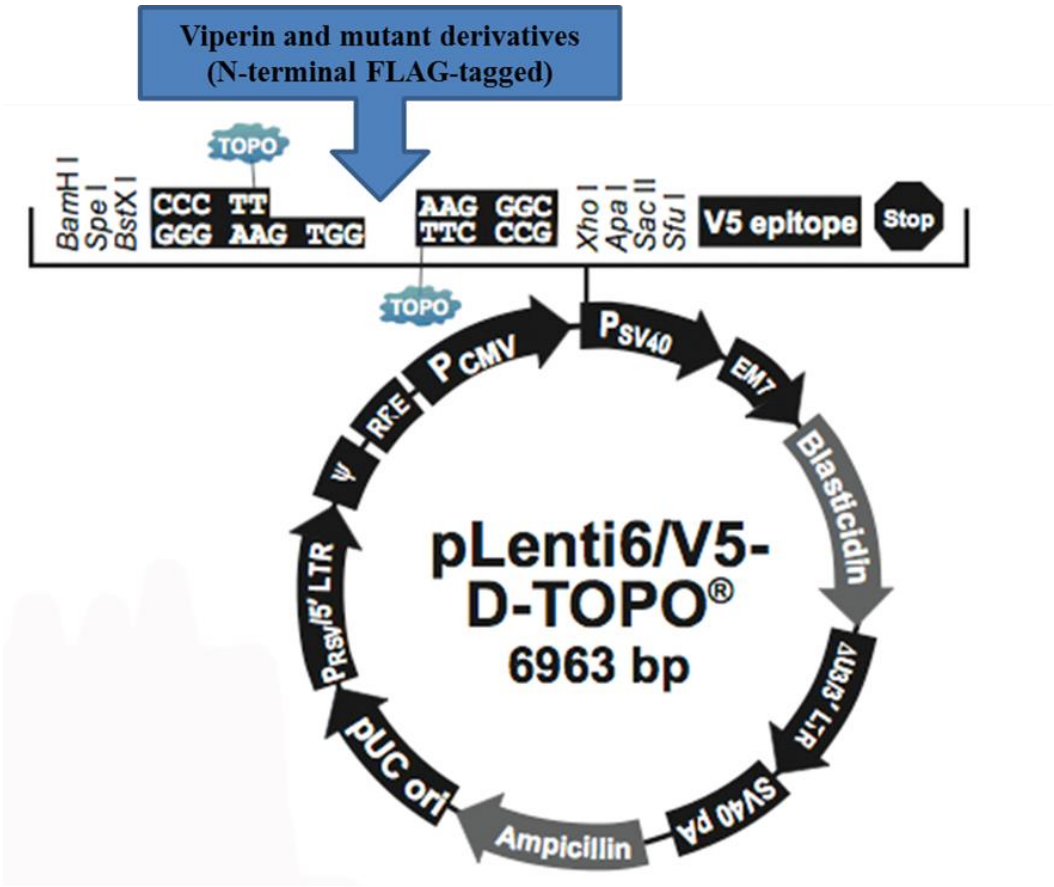

pLenti6/V5-D-TOPO-Viperin-APEX2

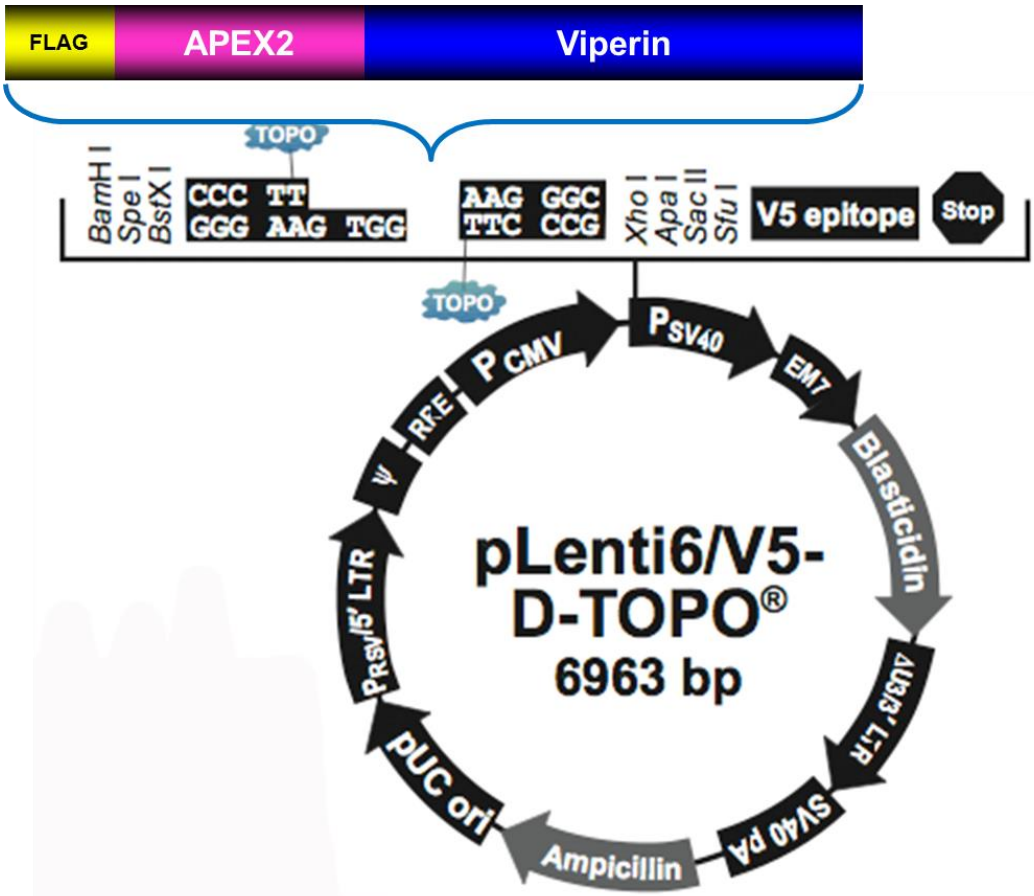

Appendix VIII: Target sequences of shRNA OSBP

A gene set of GIPZ OSBP shRNA (6 clones) target to human OSBP (accession# NM_002556) were obtained in *E. coli* glycerol stocks from Thermo Scientific (USA). The target gene sequence of each human GIPZ lentiviral shRNAmir individual clone is listed below:

Clone ID	Target gene sequence (antisense)
V2LHS_152507	TTTGCCTCGAAACTTGCTG
V2LHS_152508	TTAAGATTACACTTGTCTC
V2LHS_152509	ATAGGGATCATATGGTGTG
V3LHS_405241	TACAGACATAGTATCTCCT
V3LHS_405242	GGAATAACACTAACCTTCG
V3LHS_405243	TGTGGAATAACACTAACCT

Appendix IX: Target sequences of siRNA PEX19

A SMARTpool of ON-TARGETplus PEX19 siRNA (5 nmol) **containing** a mixture of foure siRNA target to human PEX19 (accessions NR_036493, NM_001193644, NM_002857, and NR_036492) was obtained as dry pellet from Dharmacon (part of GE Healthcare, USA, catalogue number L-012594-00-0005). The target gene sequences are listed below:

Individual siRNA	**Target sequence**
J-012594-05	CAGAAUGGUUGCAGAGUCA
J-012594-06	GAGGAAGGCUGUAGUGUCG
J-012594-07	CUUCAGAACUCCAGCAUGU
J-012594-08	GAUAUGACCUCCCAACAAG

ON-TARGETplus Non-targeting pool (5 nmol, catalogue number D-001810-10-05) was use as a control and the target sequences are provided below:

Non-targeting sequence
1) UGGUUUACAUGUCGACUAA
2) UGGUUUACAUGUUGUGUGA
3) UGGUUUACAUGUUUUCUGA
4) UGGUUUACAUGUUUUCCUA

<u>Appendix X:</u> Raw data output of the quantification of fluorescence signal using an Operetta high-content microscope and analysed with Harmony software.

1. Huh-7 cells transfected with viperin-mCherry/mCherry control followed by LD staining using BODIPY 493/503.

well#	The number of			Transfection efficiency (%)	Mean of Bodipy/	
	total cells	transfected cells	untransfected cells		transfected cells	untransfected cells
Transfection with viperin-mCherry						
1	2878	760	2118	26.41	3.45	1.06
2	3828	953	2875	24.90	2.61	0.74
3	4570	1200	3370	26.26	2.06	0.62
4	4544	1141	3403	25.11	2.46	0.69
5	4453	1118	3335	25.11	2.70	0.74
6	4982	1244	3738	24.97	2.33	0.66
7	5124	1348	3776	26.31	2.26	0.67
8	5170	1332	3838	25.76	2.27	0.65
9	4771	1295	3476	27.14	2.30	0.70
10	3774	938	2836	24.85	2.94	0.80
11	3454	860	2594	24.90	2.91	0.82
12	4280	972	3308	22.71	2.32	0.57
Average	**4319**	**1097**	**3222**	**25.37**	**2.55**	**0.73**
Transfection with mCherry control						
1	3500	1718	1782	49.09	1.33	1.22
2	4749	2317	2432	48.79	1.03	0.94
3	4891	2340	2551	47.84	1.04	0.92
4	5037	2406	2631	47.77	1.05	0.92
5	5164	2570	2594	49.77	1.16	0.97
6	4795	2247	2548	46.86	1.09	0.92
7	5122	2411	2711	47.07	1.02	0.85
8	5235	2655	2580	50.72	0.97	0.95
9	5193	2523	2670	48.58	0.99	0.90
10	5052	2428	2624	48.06	0.98	0.86
11	4890	2309	2581	47.22	1.11	0.94
12	5141	2373	2768	46.16	0.98	0.80
Average	**4897**	**2358**	**2539**	**48.16**	**1.06**	**0.93**

2. Huh-7 cells transfected with viperin-GFP/GFP control followed by peroxisome staining using mouse anti-PMP70 and subsequently Alexa Fluor 555–conjugated goat anti-mouse IgG.

well#	The number of			Transfection efficiency (%)	Mean of Bodipy/	
	total cells	transfected cells	untransfected cells		transfected cells	untransfected cells
Transfection with viperin-GFP						
1	2572	857	1715	33.32	2.29	0.83
2	3938	1395	2543	35.42	1.32	0.53
3	4540	1493	3047	32.89	1.18	0.44
4	3797	1287	2510	33.90	1.42	0.55
5	4557	1556	3001	34.15	1.18	0.46
6	3687	1306	2381	35.42	1.42	0.57
7	3592	1211	2381	33.71	1.51	0.56
8	3365	1103	2262	32.78	1.66	0.59
9	4435	1616	2819	36.44	1.13	0.48
10	4247	1432	2815	33.72	1.57	0.65
11	2896	977	1919	33.74	1.89	0.73
12	3016	1035	1981	34.32	1.98	0.75
Average	**3720**	**1272**	**2448**	**34.15**	**1.55**	**0.59**
Transfection with GFP control						
1	3149	1807	1342	57.38	0.90	1.02
2	4124	2348	1776	56.94	0.67	0.76
3	4275	2381	1894	55.70	0.67	0.70
4	4359	2398	1961	55.01	0.67	0.71
5	4731	2766	1965	58.47	0.59	0.69
6	4134	2299	1835	55.61	0.71	0.75
7	4040	2146	1894	53.12	0.75	0.70
8	4132	2178	1954	52.71	0.72	0.68
9	4063	2269	1794	55.85	0.70	0.74
10	3214	1681	1533	52.30	0.91	0.84
11	3306	1785	1521	53.99	0.83	0.82
12	3517	1973	1544	56.10	0.90	0.93
Average	**3920**	**2169**	**1751**	**55.26**	**0.75**	**0.78**

3. Huh-7 cells transfected with viperin-GFP/GFP control followed by catalase enzyme staining using goat anti-catalase and subsequently Alexa Fluor 555–conjugated goat anti-mouse IgG

well#	The number of			Transfection efficiency (%)	Mean of Bodipy/	
	total cells	transfected cells	untransfected cells		transfected cells	untransfected cells
Transfection with viperin-GFP						
1	8423	2864	5559	34.00	0.54	0.22
2	6903	2125	4778	30.78	0.70	0.26
3	6257	1902	4355	30.40	0.83	0.30
4	6810	2216	4594	32.54	0.71	0.28
5	6230	2022	4208	32.46	0.85	0.33
6	6407	1913	4494	29.86	0.91	0.31
Average	**6838**	**2174**	**4665**	**31.67**	**0.76**	**0.28**
Transfection with GFP control						
1	6313	3465	2848	54.89	0.40	0.40
2	6282	3482	2800	55.43	0.40	0.42
3	6296	3505	2791	55.67	0.41	0.43
4	6860	3962	2898	57.76	0.36	0.40
5	7141	3996	3145	55.96	0.37	0.38
6	7625	4534	3091	59.46	0.34	0.40
Average	**6753**	**3824**	**2929**	**56.53**	**0.38**	**0.40**

<u>Appendix XI:</u> Additional EM figures

X-I. Huh-7 cells were transfected with a plasmid expressing viperin-APEX2 following DAB staining.

Viperin-APEX2 (Cell#3)

Zoom in

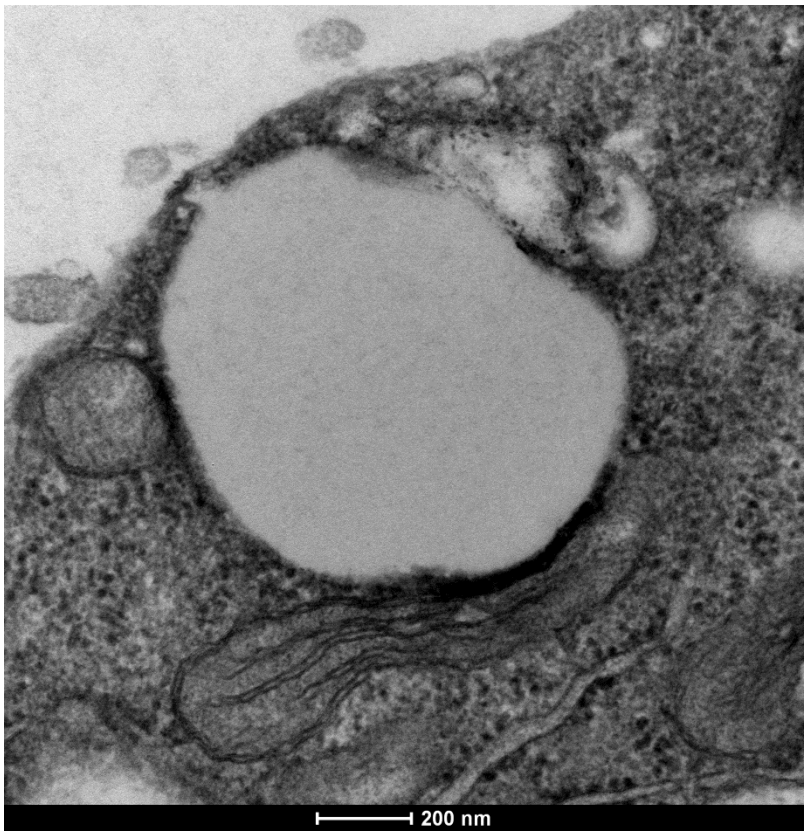

Viperin-APEX2 (Cell#4)

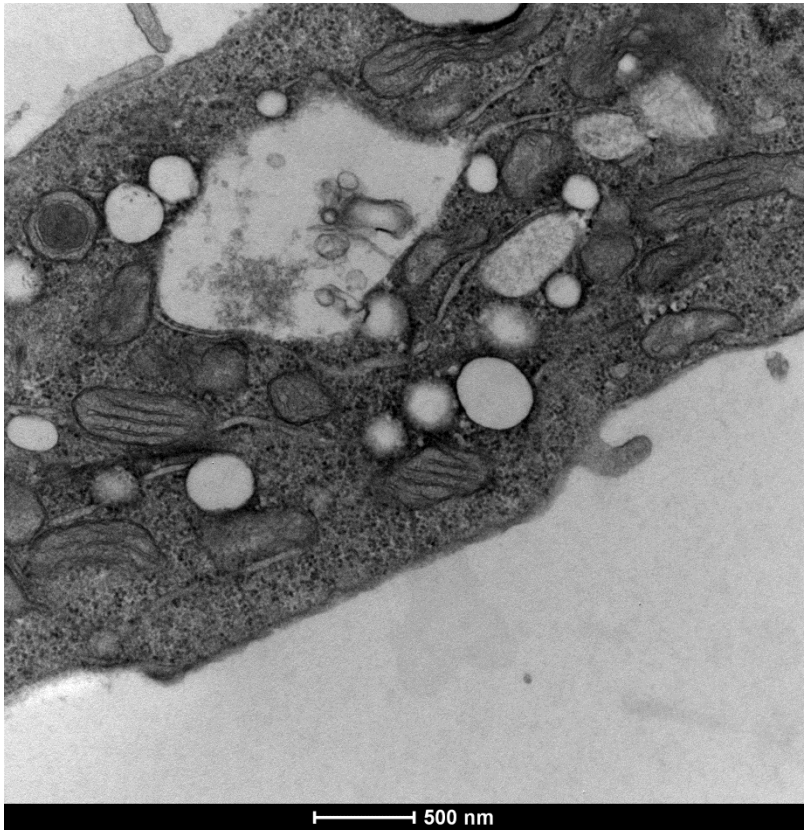

Zoom in

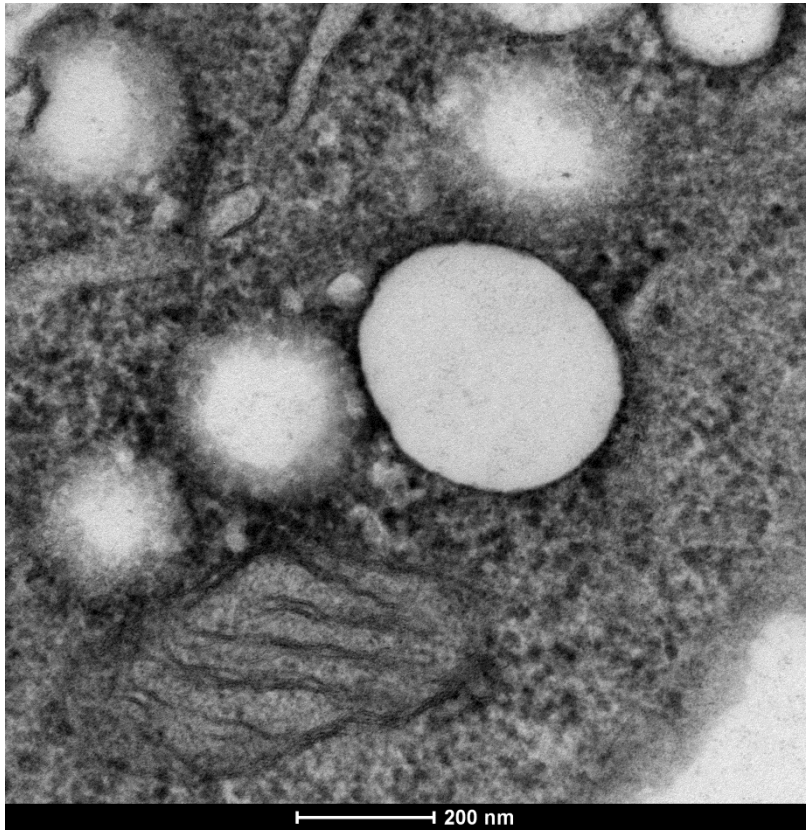

Viperin-APEX2 (Cell#5)

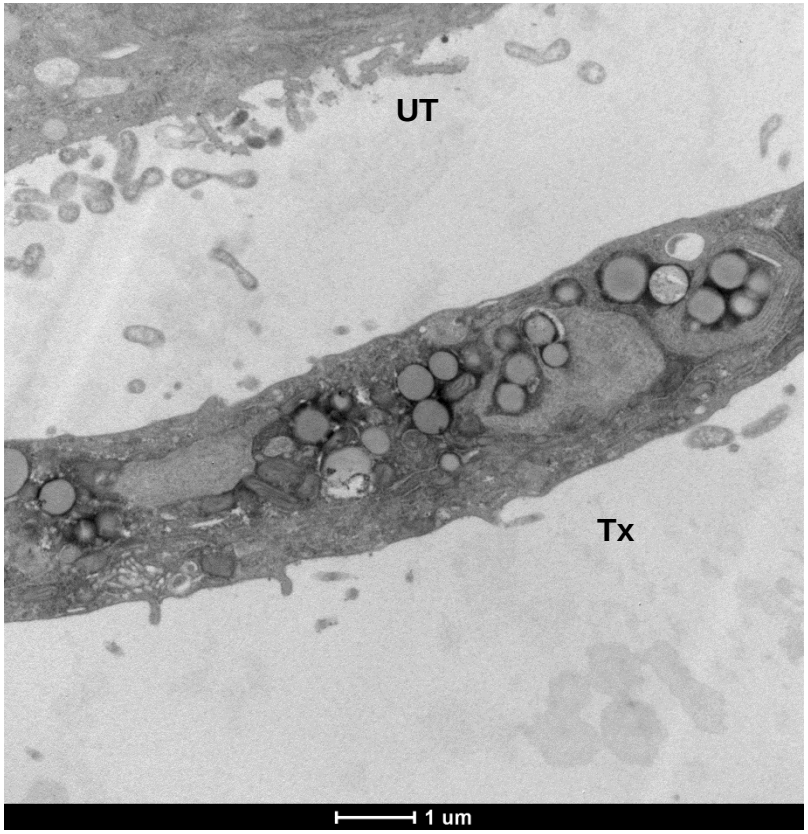

Zoom in

(Tx, Transfected cell; UT, Untransfected cell)

Viperin-APEX2 (Cell#6)

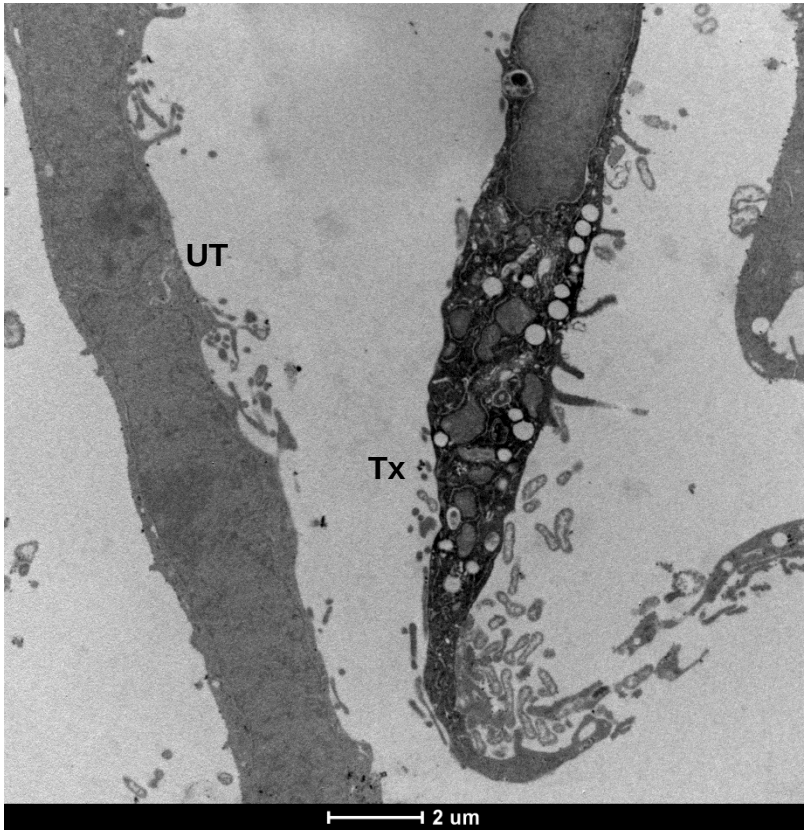

Zoom in

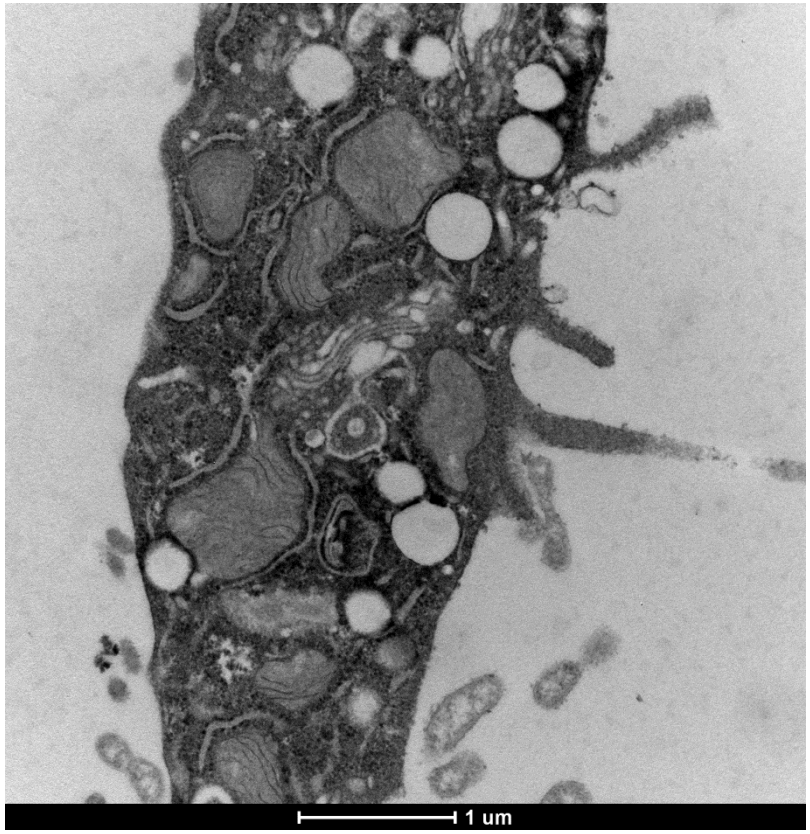

(Tx, Transfected cell; UT, Untransfected cell)

Viperin-APEX2 (Cell#7)

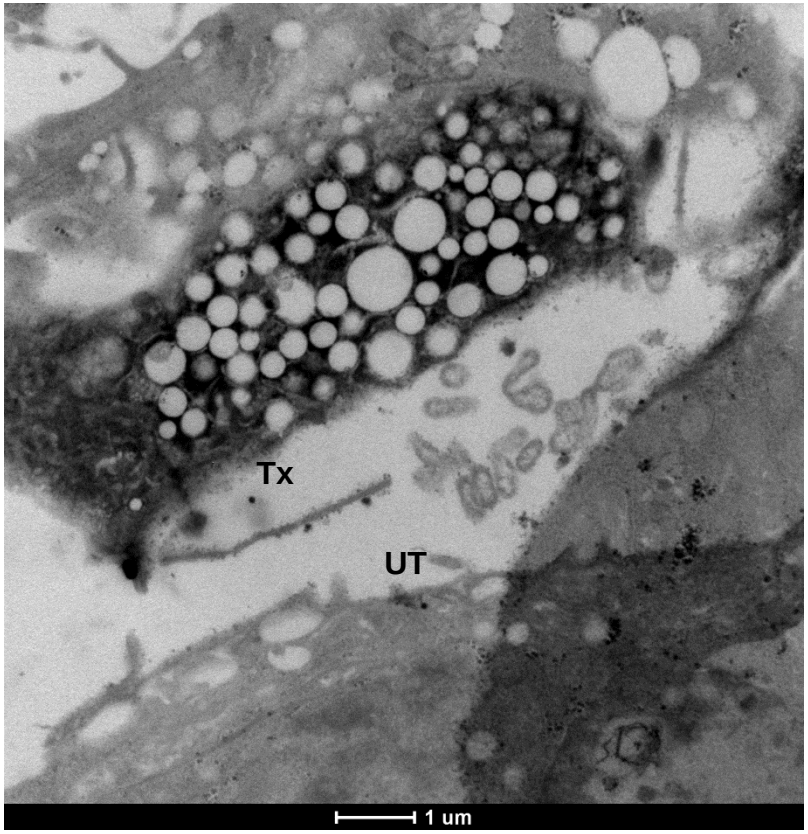

Zoom in

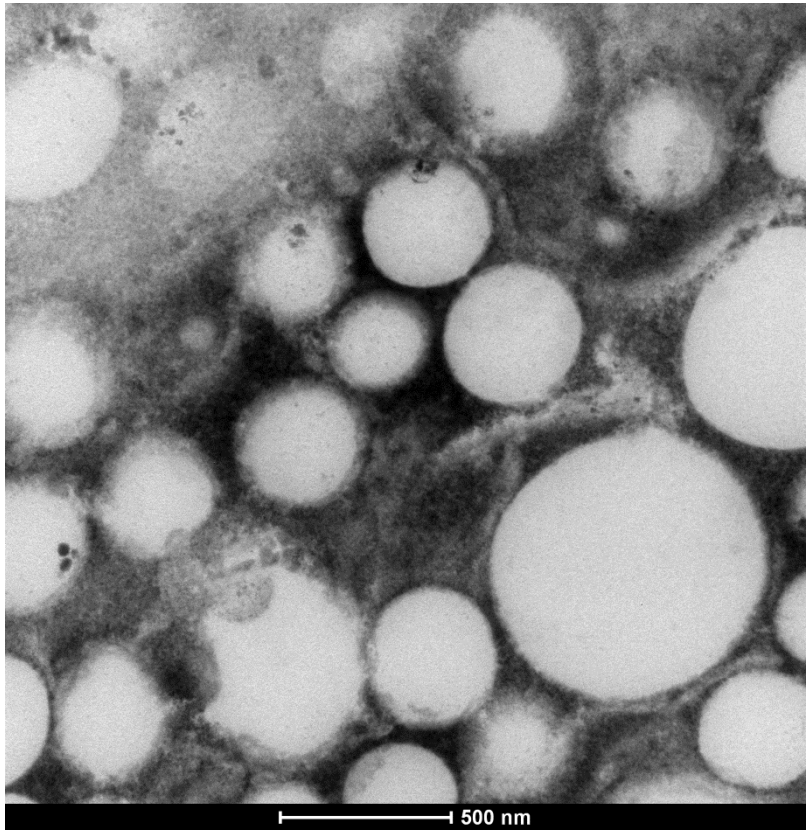

(Tx, Transfected cell; UT, Untransfected cell)

Viperin-APEX2 (Cell#8)

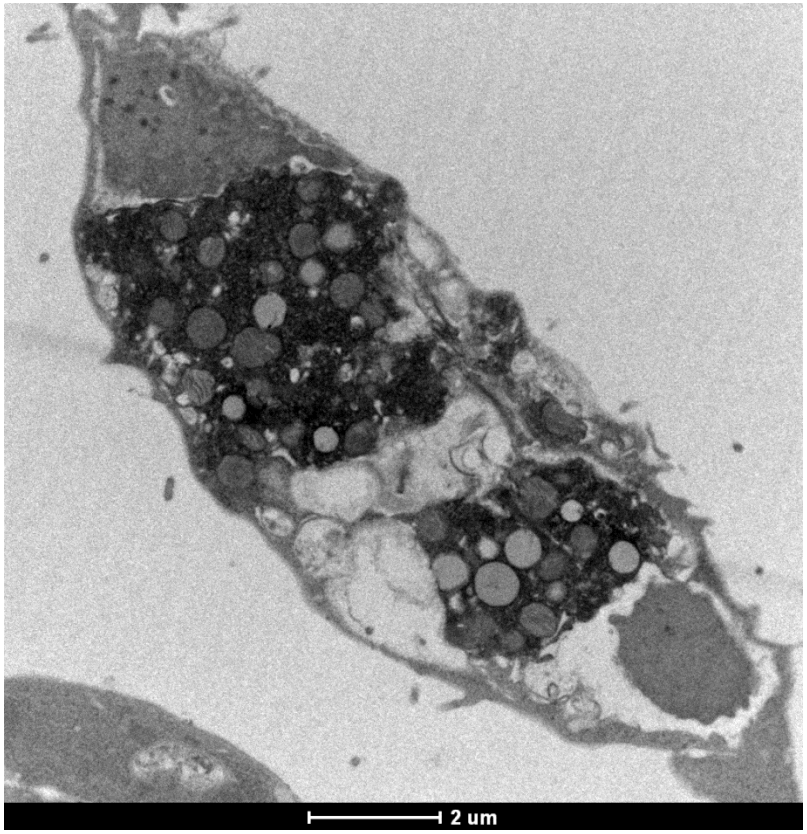

Zoom in

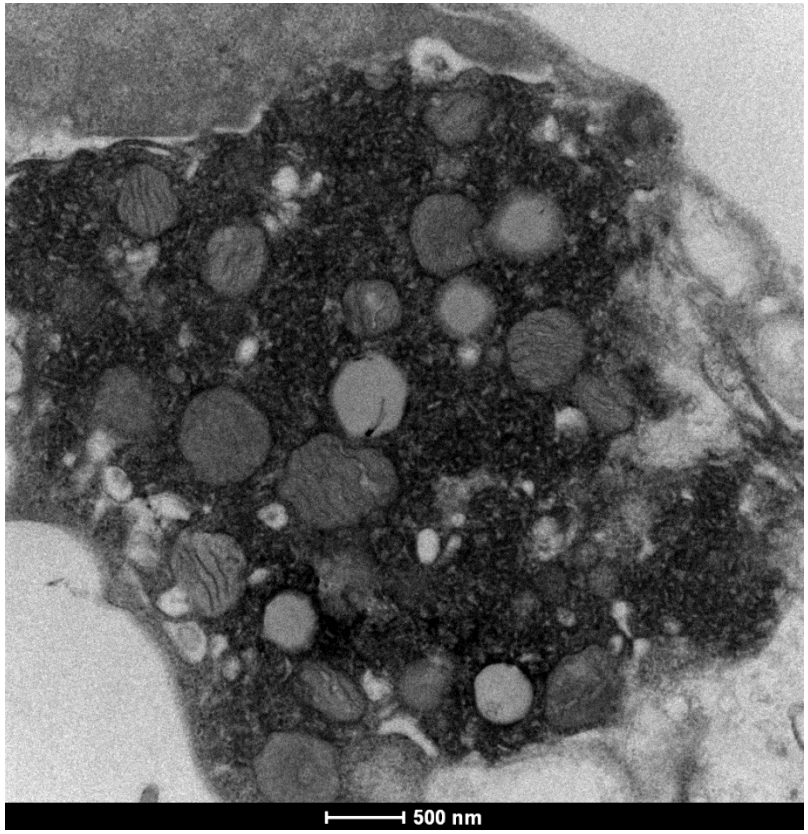

Viperin-APEX2 (Cell#9)

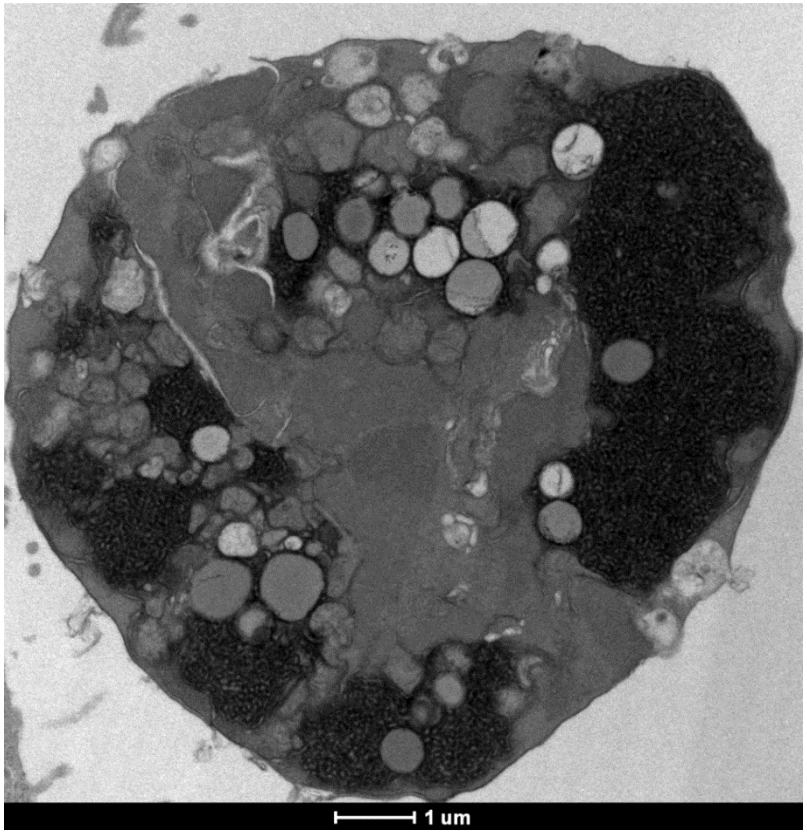

Zoom in

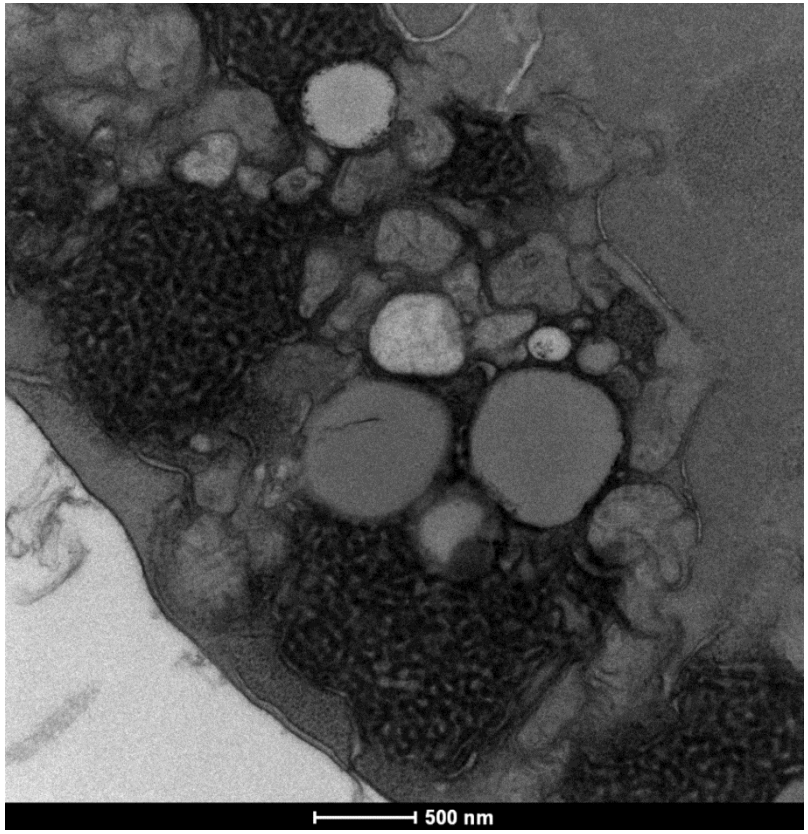

Viperin-APEX2 (Cell#10)

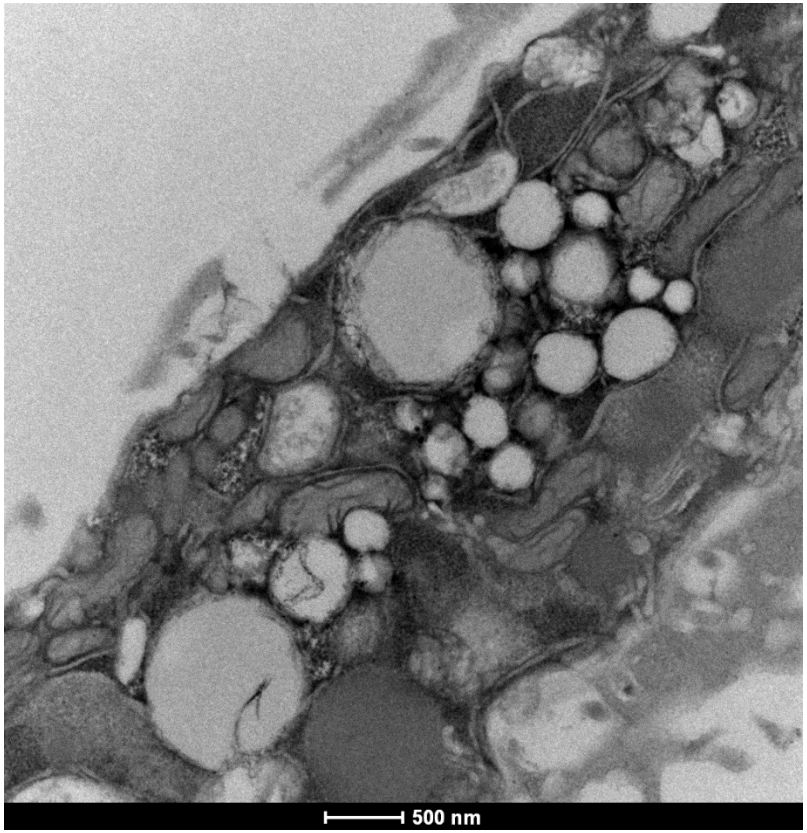

Zoom in

Viperin-APEX2 (Cell#11)

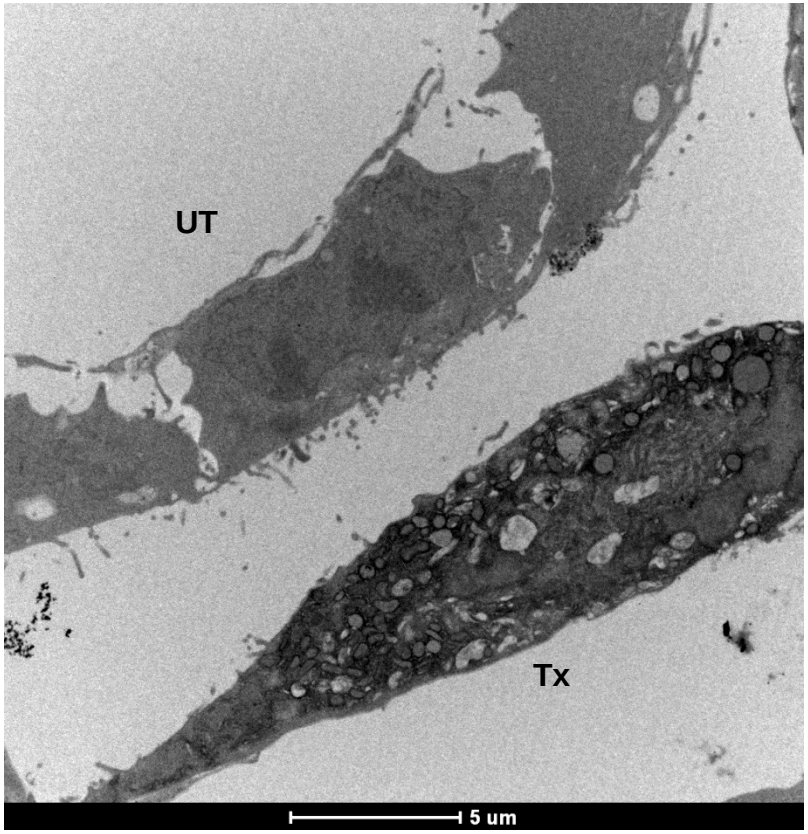

Zoom in

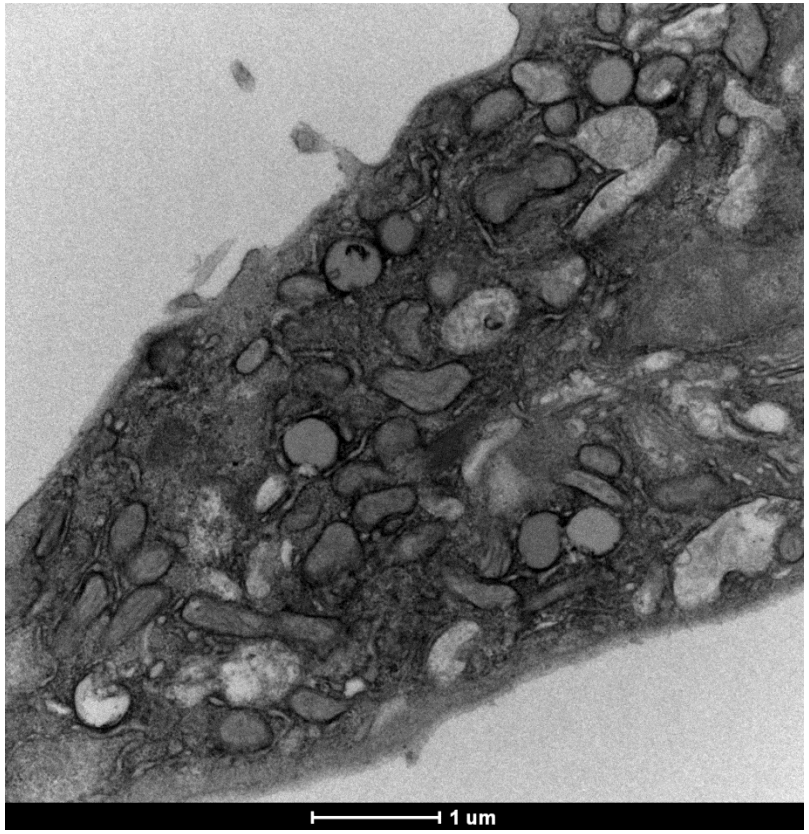

(Tx, Transfected cell; UT, Untransfected cell)

Viperin-APEX2 (Cell#12)

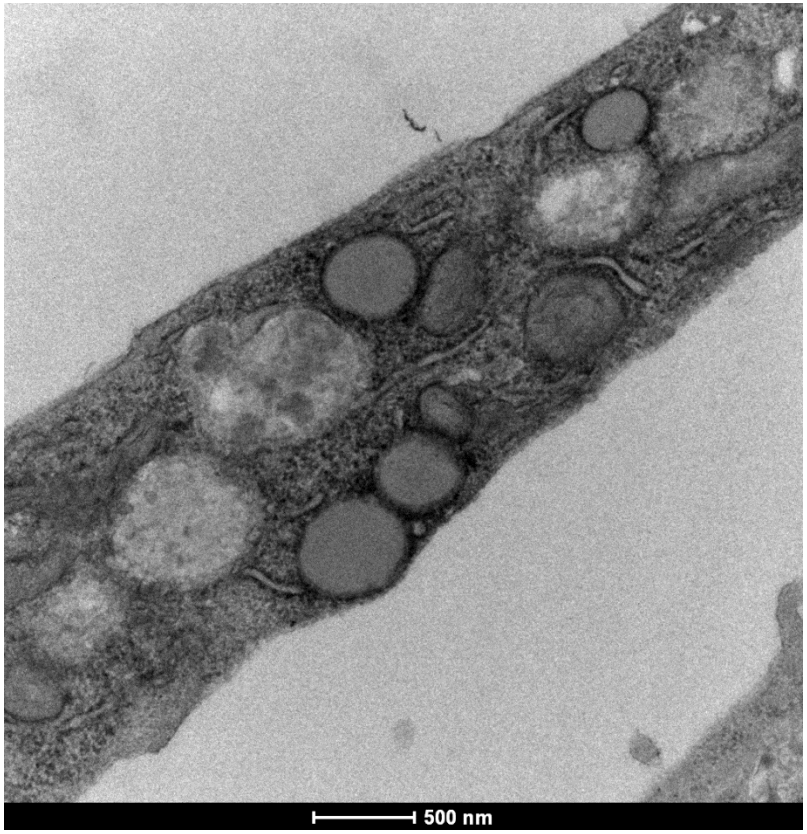

Zoom in

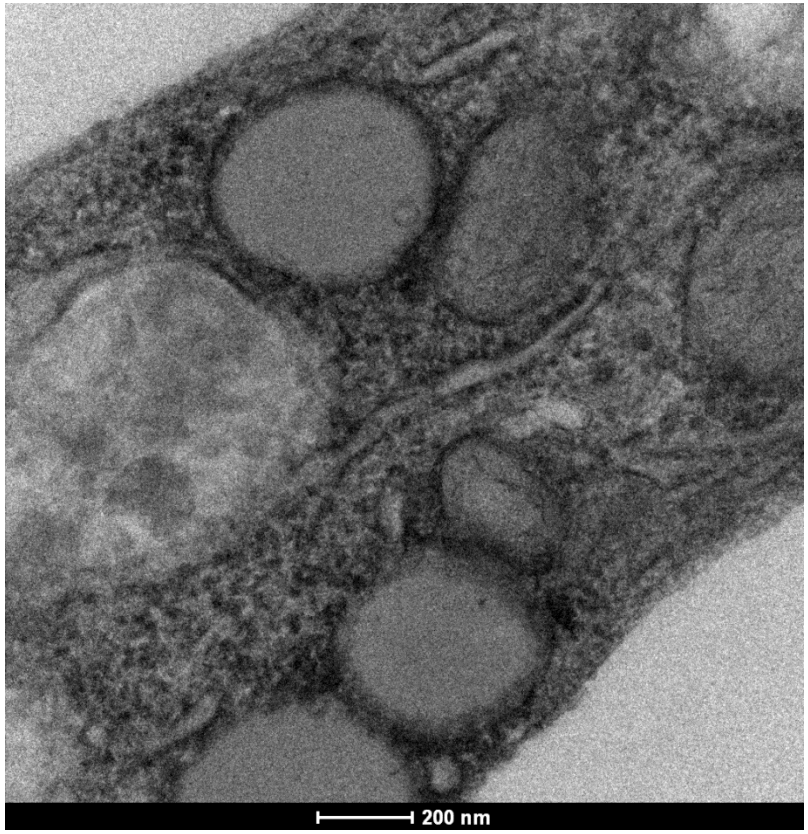

Viperin-APEX2 (Cell#13)

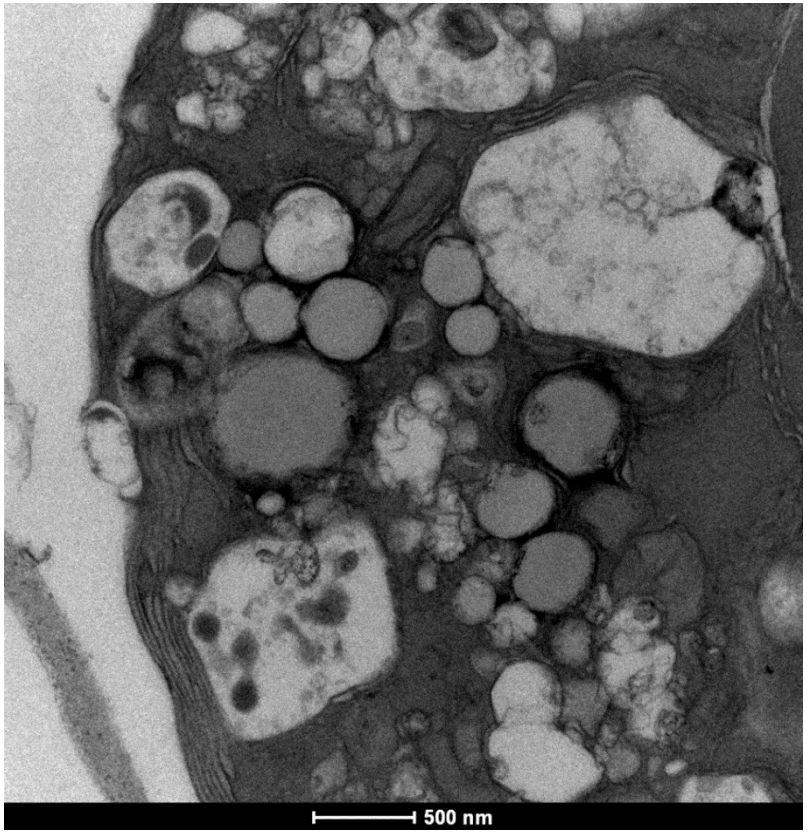

Zoom in

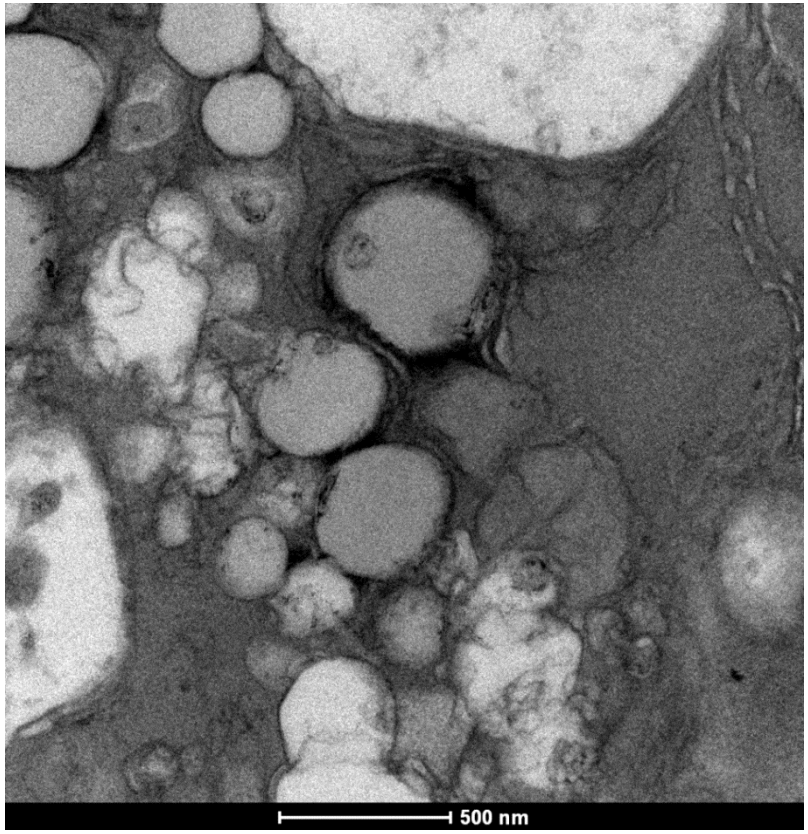

X-II. Huh-7 cells were transfected with a plasmid expressing APEX2 control following DAB staining.

APEX2 control (Cell#2)

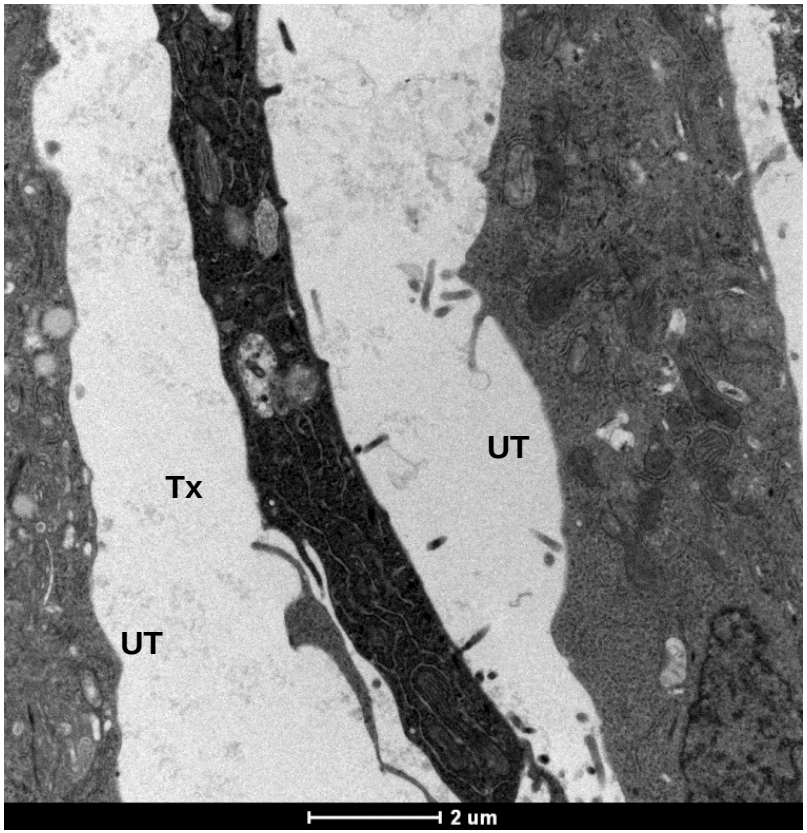

(Tx, Transfected cell; UT, Untransfected cell)

APEX2 control (Cell#3)

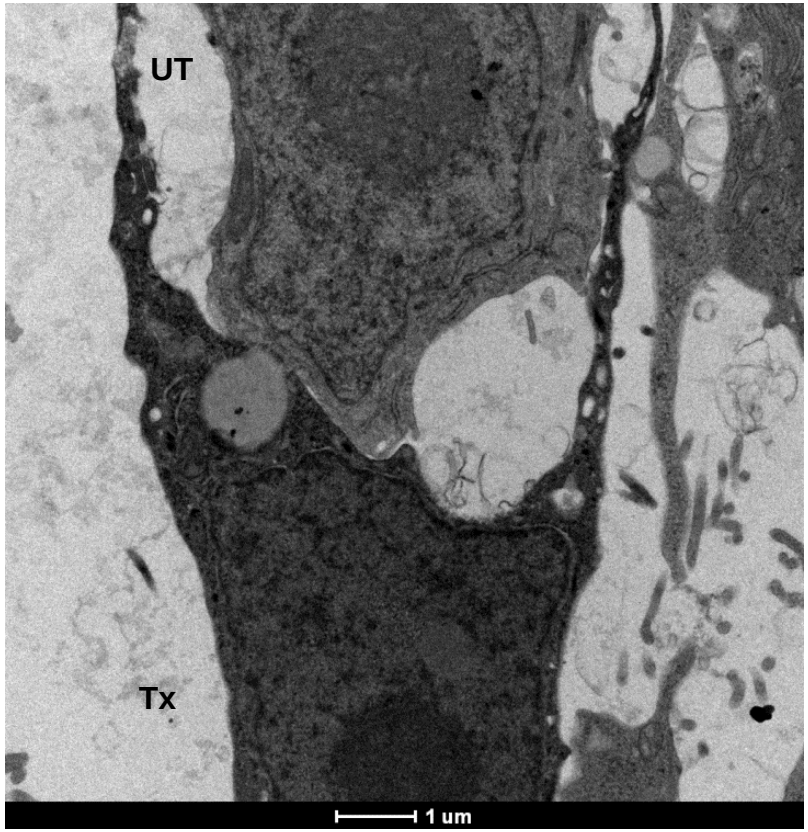

(Tx, Transfected cell; UT, Untransfected cell)

APEX2 control (Cell#4)

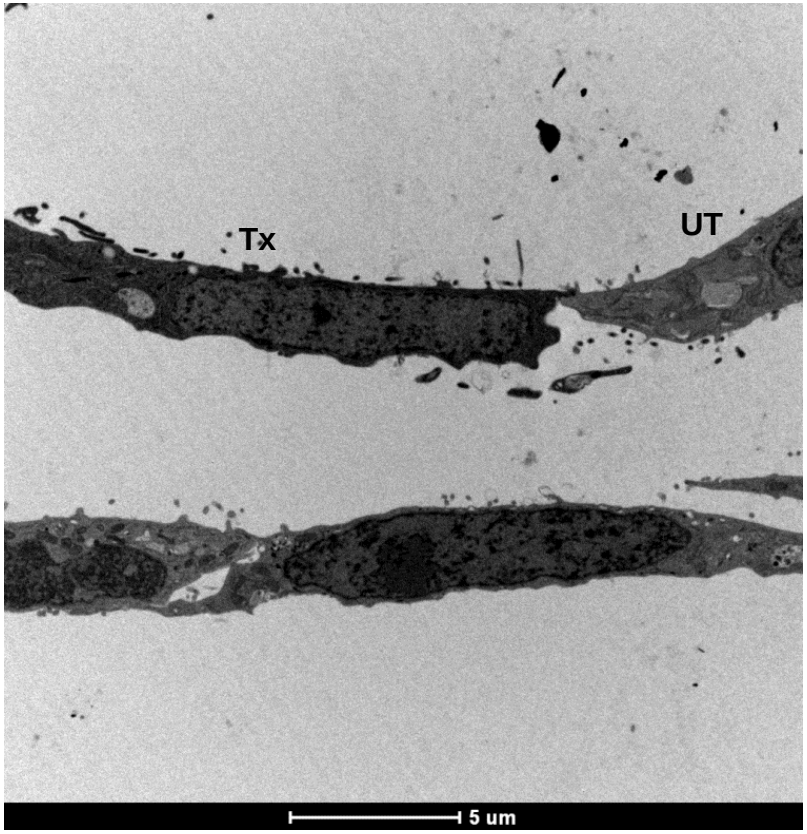

Zoom in

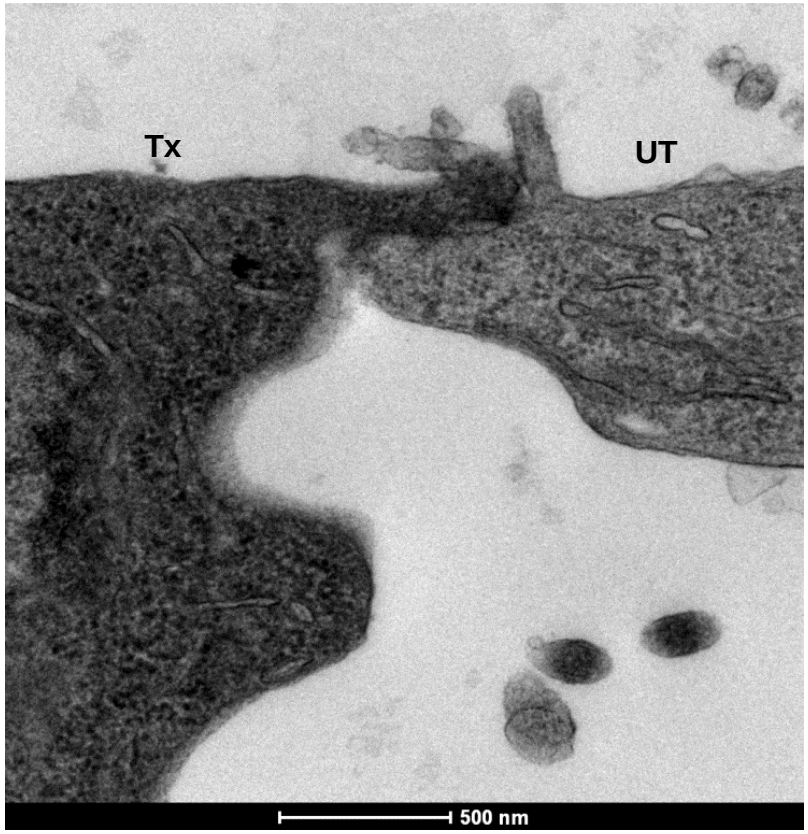

(Tx, Transfected cell; UT, Untransfected cell)

X-III. Huh-7 stably expressing T7 RNA polymerase cell line was transfected with a plasmid expressing viperin-APEX2 and pTM1(NS3-5B)/NS5A-GFP following DAB staining.

Huh-7/T7 + viperin-APEX2 (Cell#2)

Zoom in

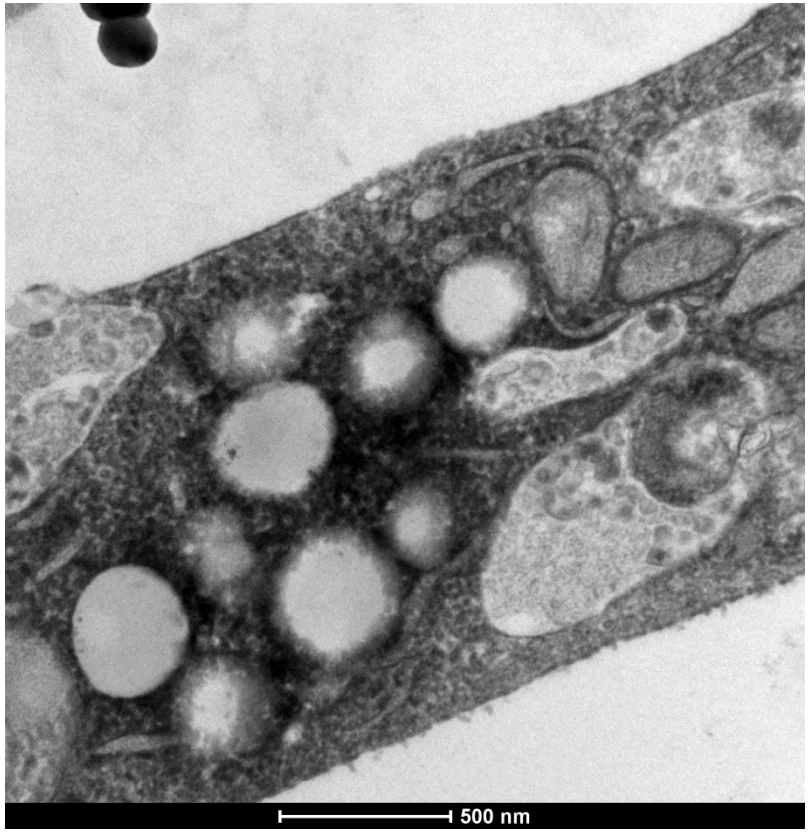

Huh-7/T7 + viperin-APEX2 (Cell#3)

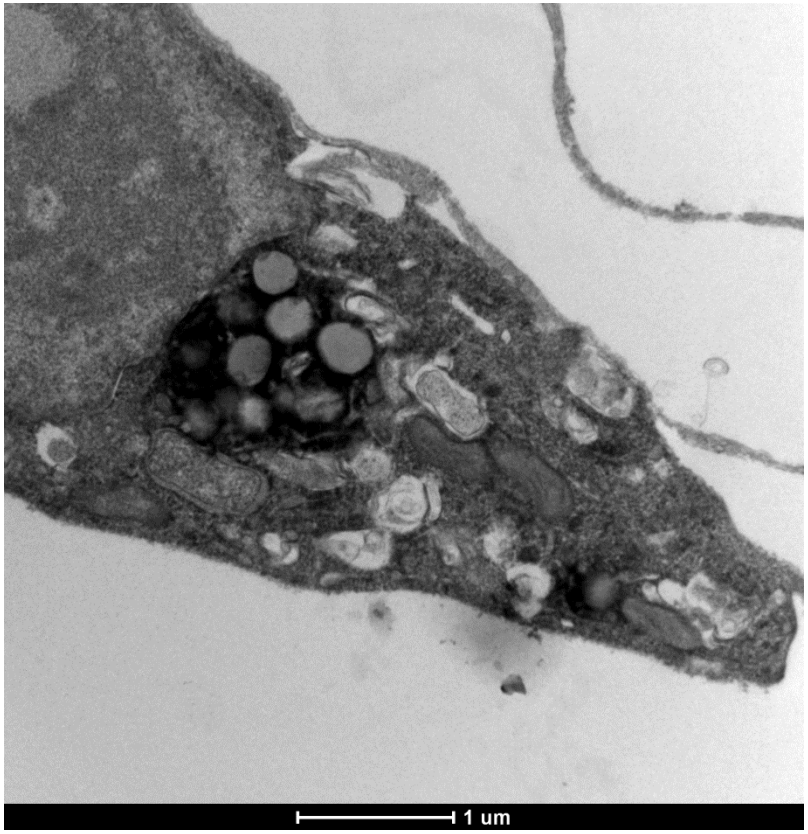

Zoom in

Huh-7/T7 + viperin-APEX2 (Cell#4)

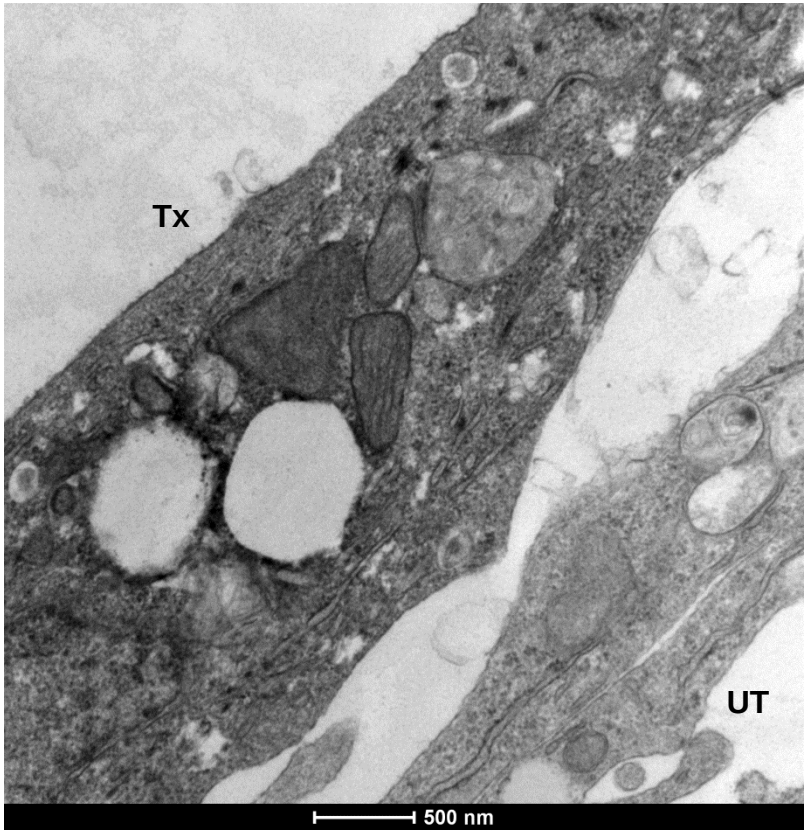

Zoom in

(Tx, Transfected cell; UT, Untransfected cell)

X-IV. Huh-7 stably expressing T7 RNA polymerase cell line was transfected with a plasmid expressing APEX2 control pTM1(NS3-5B)/NS5A-GFP following DAB staining.

Huh-7/T7 + APEX2 control (Cell#2)

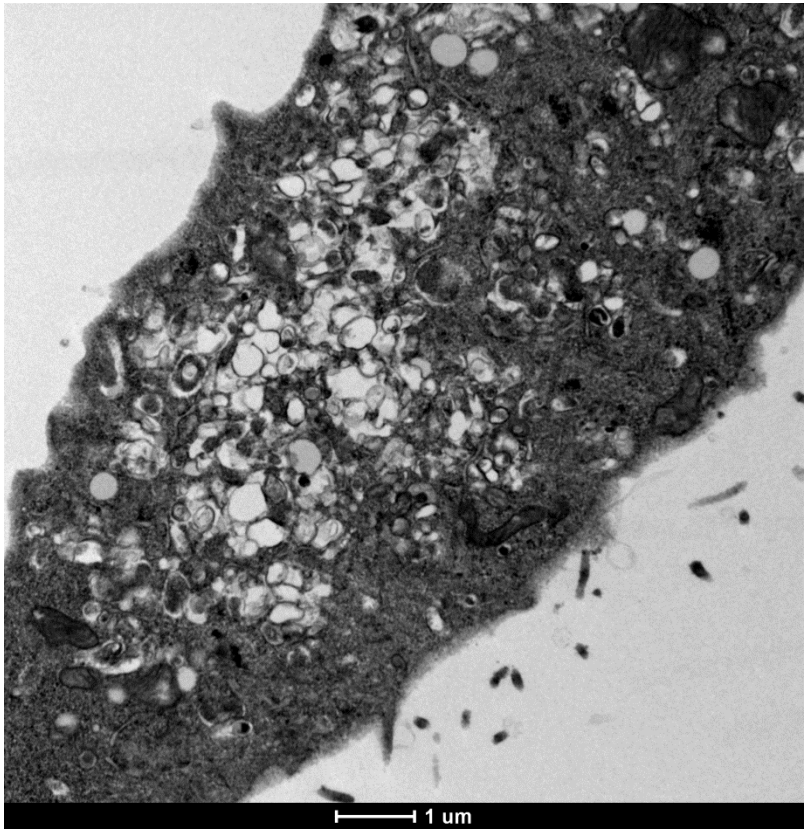

Zoom in

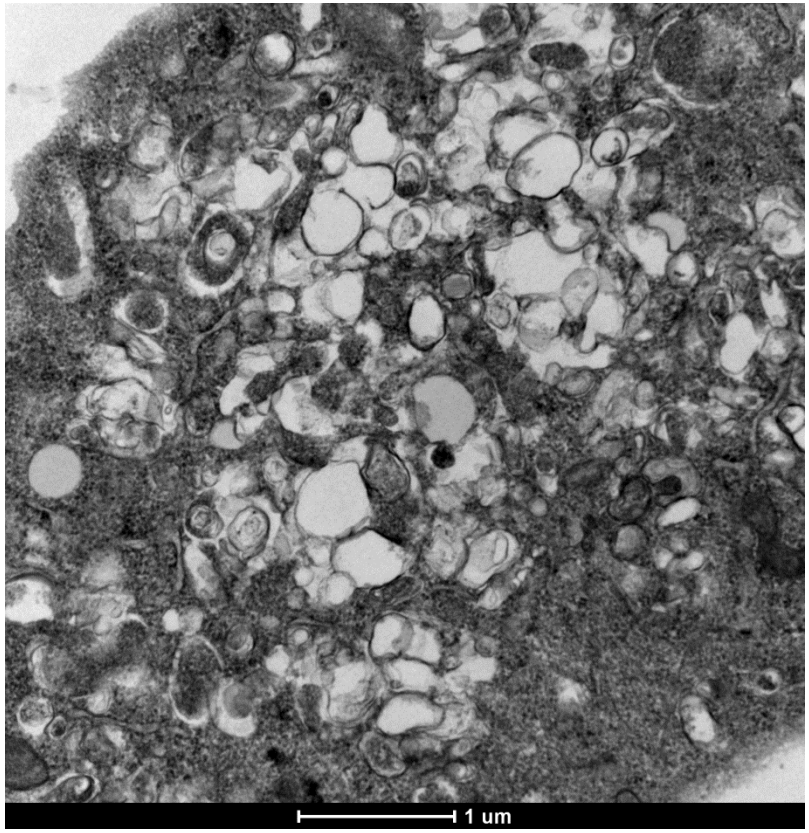

Huh-7/T7 + APEX2 control (Cell#3)

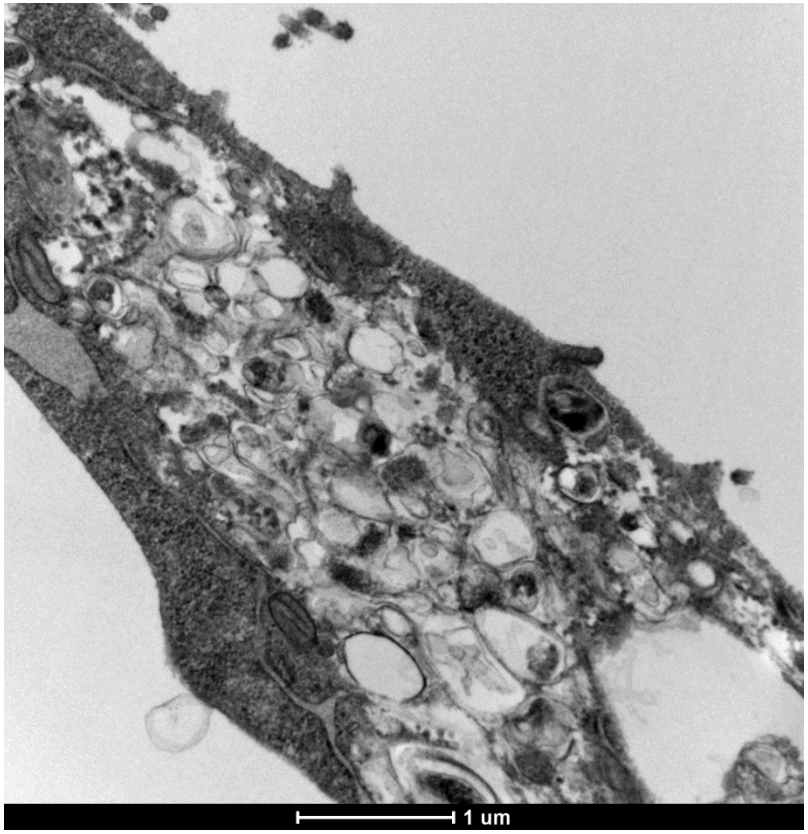

Zoom in

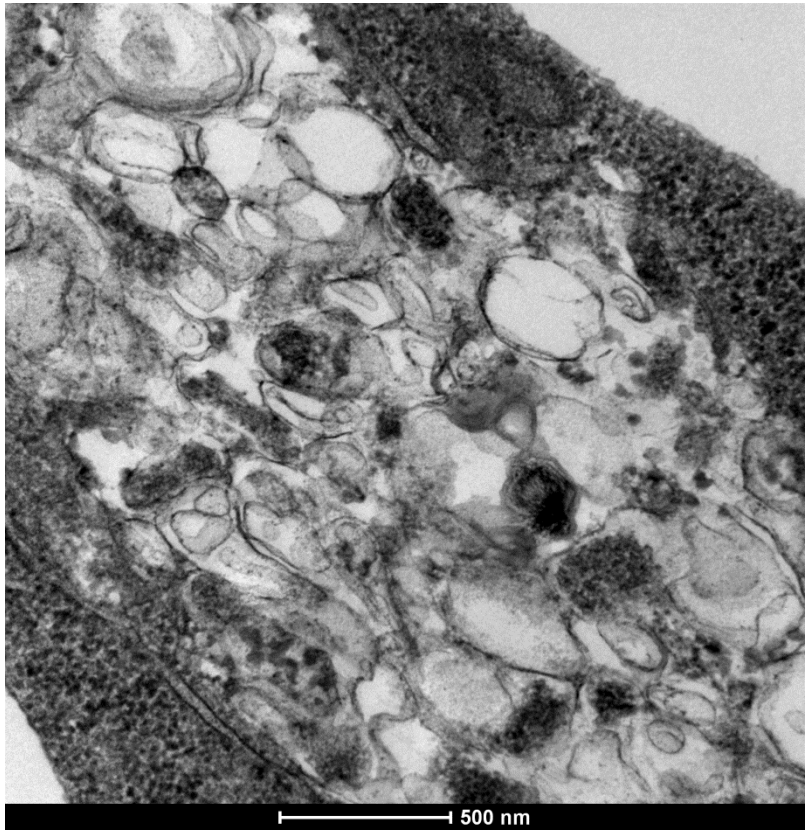

References

AFONSO, C. L., AMARASINGHE, G. K., BANYAI, K., BAO, Y., BASLER, C. F., BAVARI, S., BEJERMAN, N., BLASDELL, K. R., BRIAND, F. X., BRIESE, T., BUKREYEV, A., CALISHER, C. H., CHANDRAN, K., CHENG, J., CLAWSON, A. N., COLLINS, P. L., DIETZGEN, R. G., DOLNIK, O., DOMIER, L. L., DURRWALD, R., DYE, J. M., EASTON, A. J., EBIHARA, H., FARKAS, S. L., FREITAS-ASTUA, J., FORMENTY, P., FOUCHIER, R. A., FU, Y., GHEDIN, E., GOODIN, M. M., HEWSON, R., HORIE, M., HYNDMAN, T. H., JIANG, D., KITAJIMA, E. W., KOBINGER, G. P., KONDO, H., KURATH, G., LAMB, R. A., LENARDON, S., LEROY, E. M., LI, C. X., LIN, X. D., LIU, L., LONGDON, B., MARTON, S., MAISNER, A., MUHLBERGER, E., NETESOV, S. V., NOWOTNY, N., PATTERSON, J. L., PAYNE, S. L., PAWESKA, J. T., RANDALL, R. E., RIMA, B. K., ROTA, P., RUBBENSTROTH, D., SCHWEMMLE, M., SHI, M., SMITHER, S. J., STENGLEIN, M. D., STONE, D. M., TAKADA, A., TERREGINO, C., TESH, R. B., TIAN, J. H., TOMONAGA, K., TORDO, N., TOWNER, J. S., VASILAKIS, N., VERBEEK, M., VOLCHKOV, V. E., WAHL-JENSEN, V., WALSH, J. A., WALKER, P. J., WANG, D., WANG, L. F., WETZEL, T., WHITFIELD, A. E., XIE, J. T., YUEN, K. Y., ZHANG, Y. Z. & KUHN, J. H. 2016. Taxonomy of the order Mononegavirales: update 2016. *Arch Virol,* 161**,** 2351-60.

AGNELLO, V., ABEL, G., ELFAHAL, M., KNIGHT, G. B. & ZHANG, Q. X. 1999. Hepatitis C virus and other flaviviridae viruses enter cells via low density lipoprotein receptor. *Proc Natl Acad Sci U S A,* 96**,** 12766-71.

AGRAWAL, G. & SUBRAMANI, S. 2016. De novo peroxisome biogenesis: Evolving concepts and conundrums. *Biochim Biophys Acta,* 1863**,** 892-901.

ALEXOPOULOU, L., HOLT, A. C., MEDZHITOV, R. & FLAVELL, R. A. 2001. Recognition of double-stranded RNA and activation of NF-kappaB by Toll-like receptor 3. *Nature,* 413**,** 732-8.

ALOIA, A. L., LOCARNINI, S. & BEARD, M. R. 2012. Antiviral resistance and direct-acting antiviral agents for HCV. *Antivir Ther,* 17**,** 1147-62.

ALTER, G., SUSCOVICH, T. J., TEIGEN, N., MEIER, A., STREECK, H., BRANDER, C. & ALTFELD, M. 2007. Single-stranded RNA derived from HIV-1 serves as a potent activator of NK cells. *J Immunol,* 178**,** 7658-66.

ALTER, M. J. 1995. Epidemiology of hepatitis C in the West. *Semin Liver Dis,* 15**,** 5-14.

AMAKO, Y., SARKESHIK, A., HOTTA, H., YATES, J., 3RD & SIDDIQUI, A. 2009. Role of oxysterol binding protein in hepatitis C virus infection. *J Virol,* 83**,** 9237-46.

AMINI-BAVIL-OLYAEE, S., CHOI, Y. J., LEE, J. H., SHI, M., HUANG, I. C., FARZAN, M. & JUNG, J. U. 2013. The antiviral effector IFITM3 disrupts intracellular cholesterol homeostasis to block viral entry. *Cell Host Microbe,* 13**,** 452-64.

ANDRE, P., KOMURIAN-PRADEL, F., DEFORGES, S., PERRET, M., BERLAND, J. L., SODOYER, M., POL, S., BRECHOT, C., PARANHOS-BACCALA, G. &

LOTTEAU, V. 2002. Characterization of low- and very-low-density hepatitis C virus RNA-containing particles. *J Virol,* 76**,** 6919-28.

APPEL, N., PIETSCHMANN, T. & BARTENSCHLAGER, R. 2005. Mutational analysis of hepatitis C virus nonstructural protein 5A: potential role of differential phosphorylation in RNA replication and identification of a genetically flexible domain. *J Virol,* 79**,** 3187-94.

APPEL, N., ZAYAS, M., MILLER, S., KRIJNSE-LOCKER, J., SCHALLER, T., FRIEBE, P., KALLIS, S., ENGEL, U. & BARTENSCHLAGER, R. 2008. Essential role of domain III of nonstructural protein 5A for hepatitis C virus infectious particle assembly. *PLoS Pathog,* 4**,** e1000035.

ASSELAH, T., RUBBIA-BRANDT, L., MARCELLIN, P. & NEGRO, F. 2006. Steatosis in chronic hepatitis C: why does it really matter? *Gut,* 55**,** 123-30.

BAIN, C., FATMI, A., ZOULIM, F., ZARSKI, J. P., TREPO, C. & INCHAUSPE, G. 2001. Impaired allostimulatory function of dendritic cells in chronic hepatitis C infection. *Gastroenterology,* 120**,** 512-24.

BANKWITZ, D., STEINMANN, E., BITZEGEIO, J., CIESEK, S., FRIESLAND, M., HERRMANN, E., ZEISEL, M. B., BAUMERT, T. F., KECK, Z. Y., FOUNG, S. K., PECHEUR, E. I. & PIETSCHMANN, T. 2010. Hepatitis C virus hypervariable region 1 modulates receptor interactions, conceals the CD81 binding site, and protects conserved neutralizing epitopes. *J Virol,* 84**,** 5751-63.

BARBA, G., HARPER, F., HARADA, T., KOHARA, M., GOULINET, S., MATSUURA, Y., EDER, G., SCHAFF, Z., CHAPMAN, M. J., MIYAMURA, T. & BRECHOT, C. 1997. Hepatitis C virus core protein shows a cytoplasmic localization and associates to cellular lipid storage droplets. *Proc Natl Acad Sci U S A,* 94**,** 1200-5.

BARTENSCHLAGER, R. 2002. Hepatitis C virus replicons: potential role for drug development. *Nat Rev Drug Discov,* 1**,** 911-6.

BARTENSCHLAGER, R., PENIN, F., LOHMANN, V. & ANDRE, P. 2011. Assembly of infectious hepatitis C virus particles. *Trends Microbiol,* 19**,** 95-103.

BARTH, H., SCHAFER, C., ADAH, M. I., ZHANG, F., LINHARDT, R. J., TOYODA, H., KINOSHITA-TOYODA, A., TOIDA, T., VAN KUPPEVELT, T. H., DEPLA, E., VON WEIZSACKER, F., BLUM, H. E. & BAUMERT, T. F. 2003. Cellular binding of hepatitis C virus envelope glycoprotein E2 requires cell surface heparan sulfate. *J Biol Chem,* 278**,** 41003-12.

BARTOSCH, B., DUBUISSON, J. & COSSET, F. L. 2003. Infectious hepatitis C virus pseudo-particles containing functional E1-E2 envelope protein complexes. *J Exp Med,* 197**,** 633-42.

BEARD, M. R., ABELL, G., HONDA, M., CARROLL, A., GARTLAND, M., CLARKE, B., SUZUKI, K., LANFORD, R., SANGAR, D. V. & LEMON, S. M. 1999. An infectious molecular clone of a Japanese genotype 1b hepatitis C virus. *Hepatology,* 30**,** 316-24.

BEHRENS, S. E., TOMEI, L. & DE FRANCESCO, R. 1996. Identification and properties of the RNA-dependent RNA polymerase of hepatitis C virus. *EMBO J,* 15**,** 12-22.

BEIGNON, A. S., MCKENNA, K., SKOBERNE, M., MANCHES, O., DASILVA, I., KAVANAGH, D. G., LARSSON, M., GORELICK, R. J., LIFSON, J. D. &

BHARDWAJ, N. 2005. Endocytosis of HIV-1 activates plasmacytoid dendritic cells via Toll-like receptor-viral RNA interactions. *J Clin Invest,* 115**,** 3265-75.

BELLER, M., THIEL, K., THUL, P. J. & JACKLE, H. 2010. Lipid droplets: a dynamic organelle moves into focus. *FEBS Lett,* 584**,** 2176-82.

BENDER, S., REUTER, A., EBERLE, F., EINHORN, E., BINDER, M. & BARTENSCHLAGER, R. 2015. Activation of Type I and III Interferon Response by Mitochondrial and Peroxisomal MAVS and Inhibition by Hepatitis C Virus. *PLoS Pathog,* 11**,** e1005264.

BIGGER, C. B., GUERRA, B., BRASKY, K. M., HUBBARD, G., BEARD, M. R., LUXON, B. A., LEMON, S. M. & LANFORD, R. E. 2004. Intrahepatic gene expression during chronic hepatitis C virus infection in chimpanzees. *J Virol,* 78**,** 13779-92.

BLANCHARD, E., BELOUZARD, S., GOUESLAIN, L., WAKITA, T., DUBUISSON, J., WYCHOWSKI, C. & ROUILLE, Y. 2006. Hepatitis C virus entry depends on clathrin-mediated endocytosis. *J Virol,* 80**,** 6964-72.

BLIGHT, K. J., KOLYKHALOV, A. A. & RICE, C. M. 2000. Efficient initiation of HCV RNA replication in cell culture. *Science,* 290**,** 1972-4.

BLIGHT, K. J., MCKEATING, J. A. & RICE, C. M. 2002. Highly permissive cell lines for subgenomic and genomic hepatitis C virus RNA replication. *J Virol,* 76**,** 13001-14.

BLIGHT, K. J. & NORGARD, E. A. 2006. HCV Replicon Systems. *In:* TAN, S. L. (ed.) *Hepatitis C Viruses: Genomes and Molecular Biology.* Norfolk (UK).

BOISVERT, M. & SHOUKRY, N. H. 2016. Type III Interferons in Hepatitis C Virus Infection. *Front Immunol,* 7**,** 628.

BOUDINOT, P., RIFFAULT, S., SALHI, S., CARRAT, C., SEDLIK, C., MAHMOUDI, N., CHARLEY, B. & BENMANSOUR, A. 2000. Vesicular stomatitis virus and pseudorabies virus induce a vig1/cig5 homologue in mouse dendritic cells via different pathways. *J Gen Virol,* 81**,** 2675-82.

BOUFFARD, P., HAYASHI, P. H., ACEVEDO, R., LEVY, N. & ZELDIS, J. B. 1992. Hepatitis C virus is detected in a monocyte/macrophage subpopulation of peripheral blood mononuclear cells of infected patients. *J Infect Dis,* 166**,** 1276-80.

BOULANT, S., MONTSERRET, R., HOPE, R. G., RATINIER, M., TARGETT-ADAMS, P., LAVERGNE, J. P., PENIN, F. & MCLAUCHLAN, J. 2006. Structural determinants that target the hepatitis C virus core protein to lipid droplets. *J Biol Chem,* 281**,** 22236-47.

BOULANT, S., VANBELLE, C., EBEL, C., PENIN, F. & LAVERGNE, J. P. 2005. Hepatitis C virus core protein is a dimeric alpha-helical protein exhibiting membrane protein features. *J Virol,* 79**,** 11353-65.

BOWDEN, D. S. & BERZSENYI, M. D. 2006. Chronic hepatitis C virus infection: genotyping and its clinical role. *Future Microbiol,* 1**,** 103-12.

BRASS, V., BERKE, J. M., MONTSERRET, R., BLUM, H. E., PENIN, F. & MORADPOUR, D. 2008. Structural determinants for membrane association and dynamic organization of the hepatitis C virus NS3-4A complex. *Proc Natl Acad Sci U S A,* 105**,** 14545-50.

BRAZZOLI, M., BIANCHI, A., FILIPPINI, S., WEINER, A., ZHU, Q., PIZZA, M. & CROTTA, S. 2008. CD81 is a central regulator of cellular events required for hepatitis C virus infection of human hepatocytes. *J Virol,* 82**,** 8316-29.

BRODSKY, L. I., WAHED, A. S., LI, J., TAVIS, J. E., TSUKAHARA, T. & TAYLOR, M. W. 2007. A novel unsupervised method to identify genes important in the anti-viral response: application to interferon/ribavirin in hepatitis C patients. *PLoS One,* 2**,** e584.

BRUCKNER, A., POLGE, C., LENTZE, N., AUERBACH, D. & SCHLATTNER, U. 2009. Yeast two-hybrid, a powerful tool for systems biology. *Int J Mol Sci,* 10**,** 2763-88.

BRUENING, J., WEIGEL, B. & GEROLD, G. 2017. The Role of Type III Interferons in Hepatitis C Virus Infection and Therapy. *J Immunol Res,* 2017**,** 7232361.

CALLE SERRANO, B. & MANNS, M. P. 2012. HCV's days are numbered: next-generation direct-acting antivirals and host-targeting agents. *Antivir Ther,* 17**,** 1133-46.

CARDENAS, W. B., LOO, Y. M., GALE, M., JR., HARTMAN, A. L., KIMBERLIN, C. R., MARTINEZ-SOBRIDO, L., SAPHIRE, E. O. & BASLER, C. F. 2006. Ebola virus VP35 protein binds double-stranded RNA and inhibits alpha/beta interferon production induced by RIG-I signaling. *J Virol,* 80**,** 5168-78.

CARRERE-KREMER, S., MONTPELLIER-PALA, C., COCQUEREL, L., WYCHOWSKI, C., PENIN, F. & DUBUISSON, J. 2002. Subcellular localization and topology of the p7 polypeptide of hepatitis C virus. *J Virol,* 76**,** 3720-30.

CHAN, Y. L., CHANG, T. H., LIAO, C. L. & LIN, Y. L. 2008. The Cellular antiviral protein viperin is attenuated by proteasome-mediated protein degradation in Japanese Encephalitis Virus-infected cells. *Journal of Virology,* 82**,** 10455-10464.

CHHABRA, P., RANJAN, P., CROMEANS, T., SAMBHARA, S. & VINJE, J. 2017. Critical role of RIG-I and MDA5 in early and late stages of Tulane virus infection. *J Gen Virol,* 98**,** 1016-1026.

CHIEN, C. T., BARTEL, P. L., STERNGLANZ, R. & FIELDS, S. 1991. The two-hybrid system: a method to identify and clone genes for proteins that interact with a protein of interest. *Proc Natl Acad Sci U S A,* 88**,** 9578-82.

CHIN, K. C. & CRESSWELL, P. 2001. Viperin (cig5), an IFN-inducible antiviral protein directly induced by human cytomegalovirus. *Proceedings of the National Academy of Sciences of the United States of America,* 98**,** 15125-15130.

CHOO, Q. L., KUO, G., WEINER, A. J., OVERBY, L. R., BRADLEY, D. W. & HOUGHTON, M. 1989. Isolation of a cDNA clone derived from a blood-borne non-A, non-B viral hepatitis genome. *Science,* 244**,** 359-62.

CHUKKAPALLI, V. & RANDALL, G. 2014. Hepatitis C virus replication compartment formation: mechanism and drug target. *Gastroenterology,* 146**,** 1164-7.

COLLER, K. E., BERGER, K. L., HEATON, N. S., COOPER, J. D., YOON, R. & RANDALL, G. 2009. RNA interference and single particle tracking analysis of hepatitis C virus endocytosis. *PLoS Pathog,* 5**,** e1000702.

COUNIHAN, N. A., RAWLINSON, S. M. & LINDENBACH, B. D. 2011. Trafficking of hepatitis C virus core protein during virus particle assembly. *PLoS Pathog,* 7**,** e1002302.

CUI, S., EISENACHER, K., KIRCHHOFER, A., BRZOZKA, K., LAMMENS, A., LAMMENS, K., FUJITA, T., CONZELMANN, K. K., KRUG, A. & HOPFNER, K. P. 2008. The C-terminal regulatory domain is the RNA 5'-triphosphate sensor of RIG-I. *Mol Cell,* 29**,** 169-79.

DAFFIS, S., SAMUEL, M. A., SUTHAR, M. S., GALE, M., JR. & DIAMOND, M. S. 2008. Toll-like receptor 3 has a protective role against West Nile virus infection. *J Virol,* 82**,** 10349-58.

DAO THI, V. L., GRANIER, C., ZEISEL, M. B., GUERIN, M., MANCIP, J., GRANIO, O., PENIN, F., LAVILLETTE, D., BARTENSCHLAGER, R., BAUMERT, T. F., COSSET, F. L. & DREUX, M. 2012. Characterization of hepatitis C virus particle subpopulations reveals multiple usage of the scavenger receptor BI for entry steps. *J Biol Chem,* 287**,** 31242-57.

DAVIS, G. L., ALTER, M. J., EL-SERAG, H., POYNARD, T. & JENNINGS, L. W. 2010. Aging of hepatitis C virus (HCV)-infected persons in the United States: a multiple cohort model of HCV prevalence and disease progression. *Gastroenterology,* 138**,** 513-21, 521 e1-6.

DE VEER, M. J., HOLKO, M., FREVEL, M., WALKER, E., DER, S., PARANJAPE, J. M., SILVERMAN, R. H. & WILLIAMS, B. R. 2001. Functional classification of interferon-stimulated genes identified using microarrays. *J Leukoc Biol,* 69**,** 912-20.

DEFILIPPIS, V. R., ROBINSON, B., KECK, T. M., HANSEN, S. G., NELSON, J. A. & FRUH, K. J. 2006. Interferon regulatory factor 3 is necessary for induction of antiviral genes during human cytomegalovirus infection. *J Virol,* 80**,** 1032-7.

DI MARCO, S., VOLPARI, C., TOMEI, L., ALTAMURA, S., HARPER, S., NARJES, F., KOCH, U., ROWLEY, M., DE FRANCESCO, R., MIGLIACCIO, G. & CARFI, A. 2005. Interdomain communication in hepatitis C virus polymerase abolished by small molecule inhibitors bound to a novel allosteric site. *J Biol Chem,* 280**,** 29765-70.

DIEBOLD, S. S., KAISHO, T., HEMMI, H., AKIRA, S. & REIS E SOUSA, C. 2004. Innate antiviral responses by means of TLR7-mediated recognition of single-stranded RNA. *Science,* 303**,** 1529-31.

DIXIT, E., BOULANT, S., ZHANG, Y., LEE, A. S., ODENDALL, C., SHUM, B., HACOHEN, N., CHEN, Z. J., WHELAN, S. P., FRANSEN, M., NIBERT, M. L., SUPERTI-FURGA, G. & KAGAN, J. C. 2010. Peroxisomes are signaling platforms for antiviral innate immunity. *Cell,* 141**,** 668-81.

DOLGANIUC, A., GARCIA, C., KODYS, K. & SZABO, G. 2006. Distinct Toll-like receptor expression in monocytes and T cells in chronic HCV infection. *World J Gastroenterol,* 12**,** 1198-204.

DOLGANIUC, A., OAK, S., KODYS, K., GOLENBOCK, D. T., FINBERG, R. W., KURT-JONES, E. & SZABO, G. 2004. Hepatitis C core and nonstructural 3 proteins trigger toll-like receptor 2-mediated pathways and inflammatory activation. *Gastroenterology,* 127**,** 1513-24.

DORE, G. J., MACDONALD, M., LAW, M. G. & KALDOR, J. M. 2003. Epidemiology of hepatitis C virus infection in Australia. *Aust Fam Physician,* 32**,** 796-8.

DORNHOFF, H., SIEBLER, J. & NEURATH, M. F. 2011. Potential role of interferon-lambda in the treatment of inflammation and cancer: an update. *Int J Infereron Cytokine Mediator Res,* 3**,** 51-7.

DUBUISSON, J., HSU, H. H., CHEUNG, R. C., GREENBERG, H. B., RUSSELL, D. G. & RICE, C. M. 1994. Formation and intracellular localization of hepatitis C virus envelope glycoprotein complexes expressed by recombinant vaccinia and Sindbis viruses. *J Virol,* 68**,** 6147-60.

DUSCHENE, K. S. & BRODERICK, J. B. 2010. The antiviral protein viperin is a radical SAM enzyme. *FEBS Lett,* 584**,** 1263-7.

DUVET, S., COCQUEREL, L., PILLEZ, A., CACAN, R., VERBERT, A., MORADPOUR, D., WYCHOWSKI, C. & DUBUISSON, J. 1998. Hepatitis C virus glycoprotein complex localization in the endoplasmic reticulum involves a determinant for retention and not retrieval. *J Biol Chem,* 273**,** 32088-95.

EGGER, D., WOLK, B., GOSERT, R., BIANCHI, L., BLUM, H. E., MORADPOUR, D. & BIENZ, K. 2002. Expression of hepatitis C virus proteins induces distinct membrane alterations including a candidate viral replication complex. *J Virol,* 76**,** 5974-84.

ERRETT, J. S., SUTHAR, M. S., MCMILLAN, A., DIAMOND, M. S. & GALE, M., JR. 2013. The essential, nonredundant roles of RIG-I and MDA5 in detecting and controlling West Nile virus infection. *J Virol,* 87**,** 11416-25.

EVANS, M. J., RICE, C. M. & GOFF, S. P. 2004. Phosphorylation of hepatitis C virus nonstructural protein 5A modulates its protein interactions and viral RNA replication. *Proc Natl Acad Sci U S A,* 101**,** 13038-43.

EVANS, M. J., VON HAHN, T., TSCHERNE, D. M., SYDER, A. J., PANIS, M., WOLK, B., HATZIIOANNOU, T., MCKEATING, J. A., BIENIASZ, P. D. & RICE, C. M. 2007. Claudin-1 is a hepatitis C virus co-receptor required for a late step in entry. *Nature,* 446**,** 801-5.

EYRE, N. S., DRUMMER, H. E. & BEARD, M. R. 2010. The SR-BI partner PDZK1 facilitates hepatitis C virus entry. *PLoS Pathog,* 6**,** e1001130.

EYRE, N. S., FICHES, G. N., ALOIA, A. L., HELBIG, K. J., MCCARTNEY, E. M., MCERLEAN, C. S., LI, K., AGGARWAL, A., TURVILLE, S. G. & BEARD, M. R. 2014. Dynamic imaging of the hepatitis C virus NS5A protein during a productive infection. *J Virol,* 88**,** 3636-52.

EYRE, N. S., HAMPTON-SMITH, R. J., ALOIA, A. L., EDDES, J. S., SIMPSON, K. J., HOFFMANN, P. & BEARD, M. R. 2016. Phosphorylation of NS5A Serine-235 is essential to hepatitis C virus RNA replication and normal replication compartment formation. *Virology,* 491**,** 27-44.

FARQUHAR, M. J., HU, K., HARRIS, H. J., DAVIS, C., BRIMACOMBE, C. L., FLETCHER, S. J., BAUMERT, T. F., RAPPOPORT, J. Z., BALFE, P. & MCKEATING, J. A. 2012. Hepatitis C virus induces CD81 and claudin-1 endocytosis. *J Virol,* 86**,** 4305-16.

FAUL, E. J., WANJALLA, C. N., SUTHAR, M. S., GALE, M., WIRBLICH, C. & SCHNELL, M. J. 2010. Rabies virus infection induces type I interferon production in an IPS-1 dependent manner while dendritic cell activation relies on IFNAR signaling. *PLoS Pathog,* 6**,** e1001016.

FEINSTONE, S. M., KAPIKIAN, A. Z., PURCELL, R. H., ALTER, H. J. & HOLLAND, P. V. 1975. Transfusion-associated hepatitis not due to viral hepatitis type A or B. *N Engl J Med,* 292**,** 767-70.

FELD, J. J. & HOOFNAGLE, J. H. 2005. Mechanism of action of interferon and ribavirin in treatment of hepatitis C. *Nature,* 436**,** 967-72.

FERRARIS, P., BLANCHARD, E. & ROINGEARD, P. 2010. Ultrastructural and biochemical analyses of hepatitis C virus-associated host cell membranes. *J Gen Virol,* 91**,** 2230-7.

FICHES, G. N., EYRE, N. S., ALOIA, A. L., VAN DER HOEK, K., BETZ-STABLEIN, B., LUCIANI, F., CHOPRA, A. & BEARD, M. R. 2016. HCV RNA traffic and association with NS5A in living cells. *Virology,* 493**,** 60-74.

FIELDS, S. & SONG, O. 1989. A novel genetic system to detect protein-protein interactions. *Nature,* 340**,** 245-6.

FINK, J., GU, F., LING, L., TOLFVENSTAM, T., OLFAT, F., CHIN, K. C., AW, P., GEORGE, J., KUZNETSOV, V. A., SCHREIBER, M., VASUDEVAN, S. G. & HIBBERD, M. L. 2007. Host gene expression profiling of dengue virus infection in cell lines and patients. *PLoS Negl Trop Dis,* 1**,** e86.

FOSTER, G. R. 2010. Pegylated interferons for the treatment of chronic hepatitis C: pharmacological and clinical differences between peginterferon-alpha-2a and peginterferon-alpha-2b. *Drugs,* 70**,** 147-65.

FOY, E., LI, K., SUMPTER, R., LOO, Y. M., JOHNSON, C. L., WANG, C. F., FISH, P. M., YONEYAMA, M., FUJITA, T., LEMON, S. M. & GALE, M. 2005. Control of antiviral defenses through hepatitis C virus disruption of retinoic acid-inducible gene-I signaling. *Proceedings of the National Academy of Sciences of the United States of America,* 102**,** 2986-2991.

FREDERICKSEN, B. L., KELLER, B. C., FORNEK, J., KATZE, M. G. & GALE, M. 2008a. Establishment and maintenance of the innate antiviral response to west nile virus involves both RIG-I and MDA5 signaling through IPS-1. *Journal of Virology,* 82**,** 609-616.

FREDERICKSEN, B. L., KELLER, B. C., FORNEK, J., KATZE, M. G. & GALE, M., JR. 2008b. Establishment and maintenance of the innate antiviral response to West Nile Virus involves both RIG-I and MDA5 signaling through IPS-1. *J Virol,* 82**,** 609-16.

FREEMAN, A. J., DORE, G. J., LAW, M. G., THORPE, M., VON OVERBECK, J., LLOYD, A. R., MARINOS, G. & KALDOR, J. M. 2001. Estimating progression to cirrhosis in chronic hepatitis C virus infection. *Hepatology,* 34**,** 809-16.

FRIED, M. W., PETER, J., HOOTS, K., GAGLIO, P. J., TALBUT, D., DAVIS, P. C., KEY, N. S., WHITE, G. C., LINDBLAD, L., RICKLES, F. R. & ABSHIRE, T. C. 2002. Hepatitis C in adults and adolescents with hemophilia: a randomized, controlled trial of interferon alfa-2b and ribavirin. *Hepatology,* 36**,** 967-72.

GAO, L., AIZAKI, H., HE, J. W. & LAI, M. M. 2004. Interactions between viral nonstructural proteins and host protein hVAP-33 mediate the formation of hepatitis C virus RNA replication complex on lipid raft. *J Virol,* 78**,** 3480-8.

GAO, M., NETTLES, R. E., BELEMA, M., SNYDER, L. B., NGUYEN, V. N., FRIDELL, R. A., SERRANO-WU, M. H., LANGLEY, D. R., SUN, J. H., O'BOYLE, D. R., 2ND, LEMM, J. A., WANG, C., KNIPE, J. O., CHIEN, C.,

COLONNO, R. J., GRASELA, D. M., MEANWELL, N. A. & HAMANN, L. G. 2010. Chemical genetics strategy identifies an HCV NS5A inhibitor with a potent clinical effect. *Nature,* 465**,** 96-100.

GE, D., FELLAY, J., THOMPSON, A. J., SIMON, J. S., SHIANNA, K. V., URBAN, T. J., HEINZEN, E. L., QIU, P., BERTELSEN, A. H., MUIR, A. J., SULKOWSKI, M., MCHUTCHISON, J. G. & GOLDSTEIN, D. B. 2009. Genetic variation in IL28B predicts hepatitis C treatment-induced viral clearance. *Nature,* 461**,** 399-401.

GENTZSCH, J., BROHM, C., STEINMANN, E., FRIESLAND, M., MENZEL, N., VIEYRES, G., PERIN, P. M., FRENTZEN, A., KADERALI, L. & PIETSCHMANN, T. 2013. hepatitis c Virus p7 is critical for capsid assembly and envelopment. *PLoS Pathog,* 9**,** e1003355.

GERMI, R., CRANCE, J. M., GARIN, D., GUIMET, J., LORTAT-JACOB, H., RUIGROK, R. W., ZARSKI, J. P. & DROUET, E. 2002. Cellular glycosaminoglycans and low density lipoprotein receptor are involved in hepatitis C virus adsorption. *J Med Virol,* 68**,** 206-15.

GIANNI, T. & CAMPADELLI-FIUME, G. 2012. alphaVbeta3-integrin relocalizes nectin1 and routes herpes simplex virus to lipid rafts. *J Virol,* 86**,** 2850-5.

GITLIN, L., BARCHET, W., GILFILLAN, S., CELLA, M., BEUTLER, B., FLAVELL, R. A., DIAMOND, M. S. & COLONNA, M. 2006. Essential role of mda-5 in type I IFN responses to polyriboinosinic:polyribocytidylic acid and encephalomyocarditis picornavirus. *Proc Natl Acad Sci U S A,* 103**,** 8459-64.

GITLIN, L., BENOIT, L., SONG, C., CELLA, M., GILFILLAN, S., HOLTZMAN, M. J. & COLONNA, M. 2010. Melanoma differentiation-associated gene 5 (MDA5) is involved in the innate immune response to Paramyxoviridae infection in vivo. *PLoS Pathog,* 6**,** e1000734.

GLUE, P., FANG, J. W., ROUZIER-PANIS, R., RAFFANEL, C., SABO, R., GUPTA, S. K., SALFI, M. & JACOBS, S. 2000. Pegylated interferon-alpha2b: pharmacokinetics, pharmacodynamics, safety, and preliminary efficacy data. Hepatitis C Intervention Therapy Group. *Clin Pharmacol Ther,* 68**,** 556-67.

GOFFARD, A. & DUBUISSON, J. 2003. Glycosylation of hepatitis C virus envelope proteins. *Biochimie,* 85**,** 295-301.

GOH, P. Y., TAN, Y. J., LIM, S. P., LIM, S. G., TAN, Y. H. & HONG, W. J. 2001. The hepatitis C virus core protein interacts with NS5A and activates its caspase-mediated proteolytic cleavage. *Virology,* 290**,** 224-36.

GOSERT, R., EGGER, D., LOHMANN, V., BARTENSCHLAGER, R., BLUM, H. E., BIENZ, K. & MORADPOUR, D. 2003. Identification of the hepatitis C virus RNA replication complex in Huh-7 cells harboring subgenomic replicons. *J Virol,* 77**,** 5487-92.

GOUTAGNY, N., FATMI, A., DE LEDINGHEN, V., PENIN, F., COUZIGOU, P., INCHAUSPE, G. & BAIN, C. 2003. Evidence of viral replication in circulating dendritic cells during hepatitis C virus infection. *J Infect Dis,* 187**,** 1951-8.

GOUTTENOIRE, J., ROINGEARD, P., PENIN, F. & MORADPOUR, D. 2010. Amphipathic alpha-helix AH2 is a major determinant for the oligomerization of hepatitis C virus nonstructural protein 4B. *J Virol,* 84**,** 12529-37.

GRABENBAUER, M., SATZLER, K., BAUMGART, E. & FAHIMI, H. D. 2000. Three-dimensional ultrastructural analysis of peroxisomes in HepG2 cells. Absence of peroxisomal reticulum but evidence of close spatial association with the endoplasmic reticulum. *Cell Biochem Biophys,* 32 Spring**,** 37-49.

GRAKOUI, A., MCCOURT, D. W., WYCHOWSKI, C., FEINSTONE, S. M. & RICE, C. M. 1993. A second hepatitis C virus-encoded proteinase. *Proc Natl Acad Sci U S A,* 90**,** 10583-7.

GRANDVAUX, N., SERVANT, M. J., TENOEVER, B., SEN, G. C., BALACHANDRAN, S., BARBER, G. N., LIN, R. & HISCOTT, J. 2002. Transcriptional profiling of interferon regulatory factor 3 target genes: direct involvement in the regulation of interferon-stimulated genes. *J Virol,* 76**,** 5532-9.

GRANT, A., PONIA, S. S., TRIPATHI, S., BALASUBRAMANIAM, V., MIORIN, L., SOURISSEAU, M., SCHWARZ, M. C., SANCHEZ-SECO, M. P., EVANS, M. J., BEST, S. M. & GARCIA-SASTRE, A. 2016. Zika Virus Targets Human STAT2 to Inhibit Type I Interferon Signaling. *Cell Host Microbe,* 19**,** 882-90.

GRIFFIN, S. D., BEALES, L. P., CLARKE, D. S., WORSFOLD, O., EVANS, S. D., JAEGER, J., HARRIS, M. P. & ROWLANDS, D. J. 2003. The p7 protein of hepatitis C virus forms an ion channel that is blocked by the antiviral drug, Amantadine. *FEBS Lett,* 535**,** 34-8.

GUILLOT, L., LE GOFFIC, R., BLOCH, S., ESCRIOU, N., AKIRA, S., CHIGNARD, M. & SI-TAHAR, M. 2005. Involvement of toll-like receptor 3 in the immune response of lung epithelial cells to double-stranded RNA and influenza A virus. *J Biol Chem,* 280**,** 5571-80.

GUO, Y., CORDES, K. R., FARESE, R. V., JR. & WALTHER, T. C. 2009. Lipid droplets at a glance. *J Cell Sci,* 122**,** 749-52.

HABJAN, M., ANDERSSON, I., KLINGSTROM, J., SCHUMANN, M., MARTIN, A., ZIMMERMANN, P., WAGNER, V., PICHLMAIR, A., SCHNEIDER, U., MUHLBERGER, E., MIRAZIMI, A. & WEBER, F. 2008. Processing of genome 5' termini as a strategy of negative-strand RNA viruses to avoid RIG-I-dependent interferon induction. *PLoS One,* 3**,** e2032.

HADZIYANNIS, S. J., SETTE, H., JR., MORGAN, T. R., BALAN, V., DIAGO, M., MARCELLIN, P., RAMADORI, G., BODENHEIMER, H., JR., BERNSTEIN, D., RIZZETTO, M., ZEUZEM, S., POCKROS, P. J., LIN, A., ACKRILL, A. M. & GROUP, P. I. S. 2004. Peginterferon-alpha2a and ribavirin combination therapy in chronic hepatitis C: a randomized study of treatment duration and ribavirin dose. *Ann Intern Med,* 140**,** 346-55.

HAMAMOTO, I., NISHIMURA, Y., OKAMOTO, T., AIZAKI, H., LIU, M., MORI, Y., ABE, T., SUZUKI, T., LAI, M. M., MIYAMURA, T., MORIISHI, K. & MATSUURA, Y. 2005. Human VAP-B is involved in hepatitis C virus replication through interaction with NS5A and NS5B. *J Virol,* 79**,** 13473-82.

HAN, J. Q. & BARTON, D. J. 2002. Activation and evasion of the antiviral 2'-5' oligoadenylate synthetase/ribonuclease L pathway by hepatitis C virus mRNA. *RNA,* 8**,** 512-25.

HAQSHENAS, G., MACKENZIE, J. M., DONG, X. & GOWANS, E. J. 2007. Hepatitis C virus p7 protein is localized in the endoplasmic reticulum when it is encoded by a replication-competent genome. *J Gen Virol,* 88**,** 134-42.

HARRIS, H. J., DAVIS, C., MULLINS, J. G., HU, K., GOODALL, M., FARQUHAR, M. J., MEE, C. J., MCCAFFREY, K., YOUNG, S., DRUMMER, H., BALFE, P. & MCKEATING, J. A. 2010. Claudin association with CD81 defines hepatitis C virus entry. *J Biol Chem,* 285**,** 21092-102.

HEE, J. S. & CRESSWELL, P. 2017. Viperin interaction with mitochondrial antiviral signaling protein (MAVS) limits viperin-mediated inhibition of the interferon response in macrophages. *PLoS One,* 12**,** e0172236.

HEIL, F., HEMMI, H., HOCHREIN, H., AMPENBERGER, F., KIRSCHNING, C., AKIRA, S., LIPFORD, G., WAGNER, H. & BAUER, S. 2004. Species-specific recognition of single-stranded RNA via toll-like receptor 7 and 8. *Science,* 303**,** 1526-9.

HELBIG, K. J. & BEARD, M. R. 2014. The role of viperin in the innate antiviral response. *J Mol Biol,* 426**,** 1210-9.

HELBIG, K. J., CARR, J. M., CALVERT, J. K., WATI, S., CLARKE, J. N., EYRE, N. S., NARAYANA, S. K., FICHES, G. N., MCCARTNEY, E. M. & BEARD, M. R. 2013. Viperin is induced following dengue virus type-2 (DENV-2) infection and has anti-viral actions requiring the C-terminal end of viperin. *PLoS Negl Trop Dis,* 7**,** e2178.

HELBIG, K. J., EYRE, N. S., YIP, E., NARAYANA, S., LI, K., FICHES, G., MCCARTNEY, E. M., JANGRA, R. K., LEMON, S. M. & BEARD, M. R. 2011. The antiviral protein viperin inhibits hepatitis C virus replication via interaction with nonstructural protein 5A. *Hepatology,* 54**,** 1506-17.

HELBIG, K. J., LAU, D. T. Y., SEMENDRIC, L., HARLEY, H. A. J. & BEARD, M. R. 2005. Analysis of ISG expression in chronic hepatitis C identifies viperin as a potential antiviral effector. *Hepatology,* 42**,** 702-710.

HEMMI, H., TAKEUCHI, O., KAWAI, T., KAISHO, T., SATO, S., SANJO, H., MATSUMOTO, M., HOSHINO, K., WAGNER, H., TAKEDA, K. & AKIRA, S. 2000. A Toll-like receptor recognizes bacterial DNA. *Nature,* 408**,** 740-5.

HETTEMA, E. H., DISTEL, B. & TABAK, H. F. 1999. Import of proteins into peroxisomes. *Biochimica Et Biophysica Acta-Molecular Cell Research,* 1451**,** 17-34.

HEWSON, C. A., JARDINE, A., EDWARDS, M. R., LAZA-STANCA, V. & JOHNSTON, S. L. 2005. Toll-like receptor 3 is induced by and mediates antiviral activity against rhinovirus infection of human bronchial epithelial cells. *J Virol,* 79**,** 12273-9.

HIJIKATA, M., MIZUSHIMA, H., AKAGI, T., MORI, S., KAKIUCHI, N., KATO, N., TANAKA, T., KIMURA, K. & SHIMOTOHNO, K. 1993. Two distinct proteinase activities required for the processing of a putative nonstructural precursor protein of hepatitis C virus. *J Virol,* 67**,** 4665-75.

HINSON, E. R. & CRESSWELL, P. 2009a. The antiviral protein, viperin, localizes to lipid droplets via its N-terminal amphipathic alpha-helix. *Proc Natl Acad Sci U S A,* 106**,** 20452-7.

HINSON, E. R. & CRESSWELL, P. 2009b. The N-terminal amphipathic alpha-helix of viperin mediates localization to the cytosolic face of the endoplasmic reticulum and inhibits protein secretion. *J Biol Chem,* 284**,** 4705-12.

HINSON, E. R., JOSHI, N. S., CHEN, J. H., RAHNER, C., JUNG, Y. W., WANG, X. Y., KAECH, S. M. & CRESSWELL, P. 2010. Viperin is highly induced in neutrophils and macrophages during acute and chronic lymphocytic Choriomeningitis virus infection. *Journal of Immunology,* 184**,** 5723-5731.

HORNER, S. M. & GALE, M., JR. 2013. Regulation of hepatic innate immunity by hepatitis C virus. *Nat Med,* 19**,** 879-88.

HORNER, S. M., LIU, H. M., PARK, H. S., BRILEY, J. & GALE, M., JR. 2011. Mitochondrial-associated endoplasmic reticulum membranes (MAM) form innate immune synapses and are targeted by hepatitis C virus. *Proc Natl Acad Sci U S A,* 108**,** 14590-5.

HORSCROFT, N., LAI, V. C., CHENEY, W., YAO, N., WU, J. Z., HONG, Z. & ZHONG, W. 2005. Replicon cell culture system as a valuable tool in antiviral drug discovery against hepatitis C virus. *Antivir Chem Chemother,* 16**,** 1-12.

HSU, M., ZHANG, J., FLINT, M., LOGVINOFF, C., CHENG-MAYER, C., RICE, C. M. & MCKEATING, J. A. 2003. Hepatitis C virus glycoproteins mediate pH-dependent cell entry of pseudotyped retroviral particles. *Proc Natl Acad Sci U S A,* 100**,** 7271-6.

HUANG, L., HWANG, J., SHARMA, S. D., HARGITTAI, M. R., CHEN, Y., ARNOLD, J. J., RANEY, K. D. & CAMERON, C. E. 2005. Hepatitis C virus nonstructural protein 5A (NS5A) is an RNA-binding protein. *J Biol Chem,* 280**,** 36417-28.

HUGLE, T., FEHRMANN, F., BIECK, E., KOHARA, M., KRAUSSLICH, H. G., RICE, C. M., BLUM, H. E. & MORADPOUR, D. 2001. The hepatitis C virus nonstructural protein 4B is an integral endoplasmic reticulum membrane protein. *Virology,* 284**,** 70-81.

IKEDA, M., ABE, K., DANSAKO, H., NAKAMURA, T., NAKA, K. & KATO, N. 2005. Efficient replication of a full-length hepatitis C virus genome, strain O, in cell culture, and development of a luciferase reporter system. *Biochem Biophys Res Commun,* 329**,** 1350-9.

IKEDA, M., YI, M., LI, K. & LEMON, S. M. 2002. Selectable subgenomic and genome-length dicistronic RNAs derived from an infectious molecular clone of the HCV-N strain of hepatitis C virus replicate efficiently in cultured Huh7 cells. *J Virol,* 76**,** 2997-3006.

IMAIZUMI, T., KUMAGAI, M., TAIMA, K., FUJITA, T., YOSHIDA, H. & SATOH, K. 2005. Involvement of retinoic acid-inducible gene-I in the IFN-{gamma}/STAT1 signalling pathway in BEAS-2B cells. *Eur Respir J,* 25**,** 1077-83.

JENSEN, D. M. 2011. A new era of hepatitis C therapy begins. *N Engl J Med,* 364**,** 1272-4.

JIANG, D., GUO, H., XU, C., CHANG, J., GU, B., WANG, L., BLOCK, T. M. & GUO, J. T. 2008. Identification of three interferon-inducible cellular enzymes that inhibit the replication of hepatitis C virus. *J Virol,* 82**,** 1665-78.

JIANG, D., WEIDNER, J. M., QING, M., PAN, X. B., GUO, H., XU, C., ZHANG, X., BIRK, A., CHANG, J., SHI, P. Y., BLOCK, T. M. & GUO, J. T. 2010. Identification of five interferon-induced cellular proteins that inhibit west nile virus and dengue virus infections. *J Virol,* 84**,** 8332-41.

JIANG, F., RAMANATHAN, A., MILLER, M. T., TANG, G. Q., GALE, M., JR., PATEL, S. S. & MARCOTRIGIANO, J. 2011. Structural basis of RNA recognition and activation by innate immune receptor RIG-I. *Nature,* 479**,** 423-7.

JIRASKO, V., MONTSERRET, R., APPEL, N., JANVIER, A., EUSTACHI, L., BROHM, C., STEINMANN, E., PIETSCHMANN, T., PENIN, F. & BARTENSCHLAGER, R. 2008. Structural and functional characterization of nonstructural protein 2 for its role in hepatitis C virus assembly. *J Biol Chem,* 283**,** 28546-62.

JONES, C. T., MURRAY, C. L., EASTMAN, D. K., TASSELLO, J. & RICE, C. M. 2007. Hepatitis C virus p7 and NS2 proteins are essential for production of infectious virus. *J Virol,* 81**,** 8374-83.

JONES, D. M. & MCLAUCHLAN, J. 2010. Hepatitis C virus: assembly and release of virus particles. *J Biol Chem,* 285**,** 22733-9.

JONES, D. M., PATEL, A. H., TARGETT-ADAMS, P. & MCLAUCHLAN, J. 2009. The hepatitis C virus NS4B protein can trans-complement viral RNA replication and modulates production of infectious virus. *J Virol,* 83**,** 2163-77.

JONES, J. M., MORRELL, J. C. & GOULD, S. J. 2004. PEX19 is a predominantly cytosolic chaperone and import receptor for class 1 peroxisomal membrane proteins. *J Cell Biol,* 164**,** 57-67.

KANEKO, T., TANJI, Y., SATOH, S., HIJIKATA, M., ASABE, S., KIMURA, K. & SHIMOTOHNO, K. 1994. Production of two phosphoproteins from the NS5A region of the hepatitis C viral genome. *Biochem Biophys Res Commun,* 205**,** 320-6.

KANG, D. C., GOPALKRISHNAN, R. V., LIN, L., RANDOLPH, A., VALERIE, K., PESTKA, S. & FISHER, P. B. 2004. Expression analysis and genomic characterization of human melanoma differentiation associated gene-5, mda-5: a novel type I interferon-responsive apoptosis-inducing gene. *Oncogene,* 23**,** 1789-800.

KANG, D. C., GOPALKRISHNAN, R. V., WU, Q., JANKOWSKY, E., PYLE, A. M. & FISHER, P. B. 2002. mda-5: An interferon-inducible putative RNA helicase with double-stranded RNA-dependent ATPase activity and melanoma growth-suppressive properties. *Proc Natl Acad Sci U S A,* 99**,** 637-42.

KATO, H., SATO, S., YONEYAMA, M., YAMAMOTO, M., UEMATSU, S., MATSUI, K., TSUJIMURA, T., TAKEDA, K., FUJITA, T., TAKEUCHI, O. & AKIRA, S. 2005. Cell type-specific involvement of RIG-I in antiviral response. *Immunity,* 23**,** 19-28.

KATO, H., TAKEUCHI, O., MIKAMO-SATOH, E., HIRAI, R., KAWAI, T., MATSUSHITA, K., HIIRAGI, A., DERMODY, T. S., FUJITA, T. & AKIRA, S. 2008. Length-dependent recognition of double-stranded ribonucleic acids by retinoic acid-inducible gene-I and melanoma differentiation-associated gene 5. *J Exp Med,* 205**,** 1601-10.

KATO, H., TAKEUCHI, O., SATO, S., YONEYAMA, M., YAMAMOTO, M., MATSUI, K., UEMATSU, S., JUNG, A., KAWAI, T., ISHII, K. J., YAMAGUCHI, O., OTSU, K., TSUJIMURA, T., KOH, C. S., REIS E SOUSA, C., MATSUURA, Y., FUJITA, T. & AKIRA, S. 2006. Differential roles of

MDA5 and RIG-I helicases in the recognition of RNA viruses. *Nature,* 441**,** 101-5.

KATZE, M. G., HE, Y. & GALE, M., JR. 2002. Viruses and interferon: a fight for supremacy. *Nat Rev Immunol,* 2**,** 675-87.

KAWAI, T. & AKIRA, S. 2008. Toll-like receptor and RIG-I-like receptor signaling. *Ann N Y Acad Sci,* 1143**,** 1-20.

KAWAI, T., TAKAHASHI, K., SATO, S., COBAN, C., KUMAR, H., KATO, H., ISHII, K. J., TAKEUCHI, O. & AKIRA, S. 2005. IPS-1, an adaptor triggering RIG-I- and Mda5-mediated type I interferon induction. *Nat Immunol,* 6**,** 981-8.

KEATING, G. M. 2015. Ledipasvir/Sofosbuvir: a review of its use in chronic hepatitis C. *Drugs,* 75**,** 675-85.

KHAIBOULLINA, S. F., RIZVANOV, A. A., HOLBROOK, M. R. & ST JEOR, S. 2005. Yellow fever virus strains Asibi and 17D-204 infect human umbilical cord endothelial cells and induce novel changes in gene expression. *Virology,* 342**,** 167-76.

KIM, S., WELSCH, C., YI, M. & LEMON, S. M. 2011. Regulation of the production of infectious genotype 1a hepatitis C virus by NS5A domain III. *J Virol,* 85**,** 6645-56.

KNIGHT, E., JR. & KORANT, B. D. 1979. Fibroblast interferon induces synthesis of four proteins in human fibroblast cells. *Proc Natl Acad Sci U S A,* 76**,** 1824-7.

KOTENKO, S. V., GALLAGHER, G., BAURIN, V. V., LEWIS-ANTES, A., SHEN, M., SHAH, N. K., LANGER, J. A., SHEIKH, F., DICKENSHEETS, H. & DONNELLY, R. P. 2003. IFN-lambdas mediate antiviral protection through a distinct class II cytokine receptor complex. *Nat Immunol,* 4**,** 69-77.

KOUTSOUDAKIS, G., KAUL, A., STEINMANN, E., KALLIS, S., LOHMANN, V., PIETSCHMANN, T. & BARTENSCHLAGER, R. 2006. Characterization of the early steps of hepatitis C virus infection by using luciferase reporter viruses. *J Virol,* 80**,** 5308-20.

KOWALINSKI, E., LUNARDI, T., MCCARTHY, A. A., LOUBER, J., BRUNEL, J., GRIGOROV, B., GERLIER, D. & CUSACK, S. 2011. Structural basis for the activation of innate immune pattern-recognition receptor RIG-I by viral RNA. *Cell,* 147**,** 423-35.

KRIEGER, N., LOHMANN, V. & BARTENSCHLAGER, R. 2001. Enhancement of hepatitis C virus RNA replication by cell culture-adaptive mutations. *J Virol,* 75**,** 4614-24.

KUMAR, A., HOU, S., AIRO, A. M., LIMONTA, D., MANCINELLI, V., BRANTON, W., POWER, C. & HOBMAN, T. C. 2016. Zika virus inhibits type-I interferon production and downstream signaling. *EMBO Rep,* 17**,** 1766-1775.

KUMAR, H., KAWAI, T., KATO, H., SATO, S., TAKAHASHI, K., COBAN, C., YAMAMOTO, M., UEMATSU, S., ISHII, K. J., TAKEUCHI, O. & AKIRA, S. 2006. Essential role of IPS-1 in innate immune responses against RNA viruses. *J Exp Med,* 203**,** 1795-803.

LE GUILLOU-GUILLEMETTE, H., VALLET, S., GAUDY-GRAFFIN, C., PAYAN, C., PIVERT, A., GOUDEAU, A. & LUNEL-FABIANI, F. 2007. Genetic diversity of the hepatitis C virus: impact and issues in the antiviral therapy. *World J Gastroenterol,* 13**,** 2416-26.

LEE, H. K., LUND, J. M., RAMANATHAN, B., MIZUSHIMA, N. & IWASAKI, A. 2007. Autophagy-dependent viral recognition by plasmacytoid dendritic cells. *Science,* 315**,** 1398-401.

LEE, J., WU, C. C., LEE, K. J., CHUANG, T. H., KATAKURA, K., LIU, Y. T., CHAN, M., TAWATAO, R., CHUNG, M., SHEN, C., COTTAM, H. B., LAI, M. M., RAZ, E. & CARSON, D. A. 2006. Activation of anti-hepatitis C virus responses via Toll-like receptor 7. *Proc Natl Acad Sci U S A,* 103**,** 1828-33.

LI, K., FOY, E., FERREON, J. C., NAKAMURA, M., FERREON, A. C., IKEDA, M., RAY, S. C., GALE, M., JR. & LEMON, S. M. 2005a. Immune evasion by hepatitis C virus NS3/4A protease-mediated cleavage of the Toll-like receptor 3 adaptor protein TRIF. *Proc Natl Acad Sci U S A,* 102**,** 2992-7.

LI, K., LI, N. L., WEI, D., PFEFFER, S. R., FAN, M. & PFEFFER, L. M. 2012. Activation of chemokine and inflammatory cytokine response in hepatitis C virus-infected hepatocytes depends on Toll-like receptor 3 sensing of hepatitis C virus double-stranded RNA intermediates. *Hepatology,* 55**,** 666-75.

LI, X. D., SUN, L., SETH, R. B., PINEDA, G. & CHEN, Z. J. 2005b. Hepatitis C virus protease NS3/4A cleaves mitochondrial antiviral signaling protein off the mitochondria to evade innate immunity. *Proc Natl Acad Sci U S A,* 102**,** 17717-22.

LIN, T. I., LENZ, O., FANNING, G., VERBINNEN, T., DELOUVROY, F., SCHOLLIERS, A., VERMEIREN, K., ROSENQUIST, A., EDLUND, M., SAMUELSSON, B., VRANG, L., DE KOCK, H., WIGERINCK, P., RABOISSON, P. & SIMMEN, K. 2009. In vitro activity and preclinical profile of TMC435350, a potent hepatitis C virus protease inhibitor. *Antimicrob Agents Chemother,* 53**,** 1377-85.

LINDENBACH, B. D., EVANS, M. J., SYDER, A. J., WOLK, B., TELLINGHUISEN, T. L., LIU, C. C., MARUYAMA, T., HYNES, R. O., BURTON, D. R., MCKEATING, J. A. & RICE, C. M. 2005. Complete replication of hepatitis C virus in cell culture. *Science,* 309**,** 623-6.

LINDENBACH, B. D., MEULEMAN, P., PLOSS, A., VANWOLLEGHEM, T., SYDER, A. J., MCKEATING, J. A., LANFORD, R. E., FEINSTONE, S. M., MAJOR, M. E., LEROUX-ROELS, G. & RICE, C. M. 2006. Cell culture-grown hepatitis C virus is infectious in vivo and can be recultured in vitro. *Proc Natl Acad Sci U S A,* 103**,** 3805-9.

LINDENBACH, B. D. & RICE, C. M. 2013. The ins and outs of hepatitis C virus entry and assembly. *Nat Rev Microbiol,* 11**,** 688-700.

LO, S. Y., MASIARZ, F., HWANG, S. B., LAI, M. M. & OU, J. H. 1995. Differential subcellular localization of hepatitis C virus core gene products. *Virology,* 213**,** 455-61.

LOHMANN, V., KORNER, F., DOBIERZEWSKA, A. & BARTENSCHLAGER, R. 2001. Mutations in hepatitis C virus RNAs conferring cell culture adaptation. *J Virol,* 75**,** 1437-49.

LOHMANN, V., KORNER, F., KOCH, J., HERIAN, U., THEILMANN, L. & BARTENSCHLAGER, R. 1999. Replication of subgenomic hepatitis C virus RNAs in a hepatoma cell line. *Science,* 285**,** 110-3.

LOO, Y. M., FORNEK, J., CROCHET, N., BAJWA, G., PERWITASARI, O., MARTINEZ-SOBRIDO, L., AKIRA, S., GILL, M. A., GARCIA-SASTRE, A., KATZE, M. G. & GALE, M., JR. 2008. Distinct RIG-I and MDA5 signaling by RNA viruses in innate immunity. *J Virol,* 82**,** 335-45.

LOO, Y. M. & GALE, M., JR. 2011. Immune signaling by RIG-I-like receptors. *Immunity,* 34**,** 680-92.

LOO, Y. M., OWEN, D. M., LI, K., ERICKSON, A. K., JOHNSON, C. L., FISH, P. M., CARNEY, D. S., WANG, T., ISHIDA, H., YONEYAMA, M., FUJITA, T., SAITO, T., LEE, W. M., HAGEDORN, C. H., LAU, D. T., WEINMAN, S. A., LEMON, S. M. & GALE, M., JR. 2006. Viral and therapeutic control of IFN-beta promoter stimulator 1 during hepatitis C virus infection. *Proc Natl Acad Sci U S A,* 103**,** 6001-6.

LORENZ, I. C., MARCOTRIGIANO, J., DENTZER, T. G. & RICE, C. M. 2006. Structure of the catalytic domain of the hepatitis C virus NS2-3 protease. *Nature,* 442**,** 831-5.

LUND, J. M., ALEXOPOULOU, L., SATO, A., KAROW, M., ADAMS, N. C., GALE, N. W., IWASAKI, A. & FLAVELL, R. A. 2004. Recognition of single-stranded RNA viruses by Toll-like receptor 7. *Proc Natl Acad Sci U S A,* 101**,** 5598-603.

LUNDIN, M., MONNE, M., WIDELL, A., VON HEIJNE, G. & PERSSON, M. A. 2003. Topology of the membrane-associated hepatitis C virus protein NS4B. *J Virol,* 77**,** 5428-38.

MAGALHAES, A. C., FERREIRA, A. R., GOMES, S., VIEIRA, M., GOUVEIA, A., VALENCA, I., ISLINGER, M., NASCIMENTO, R., SCHRADER, M., KAGAN, J. C. & RIBEIRO, D. 2016. Peroxisomes are platforms for cytomegalovirus' evasion from the cellular immune response. *Sci Rep,* 6**,** 26028.

MANES, S., DEL REAL, G. & MARTINEZ, A. C. 2003. Pathogens: raft hijackers. *Nat Rev Immunol,* 3**,** 557-68.

MANNS, M. P., MCHUTCHISON, J. G., GORDON, S. C., RUSTGI, V. K., SHIFFMAN, M., REINDOLLAR, R., GOODMAN, Z. D., KOURY, K., LING, M. & ALBRECHT, J. K. 2001. Peginterferon alfa-2b plus ribavirin compared with interferon alfa-2b plus ribavirin for initial treatment of chronic hepatitis C: a randomised trial. *Lancet,* 358**,** 958-65.

MARIE, I., DURBIN, J. E. & LEVY, D. E. 1998. Differential viral induction of distinct interferon-alpha genes by positive feedback through interferon regulatory factor-7. *EMBO J,* 17**,** 6660-9.

MARKS, K. M. & JACOBSON, I. M. 2012. The first wave: HCV NS3 protease inhibitors telaprevir and boceprevir. *Antivir Ther,* 17**,** 1119-31.

MARTELL, J. D., DEERINCK, T. J., SANCAK, Y., POULOS, T. L., MOOTHA, V. K., SOSINSKY, G. E., ELLISMAN, M. H. & TING, A. Y. 2012. Engineered ascorbate peroxidase as a genetically encoded reporter for electron microscopy. *Nat Biotechnol,* 30**,** 1143-8.

MARTIN, D. N. & UPRICHARD, S. L. 2013. Identification of transferrin receptor 1 as a hepatitis C virus entry factor. *Proc Natl Acad Sci U S A,* 110**,** 10777-82.

MASAKI, T., SUZUKI, R., MURAKAMI, K., AIZAKI, H., ISHII, K., MURAYAMA, A., DATE, T., MATSUURA, Y., MIYAMURA, T., WAKITA, T. & SUZUKI, T.

2008. Interaction of hepatitis C virus nonstructural protein 5A with core protein is critical for the production of infectious virus particles. *J Virol,* 82**,** 7964-76.

MCCARTNEY, E. M., EYRE, N. S. & BEARD, M. R. 2011. Border patrol intensifies for hepatitis C virus entry. *Hepatology,* 54**,** 1472-5.

MCCARTNEY, S. A., THACKRAY, L. B., GITLIN, L., GILFILLAN, S., VIRGIN, H. W. & COLONNA, M. 2008. MDA-5 recognition of a murine norovirus. *PLoS Pathog,* 4**,** e1000108.

MCGILLIVARY, G., JORDAN, Z. B., PEEPLES, M. E. & BAKALETZ, L. O. 2013. Replication of respiratory syncytial virus is inhibited by the host defense molecule viperin. *J Innate Immun,* 5**,** 60-71.

MCLAUCHLAN, J., LEMBERG, M. K., HOPE, G. & MARTOGLIO, B. 2002. Intramembrane proteolysis promotes trafficking of hepatitis C virus core protein to lipid droplets. *EMBO J,* 21**,** 3980-8.

MELCHJORSEN, J., JENSEN, S. B., MALMGAARD, L., RASMUSSEN, S. B., WEBER, F., BOWIE, A. G., MATIKAINEN, S. & PALUDAN, S. R. 2005. Activation of innate defense against a paramyxovirus is mediated by RIG-I and TLR7 and TLR8 in a cell-type-specific manner. *J Virol,* 79**,** 12944-51.

MESMIN, B., BIGAY, J., MOSER VON FILSECK, J., LACAS-GERVAIS, S., DRIN, G. & ANTONNY, B. 2013. A four-step cycle driven by PI(4)P hydrolysis directs sterol/PI(4)P exchange by the ER-Golgi tether OSBP. *Cell,* 155**,** 830-43.

METZ, P., DAZERT, E., RUGGIERI, A., MAZUR, J., KADERALI, L., KAUL, A., ZEUGE, U., WINDISCH, M. P., TRIPPLER, M., LOHMANN, V., BINDER, M., FRESE, M. & BARTENSCHLAGER, R. 2012. Identification of type I and type II interferon-induced effectors controlling hepatitis C virus replication. *Hepatology,* 56**,** 2082-93.

MEYLAN, E., CURRAN, J., HOFMANN, K., MORADPOUR, D., BINDER, M., BARTENSCHLAGER, R. & TSCHOPP, J. 2005. Cardif is an adaptor protein in the RIG-I antiviral pathway and is targeted by hepatitis C virus. *Nature,* 437**,** 1167-72.

MILIC, N. L., DAVIS, S., CARR, J. M., ISBERG, S., BEARD, M. R. & HELBIG, K. J. 2015. Sequence analysis and characterisation of virally induced viperin in the saltwater crocodile (Crocodylus porosus). *Dev Comp Immunol,* 51**,** 108-15.

MIYANARI, Y., ATSUZAWA, K., USUDA, N., WATASHI, K., HISHIKI, T., ZAYAS, M., BARTENSCHLAGER, R., WAKITA, T., HIJIKATA, M. & SHIMOTOHNO, K. 2007. The lipid droplet is an important organelle for hepatitis C virus production. *Nat Cell Biol,* 9**,** 1089-97.

MOHAN, N., GONZALEZ-PERALTA, R. P., FUJISAWA, T., CHANG, M. H., HELLER, S., JARA, P., KELLY, D., MIELI-VERGANI, G., SHAH, U. & MURRAY, K. F. 2010. Chronic hepatitis C virus infection in children. *J Pediatr Gastroenterol Nutr,* 50**,** 123-31.

MONAZAHIAN, M., BOHME, I., BONK, S., KOCH, A., SCHOLZ, C., GRETHE, S. & THOMSSEN, R. 1999. Low density lipoprotein receptor as a candidate receptor for hepatitis C virus. *J Med Virol,* 57**,** 223-9.

MORADPOUR, D., BRASS, V., BIECK, E., FRIEBE, P., GOSERT, R., BLUM, H. E., BARTENSCHLAGER, R., PENIN, F. & LOHMANN, V. 2004. Membrane

association of the RNA-dependent RNA polymerase is essential for hepatitis C virus RNA replication. *J Virol,* 78**,** 13278-84.

MORADPOUR, D., GOSERT, R., EGGER, D., PENIN, F., BLUM, H. E. & BIENZ, K. 2003. Membrane association of hepatitis C virus nonstructural proteins and identification of the membrane alteration that harbors the viral replication complex. *Antiviral Res,* 60**,** 103-9.

MORADPOUR, D., PENIN, F. & RICE, C. M. 2007. Replication of hepatitis C virus. *Nat Rev Microbiol,* 5**,** 453-63.

MORIKAWA, K., LANGE, C. M., GOUTTENOIRE, J., MEYLAN, E., BRASS, V., PENIN, F. & MORADPOUR, D. 2011. Nonstructural protein 3-4A: the Swiss army knife of hepatitis C virus. *J Viral Hepat,* 18**,** 305-15.

MORIYA, K., FUJIE, H., SHINTANI, Y., YOTSUYANAGI, H., TSUTSUMI, T., ISHIBASHI, K., MATSUURA, Y., KIMURA, S., MIYAMURA, T. & KOIKE, K. 1998. The core protein of hepatitis C virus induces hepatocellular carcinoma in transgenic mice. *Nat Med,* 4**,** 1065-7.

MORIYA, K., YOTSUYANAGI, H., SHINTANI, Y., FUJIE, H., ISHIBASHI, K., MATSUURA, Y., MIYAMURA, T. & KOIKE, K. 1997. Hepatitis C virus core protein induces hepatic steatosis in transgenic mice. *J Gen Virol,* 78 (Pt 7)**,** 1527-31.

MOSCHONAS, A., IOANNOU, M. & ELIOPOULOS, A. G. 2012. CD40 stimulates a "feed-forward" NF-kappaB-driven molecular pathway that regulates IFN-beta expression in carcinoma cells. *J Immunol,* 188**,** 5521-7.

NAKABAYASHI, H., TAKETA, K., MIYANO, K., YAMANE, T. & SATO, J. 1982. Growth of human hepatoma cells lines with differentiated functions in chemically defined medium. *Cancer Res,* 42**,** 3858-63.

NARAYANA, S. K., HELBIG, K. J., MCCARTNEY, E. M., EYRE, N. S., BULL, R. A., ELTAHLA, A., LLOYD, A. R. & BEARD, M. R. 2015. The Interferon-induced Transmembrane Proteins, IFITM1, IFITM2, and IFITM3 Inhibit Hepatitis C Virus Entry. *J Biol Chem,* 290**,** 25946-59.

NASR, N., MADDOCKS, S., TURVILLE, S. G., HARMAN, A. N., WOOLGER, N., HELBIG, K. J., WILKINSON, J., BYE, C. R., WRIGHT, T. K., RAMBUKWELLE, D., DONAGHY, H., BEARD, M. R. & CUNNINGHAM, A. L. 2012. HIV-1 infection of human macrophages directly induces viperin which inhibits viral production. *Blood,* 120**,** 778-88.

NEGISHI, H., OSAWA, T., OGAMI, K., OUYANG, X., SAKAGUCHI, S., KOSHIBA, R., YANAI, H., SEKO, Y., SHITARA, H., BISHOP, K., YONEKAWA, H., TAMURA, T., KAISHO, T., TAYA, C., TANIGUCHI, T. & HONDA, K. 2008. A critical link between Toll-like receptor 3 and type II interferon signaling pathways in antiviral innate immunity. *Proc Natl Acad Sci U S A,* 105**,** 20446-51.

NIELSEN, S. U., BASSENDINE, M. F., BURT, A. D., BEVITT, D. J. & TOMS, G. L. 2004. Characterization of the genome and structural proteins of hepatitis C virus resolved from infected human liver. *J Gen Virol,* 85**,** 1497-507.

NIEPMANN, M. 2013. Hepatitis C virus RNA translation. *Curr Top Microbiol Immunol,* 369**,** 143-66.

ODENDALL, C., DIXIT, E., STAVRU, F., BIERNE, H., FRANZ, K. M., DURBIN, A. F., BOULANT, S., GEHRKE, L., COSSART, P. & KAGAN, J. C. 2014. Diverse

intracellular pathogens activate type III interferon expression from peroxisomes. *Nat Immunol,* 15**,** 717-26.

ORGANISATION, W. H. 2014. Hepatitis C Factsheet No. 164.

OSHIUMI, H., OKAMOTO, M., FUJII, K., KAWANISHI, T., MATSUMOTO, M., KOIKE, S. & SEYA, T. 2011. The TLR3/TICAM-1 pathway is mandatory for innate immune responses to poliovirus infection. *J Immunol,* 187**,** 5320-7.

PAVLOVIC, D., NEVILLE, D. C., ARGAUD, O., BLUMBERG, B., DWEK, R. A., FISCHER, W. B. & ZITZMANN, N. 2003. The hepatitis C virus p7 protein forms an ion channel that is inhibited by long-alkyl-chain iminosugar derivatives. *Proc Natl Acad Sci U S A,* 100**,** 6104-8.

PAWLOTSKY, J. M. 2006. Therapy of hepatitis C: from empiricism to eradication. *Hepatology,* 43**,** S207-20.

PERRY, A. K., CHEN, G., ZHENG, D., TANG, H. & CHENG, G. 2005. The host type I interferon response to viral and bacterial infections. *Cell Res,* 15**,** 407-22.

PESTKA, S., KRAUSE, C. D. & WALTER, M. R. 2004. Interferons, interferon-like cytokines, and their receptors. *Immunol Rev,* 202**,** 8-32.

PESTKA, S., LANGER, J. A., ZOON, K. C. & SAMUEL, C. E. 1987. Interferons and their actions. *Annu Rev Biochem,* 56**,** 727-77.

PETRACCA, R., FALUGI, F., GALLI, G., NORAIS, N., ROSA, D., CAMPAGNOLI, S., BURGIO, V., DI STASIO, E., GIARDINA, B., HOUGHTON, M., ABRIGNANI, S. & GRANDI, G. 2000. Structure-function analysis of hepatitis C virus envelope-CD81 binding. *J Virol,* 74**,** 4824-30.

PHIPPS, S., LAM, C. E., MAHALINGAM, S., NEWHOUSE, M., RAMIREZ, R., ROSENBERG, H. F., FOSTER, P. S. & MATTHAEI, K. I. 2007. Eosinophils contribute to innate antiviral immunity and promote clearance of respiratory syncytial virus. *Blood,* 110**,** 1578-86.

PIETSCHMANN, T., KAUL, A., KOUTSOUDAKIS, G., SHAVINSKAYA, A., KALLIS, S., STEINMANN, E., ABID, K., NEGRO, F., DREUX, M., COSSET, F. L. & BARTENSCHLAGER, R. 2006. Construction and characterization of infectious intragenotypic and intergenotypic hepatitis C virus chimeras. *Proc Natl Acad Sci U S A,* 103**,** 7408-13.

PILERI, P., UEMATSU, Y., CAMPAGNOLI, S., GALLI, G., FALUGI, F., PETRACCA, R., WEINER, A. J., HOUGHTON, M., ROSA, D., GRANDI, G. & ABRIGNANI, S. 1998. Binding of hepatitis C virus to CD81. *Science,* 282**,** 938-41.

PLOSS, A., EVANS, M. J., GAYSINSKAYA, V. A., PANIS, M., YOU, H., DE JONG, Y. P. & RICE, C. M. 2009. Human occludin is a hepatitis C virus entry factor required for infection of mouse cells. *Nature,* 457**,** 882-6.

PLUMET, S., HERSCHKE, F., BOURHIS, J. M., VALENTIN, H., LONGHI, S. & GERLIER, D. 2007. Cytosolic 5'-triphosphate ended viral leader transcript of measles virus as activator of the RIG I-mediated interferon response. *PLoS One,* 2**,** e279.

POPESCU, C. I., CALLENS, N., TRINEL, D., ROINGEARD, P., MORADPOUR, D., DESCAMPS, V., DUVERLIE, G., PENIN, F., HELIOT, L., ROUILLE, Y. & DUBUISSON, J. 2011a. NS2 protein of hepatitis C virus interacts with structural and non-structural proteins towards virus assembly. *PLoS Pathog,* 7**,** e1001278.

POPESCU, C. I., ROUILLE, Y. & DUBUISSON, J. 2011b. Hepatitis C virus assembly imaging. *Viruses,* 3**,** 2238-54.

PROSSER, D. C., TRAN, D., GOUGEON, P. Y., VERLY, C. & NGSEE, J. K. 2008. FFAT rescues VAPA-mediated inhibition of ER-to-Golgi transport and VAPB-mediated ER aggregation. *J Cell Sci,* 121**,** 3052-61.

PROUD, D., TURNER, R. B., WINTHER, B., WIEHLER, S., TIESMAN, J. P., REICHLING, T. D., JUHLIN, K. D., FULMER, A. W., HO, B. Y., WALANSKI, A. A., POORE, C. L., MIZOGUCHI, H., JUMP, L., MOORE, M. L., ZUKOWSKI, C. K. & CLYMER, J. W. 2008. Gene expression profiles during in vivo human rhinovirus infection: insights into the host response. *Am J Respir Crit Care Med,* 178**,** 962-8.

QIU, L. Q., CRESSWELL, P. & CHIN, K. C. 2009. Viperin is required for optimal Th2 responses and T-cell receptor-mediated activation of NF-kappaB and AP-1. *Blood,* 113**,** 3520-9.

RASSA, J. C., MEYERS, J. L., ZHANG, Y., KUDARAVALLI, R. & ROSS, S. R. 2002. Murine retroviruses activate B cells via interaction with toll-like receptor 4. *Proc Natl Acad Sci U S A,* 99**,** 2281-6.

RAUCH, A., KUTALIK, Z., DESCOMBES, P., CAI, T., DI IULIO, J., MUELLER, T., BOCHUD, M., BATTEGAY, M., BERNASCONI, E., BOROVICKA, J., COLOMBO, S., CERNY, A., DUFOUR, J. F., FURRER, H., GUNTHARD, H. F., HEIM, M., HIRSCHEL, B., MALINVERNI, R., MORADPOUR, D., MULLHAUPT, B., WITTECK, A., BECKMANN, J. S., BERG, T., BERGMANN, S., NEGRO, F., TELENTI, A., BOCHUD, P. Y., SWISS HEPATITIS, C. C. S. & SWISS, H. I. V. C. S. 2010. Genetic variation in IL28B is associated with chronic hepatitis C and treatment failure: a genome-wide association study. *Gastroenterology,* 138**,** 1338-45, 1345 e1-7.

RAYCHAUDHURI, S. & PRINZ, W. A. 2010. The diverse functions of oxysterol-binding proteins. *Annu Rev Cell Dev Biol,* 26**,** 157-77.

RAZALI, K., AMIN, J., DORE, G. J., LAW, M. G. & GROUP, H. C. V. P. W. 2009. Modelling and calibration of the hepatitis C epidemic in Australia. *Stat Methods Med Res,* 18**,** 253-70.

RAZALI, K., THEIN, H. H., BELL, J., COOPER-STANBURY, M., DOLAN, K., DORE, G., GEORGE, J., KALDOR, J., KARVELAS, M., LI, J., MAHER, L., MCGREGOR, S., HELLARD, M., POEDER, F., QUAINE, J., STEWART, K., TYRRELL, H., WELTMAN, M., WESTCOTT, O., WODAK, A. & LAW, M. 2007. Modelling the hepatitis C virus epidemic in Australia. *Drug Alcohol Depend,* 91**,** 228-35.

RAZAVI, H., WAKED, I., SARRAZIN, C., MYERS, R. P., IDILMAN, R., CALINAS, F., VOGEL, W., MENDES CORREA, M. C., HEZODE, C., LAZARO, P., AKARCA, U., ALEMAN, S., BALIK, I., BERG, T., BIHL, F., BILODEAU, M., BLASCO, A. J., BRANDAO MELLO, C. E., BRUGGMANN, P., BUTI, M., CALLEJA, J. L., CHEINQUER, H., CHRISTENSEN, P. B., CLAUSEN, M., COELHO, H. S., CRAMP, M. E., DORE, G. J., DOSS, W., DUBERG, A. S., EL-SAYED, M. H., ERGOR, G., ESMAT, G., FALCONER, K., FELIX, J., FERRAZ, M. L., FERREIRA, P. R., FRANKOVA, S., GARCIA-SAMANIEGO, J., GERSTOFT, J., GIRIA, J. A., GONCALES, F. L., JR., GOWER, E.,

GSCHWANTLER, M., GUIMARAES PESSOA, M., HINDMAN, S. J., HOFER, H., HUSA, P., KABERG, M., KAITA, K. D., KAUTZ, A., KAYMAKOGLU, S., KRAJDEN, M., KRARUP, H., LALEMAN, W., LAVANCHY, D., MARINHO, R. T., MAROTTA, P., MAUSS, S., MORENO, C., MURPHY, K., NEGRO, F., NEMECEK, V., ORMECI, N., OVREHUS, A. L., PARKES, J., PASINI, K., PELTEKIAN, K. M., RAMJI, A., REIS, N., ROBERTS, S. K., ROSENBERG, W. M., ROUDOT-THORAVAL, F., RYDER, S. D., SARMENTO-CASTRO, R., SEMELA, D., SHERMAN, M., SHIHA, G. E., SIEVERT, W., SPERL, J., STARKEL, P., STAUBER, R. E., THOMPSON, A. J., URBANEK, P., VAN DAMME, P., VAN THIEL, I., VAN VLIERBERGHE, H., VANDIJCK, D., WEDEMEYER, H., WEIS, N., WIEGAND, J., YOSRY, A., ZEKRY, A., CORNBERG, M., MULLHAUPT, B. & ESTES, C. 2014. The present and future disease burden of hepatitis C virus (HCV) infection with today's treatment paradigm. *J Viral Hepat,* 21 Suppl 1**,** 34-59.

ROBINSON, M., YANG, H., SUN, S. C., PENG, B., TIAN, Y., PAGRATIS, N., GREENSTEIN, A. E. & DELANEY, W. E. T. 2010. Novel hepatitis C virus reporter replicon cell lines enable efficient antiviral screening against genotype 1a. *Antimicrob Agents Chemother,* 54**,** 3099-106.

ROMERO-BREY, I. & BARTENSCHLAGER, R. 2014. Membranous replication factories induced by plus-strand RNA viruses. *Viruses,* 6**,** 2826-57.

ROMERO-BREY, I., MERZ, A., CHIRAMEL, A., LEE, J. Y., CHLANDA, P., HASELMAN, U., SANTARELLA-MELLWIG, R., HABERMANN, A., HOPPE, S., KALLIS, S., WALTHER, P., ANTONY, C., KRIJNSE-LOCKER, J. & BARTENSCHLAGER, R. 2012. Three-dimensional architecture and biogenesis of membrane structures associated with hepatitis C virus replication. *PLoS Pathog,* 8**,** e1003056.

ROTH-CROSS, J. K., BENDER, S. J. & WEISS, S. R. 2008. Murine coronavirus mouse hepatitis virus is recognized by MDA5 and induces type I interferon in brain macrophages/microglia. *J Virol,* 82**,** 9829-38.

ROTHENFUSSER, S., GOUTAGNY, N., DIPERNA, G., GONG, M., MONKS, B. G., SCHOENEMEYER, A., YAMAMOTO, M., AKIRA, S. & FITZGERALD, K. A. 2005. The RNA helicase Lgp2 inhibits TLR-independent sensing of viral replication by retinoic acid-inducible gene-I. *J Immunol,* 175**,** 5260-8.

RUDD, B. D., BURSTEIN, E., DUCKETT, C. S., LI, X. & LUKACS, N. W. 2005. Differential role for TLR3 in respiratory syncytial virus-induced chemokine expression. *J Virol,* 79**,** 3350-7.

SACKSTEDER, K. A., JONES, J. M., SOUTH, S. T., LI, X., LIU, Y. & GOULD, S. J. 2000. PEX19 binds multiple peroxisomal membrane proteins, is predominantly cytoplasmic, and is required for peroxisome membrane synthesis. *J Cell Biol,* 148**,** 931-44.

SAHA, S. K., PIETRAS, E. M., HE, J. Q., KANG, J. R., LIU, S. Y., OGANESYAN, G., SHAHANGIAN, A., ZARNEGAR, B., SHIBA, T. L., WANG, Y. & CHENG, G. 2006. Regulation of antiviral responses by a direct and specific interaction between TRAF3 and Cardif. *EMBO J,* 25**,** 3257-63.

SAINZ, B., JR., BARRETTO, N., MARTIN, D. N., HIRAGA, N., IMAMURA, M., HUSSAIN, S., MARSH, K. A., YU, X., CHAYAMA, K., ALREFAI, W. A. &

UPRICHARD, S. L. 2012. Identification of the Niemann-Pick C1-like 1 cholesterol absorption receptor as a new hepatitis C virus entry factor. *Nat Med,* 18**,** 281-5.

SAITO, T., HIRAI, R., LOO, Y. M., OWEN, D., JOHNSON, C. L., SINHA, S. C., AKIRA, S., FUJITA, T. & GALE, M., JR. 2007. Regulation of innate antiviral defenses through a shared repressor domain in RIG-I and LGP2. *Proc Natl Acad Sci U S A,* 104**,** 582-7.

SAITO, T., OWEN, D. M., JIANG, F., MARCOTRIGIANO, J. & GALE, M., JR. 2008. Innate immunity induced by composition-dependent RIG-I recognition of hepatitis C virus RNA. *Nature,* 454**,** 523-7.

SAITOH, T., SATOH, T., YAMAMOTO, N., UEMATSU, S., TAKEUCHI, O., KAWAI, T. & AKIRA, S. 2011. Antiviral protein Viperin promotes Toll-like receptor 7- and Toll-like receptor 9-mediated type I interferon production in plasmacytoid dendritic cells. *Immunity,* 34**,** 352-63.

SAKAI, A., CLAIRE, M. S., FAULK, K., GOVINDARAJAN, S., EMERSON, S. U., PURCELL, R. H. & BUKH, J. 2003. The p7 polypeptide of hepatitis C virus is critical for infectivity and contains functionally important genotype-specific sequences. *Proc Natl Acad Sci U S A,* 100**,** 11646-51.

SANG, Y., BERGKAMP, J. & BLECHA, F. 2014. Molecular evolution of the porcine type I interferon family: subtype-specific expression and antiviral activity. *PLoS One,* 9**,** e112378.

SARASIN-FILIPOWICZ, M., OAKELEY, E. J., DUONG, F. H., CHRISTEN, V., TERRACCIANO, L., FILIPOWICZ, W. & HEIM, M. H. 2008. Interferon signaling and treatment outcome in chronic hepatitis C. *Proc Natl Acad Sci U S A,* 105**,** 7034-9.

SATO, K., ISHIKAWA, T., OKUMURA, A., YAMAUCHI, T., SATO, S., AYADA, M., MATSUMOTO, E., HOTTA, N., OOHASHI, T., FUKUZAWA, Y. & KAKUMU, S. 2007. Expression of Toll-like receptors in chronic hepatitis C virus infection. *J Gastroenterol Hepatol,* 22**,** 1627-32.

SATO, M., HATA, N., ASAGIRI, M., NAKAYA, T., TANIGUCHI, T. & TANAKA, N. 1998. Positive feedback regulation of type I IFN genes by the IFN-inducible transcription factor IRF-7. *FEBS Lett,* 441**,** 106-10.

SCARSELLI, E., ANSUINI, H., CERINO, R., ROCCASECCA, R. M., ACALI, S., FILOCAMO, G., TRABONI, C., NICOSIA, A., CORTESE, R. & VITELLI, A. 2002. The human scavenger receptor class B type I is a novel candidate receptor for the hepatitis C virus. *EMBO J,* 21**,** 5017-25.

SCHALLER, T., APPEL, N., KOUTSOUDAKIS, G., KALLIS, S., LOHMANN, V., PIETSCHMANN, T. & BARTENSCHLAGER, R. 2007. Analysis of hepatitis C virus superinfection exclusion by using novel fluorochrome gene-tagged viral genomes. *J Virol,* 81**,** 4591-603.

SCHERER, W. F., SYVERTON, J. T. & GEY, G. O. 1953. Studies on the propagation in vitro of poliomyelitis viruses. IV. Viral multiplication in a stable strain of human malignant epithelial cells (strain HeLa) derived from an epidermoid carcinoma of the cervix. *J Exp Med,* 97**,** 695-710.

SCHMIDT-MENDE, J., BIECK, E., HUGLE, T., PENIN, F., RICE, C. M., BLUM, H. E. & MORADPOUR, D. 2001. Determinants for membrane association of the hepatitis C virus RNA-dependent RNA polymerase. *J Biol Chem,* 276**,** 44052-63.

SCHNEIDER, W. M., CHEVILLOTTE, M. D. & RICE, C. M. 2014. Interferon-stimulated genes: a complex web of host defenses. *Annu Rev Immunol,* 32**,** 513-45.

SCHNELL, U., DIJK, F., SJOLLEMA, K. A. & GIEPMANS, B. N. 2012. Immunolabeling artifacts and the need for live-cell imaging. *Nat Methods,* 9**,** 152-8.

SCHOGGINS, J. W. & RICE, C. M. 2011. Interferon-stimulated genes and their antiviral effector functions. *Curr Opin Virol,* 1**,** 519-25.

SCHOGGINS, J. W., WILSON, S. J., PANIS, M., MURPHY, M. Y., JONES, C. T., BIENIASZ, P. & RICE, C. M. 2011. A diverse range of gene products are effectors of the type I interferon antiviral response. *Nature,* 472**,** 481-5.

SCHRADER, M. 2006. Shared components of mitochondrial and peroxisomal division. *Biochim Biophys Acta,* 1763**,** 531-41.

SCHRADER, M., GRILLE, S., FAHIMI, H. D. & ISLINGER, M. 2013. Peroxisome interactions and cross-talk with other subcellular compartments in animal cells. *Subcell Biochem,* 69**,** 1-22.

SCHROEDER, C. 2010. Cholesterol-binding viral proteins in virus entry and morphogenesis. *Subcell Biochem,* 51**,** 77-108.

SELBY, M. J., GLAZER, E., MASIARZ, F. & HOUGHTON, M. 1994. Complex processing and protein:protein interactions in the E2:NS2 region of HCV. *Virology,* 204**,** 114-22.

SEN, A., PRUIJSSERS, A. J., DERMODY, T. S., GARCIA-SASTRE, A. & GREENBERG, H. B. 2011. The early interferon response to rotavirus is regulated by PKR and depends on MAVS/IPS-1, RIG-I, MDA-5, and IRF3. *J Virol,* 85**,** 3717-32.

SEN, G. C. 2001. Viruses and interferons. *Annu Rev Microbiol,* 55**,** 255-81.

SEO, J. Y., YANEVA, R., HINSON, E. R. & CRESSWELL, P. 2011. Human cytomegalovirus directly induces the antiviral protein viperin to enhance infectivity. *Science,* 332**,** 1093-7.

SETH, R. B., SUN, L., EA, C. K. & CHEN, Z. J. 2005. Identification and characterization of MAVS, a mitochondrial antiviral signaling protein that activates NF-kappaB and IRF 3. *Cell,* 122**,** 669-82.

SEVERA, M., COCCIA, E. M. & FITZGERALD, K. A. 2006a. Toll-like receptor-dependent and -independent viperin gene expression and counter-regulation by PRDI-binding factor-1/BLIMP1. *J Biol Chem,* 281**,** 26188-95.

SEVERA, M., COCCIA, E. M. & FITZGERALD, K. A. 2006b. Toll-like receptor-dependent and -independent viperin gene expression and counter-regulation by PRDI-binding factor-1/BLIMP1. *Journal of Biological Chemistry,* 281**,** 26188-26195.

SHARMA, S. D. 2010. Hepatitis C virus: molecular biology & current therapeutic options. *Indian J Med Res,* 131**,** 17-34.

SHAVETA, G., SHI, J., CHOW, V. T. & SONG, J. 2010. Structural characterization reveals that viperin is a radical S-adenosyl-L-methionine (SAM) enzyme. *Biochem Biophys Res Commun,* 391**,** 1390-5.

SHI, S. T., POLYAK, S. J., TU, H., TAYLOR, D. R., GRETCH, D. R. & LAI, M. M. 2002. Hepatitis C virus NS5A colocalizes with the core protein on lipid droplets and interacts with apolipoproteins. *Virology,* 292**,** 198-210.

SHIMAKAMI, T., HIJIKATA, M., LUO, H., MA, Y. Y., KANEKO, S., SHIMOTOHNO, K. & MURAKAMI, S. 2004. Effect of interaction between hepatitis C virus NS5A and NS5B on hepatitis C virus RNA replication with the hepatitis C virus replicon. *J Virol,* 78**,** 2738-48.

SHIN, E. C., SUNG, P. S. & PARK, S. H. 2016. Immune responses and immunopathology in acute and chronic viral hepatitis. *Nat Rev Immunol,* 16**,** 509-23.

SIEVERT, W., ALTRAIF, I., RAZAVI, H. A., ABDO, A., AHMED, E. A., ALOMAIR, A., AMARAPURKAR, D., CHEN, C. H., DOU, X., EL KHAYAT, H., ELSHAZLY, M., ESMAT, G., GUAN, R., HAN, K. H., KOIKE, K., LARGEN, A., MCCAUGHAN, G., MOGAWER, S., MONIS, A., NAWAZ, A., PIRATVISUTH, T., SANAI, F. M., SHARARA, A. I., SIBBEL, S., SOOD, A., SUH, D. J., WALLACE, C., YOUNG, K. & NEGRO, F. 2011. A systematic review of hepatitis C virus epidemiology in Asia, Australia and Egypt. *Liver Int,* 31 Suppl 2**,** 61-80.

SILVENNOINEN, O., IHLE, J. N., SCHLESSINGER, J. & LEVY, D. E. 1993. Interferon-induced nuclear signalling by Jak protein tyrosine kinases. *Nature,* 366**,** 583-5.

SIMMONDS, P., BUKH, J., COMBET, C., DELEAGE, G., ENOMOTO, N., FEINSTONE, S., HALFON, P., INCHAUSPE, G., KUIKEN, C., MAERTENS, G., MIZOKAMI, M., MURPHY, D. G., OKAMOTO, H., PAWLOTSKY, J. M., PENIN, F., SABLON, E., SHIN, I. T., STUYVER, L. J., THIEL, H. J., VIAZOV, S., WEINER, A. J. & WIDELL, A. 2005. Consensus proposals for a unified system of nomenclature of hepatitis C virus genotypes. *Hepatology,* 42**,** 962-73.

SKEHEL, P. A., FABIAN-FINE, R. & KANDEL, E. R. 2000. Mouse VAP33 is associated with the endoplasmic reticulum and microtubules. *Proc Natl Acad Sci U S A,* 97**,** 1101-6.

SKLAN, E. H., CHARUWORN, P., PANG, P. S. & GLENN, J. S. 2009. Mechanisms of HCV survival in the host. *Nat Rev Gastroenterol Hepatol,* 6**,** 217-27.

SMITH, D. B., BUKH, J., KUIKEN, C., MUERHOFF, A. S., RICE, C. M., STAPLETON, J. T. & SIMMONDS, P. 2014. Expanded classification of hepatitis C virus into 7 genotypes and 67 subtypes: updated criteria and genotype assignment web resource. *Hepatology,* 59**,** 318-27.

SMITH, J. J. & AITCHISON, J. D. 2013. Peroxisomes take shape. *Nat Rev Mol Cell Biol,* 14**,** 803-17.

SOSINSKY, G. E., GIEPMANS, B. N., DEERINCK, T. J., GAIETTA, G. M. & ELLISMAN, M. H. 2007. Markers for correlated light and electron microscopy. *Methods Cell Biol,* 79**,** 575-91.

SOURISSEAU, M., MICHTA, M. L., ZONY, C., ISRAELOW, B., HOPCRAFT, S. E., NARBUS, C. M., PARRA MARTIN, A. & EVANS, M. J. 2013. Temporal

analysis of hepatitis C virus cell entry with occludin directed blocking antibodies. *PLoS Pathog,* 9**,** e1003244.

STEINBERG, S. J., RAYMOND, G. V., BRAVERMAN, N. E. & MOSER, A. B. 1993. Peroxisome Biogenesis Disorders, Zellweger Syndrome Spectrum. *In:* PAGON, R. A., ADAM, M. P., ARDINGER, H. H., WALLACE, S. E., AMEMIYA, A., BEAN, L. J. H., BIRD, T. D., LEDBETTER, N., MEFFORD, H. C., SMITH, R. J. H. & STEPHENS, K. (eds.) *GeneReviews(R).* Seattle (WA).

STEINMANN, E., PENIN, F., KALLIS, S., PATEL, A. H., BARTENSCHLAGER, R. & PIETSCHMANN, T. 2007. Hepatitis C virus p7 protein is crucial for assembly and release of infectious virions. *PLoS Pathog,* 3**,** e103.

STIRNWEISS, A., KSIENZYK, A., KLAGES, K., RAND, U., GRASHOFF, M., HAUSER, H. & KROGER, A. 2010. IFN regulatory factor-1 bypasses IFN-mediated antiviral effects through viperin gene induction. *J Immunol,* 184**,** 5179-85.

STRAUSS, M. P., LIEW, A. T., TURNBULL, L., WHITCHURCH, C. B., MONAHAN, L. G. & HARRY, E. J. 2012. 3D-SIM super resolution microscopy reveals a bead-like arrangement for FtsZ and the division machinery: implications for triggering cytokinesis. *PLoS Biol,* 10**,** e1001389.

SU, A. I., PEZACKI, J. P., WODICKA, L., BRIDEAU, A. D., SUPEKOVA, L., THIMME, R., WIELAND, S., BUKH, J., PURCELL, R. H., SCHULTZ, P. G. & CHISARI, F. V. 2002. Genomic analysis of the host response to hepatitis C virus infection. *Proc Natl Acad Sci U S A,* 99**,** 15669-74.

SUMPTER, R., JR., LOO, Y. M., FOY, E., LI, K., YONEYAMA, M., FUJITA, T., LEMON, S. M. & GALE, M., JR. 2005. Regulating intracellular antiviral defense and permissiveness to hepatitis C virus RNA replication through a cellular RNA helicase, RIG-I. *J Virol,* 79**,** 2689-99.

SUNG, V. M., SHIMODAIRA, S., DOUGHTY, A. L., PICCHIO, G. R., CAN, H., YEN, T. S., LINDSAY, K. L., LEVINE, A. M. & LAI, M. M. 2003. Establishment of B-cell lymphoma cell lines persistently infected with hepatitis C virus in vivo and in vitro: the apoptotic effects of virus infection. *J Virol,* 77**,** 2134-46.

SUZUKI, T., ISHII, K., AIZAKI, H. & WAKITA, T. 2007. Hepatitis C viral life cycle. *Adv Drug Deliv Rev,* 59**,** 1200-12.

SZRETTER, K. J., BRIEN, J. D., THACKRAY, L. B., VIRGIN, H. W., CRESSWELL, P. & DIAMOND, M. S. 2011. The interferon-inducible gene viperin restricts West Nile virus pathogenesis. *J Virol,* 85**,** 11557-66.

TAI, A. W. & SALLOUM, S. 2011. The role of the phosphatidylinositol 4-kinase PI4KA in hepatitis C virus-induced host membrane rearrangement. *PLoS One,* 6**,** e26300.

TAI, C. L., CHI, W. K., CHEN, D. S. & HWANG, L. H. 1996. The helicase activity associated with hepatitis C virus nonstructural protein 3 (NS3). *J Virol,* 70**,** 8477-84.

TAKAHASHI, K., ASABE, S., WIELAND, S., GARAIGORTA, U., GASTAMINZA, P., ISOGAWA, M. & CHISARI, F. V. 2010. Plasmacytoid dendritic cells sense hepatitis C virus-infected cells, produce interferon, and inhibit infection. *Proc Natl Acad Sci U S A,* 107**,** 7431-6.

TAN, K. S., OLFAT, F., PHOON, M. C., HSU, J. P., HOWE, J. L., SEET, J. E., CHIN, K. C. & CHOW, V. T. 2012. In vivo and in vitro studies on the antiviral activities of viperin against influenza H1N1 virus infection. *J Gen Virol,* 93**,** 1269-77.

TANAKA, Y., NISHIDA, N., SUGIYAMA, M., KUROSAKI, M., MATSUURA, K., SAKAMOTO, N., NAKAGAWA, M., KORENAGA, M., HINO, K., HIGE, S., ITO, Y., MITA, E., TANAKA, E., MOCHIDA, S., MURAWAKI, Y., HONDA, M., SAKAI, A., HIASA, Y., NISHIGUCHI, S., KOIKE, A., SAKAIDA, I., IMAMURA, M., ITO, K., YANO, K., MASAKI, N., SUGAUCHI, F., IZUMI, N., TOKUNAGA, K. & MIZOKAMI, M. 2009. Genome-wide association of IL28B with response to pegylated interferon-alpha and ribavirin therapy for chronic hepatitis C. *Nat Genet,* 41**,** 1105-9.

TANG, H. B., LU, Z. L., WEI, X. K., ZHONG, T. Z., ZHONG, Y. Z., OUYANG, L. X., LUO, Y., XING, X. W., LIAO, F., PENG, K. K., DENG, C. Q., MINAMOTO, N. & LUO, T. R. 2016. Viperin inhibits rabies virus replication via reduced cholesterol and sphingomyelin and is regulated upstream by TLR4. *Sci Rep,* 6**,** 30529.

TARANTINO, G., DI CRISTINA, A., PIPITONE, R., ALMASIO, P. L., DI VITA, G., CRAXI, A. & GRIMAUDO, S. 2013. In vivo liver expression of TLR2, TLR3 and TLR7 in chronic hepatitis C. *J Biol Regul Homeost Agents,* 27**,** 233-9.

TARGETT-ADAMS, P., GRAHAM, E. J., MIDDLETON, J., PALMER, A., SHAW, S. M., LAVENDER, H., BRAIN, P., TRAN, T. D., JONES, L. H., WAKENHUT, F., STAMMEN, B., PRYDE, D., PICKFORD, C. & WESTBY, M. 2011. Small molecules targeting hepatitis C virus-encoded NS5A cause subcellular redistribution of their target: insights into compound modes of action. *J Virol,* 85**,** 6353-68.

TELLINGHUISEN, T. L., EVANS, M. J., VON HAHN, T., YOU, S. & RICE, C. M. 2007. Studying hepatitis C virus: making the best of a bad virus. *J Virol,* 81**,** 8853-67.

TELLINGHUISEN, T. L., FOSS, K. L. & TREADAWAY, J. 2008a. Regulation of hepatitis C virion production via phosphorylation of the NS5A protein. *PLoS Pathog,* 4**,** e1000032.

TELLINGHUISEN, T. L., FOSS, K. L., TREADAWAY, J. C. & RICE, C. M. 2008b. Identification of residues required for RNA replication in domains II and III of the hepatitis C virus NS5A protein. *J Virol,* 82**,** 1073-83.

TELLINGHUISEN, T. L., MARCOTRIGIANO, J., GORBALENYA, A. E. & RICE, C. M. 2004. The NS5A protein of hepatitis C virus is a zinc metalloprotein. *J Biol Chem,* 279**,** 48576-87.

TENG, T. S., FOO, S. S., SIMAMARTA, D., LUM, F. M., TEO, T. H., LULLA, A., YEO, N. K., KOH, E. G., CHOW, A., LEO, Y. S., MERITS, A., CHIN, K. C. & NG, L. F. 2012. Viperin restricts chikungunya virus replication and pathology. *J Clin Invest,* 122**,** 4447-60.

THOMAS, D. L. 2013. Global control of hepatitis C: where challenge meets opportunity. *Nat Med,* 19**,** 850-8.

THOMAS, D. L., THIO, C. L., MARTIN, M. P., QI, Y., GE, D., O'HUIGIN, C., KIDD, J., KIDD, K., KHAKOO, S. I., ALEXANDER, G., GOEDERT, J. J., KIRK, G. D., DONFIELD, S. M., ROSEN, H. R., TOBLER, L. H., BUSCH, M. P.,

MCHUTCHISON, J. G., GOLDSTEIN, D. B. & CARRINGTON, M. 2009. Genetic variation in IL28B and spontaneous clearance of hepatitis C virus. *Nature,* 461**,** 798-801.

THOMSSEN, R., BONK, S., PROPFE, C., HEERMANN, K. H., KOCHEL, H. G. & UY, A. 1992. Association of hepatitis C virus in human sera with beta-lipoprotein. *Med Microbiol Immunol,* 181**,** 293-300.

TITORENKO, V. I. & RACHUBINSKI, R. A. 2001. The life cycle of the peroxisome. *Nat Rev Mol Cell Biol,* 2**,** 357-68.

TU, H., GAO, L., SHI, S. T., TAYLOR, D. R., YANG, T., MIRCHEFF, A. K., WEN, Y., GORBALENYA, A. E., HWANG, S. B. & LAI, M. M. 1999. Hepatitis C virus RNA polymerase and NS5A complex with a SNARE-like protein. *Virology,* 263**,** 30-41.

TURSI, A., BRANDIMANTE, G., CHIARELLI, F., SPAGNOLI, A. & TORELLO, M. 2002. Detection of HCV RNA in gastric mucosa-associated lymphoid tissue by in situ hybridization: evidence of a new extrahepatic localization of HCV with increased risk of gastric malt lymphoma. *Am J Gastroenterol,* 97**,** 1802-6.

UPADHYAY, A. S., VONDERSTEIN, K., PICHLMAIR, A., STEHLING, O., BENNETT, K. L., DOBLER, G., GUO, J. T., SUPERTI-FURGA, G., LILL, R., OVERBY, A. K. & WEBER, F. 2014. Viperin is an iron-sulfur protein that inhibits genome synthesis of tick-borne encephalitis virus via radical SAM domain activity. *Cell Microbiol,* 16**,** 834-48.

UZRI, D. & GEHRKE, L. 2009. Nucleotide sequences and modifications that determine RIG-I/RNA binding and signaling activities. *J Virol,* 83**,** 4174-84.

VAN CRIEKINGE, W. & BEYAERT, R. 1999. Yeast Two-Hybrid: State of the Art. *Biol Proced Online,* 2**,** 1-38.

VAN DER HOEK, K. H., EYRE, N. S., SHUE, B., KHANTISITTHIPORN, O., GLAB-AMPI, K., CARR, J. M., GARTNER, M. J., JOLLY, L. A., THOMAS, P. Q., ADIKUSUMA, F., JANKOVIC-KARASOULOS, T., ROBERTS, C. T., HELBIG, K. J. & BEARD, M. R. 2017. Viperin is an important host restriction factor in control of Zika virus infection. *Sci Rep,* 7**,** 4475.

VAZQUEZ, C. & HORNER, S. M. 2015. MAVS Coordination of Antiviral Innate Immunity. *J Virol,* 89**,** 6974-7.

VEIT, M. & THAA, B. 2011. Association of influenza virus proteins with membrane rafts. *Adv Virol,* 2011**,** 370606.

VENKATARAMAN, T., VALDES, M., ELSBY, R., KAKUTA, S., CACERES, G., SAIJO, S., IWAKURA, Y. & BARBER, G. N. 2007. Loss of DExD/H box RNA helicase LGP2 manifests disparate antiviral responses. *J Immunol,* 178**,** 6444-55.

VONDERSTEIN, K., NILSSON, E., HUBEL, P., NYGARD SKALMAN, L., UPADHYAY, A., PASTO, J., PICHLMAIR, A., LUNDMARK, R. & OVERBY, A. K. 2017. Viperin targets flavivirus virulence by inducing assembly of non-infectious capsid particles. *J Virol*.

WAKITA, T., PIETSCHMANN, T., KATO, T., DATE, T., MIYAMOTO, M., ZHAO, Z., MURTHY, K., HABERMANN, A., KRAUSSLICH, H. G., MIZOKAMI, M., BARTENSCHLAGER, R. & LIANG, T. J. 2005. Production of infectious hepatitis C virus in tissue culture from a cloned viral genome. *Nat Med,* 11**,** 791-6.

WANDERS, R. J. 2004. Peroxisomes, lipid metabolism, and peroxisomal disorders. *Mol Genet Metab,* 83**,** 16-27.
WANDERS, R. J. & WATERHAM, H. R. 2006. Biochemistry of mammalian peroxisomes revisited. *Annu Rev Biochem,* 75**,** 295-332.
WANG, C., PFLUGHEBER, J., SUMPTER, R., JR., SODORA, D. L., HUI, D., SEN, G. C. & GALE, M., JR. 2003. Alpha interferon induces distinct translational control programs to suppress hepatitis C virus RNA replication. *J Virol,* 77**,** 3898-912.
WANG, H., PERRY, J. W., LAURING, A. S., NEDDERMANN, P., DE FRANCESCO, R. & TAI, A. W. 2014. Oxysterol-binding protein is a phosphatidylinositol 4-kinase effector required for HCV replication membrane integrity and cholesterol trafficking. *Gastroenterology,* 146**,** 1373-85 e1-11.
WANG, H. & SZTALRYD, C. 2011. Oxidative tissue: perilipin 5 links storage with the furnace. *Trends Endocrinol Metab,* 22**,** 197-203.
WANG, H. & TAI, A. W. 2016. Mechanisms of Cellular Membrane Reorganization to Support Hepatitis C Virus Replication. *Viruses,* 8.
WANG, J. P., LIU, P., LATZ, E., GOLENBOCK, D. T., FINBERG, R. W. & LIBRATY, D. H. 2006. Flavivirus activation of plasmacytoid dendritic cells delineates key elements of TLR7 signaling beyond endosomal recognition. *J Immunol,* 177**,** 7114-21.
WANG, N., LIANG, Y., DEVARAJ, S., WANG, J., LEMON, S. M. & LI, K. 2009a. Toll-like receptor 3 mediates establishment of an antiviral state against hepatitis C virus in hepatoma cells. *J Virol,* 83**,** 9824-34.
WANG, S., WU, X., PAN, T., SONG, W., WANG, Y., ZHANG, F. & YUAN, Z. 2012. Viperin inhibits hepatitis C virus replication by interfering with binding of NS5A to host protein hVAP-33. *J Gen Virol,* 93**,** 83-92.
WANG, T., TOWN, T., ALEXOPOULOU, L., ANDERSON, J. F., FIKRIG, E. & FLAVELL, R. A. 2004. Toll-like receptor 3 mediates West Nile virus entry into the brain causing lethal encephalitis. *Nat Med,* 10**,** 1366-73.
WANG, W., FU, Y. J., ZU, Y. G., WU, N., REICHLING, J. & EFFERTH, T. 2009b. Lipid rafts play an important role in the vesicular stomatitis virus life cycle. *Arch Virol,* 154**,** 595-600.
WANG, X. Y., HINSON, E. R. & CRESSWELL, P. 2007. The interferon-inducible protein viperin inhibits influenza virus release by perturbing lipid rafts. *Cell Host & Microbe,* 2**,** 96-105.
WEBER, M., GAWANBACHT, A., HABJAN, M., RANG, A., BORNER, C., SCHMIDT, A. M., VEITINGER, S., JACOB, R., DEVIGNOT, S., KOCHS, G., GARCIA-SASTRE, A. & WEBER, F. 2013. Incoming RNA virus nucleocapsids containing a 5'-triphosphorylated genome activate RIG-I and antiviral signaling. *Cell Host Microbe,* 13**,** 336-46.
WEIHOFEN, A., BINNS, K., LEMBERG, M. K., ASHMAN, K. & MARTOGLIO, B. 2002. Identification of signal peptide peptidase, a presenilin-type aspartic protease. *Science,* 296**,** 2215-8.
WEIR, M. L., XIE, H., KLIP, A. & TRIMBLE, W. S. 2001. VAP-A binds promiscuously to both v- and tSNAREs. *Biochem Biophys Res Commun,* 286**,** 616-21.
WHITE, L. K., SALI, T., ALVARADO, D., GATTI, E., PIERRE, P., STREBLOW, D. & DEFILIPPIS, V. R. 2011. Chikungunya virus induces IPS-1-dependent innate

immune activation and protein kinase R-independent translational shutoff. *J Virol,* 85**,** 606-20.

WILKINS, C., WOODWARD, J., LAU, D. T., BARNES, A., JOYCE, M., MCFARLANE, N., MCKEATING, J. A., TYRRELL, D. L. & GALE, M., JR. 2013. IFITM1 is a tight junction protein that inhibits hepatitis C virus entry. *Hepatology,* 57**,** 461-9.

WOLK, B., SANSONNO, D., KRAUSSLICH, H. G., DAMMACCO, F., RICE, C. M., BLUM, H. E. & MORADPOUR, D. 2000. Subcellular localization, stability, and trans-cleavage competence of the hepatitis C virus NS3-NS4A complex expressed in tetracycline-regulated cell lines. *J Virol,* 74**,** 2293-304.

WYLES, J. P., MCMASTER, C. R. & RIDGWAY, N. D. 2002. Vesicle-associated membrane protein-associated protein-A (VAP-A) interacts with the oxysterol-binding protein to modify export from the endoplasmic reticulum. *J Biol Chem,* 277**,** 29908-18.

XU, D., HOLKO, M., SADLER, A. J., SCOTT, B., HIGASHIYAMA, S., BERKOFSKY-FESSLER, W., MCCONNELL, M. J., PANDOLFI, P. P., LICHT, J. D. & WILLIAMS, B. R. 2009. Promyelocytic leukemia zinc finger protein regulates interferon-mediated innate immunity. *Immunity,* 30**,** 802-16.

XU, L. G., WANG, Y. Y., HAN, K. J., LI, L. Y., ZHAI, Z. & SHU, H. B. 2005. VISA is an adapter protein required for virus-triggered IFN-beta signaling. *Mol Cell,* 19**,** 727-40.

YAO, N., REICHERT, P., TAREMI, S. S., PROSISE, W. W. & WEBER, P. C. 1999. Molecular views of viral polyprotein processing revealed by the crystal structure of the hepatitis C virus bifunctional protease-helicase. *Structure,* 7**,** 1353-63.

YASUI, K., WAKITA, T., TSUKIYAMA-KOHARA, K., FUNAHASHI, S. I., ICHIKAWA, M., KAJITA, T., MORADPOUR, D., WANDS, J. R. & KOHARA, M. 1998. The native form and maturation process of hepatitis C virus core protein. *J Virol,* 72**,** 6048-55.

YE, J. 2007. Reliance of host cholesterol metabolic pathways for the life cycle of hepatitis C virus. *PLoS Pathog,* 3**,** e108.

YONEYAMA, M. & FUJITA, T. 2007. Function of RIG-I-like receptors in antiviral innate immunity. *J Biol Chem,* 282**,** 15315-8.

YONEYAMA, M., KIKUCHI, M., MATSUMOTO, K., IMAIZUMI, T., MIYAGISHI, M., TAIRA, K., FOY, E., LOO, Y. M., GALE, M., JR., AKIRA, S., YONEHARA, S., KATO, A. & FUJITA, T. 2005. Shared and unique functions of the DExD/H-box helicases RIG-I, MDA5, and LGP2 in antiviral innate immunity. *J Immunol,* 175**,** 2851-8.

YONEYAMA, M., KIKUCHI, M., NATSUKAWA, T., SHINOBU, N., IMAIZUMI, T., MIYAGISHI, M., TAIRA, K., AKIRA, S. & FUJITA, T. 2004. The RNA helicase RIG-I has an essential function in double-stranded RNA-induced innate antiviral responses. *Nat Immunol,* 5**,** 730-7.

YOU, J., HOU, S., MALIK-SONI, N., XU, Z., KUMAR, A., RACHUBINSKI, R. A., FRAPPIER, L. & HOBMAN, T. C. 2015. Flavivirus Infection Impairs Peroxisome Biogenesis and Early Antiviral Signaling. *J Virol,* 89**,** 12349-61.

YU, G. Y., LEE, K. J., GAO, L. & LAI, M. M. 2006. Palmitoylation and polymerization of hepatitis C virus NS4B protein. *J Virol,* 80**,** 6013-23.

ZHANG, Y., BURKE, C. W., RYMAN, K. D. & KLIMSTRA, W. B. 2007. Identification and characterization of interferon-induced proteins that inhibit alphavirus replication. *J Virol,* 81**,** 11246-55.

ZHANG, Y., EL-FAR, M., DUPUY, F. P., ABDEL-HAKEEM, M. S., HE, Z., PROCOPIO, F. A., SHI, Y., HADDAD, E. K., ANCUTA, P., SEKALY, R. P. & SAID, E. A. 2016. HCV RNA Activates APCs via TLR7/TLR8 While Virus Selectively Stimulates Macrophages Without Inducing Antiviral Responses. *Sci Rep,* 6**,** 29447.

ZHANG, Y. L., GUO, Y. J., BIN, L. & SUN, S. H. 2009. Hepatitis C virus single-stranded RNA induces innate immunity via Toll-like receptor 7. *J Hepatol,* 51**,** 29-38.

ZHAO, H., LIN, W., KUMTHIP, K., CHENG, D., FUSCO, D. N., HOFMANN, O., JILG, N., TAI, A. W., GOTO, K., ZHANG, L., HIDE, W., JANG, J. Y., PENG, L. F. & CHUNG, R. T. 2012. A functional genomic screen reveals novel host genes that mediate interferon-alpha's effects against hepatitis C virus. *J Hepatol,* 56**,** 326-33.

ZHONG, J., GASTAMINZA, P., CHENG, G., KAPADIA, S., KATO, T., BURTON, D. R., WIELAND, S. F., UPRICHARD, S. L., WAKITA, T. & CHISARI, F. V. 2005. Robust hepatitis C virus infection in vitro. *Proc Natl Acad Sci U S A,* 102**,** 9294-9.

ZHOU, A., PARANJAPE, J. M., DER, S. D., WILLIAMS, B. R. & SILVERMAN, R. H. 1999. Interferon action in triply deficient mice reveals the existence of alternative antiviral pathways. *Virology,* 258**,** 435-40.

ZHOU, S., CERNY, A. M., ZACHARIA, A., FITZGERALD, K. A., KURT-JONES, E. A. & FINBERG, R. W. 2010. Induction and inhibition of type I interferon responses by distinct components of lymphocytic choriomeningitis virus. *J Virol,* 84**,** 9452-62.

ZHOU, Y., WANG, X., SUN, L., ZHOU, L., MA, T. C., SONG, L., WU, J. G., LI, J. L. & HO, W. Z. 2016. Toll-like receptor 3-activated macrophages confer anti-HCV activity to hepatocytes through exosomes. *FASEB J,* 30**,** 4132-4140.

ZHOU, Z., WANG, N., WOODSON, S. E., DONG, Q., WANG, J., LIANG, Y., RIJNBRAND, R., WEI, L., NICHOLS, J. E., GUO, J. T., HOLBROOK, M. R., LEMON, S. M. & LI, K. 2011. Antiviral activities of ISG20 in positive-strand RNA virus infections. *Virology,* 409**,** 175-88.

ZHU, H., CONG, J. P. & SHENK, T. 1997. Use of differential display analysis to assess the effect of human cytomegalovirus infection on the accumulation of cellular RNAs: induction of interferon-responsive RNAs. *Proc Natl Acad Sci U S A,* 94**,** 13985-90.

ZHU, H., ZHAO, H., COLLINS, C. D., ECKENRODE, S. E., RUN, Q., MCINDOE, R. A., CRAWFORD, J. M., NELSON, D. R., SHE, J. X. & LIU, C. 2003. Gene expression associated with interferon alfa antiviral activity in an HCV replicon cell line. *Hepatology,* 37**,** 1180-8.